CLASSIFICATION OF ROCK GLACIERS IN SOUTHERN COLORADO BASED ON ICE CONTENT USING RADAR INTERFEROMETRY AND THERMAL REMOTE SENSING

A Thesis

presented to

the Faculty of the Graduate School

at the University of Missouri-Columbia

In Partial Fulfillment

of the Requirements for the Degree

Master of Science

---

by

Allison Alcott

Dr. Francisco Gomez, Thesis Supervisor

MAY 2020

The undersigned, appointed by the dean of the Graduate School, have examined the thesis entitled

CLASSIFICATION OF ROCK GLACIERS IN SOUTHERN COLORADO BASED ON ICE CONTENT USING RADAR INTERFEROMETRY AND THERMAL REMOTE SENSING

presented by Allison Alcott,

a candidate for the degree of Master of Science

and hereby certify that, in their opinion, it is worthy of acceptance.

_____

Professor Francisco Gomez

_____

Professor Tandis Bidgoli

_____

Professor Clayton Blodgett

ACKNOWLEDGEMENTS

I would like to acknowledge the help I have received from the University of Missouri Department of Geoscience in the form of a teaching assistantship, which I received for the duration of my degree. I owe my ability to complete this research to the support, both financially and academically, that I received from the Department of Geosciences. I am also grateful for the Davies Scholarship, which I was awarded during my first year at Mizzou. I wish to thank Professor Francisco Gomez, my advisor, who gave me the opportunity to work on this study, and the rest of my thesis committee, Dr. Tandis Bidgoli and Dr. Clayton Blodgett. Each one has given me invaluable feedback and new perspectives. Thank you to Professor Matthew Pritchard and Dr. Kevin Reath both helped to inspire my interest in remote sensing and gave me my first research opportunity. Finally, I am unable to express how thankful I am for the friends and family who loved and supported me along the way.

TABLE OF CONTENTS

ACKNOWLEDGEMENTS ii

LIST OF FIGURES iv

ABSTRACT vii

Chapter 1. INTRODUCTION 1

Chapter 2. GEOLOGIC BACKGROUND……..8

Rock Glaciers in The Environment.....8

Classification of Rock Glaciers…….12

Genetic Classification……12

Morphological Classification…….14

Activity Classification……...16

Kinematics and Mechanics……17

Study Area…….21

Chapter 3. RADAR INTERFEROMETRY

Background……32

Method……...34

Results……43

Chapter 4. THERMAL REMOTE SENSING

Background……71

Method……...74

Results……77

Chapter 5. DISCUSSION AND CONCLUSIONS

Discussion of Radar Interferometry……...89

Discussion of Thermal Analysis……93

Sources of Uncertainty……...97

Conclusions……..101

APPENDIX A. Radar Interferometry Time Series.....112

APPENDIX B Land Surface Temperature.....142

APPENDIX C Tables…….....165
CITATIONS 169

LIST OF FIGURES

1.1 Study Area Map……4

1.2 Photograph on Rock Glacier……..5

1.3 Diagram of a Rock Glacier……6

1.4 Plan of Approach……...7

2.1 Diagram of a Rock Glacier Overlain on an Image……..24

2.2 Genetic Classification Cross Sections……25

2.3 Morphological Classifications……26

2.4 Maps of Rock Glaciers by Peak……...27

2.5 Geologic Map……...31

3.1 Radar Interferometry Concept Diagram……..48

3.2 Effect of Look Direction Diagram.....……..49

3.3 Processing Plan of Approach……...50

3.4 Map Geometry Radar Image……51

3.5 Geocoding to Radar Geometry……52

3.6 Raw Interferogram……...53

3.7 Effect of Filtering……54

3.8 Unwrapping Concept……...55

3.9 Unwrapping Error……56

3.10 Baseline Refinement……..57

3.11 Interpolation……...58

3.12 Atmospheric Removal……...59

3.13 Elevation Removal……60

3.14 Stack and Closeups……61

3.15 Time Series Images……63

3.16 Elevation Histogram……..65

3.17 Displacement of Fastest Rock Glacier.....……66

3.18 Displacement Toward Sensor……67

3.19 Low Sensitivity Displacement……...68
3.20 Inactive Time Series Plot……...69
3.21 Azimuth vs. Phase Rate…….70
4.1 Land Surface Temperature Landsat7 Image……80
4.2 Weather Time Series……81
4.3 Rock Glacier Time Series……82
4.4 Comparison of Amplitude for Weather and LST ……...83
4.5 Diagram of Comparative Amplitude……...84
4.6 Comparative Amplitude Histograms: Active vs. Inactive……...85
5.1 Seasonal Displacement……..104
5.2 Azimuth vs. Sensitivity……..105
5.3 Sensitivity vs. Phase Rate……..106
5.4 Peak Maps of Classified Rock Glaciers…….107
5.5 Examples of Culled Thermal Time Series…….111

Classification of Rock Glaciers in Southern Colorado Based on Ice Content Using Radar Interferometry and Thermal Remote Sensing

Allison Alcott

Thesis Supervisor: Dr. Francisco Gomez

ABSTRACT

Remote sensing provides a means of assessing potential water resources stored in alpine ground ice; this study focuses on rock glaciers, in particular. A rock glacier is a landform composed of block of loose debris (talus) cemented with ice. There are many ways of classifying rock glaciers; categorizing them based on activity provides context on their movement and ice content. Active rock glaciers are able to flow due to their ice content, while inactive or relict rock glaciers are unable to flow due to lack of sufficient ice. This study uses satellite based radar interferometry to identify and quantify movement of 87 rock glaciers on seven peaks in Southern Colorado. Once the active flowing rock glaciers and inactive nonflowing rock glaciers had been identified, the thermal properties of each group were studied to determine if it was possible to classify rock glaciers based on activity using satellite based thermal imaging. This was accomplished by comparing the amplitude of variation in land surface temperature derived from Landsat 7 and Landsat 8 to daily NOAA weather observations over different periods. Active rock glaciers demonstrated less variation in temperature annually than inactive rock glaciers, likely due to the ice modulating surface temperatures from below. Because rock glacier ice content affects land surface temperature over a period of 1 year, the depth to the ice was estimated using a skin depth calculation to be

between 4.8m and 6.9m. Active and inactive rock glaciers appear to have different thermal characteristics that can be identified in satellite based thermal infrared imagery. Identifying the difference between active and inactive rock glaciers could be important in identifying potential water resources in remote alpine ecosystems, and on Mars, as well as provide insight to the climatic history of the region.

Chapter 1: Introduction

Rock glaciers are dynamic landforms that are staples in alpine environments, transporting large amounts of rock debris downslope (Giardino and Vitek, 1988). A rock glacier is composed of blocks of loose rock and ice filling in the spaces between (Figure 1.3). While, transporting solid rock is an important aspect of rock glaciers, they can also act as storage for vital water sources and can feed ground water reserves from the melt and runoff of their interstitial ice (Liu et al., 2013). Their consideration as a water resource has grown in importance because they can maintain ice for centuries, despite short term changes in weather, if the climate enables it. Rock glaciers, therefore, indicate past and present periglacial and glacial climate. Changes in climate over time are reflected in the distribution of various classifications of rock glaciers. The presence of similar features on Mars indicate past Martian climates and could potentially be a subsurface ice resource that may be used for supporting human exploration (Colaprete and Jakosky, 1998).

There are two requirements for the formation of rock glaciers: 1) a supply of talus (rock material) to make up the body of the rock glacier, and 2) a climate conducive to the generation and sustenance of sub surface ice. While there are several methods to classify rock glaciers, in this study, the activity of a rock glacier will be determined by evaluating the amount of ice within a rock glacier using remote sensing methods. Active rock glaciers contain a sufficient amount of interstitial ice to be able to flow downslope by plastic deformation of the ice at depth. Inactive rock glaciers may contain interstitial ice, but they do not have enough to allow the landform to move. Fossil (or relict) rock glaciers do not have any ice in them.

This study focuses on Mt. Mestas in southern Colorado, as well as several high elevation regions near Mt. Mestas (Figure 1.1), to evaluate the utility of satellite imagery in determining rock glacier activity. Mt. Mestas has 44 rock glaciers on its flanks, including the one shown in Figure 1.2, with varying levels of activity. Some rock glaciers found there move rapidly, with ice observed only meters below the rock surface. Other rock glaciers do not exhibit any sign of movement. Having such a wide variety of rock glacier activities allows for observation of the characteristics of each activity category and the methods may be tested for future use in other locations.

Because rock glaciers are located in high elevations, on remote mountains, and on other planets, an efficient way of monitoring them is with remote sensing. This study employs two remotely sensed data methodologies in order to determine the activity of each rock glacier. The first method is radar interferometry, which can be used to directly measure rock glacier displacement over time and changes in flow rate. Rock glaciers that move are by definition active and contain ground ice. The second method of remote sensing is thermal remote sensing. Using the thermal infrared imagery, difference in signals over rock glaciers with and without ground ice may be compared and an estimate of ground ice depth can be made. If a large displacement is measured over a rock glacier using radar interferometry, then the thermal signal should indicate a smaller depth to the interstitial ground ice because there will be more ice acting as a mechanism for flow. Being able to determine the ice content of a rock glacier remotely could become an invaluable tool for identifying water sources in terrestrial alpine or Martian environments and could act as an indicator for environmental evolution due to climate change. Thermal differentiation of active and inactive rock glaciers is important because it goes beyond

just activity classification, and gives insight into the internal structure and ice content of the rock glaciers.

Figure 1.4 displays the general process for completing this study. The hypotheses for this study are as follows:

1) The movement of rock glaciers may be determined using radar interferometry on a long term scale and seasonally.
2) Thermal infrared imagery may be used to characterize the activity of rock glaciers because rock glaciers containing ice will behave differently thermally over time than rock glaciers lacking interstitial ice.
3) The depth to the ice in active rock glaciers, as determined by radar interferometry, may be determined using thermal infrared imagery.

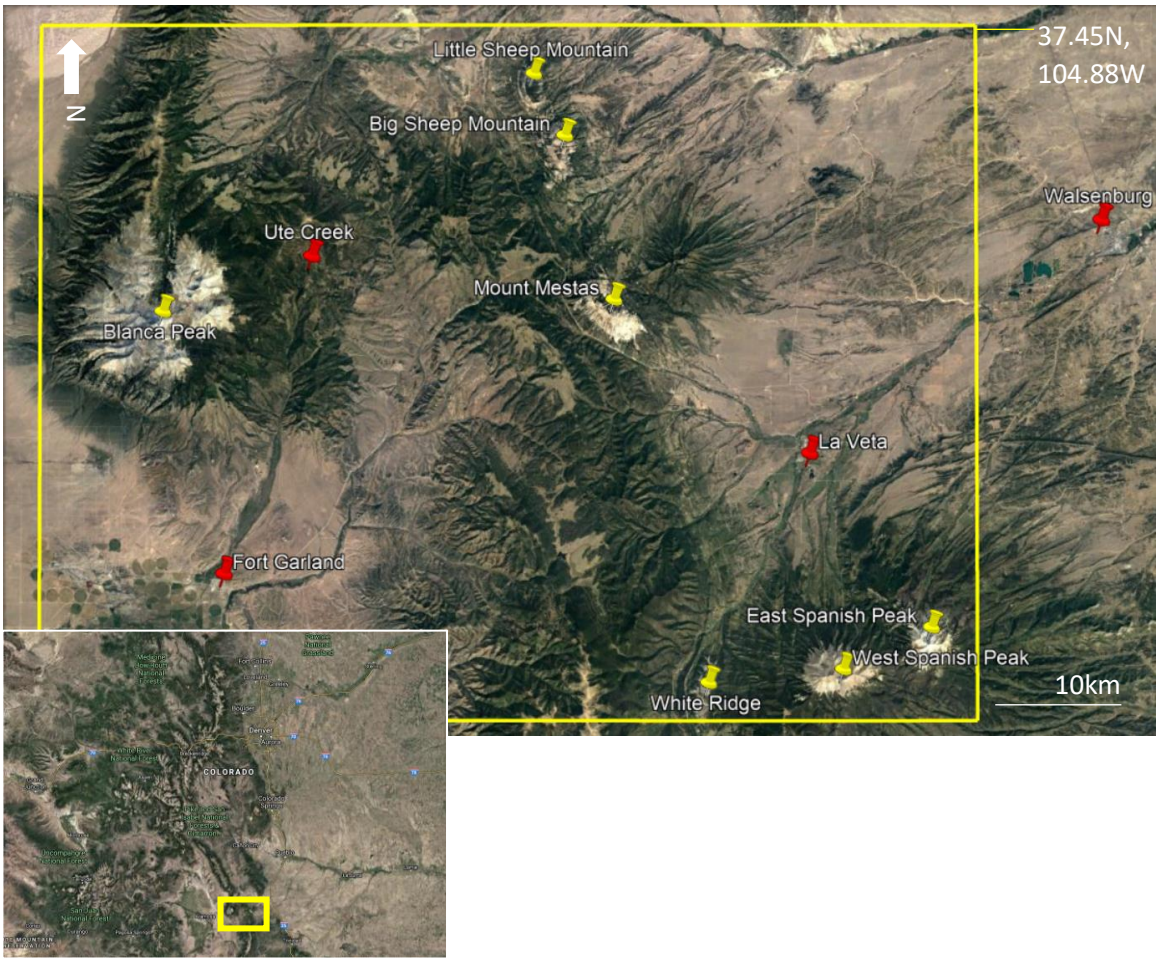

Figure 1.1: Google Earth image of the study area, outlined in the yellow box. Peaks with rock glaciers are labeled by yellow markers, NOAA Ute Creek and Walsenburg weather stations are labeled in with a red marker. The inset box shows the context of the study area box in the whole of Colorado. Fort Garland (FG) and La Veta (LV) are towns labeled for geographic context

Figure 1.2: An image taken from the surface of rock glacier number 018 on Mount Mestas in September 2019, looking southwest. The loose talus covers the surface and there is a lack of vegetation. The lighter colored talus at the toe of the rock glacier is the result of quarrying that exposed inner portions of the talus apron in the 1960s.

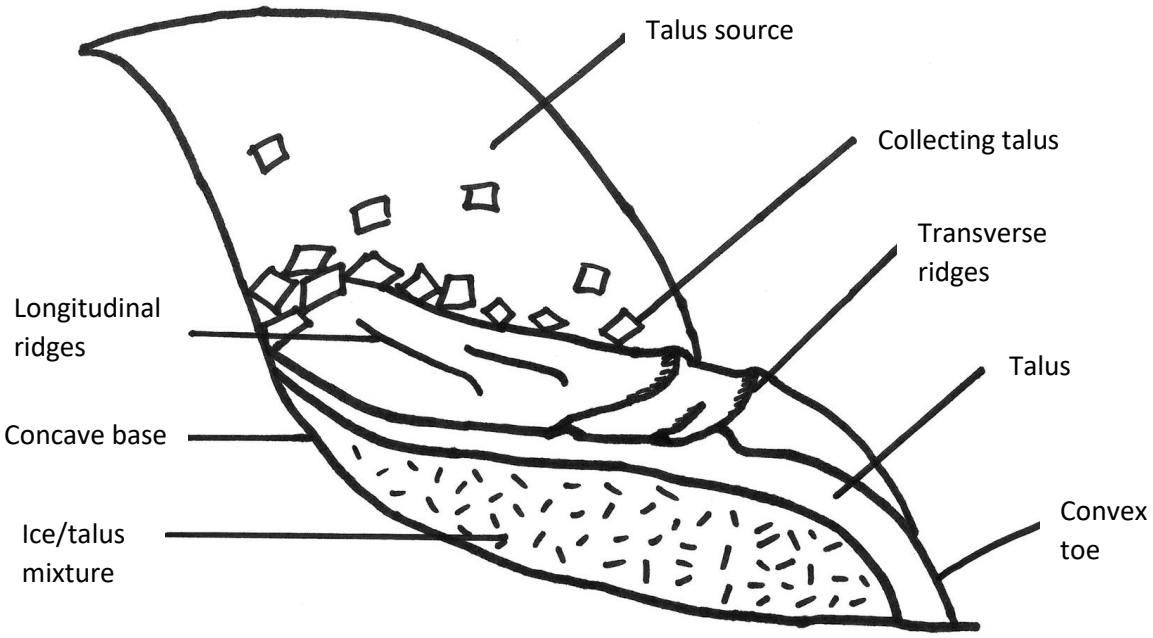

Figure 1.3: This is a basic diagram of a rock glacier, displaying both the morphological features on the surface of the rock glacier, as well as the cross-sectional composition and distribution of various layers.

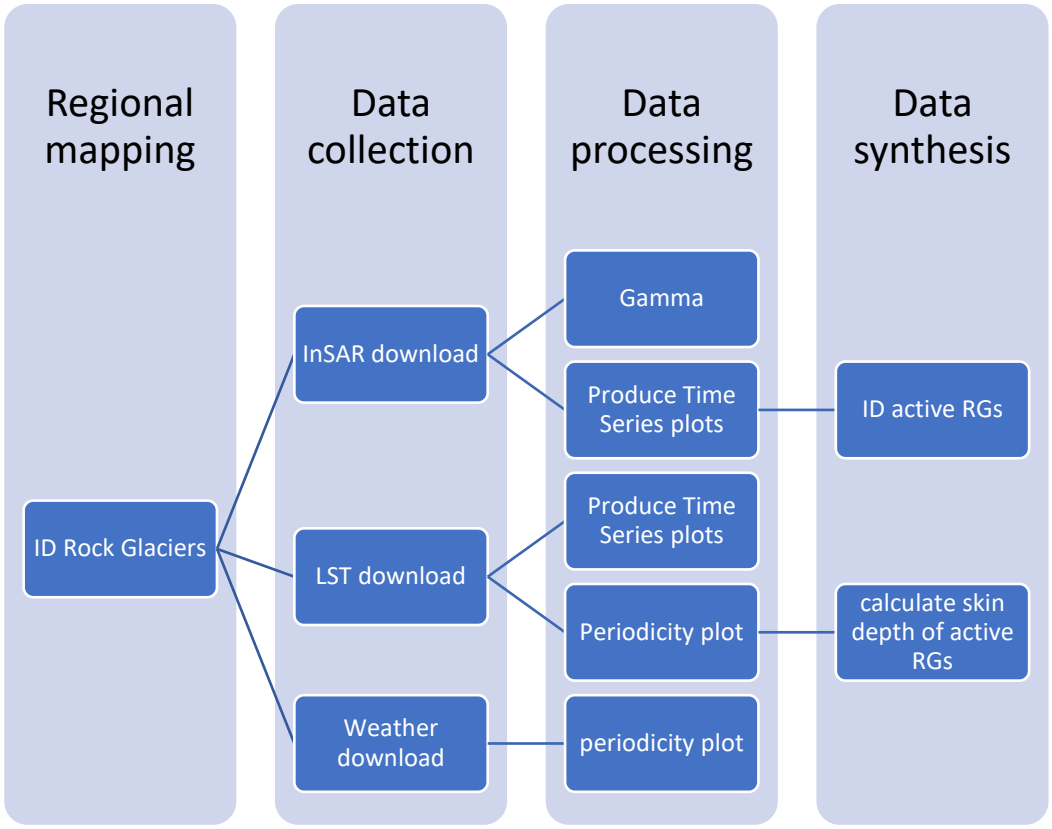

Figure 1.4: This flowchart represents the general plan of approach for the study. The final data outcomes are identifying the active rock glaciers in the region and finding the depth to the ice for all of them.

Chapter 2: Geologic Background

In the century since they were first identified, the literature surrounding rock glaciers has provided dozens of vocabulary words to label and describe them. For the purposes of this study, a rock glacier is a landform composed of rock debris and ice that is capable of flowing down a slope (Jorgensen, 2007). The debris, also known as talus or scree, is a collection of poorly sorted angular boulders, with little to no fine-grained sediment, (Jorgensen, 2007; Marker, 1990). The ice is found within the body of the rock glacier, whether in the form of a missive ice core, or interstitial, pore filling ice (Giardino and Vitek, 1988). Morphologically, all rock glaciers, regardless of classification have a concave upper portion and convex toe as a result of flow (Giardino and Vitek, 1988). They all have ridges and furrows on the surface, as well, due to their downward motion (Jorgensen, 2007; Giardino and Vitek, 1988; Martin and Whalley, 1987) (Figure 2.1). Though they vary in size, shape, location, origin, ice content and distribution, and composition, all rock glaciers form in mountain environments with a history of ice formation and little to no vegetation (Giardino and Vitek, 1988; Jorgensen, 2007).

ROCK GLACIERS IN THE ENVIRONMENT

Rock glaciers play an important role in the environments in which they form. They are indicators of permafrost and transport mass down mountain slopes (Giardino and Vitek, 1988). In alpine environments, they act as water sources and can feed ground water reserves from the melt and runoff of their interstitial ice (Liu et al., 2013). Because rock glaciers form at high elevations with low levels of precipitation, rock glaciers are important in that they store snow and ice in the winter and produce meltwater in the

summer. This cycle provides water seasonally and over longer periods of time (Brenning et al., 2007). Rock glaciers are more common than glaciers and form at lower elevations due to the insulating properties of the talus accumulation (Morris, 1981), making them a more widespread source of water than ice glaciers.

Rock glaciers form where and when the combination of several conditions is ideal. The controls on rock glacier formation are thermal conditions, including climate and heating from incoming solar radiation, talus production, and history of glaciation (Brenning et al., 2007). The more favorable the combination of these conditions, the higher the likelihood of rock glacier formation and the larger the rock glacier can grow (Morris, 1981). High rates of talus production are favorable and consistently colder climates allow for higher production of ice and longer retention of that ice. It is necessary for talus to be produced in order to insulate the ice and maintain freezing ground temperatures, which is required for the rock glacier to exist for any period of time (Jorgensen, 2007).

Rock glaciers have specific thermal requirements for formation. Formation of interstitial ice can result from periglacial activity, especially when the ground is uninsulated by snow. Access to cold air temperatures initiates freezing in the ground. There must, however, be a source of ground water, which at high elevations can originate from snow melt. This subsequently percolates into the ground and freezes (Marker, 1990). The climate needs to be cold enough overall to allow for freezing and thawing seasonally, which drives frost wedging to accumulate talus (Martin and Whalley, 1987).

The location, including elevation, slope, and aspect, of the rock glacier on the mountain also plays an important role in weather conditions because of the amount of

incoming solar radiation. The amount of solar radiation affects the ground temperature and ice production (Janke, 2007). Higher elevations have colder temperatures on average. Northern slopes have lower levels of incoming solar radiation and, maintain lower temperatures and more ice (Janke, 2007). Each factor has differing relative significance depending on regional climate (Morris, 1981). In very cold climates, the elevation and aspect play less of a role because there are more locations in which rock glaciers can form overall. In warmer climates, the elevation and aspect play a larger role because they have more control over the local temperature. Topography also provides a source of talus and location for the talus to accumulate, both of which are necessary for rock glacier production (Morris, 1981). There is no direct correlation between rock glacier size and elevation because, even at high elevation where there are cold temperatures, there are other factors which determine the size and location of rock glaciers. For example, if the climate is very cold and at a high elevation on a mountain, a rock glacier may not form if there is no source of talus (Morris, 1981).

Different environmental conditions may produce rock glaciers with different appearances (Marker, 1990). For example, rock glaciers that form in valley floors or cirque valleys have different characteristics than rock glaciers that form on the side of valleys and flow down their walls. They will have different length to width ratios, the ridges and furrows may trend in different directions.

Rock glacier formation is favored where there is a large collection of talus (Brenning et al., 2007), which keeps the ice from being exposed to direct sunlight and daily temperature fluctuations. Talus accumulation and rock glacier formation is greatest on a concave land surface (Brenning et al., 2007). Upper portions of the curve are steeper

and create an unstable rock face that can produce talus which then falls downslope and accumulates where the curve flattens out. This topography also has controls on the velocity of the rock glacier, slowing its movement as it moves downslope to the less steep area of the curved surface (Brenning et al., 2007).

Other topographic controls on rock glacier formation, especially in cirques, include valley wall height. This controls the amount of shading on the valley and the amount of talus available. The roughness and lithological composition of the cirque wall will factor into how easily it breaks apart to form talus (Brenning et al., 2007).

One final controlling factor in the formation and location of rock glaciers is the presence of vegetation. Rock glaciers form at high elevations, often above the tree line (Brenning et al., 2007). Tree roots hold loose talus together, making the slope too stable to flow. The roots are also able to keep the groundwater warmer, preventing freezing and ice accumulation (Marker, 1990). Dry, arid, mountain climates often do not have enough water to support trees or other vegetation, so ground freezing and ice production are more prevalent (Marker, 1990). Some rock glaciers are currently found below the tree line, and therefore provide evidence on the history of the rock glacier. At one point it must have formed above the tree line, flowing downslope over time to below the tree line with all the ice melting out in the process, or the climate may have historically been colder, with a lower tree line (Marker, 1990). The environmental conditions needed for rock glacier formation are very specific and the presence of rock glaciers can give insight into the climate at the time of the rock glacier's formation.

CLASSIFICATION OF ROCK GLACIERS

Since rock glaciers were first identified and described in the early twentieth century, several ways of classifying them have emerged along with much confusion regarding the terms used to do so (Jorgensen, 2007). There are four main classification systems for rock glaciers: genetic, geometric, topographic, and activity (Giardino and Vitek, 1988). The genetic classification deals with the origin and formation of rock glaciers. Some rock glaciers form from ice glaciers (ice cored, azonal, or glacially derived), whereas others develop from periglacial processes with no history of glaciation (ice cemented, zonal, or talus derived). Geometric classification is based on the shape of rock glaciers, whether they are longer they are wide (tongue shaped) or vice versa (lobe shaped) (Giardino and Vitek, 1988). Topographic or distribution-based classification deals with the landforms upon which the rock glaciers form. Some rock glaciers fill valleys, while some form down valley walls (Martin and Whalley, 1987). The final means of classifying rock glaciers is based on their activity, which directly relates to ice content. Rock glaciers are separated into active, inactive, and fossil categories based on the amount of ice contained within them and the downslope flow that results from interstitial ice (Giardino and Vitek, 1988). The activity classification is what will be used for the purposes of this study, though, in subsequent sections, the other methods of classification will also be described.

GENETIC CLASSIFICATION

The genetic classification of rock glaciers is based upon the mechanism of formation through which a rock glacier formed. There are three main classifications based on theories of formation. The first theory is the rockslide model, which states that a

rock glacier is formed by one mass wasting event depositing the rock material. This theory does describe ice within the rock glacier accounting for small amounts of creep subsequent to rock glacier formation (Martin and Whalley, 1992). The rockslide theory exemplifies the idea that a rock glacier may exhibit the same morphological characteristics but have formed in a variety of different circumstances. Different mechanisms or conditions of formation may yield a similar resulting rock glacier (Martin and Whalley, 1992).

The glacially derived theory explains that a rock glacier may form when debris accumulates on top of an active ice glacier. The debris acts as an insulator for the ice and may preserve the glacier outside the boundaries when an exposed ice glacier would retreat (Whalley, 2016). The massive ice core in the middle of a glacially derived rock glacier provides a site for deformation and the talus surface would increase the pressure of underlying ice, causing flow (Whalley, 2016). Massive ice has been observed in many rock glaciers and can extend down the length of rock glaciers (Martin and Whalley, 1992). The flow of a rock glacier that is glacially derived should follow the same principles as the flow of an ice glacier because the massive ice is the portion that is flowing (Martin and Whalley, 1992).

Some rock glaciers form in locations without any history of glaciation, so the permafrost model may be used to explain their formation (Giardino and Vitek, 1988). The permafrost model is also called the talus derived theory explains rock glacier formation as a result of periglacial processes (Whalley, 2016). The processes of seasonal freezing and thawing enables the accumulation of ice between the pores of a collection of talus. Ice lenses and interstitial pore ice act as the source of flow in the rock glacier and

flow only occurs when the rock glacier pores are completely filled or interconnected with ice (Whalley, 2016). The ice remains the portion of the rock glacier that is able to move and deform plastically, so the interconnected pores prevent pieces of talus from producing friction on each other which would impede gravitational flow forces (Whalley, 2016).

There have been observations of both massive and interstitial ice in rock glaciers (Benedict, 1986). In these cases, it seems likely that, interstitial ice must have formed at either the same time or after the massive ice core, indicating permafrost processes took place after the formation of a glacially derived rock glacier, and that periglacial climate conditions followed glacial ones (Martin and Whalley, 1992). A mixture of the two formation methods is the most likely answer to theories of rock glacier formation (Martin and Whalley, 1992). Figure 2.2 illustrates the different ice/talus distributions in rock glaciers based on their genetic classification.

MORPHOLOGICAL CLASSIFICATION

One uniting characteristic of rock glaciers is the presence of flow features such as ridges or furrows on their surface (Jorgensen, 2007; Giardino and Vitek, 1988; Martin and Whalley, 1987; Martin and Whalley, 1992). They can be either transverse (perpendicular to the direction of flow) or longitudinal (parallel to the direction of flow) (Martin and Whalley, 1992). The ridges and furrows are products of plastic flow, making them similar to the ridges and furrows on lava flows. The ridges and furrows are present on rock glaciers from every morphological category, of which there are three.

The first category is tongue shaped (Figure 2.3). These fill valley floors and are longer than they are wide (Martin and Whalley, 1987). Because they form in cirque valleys, they are more likely to form in areas with a history of glaciation and be glacial in origin (Janke, 2007). The direction of flow is parallel to the axis of the valley, allowing them to fill long valleys and giving them their distinctive shape (Liu et al., 2013). Tongue shaped rock glaciers have more visible transverse ridges that cross perpendicularly to the toe of the rock glacier (Janke, 2007).

Lobate rock glaciers are wider than they are long, having distinctive dimensions from tongue shaped rock glaciers (Martin and Whalley, 1987). They are more wedge shaped (Liu et al., 2013). They are more likely to be periglacial in origin (Janke, 2007) because they originate at the base of talus slopes (Martin and Whalley, 1987), not necessarily in a location with glacial history. Valley wall rock glaciers flow perpendicular to the direction of the valley, moving down the valley wall (Liu et al., 2013). Longitudinal ridges are more likely to be found on lobate rock glaciers than tongue shaped rock glaciers (Janke, 2007). Lobate forms cover larger areas than tongue shaped and are more common (Janke, 2007).

A third morphology that can be found among rock glaciers is the spatulate shape. They are a combination of the other two forms forming originally in a hanging valley with the characteristics of a tongue shaped rock glacier, then moving downward and widening as it expands on a valley wall like a lobate rock glacier (Martin and Whalley, 1987).

ACTIVITY CLASSIFICATION

The final method that will be discussed in detail is the one used for the remainder of this study when attempting to classify rock glaciers. There are three categories when determining the activity of rock glaciers: active, inactive, and fossil or relict. The foundation of classifying the activity of rock glaciers is based on the presence and movement of the ice inside the rock glacier.

A fossil or relict rock glacier has no ice inside it. It, therefore, would have no movement (Janke, 2007). Because a fossil rock glacier has no ice to maintain, they are found in the widest variety of different locations and climates, including lower elevations and more slope aspects (Janke, 2007), representing a past periglacial environment.

An inactive rock glacier no longer moves, though it may retain some interstitial ice, just not enough for flow (Janke, 2007). As a result, the surface topography of an inactive rock glacier can be more subdued than one actively deforming (Janke, 2007). Inactive rock glaciers are found at lower elevations than active rock glaciers because they do not have to maintain as much interstitial ice, as some has melted out (Brenning et al., 2007). Inactive rock glaciers represent a waning periglacial environment. The distribution of inactive and other types of rock glaciers do overlap since elevation is not the only variable that controls rock glacier formation (Janke, 2007). One method used to determine whether a rock glacier is classified as inactive or fossil is the presence of vegetation. Inactive rock glaciers have less vegetation cover than fossil because they have been stationary for a shorter period of time (Janke, 2007).

Active rock glaciers have enough internal ice to allow for deformation and flow. This gives the ridges and furrows on their surface a pronounced appearance and a very steep slope at their toe (Janke, 2007). They move down slope as a result of gravitationally driven flow (Martin and Whalley, 1987). Active rock glaciers form in only the most ideal conditions for rock glacier existence (high elevation, slope facing the poles, cold climate, etc. (Morris, 1981, Janke, 2007). They are not found extending to such low altitudes as the other types of rock glacier (Brenning et al., 2007). Because of the dependence on very specific regional climate conditions, active rock glaciers tend to be found in close proximity to other active rock glaciers (Liu et al., 2013). The deformation of the internal ice is what sets apart active rock glaciers, which will be covered in a subsequent section. Despite the seasonal variation of flow rates throughout the year, a rock glacier that actively flows is always classified as active (Liu et al., 2013). Active rock glaciers move at a slower pace than ice glaciers, generally at a rate of less than 1 meter per year (Whalley, 2016).

KINEMATICS AND MECHANICS

Rock glacier deformation is a process that evolves during the life cycle of a rock glacier. Over the millennial scale, rock glaciers form, flow downward, and become inactive or fossil. Over a period of hundreds of years, the climate or supply of talus can change, and the rock glacier may develop different characteristics as a result. Over decades the rock glacier can change velocity and seasonal variations occur within a year (Kaab et al., 2007). In general rock glaciers move downslope as a single body as a result of climate conditions, topography, and structure. The higher the temperature, as long as internal ice is maintained, the higher the flow rate (Liu et al., 2013).

There are believed to be two mechanisms driving rock glacier movement. The first mechanism involves the creep of internal ice. The ice may either be massive or interstitial depending on the genetic category the rock glacier falls into. The ice deforms plastically as a function of the temperature, overlying pressure, slope, and rock component characteristics (Jorgensen, 2007). The other mechanism is basal shearing. This occurs as a result of hydrostatic pressure causing melting at the base of the ice within the rock glacier. The water it produces causes decreased friction at the base and results in flow of the entire rock glacier (Jorgensen, 2007). The amount of movement that comes from basal sliding as opposed to plastic internal deformation is unknown (Martin and Whalley, 1992).

The deformation of internal ice has both random and synchronous characteristics. The rock glacier moves as a whole plastically, but the fact that the ice within the rock glacier is discontinuous and there are impurities causes folding and faulting internally, producing the furrows on the surface (Jorgensen, 2007).

Deformation is not equally distributed throughout the rock glacier. Strain is greatest at the top of the ice layer (Kaab et al., 2007). The solid rock does not deform, only the ice, so the most plastic movement would occur at the top of the ice where the displacement accumulates (Kaab et al., 2007). The different velocity in different parts of the rock glacier cause the formation of furrows (Jorgensen, 2007).

The ice within a rock glacier may not be homogeneous. Irregular topography and talus distribution cause ice production to be concentrated in some parts of the rock glacier as opposed to others. The ice within the rock glacier may not be homogenous in its internal structure, either. A soft layer in the ice will affect the movement in one of two

ways. It can be the source of movement in the ice because of the weakened structure, or it can absorb stress and dampen the movement of the entire rock glacier. The effect of a soft ice layer would depend on the location within the rock glacier, temperature, and acting force (Kaab et al., 2007).

An ice lens is an area within a rock glacier where ice has coalesced into a massive body, not necessarily at the core. They act as a source of deformation within the rock glacier (Martin and Whalley, 1992). An ice lens would have to be large or widely distributed in order to provide enough strain for the entire rock glacier to move. One small ice lens will not significantly contribute to the flow of a rock glacier. As they flow downslope, ice lenses are stretched and thinned. As they grow thinner, more friction is produced by the talus in contact with them and the deformation they create decreases (Martin and Whalley, 1992).

Because the movement of the ice is thermally dependent, increasing temperatures cause the rock glacier to increase in speed. As speed increases talus is moved away from the source more quickly and more talus will have to be produced to maintain the rock glacier at the top. Warmer temperatures and steeper slopes increase the speed of rock glacier flow and therefore increase the seasonal fluctuation of speed (Kaab et al., 2007). Seasonal temperature variations cause the rate of rock glacier movement to fluctuate by 15%, so higher velocity rock glaciers will have larger differences of rate seasonally (Kaab et al., 2007). The rate of fluctuation can increase over longer time scales of exposure to different conditions as well, because it takes time for the external heat source to diffuse energy to the internal ice (Kaab et al., 2007).

The movement of rock glaciers is similar in nature to the movement of glaciers because only the internal ice is deforming in rock glaciers. Flow rate for the ice in ice glaciers is estimated using Glen's flow law, which can be modified to include the presence of overlying debris (Konrad et al. 1999) resulting in the equation:

$$h=\left(\frac{v(n+1)}{2A(\rho g sin(\theta)^n}+\frac{\rho_d}{\rho_i}d^{n+1}\right)^{\frac{1}{n+1}}-\frac{\rho_d}{\rho_i}d.$$

In this formula h represents the ice thickness, v is the surface velocity, ρ_i represents the density of the ice, ρ_d represents the density of the debris. The thickness of the debris is represented by d, and θ represents surface slope. A and n are temperate ice-flow parameters. The use of the modified Glen's flow law to estimate rock glacier motion does have drawbacks, however. The ice is assumed to be in an uninterrupted layer, but the presence of talus within the solid ice layer or non-interconnected pores would cause aberrations in movement unaccounted for by the equation. It also lacks the contribution to movement by basal shear. There is higher basal shear stress in rock glaciers than in ice glaciers because the overlying rock has a higher density than the ice of a glacier, increasing the pressure. The basal shear stress is also increased based on the topography. Steep slopes increase the basal shear stress. Within the rock glacier, strain occurs only where the pores are interconnected with interstitial ice. The friction between talus fragments prevents flow, so deformation only occurs if the rock components are separated by ice (Martin and Whalley, 1992). The interconnectedness of pores produces hydrostatic forces in all directions and enables movement (Martin and Whalley, 1992).

The presence of liquid water also has a profound effect on the movement of a rock glacier. Movement occurs along the interface between water and ice or rock and the

volume of water affects the amount of movement. The difference in strength between the surface of the rock and the water and ice mixture is the cause of deformation of that interface. Water also produces hydrostatic pressure, with similar effects as those present due to the hydrostatic pressure from ice (Martin and Whalley, 1992).

STUDY AREA

The total extent of the study area spanned from 37 21' to 37 45' degrees latitude and from -104 53' to -105 34' degrees longitude. Other smaller features in the map area are able to support talus debris landforms including two smaller peaks called the Sheep Mountains (Figures 2.4 e and f) just North of Mount Mestas. There is also a ridge called the White Peaks (Figure 2.4 d) in the Southern portion of the study area. Each reaches a high enough elevation to have formed rock glaciers in the past, though not all the rock glaciers may be currently active.

For this study 87 rock glaciers were identified on the slopes of the peaks in the study region. A region was selected as a rock glacier if it was on an elevated peak, mostly free from vegetation, covered in igneous debris (Figure 2.5), and had visible flow features like ridges or furrows. Blanca Peak (Figure 2.4.g). had the most rock glaciers, followed by Mount Mestas (Figure 2.4.a). Some rock glaciers are known to be active, like 011 and 018 on Mount Mestas, which have recorded movement, as stated previously. Rock glacier complexes, like the branching structure of 015 and 016 were counted as separate rock glaciers due to the potential for each branch having a different activity classification. There is a mixture of lobate and tongue shaped morphologies among all the rock glaciers, but the genetic and activity classifications are not known for every rock glacier. While the rock glaciers on Mestas are necessarily periglacial in origin, the rock glaciers on

Blanca Peak and the Spanish Peaks (2.4.b and c) could be glacial, resulting from the glacial history of those two locations.

The primary location chosen for this study is a mountain in Southern Colorado called Mount Mestas. This peak in Huerfano County, Colorado has a relief of 1027m and a total elevation of 3526m. Rock glaciers of varying levels of activity can be found on its flanks in all directions, making it a good candidate to study. The mountain is composed felsite and represents the remains of a tertiary pluton. 44 rock glaciers in total have been identified on its surface, 25 have evidence of movement (Giardino et al., 1984). Because this mountain has no history of glaciation, the rock glaciers are necessarily periglacial in origin (Jorgensen, 2007; Giardino et al., 1984).

The talus source on Mount Mestas is the massive felsite of which it is composed. The weathering that produced the talus has been occurring since the Tertiary period, with the resulting debris taking on a platy form. The debris further downslope has evidence of mass movement, while the upper slopes are steeper with debris present due to frost and gelifluction (Giardino et al., 1984). Rock glacier movement is at the highest velocity in the center of the rock glacier, while it is slower around the periphery.

Previous studies have observed the rock glaciers on Mount Mestas using unconventional means. The rare presence of vegetation on actively flowing rock glaciers allows the movement history of rock glacier number 011(the southeasternmost rock glacier on Mt. Mestas) to be estimated using tree ring analysis (Giardino et al., 1984). Ground penetrating radar was also used on rock glacier number 018 to determine the mechanism of movement based on internal structure (Jorgensen, 2007). The study found continuous bedding layers within the rock glacier, ice one meter below the surface, and a

thrust fault that is not visible form the surface. 018 is also distinct in that it has an excavated toe due to roadwork in 1963, which could potentially contribute to the movement of the rock glacier (Giardino et al., 1984).

Mount Mestas is just one of several structures with rock glaciers upon their slopes. Blanca peak, the Spanish peaks (Figures 2.4 b and c), and several other smaller features with high elevation do facilitate the formation and maintenance of rock glaciers and were included in the portion of this study concerned with the thermal effects of ground ice. Not all of these features are made up of the same material as Mount Mestas and the elevation and attitude of slope face varies.

The Spanish Peaks are two igneous mountains in the western portion of the Park Plateau. They are more resistant to erosion than the surrounding area and therefore have a high relief above the sedimentary rocks of the rest of the plateau, reaching altitudes of nearly 4000m. Radiating out from around the Spanish Peaks are a series of igneous dikes that control drainage in the area (38). West Spanish Peak has morainic evidence supporting several stages Wisconsin Glacial history (39).

Blanca Peak is the largest feature in the study area with a peak reaching an elevation of 4373m (Janke, 2005; National Elevation Dataset, 1978). In the early 20th century, Siebenthal described the topographic and glacial features found on Blanca (Siebenthal, 1907). Siebenthal identified two active glaciers and several examples of "talus glaciers," which he identified as glacially derived due to the presence of morainic trains at their base. The moraines and talus debris forms are composed of granite and quartz conglomerate. Blanca is notable for hosting the Southernmost glaciers in the Rocky Mountains at a latitude of 37 degrees 35'. The features that Siebenthal described

are still visible USGS Aerial Photography of Blanca (Hoffman, 2011), including the north facing glaciers (Figure 2.4 g).

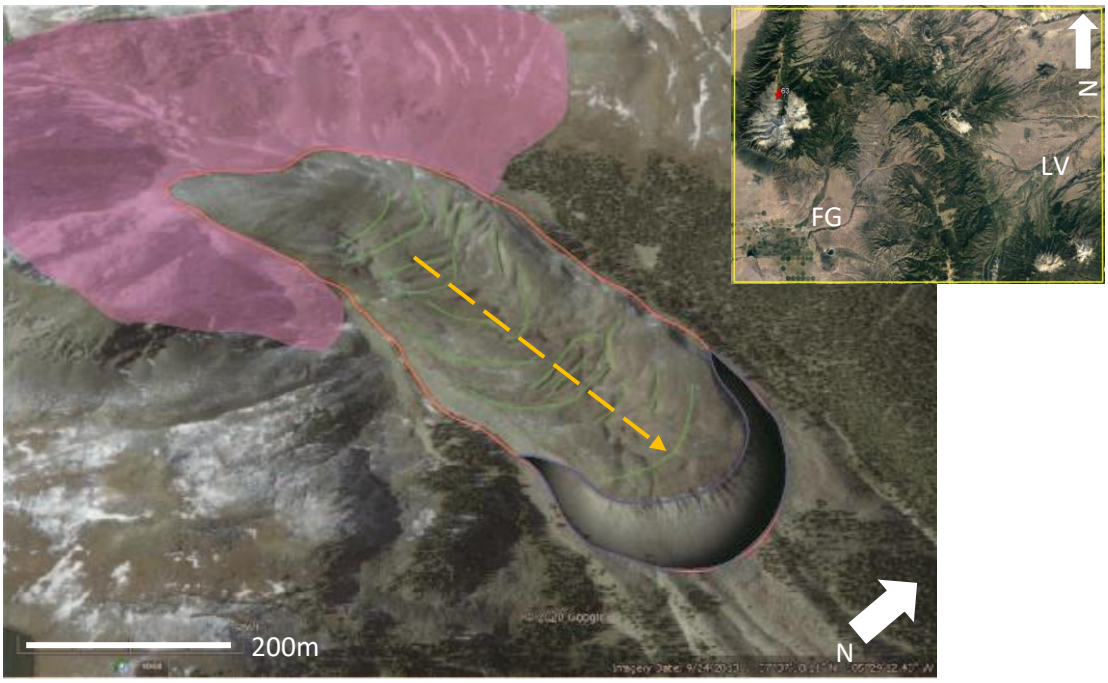

Figure 2.1: Diagram of a rock glacier as compared to a Google Earth Image 063 on Blanca. This rock glacier exemplifies the concave nature of the rock glacier location, the source of talus supply (pink), the ridges on the surface (green), both longitudinal and transverse, and the convex toe of the debris flow (blue with gradient). There is also a lack of vegetation on the surface, typical of rock glaciers. This particular tongue shaped rock glacier measures 300m across and 1100 meters from head to toe and flows downslope toward the East, as indicated by the orange dotted arrow. An overhead closeup of this rock glacier may also be seen in image 2.3.

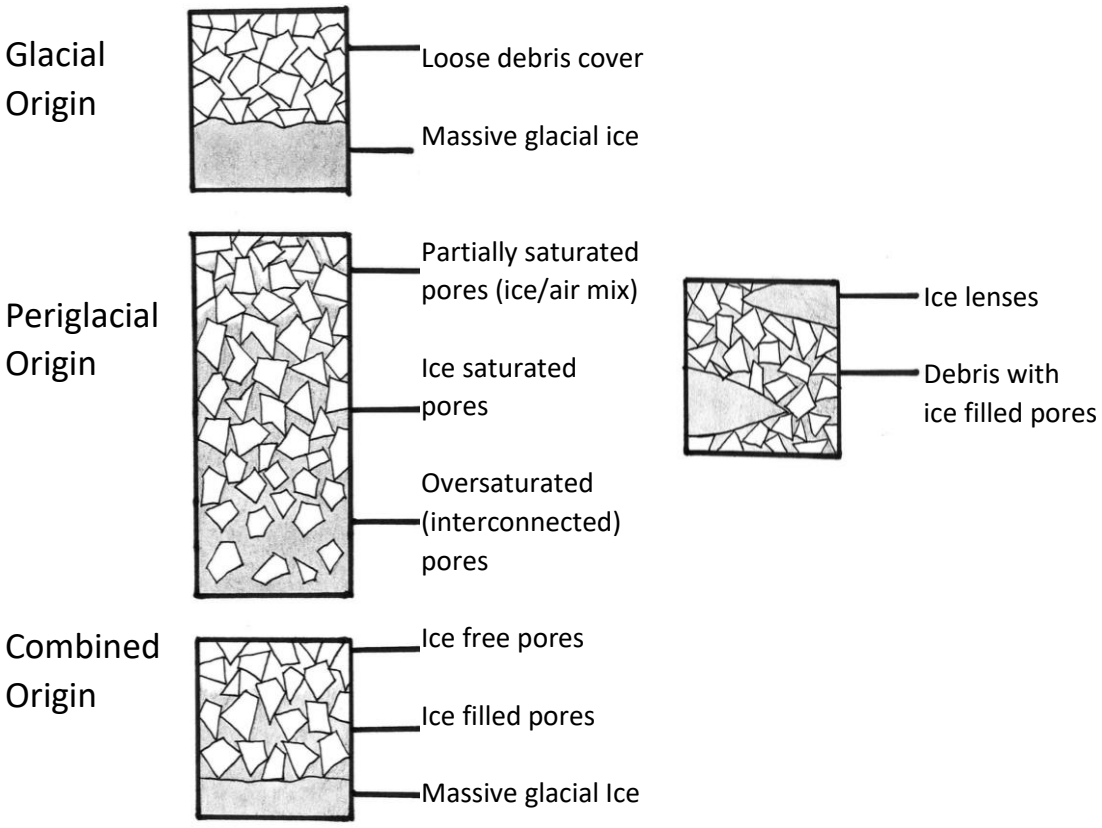

Figure 2.2: These diagrams show the difference between a massive ice core and an interstitial ice system. The interstitial ice fills the pores completely which facilitates flow, especially when the pores are interconnected. The massive ice core is likely a result of glacial formation, however ice lenses can aggregate into regions of massive ice, even in periglacial environments. The combined origin is the result of both glacial and periglacial processes and contains a massive ice core and interstitial ice

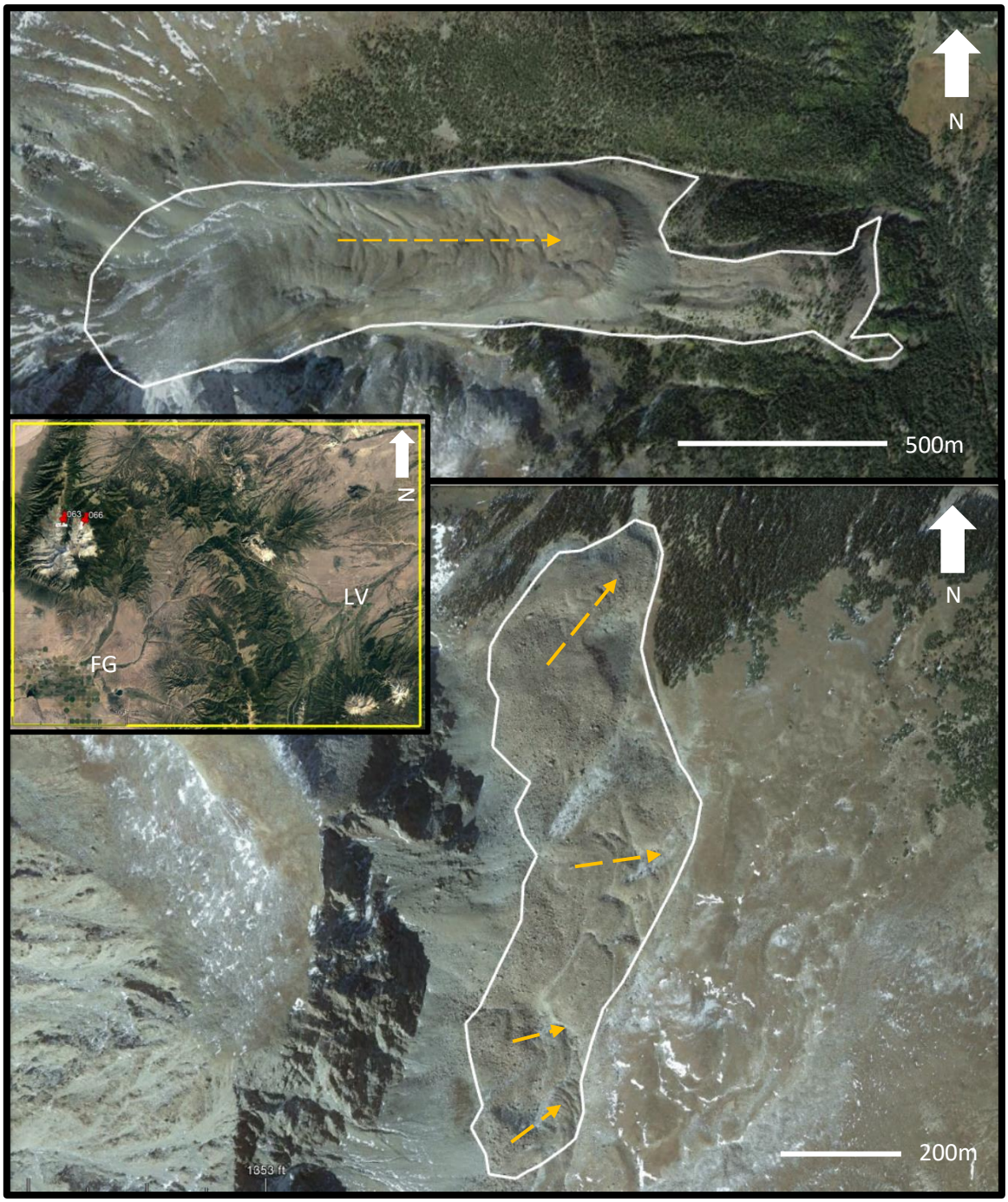

Figure 2.3: These two rock glaciers are both on the Northern side of Blanca Peak flowing eastward. 63 originates at the head of a glacial valley and 66 flows down the side of a valley from a ridge. These exemplify the differences between lobate and tongue shaped rock glaciers, with 66 representing the latter and 63 the former. With almost opposite dimensions, 66 is 300 meters long from head to toe and 1300 meters wide. Both exhibit transverse and longitudinal ridges. Flow direction is indicated by the dashed arrows

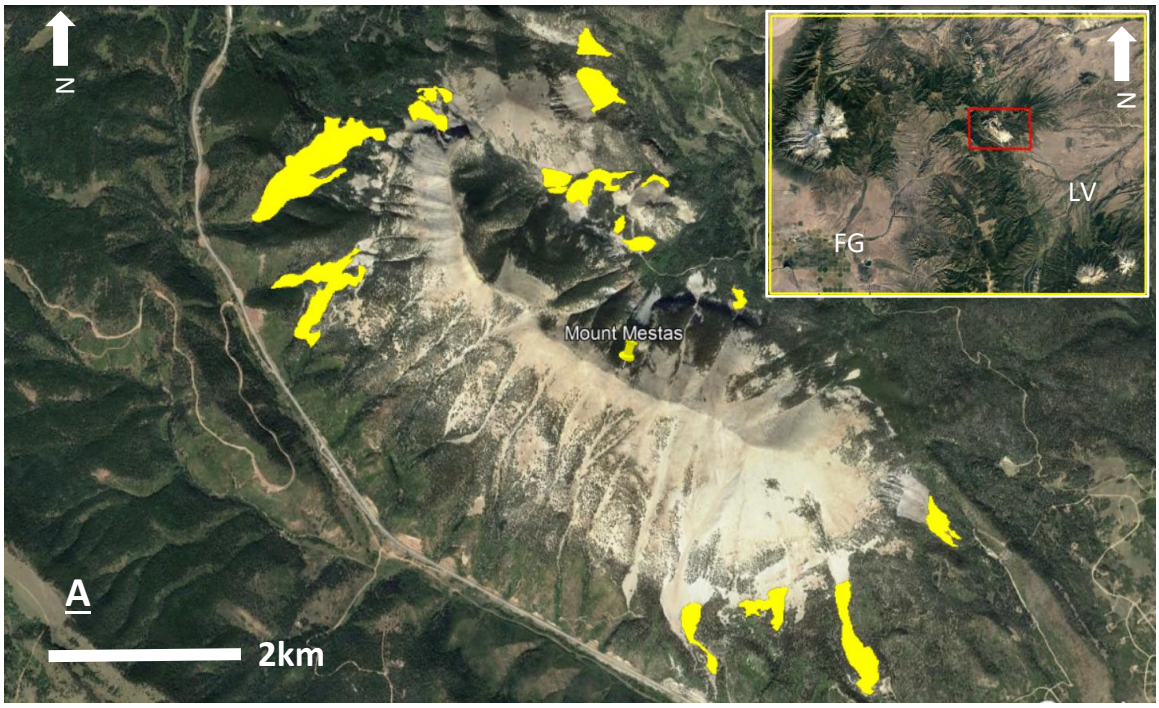
N
Mount Mestas
A
2km
N
LV
FG

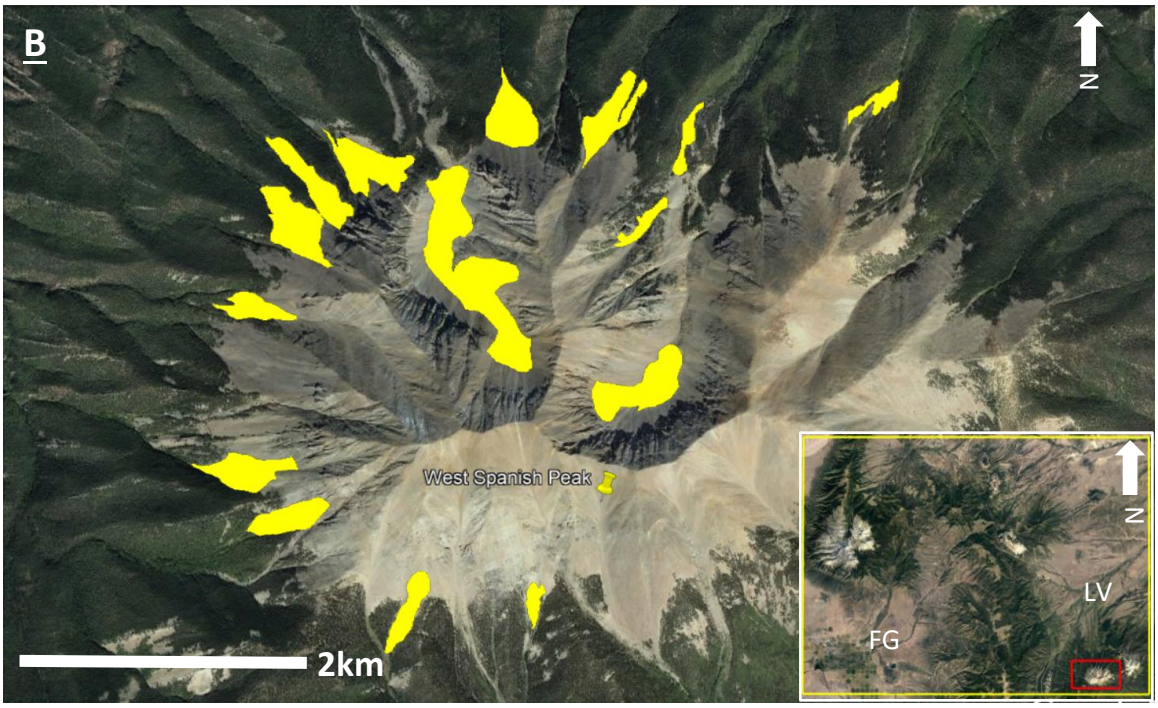
B
N
West Spanish Peak
2km
N
LV
FG

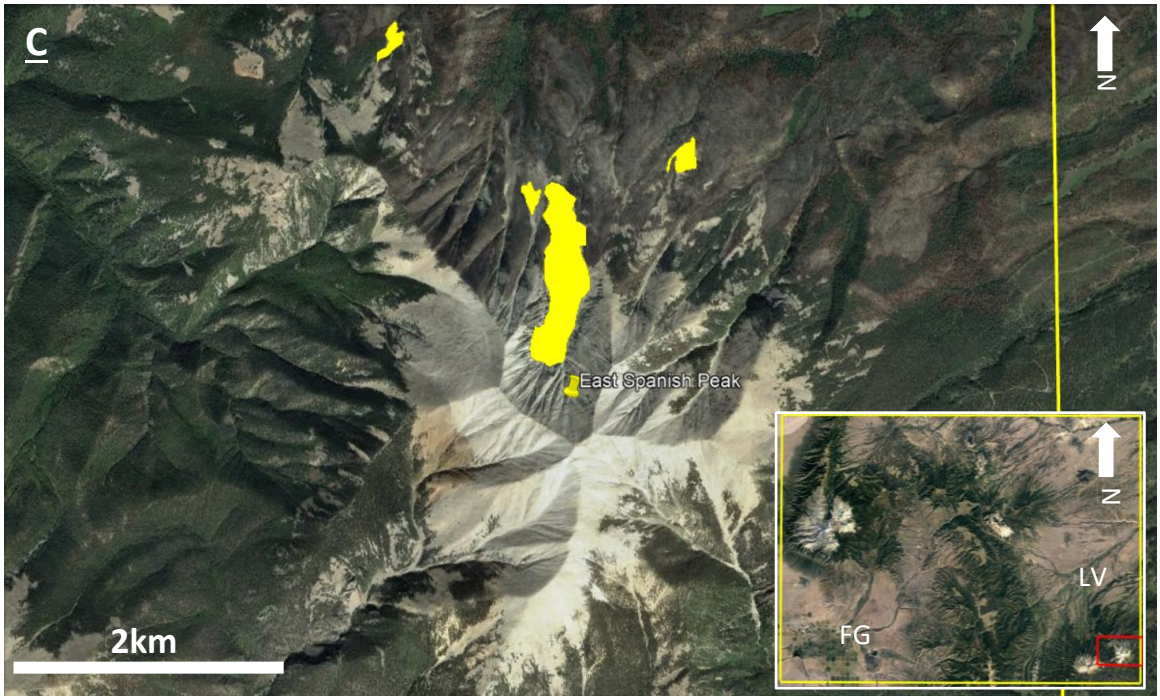
C
N
East Spanish Peak
2km
N
LV
FG

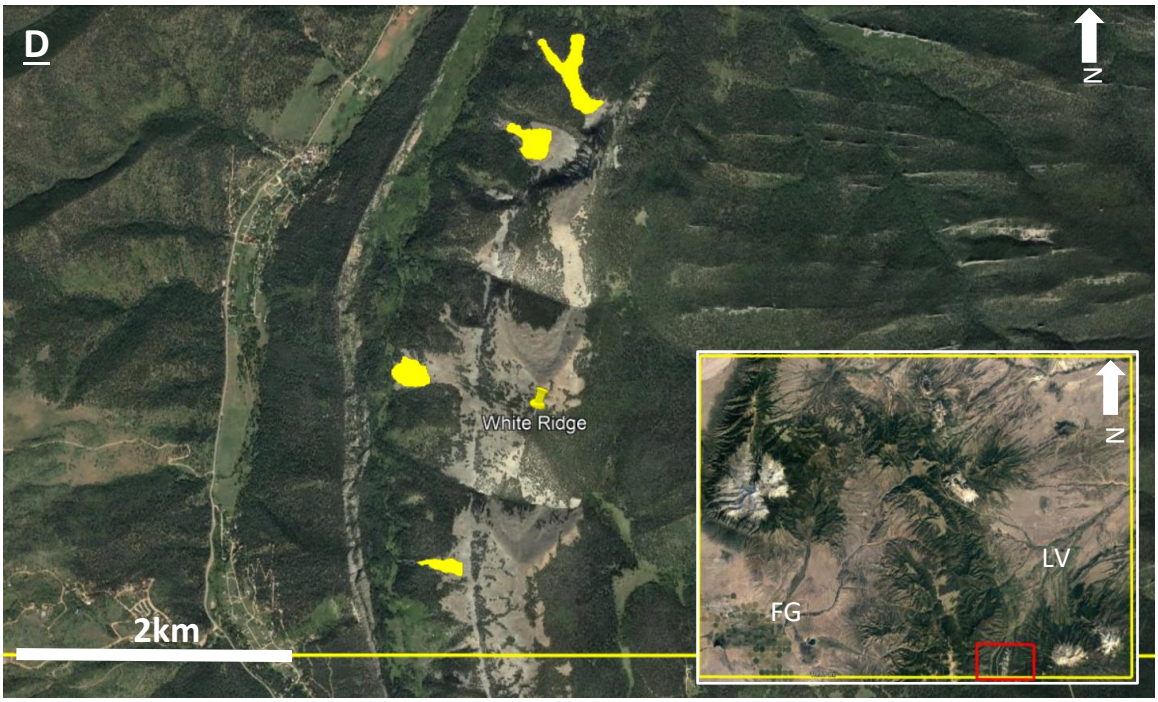
D
N
White Ridge
2km
N
LV
FG

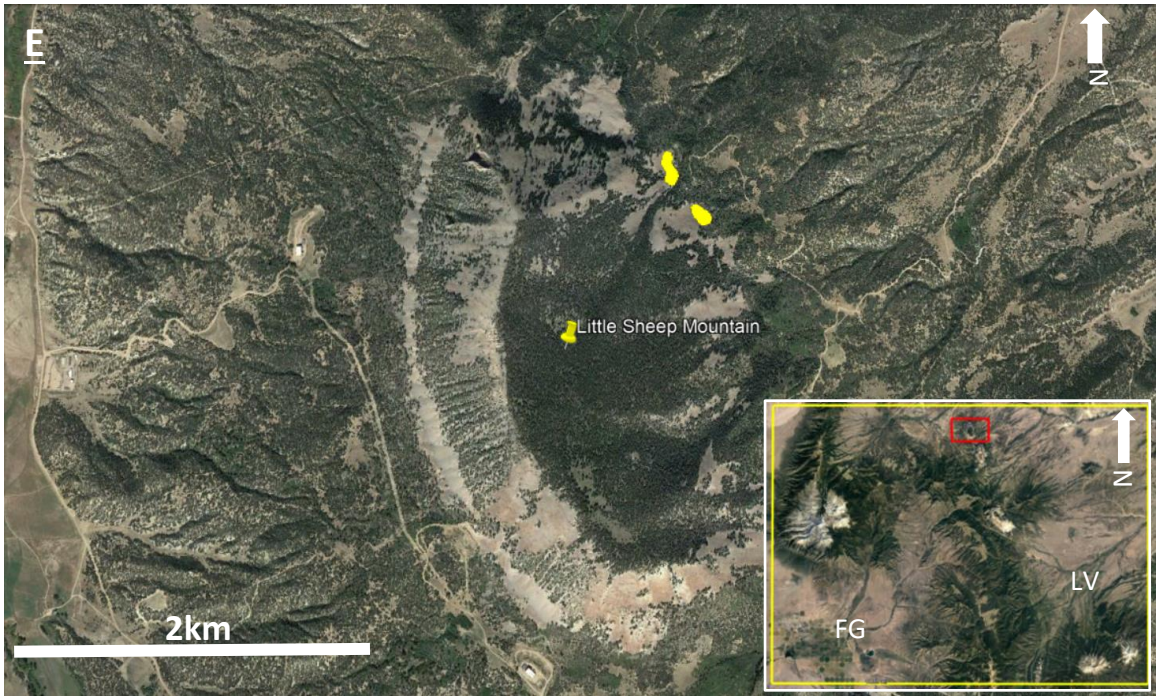
E
N
Little Sheep Mountain
2km
N
LV
FG

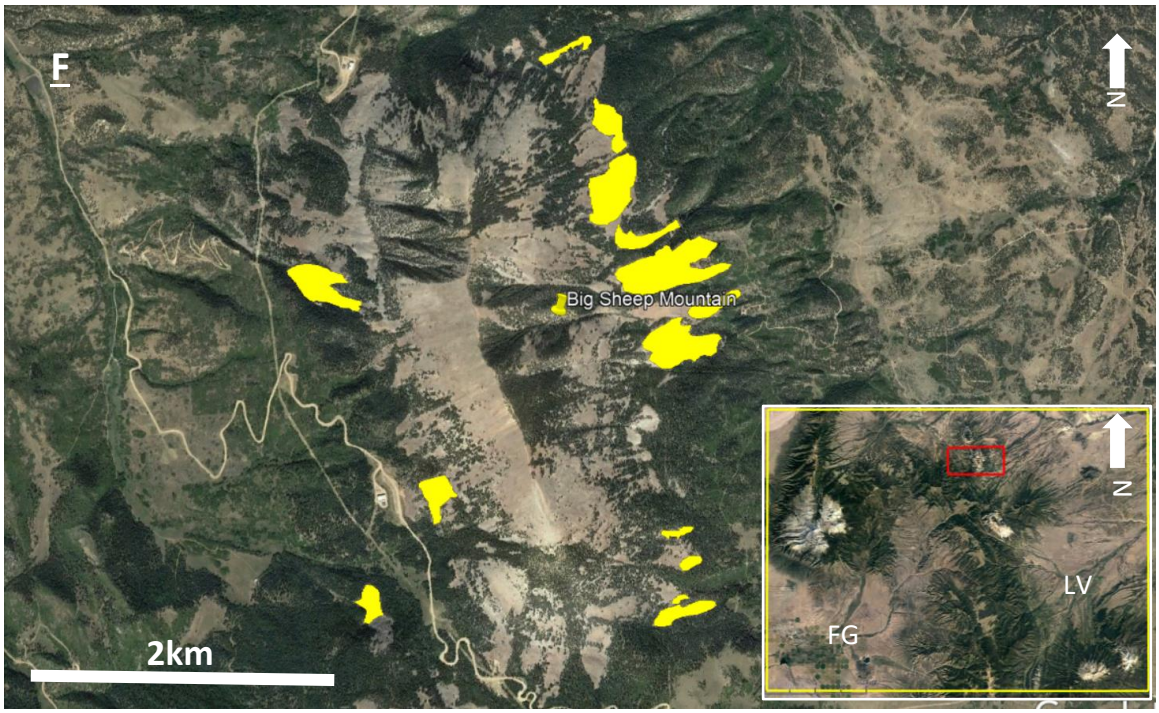
F
N
Big Sheep Mountain
2km
N
LV
FG

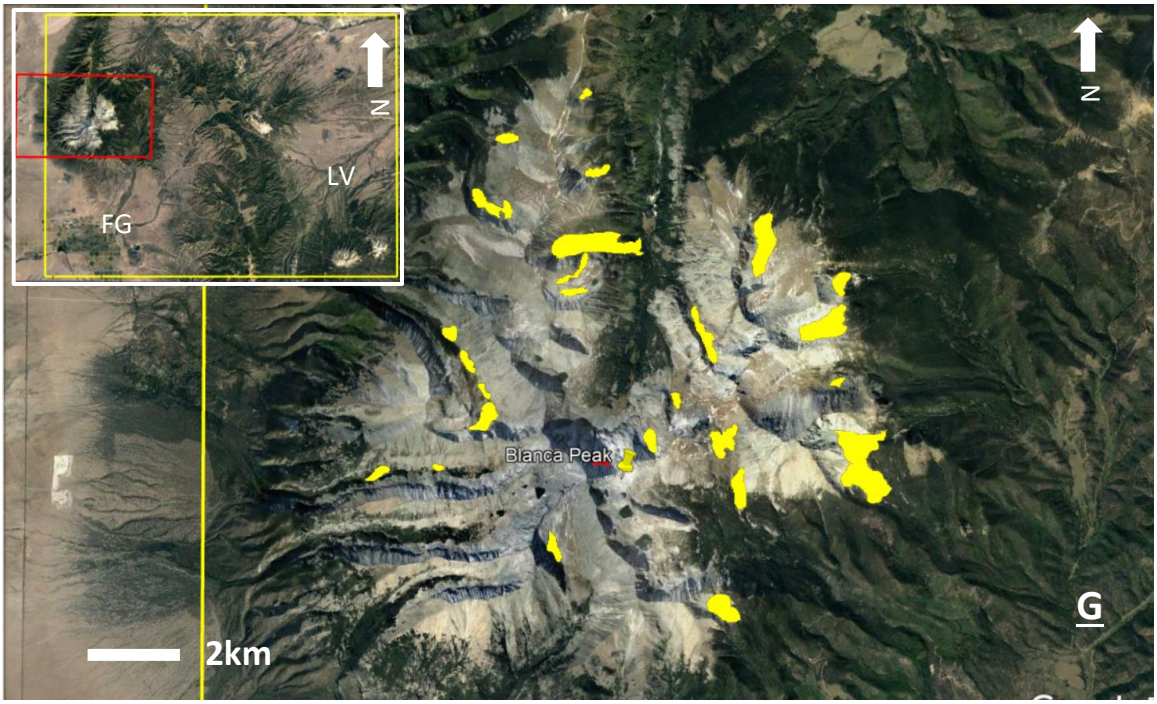

Figure 2.4: Each peak in the study region is shown separately in map view below. Along withs its location within the study region (yellow box). The rock glaciers have been blocked in yellow. The red shape on Blanca Peak (G) represents the remaining ice glacier.

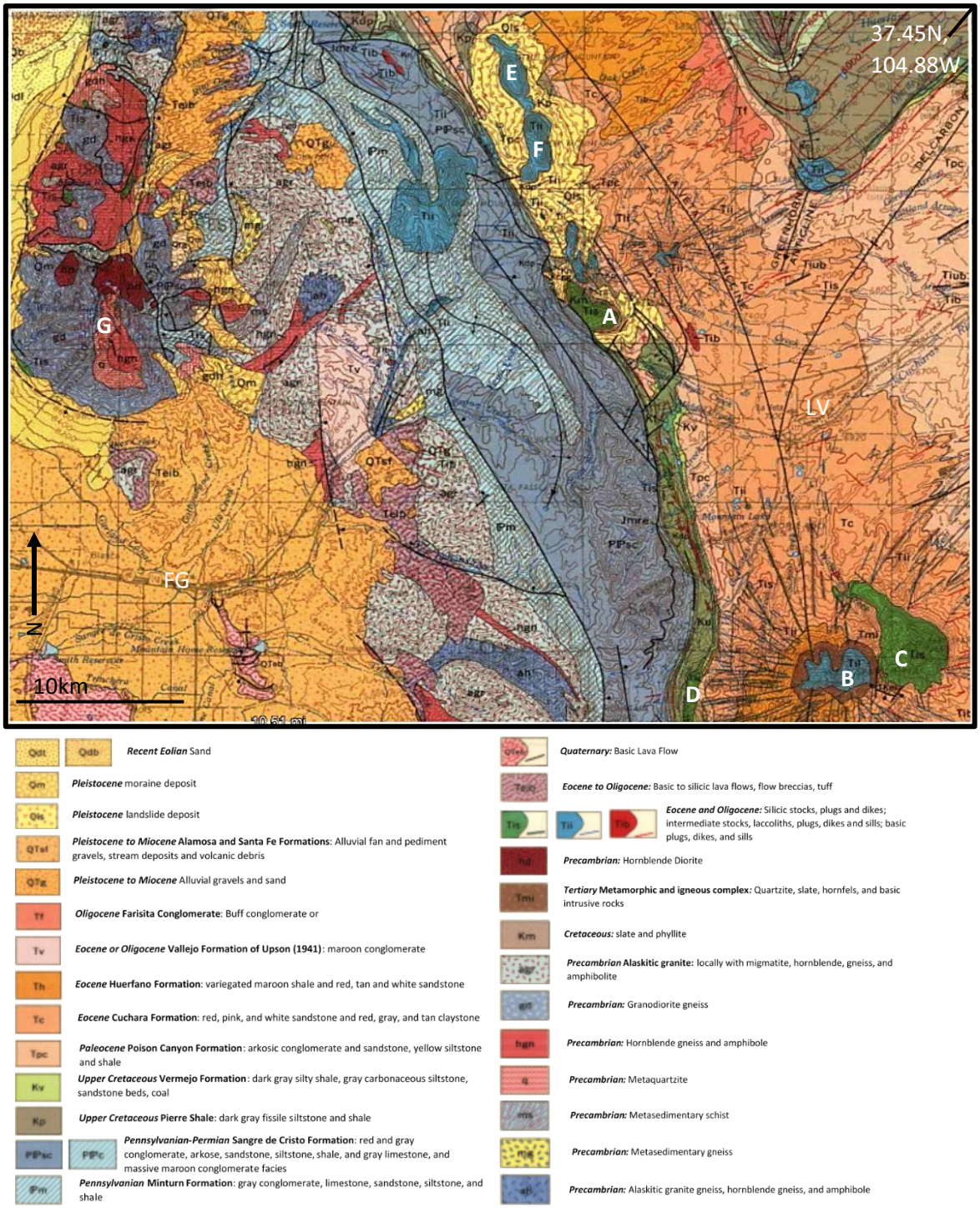

Figure 2.5: This is a portion of the Trinidad Quadrangle Geologic Map South Central Colorado by Ross B Johnson, published in 1969. The map has been cropped to the exact study region as delineated in Figure 1.1. Explanations of each of the rock units may be found on the next page. Of note are the units Tis and Tii which are present on all of the peaks specified in the study (denoted by the letters A-F corresponding to the chart in Figure 2.4) and both represent early Tertiary igneous intrusions. Tis is silicic while Tii is intermediate in composition. LV and FG represent the towns La Veta and Fort Garland.

Chapter 3: Radar Interferometry

BACKGROUND

In this study, radar interferometry is used to determine the movement of rock glaciers over time was radar interferometry, specifically using InSAR (Interferometric Synthetic Aperture Radar) analysis. Radar interferometry is a method of determining deformation or change in the structure of the surface of Earth over time. The concept relies on radar measurements of Earth from orbiting satellites that pass over the same location frequently. Changes in measurements of the line-of-sight distance from the satellite to the surface of Earth and back, based on the change in phase of the signal, indicate a change in the Earth's surface and movement. Figure 3.1 diagrams the basic concept behind Radar Interferometry.

InSAR has been used to measure deformation in many different forms, such as subsidence as a result of drought (e.g. Schmidt and Burgmann, 2003) or uplift and displacement resulting from earthquakes or volcanic activity (e.g. Burgmann et al.,2000, and references therein). InSAR has also been used to study the motion of rock glaciers in the past. Liu et al 2013 observed active rock glaciers in California and their changes in flow rate over time as a result of seasonal temperature change or large-scale climate change.

Some benefits of InSAR include the relatively high spatial resolution (meters to tens of meters) and high precision for displacement measurements. A change in elevation on the scale of millimeters can potentially be measured using InSAR imagery. The temporal resolution is on the scale of weeks which can provide information on the

seasonal changes is rate of deformation (Schmidt and Burgmann, 2003), a cycle that is especially important for temperature dependent interstitial ice in rock glaciers. Not only is the total displacement of the rock glacier able to be determined, but the rate of displacement can be clarified and even the change in rate over time (Schmidt and Burgmann, 2003).

Other benefits of InSAR include its non-reliance on weather. Though severe weather or the presence of clouds can create signatures on interferograms, many of these can be accounted for and removed, unlike in shorter wavelength (visible and near infrared) multispectral imagery (Liu et al., 2013). Like other remote sensing methods, the ability to make measurements in inaccessible areas reduces previous limitations in those regions. The high spatial resolution allows for the study of localized features and very small changes over time which cannot be determined with larger pixel sizes or different methods like pixel tracking (Liu et al., 2013).

The challenges of using InSAR include the time and computer power required to process interferograms (Schmidt and Burgmann, 2003). Furthermore, vegetation (or other changes in the nature of the backscattering surface) can introduce too much noise into interferograms for them to be useful. Fortunately, active rock glaciers have little to no vegetation. Relict rock glaciers, however, will have more vegetation which could provide a signal of movement that does not match the ground motion (Liu et al., 2013). Because imaging radar sensors are side looking and image obliquely to one side of the platform, the interferogram only measures the portion of displacement that is resolved in the line of sight direction. Any motion perpendicular to the look direction of the sensor will not be measured because the distance from the satellite to the ground has not

changed. Furthermore, InSAR phase is measured in wrapped angular units (-pi to pi radians), the integer number of complete cycles must be resolved, or “unwrapped”, independently. Thus, if the ground has shifted by more than one complete wavelength phase between two measurements, the exact amount of deformation is more difficult to determine.

Previous studies have attempted to alleviate some of the complications associated with InSAR by only processing interferograms with short time spans, in which the scene pairs were well correlated and projecting the resulting movement into the downslope direction to determine the speed of the rock glaciers (Liu et al., 2013). Alanyses of surface deformation have typically used Digital Elevation Models to remove the effect of topography on the resulting interferograms (Schmidt and Burgmann, 2003).

METHODOLOGY

The initial step was data selection. For this study, 74 scenes of Sentinel-1 data were used. The data collected represents dates from 2015-2018. TABLE 1 shows the list of InSAR scenes used in this study. Interferometric data processing was accomplished using the Gamma Remote Sensing suite of radar software tools (http://gamma-rs.ch). Figure 3.3 depicts the steps required to compete InSAR processing.Once the data were acquired, they were mosaicked into single images for each acquisition date and co registered to a single, master geometry.

Sentinel-1 data is a joint mission by the European Space Agency (ESA) and the European Commission (EC) as part of the Copernicus program, which combines satellite based and ground based observational services (https://sentinel.esa.int/web/sentinel/user-

guides/sentinel-1-sar). Sentinel- 1 utilizes the C-band (5.6cm wavelength) and can resolve pixels down to at least 5 meters, with the majority of pixels being closer to 3 meters. There are two satellites (1A and 1B) that cover the same orbit and improve the observation repeat time. They have been in orbit since 2014 and 2016 respectively and the mission was initially set to endure for 7 years. The specific Sentinel-1 data product used in this study was the Level-1 data in the form of Single Look Complex (SLC) with the complex data appearing in the range look direction. At each pixel, the complex data value takes the Cartesian form of z=x+iy or in the angular form $z = Ae^{i\omega t}$ where $A = \sqrt{x^2 + y^2}$ and ω is the arctangent of x and y in four quadrants. The angular form of the complex value contains information on the phase and amplitude of the radar.

One particularly important step in creating accurate InSAR results is geocoding the scenes (Figure 3.4) to a defined Digital Elevation Model (DEM). In this study, a 30 meter pixel DEM from the National Elevation Dataset (https://nationalmap.usgs.gov) was used. Although the DEM is lower resolution than the radar data, it is still sufficient to remove the topographic effects and refine the estimates of satellite baseline (Burgmann, et al., 2000) Geocoding is accomplished by using the DEM to simulate a radar backscatter image (Figure 3.5b) using the radar viewing geometry and orbital information. Cross correlation of simulated and acquired radar images is required to account for slight mis-registrations due to small errors in the orbital data. The geocoded images may all be aligned to each other and to the known elevation data. For the Sentinel-1 image data, separate bursts of collected data must be stitched together using the topographic geocoding corrections (Figure 3.5a).

Once all the SAR scenes are aligned in the same geometry, the next step is to form interferograms by differencing the phase values for co-registered pixels in two radar images. The value of each pixel is a complex number that can be expressed in either Cartesian or angular form. For that reason, the values of two scenes cannot be simply subtracted but a dot product of the value of the master scene and the inverse of the slave scene will produce a value from which the phase difference may be resolved: $z = |z|\exp(i\omega)$. An interferogram would be represented by

$$I = z_1 * z_2' = |z_1||z_2|e^{i(\omega_1 - \omega_2)}$$

where ω represents the phase. If each of the 74 SAR images for this study were paired with all of the others, 2701 interferogram pairs are possible. Many of these, especially those that become decorrelated due to long time spans, are not useful enough to justify the computational cost required for analyzing them. In order to create a balance between data quality and computational cost, two different sets of interferograms were paired. The first used a time difference between scenes of less than 6 months, the second used a time span of approximately one year. This combination of two different time spans was to ensure a high quality of data and coherent images, from the shorter time spans, while also being able to measure potential flow on larger time frames for slow moving rock glaciers. Limiting the time frame of differentiation limits the number of interferograms produced. With the 74 initial Sentinel-1 images, 829 interferograms were produced. 722 resulted from the 6 month time span differentiation, while 107 resulted from the one year differentiation. Processing so many interferograms requires a significant amount of time and computing power, so including interferograms with a time

span of eight or nine months would be too taxing and would not provide the quality of data to make it worth the labor, due to incoherence.

Once the scene pairs have been differenced (Figure 3.6), the next step involves spatially filtering the resulting interferogram to reduce noise and improve coherence. Interferograms are datasets containing complex values of the differential phase information in each pixel of the image. The filtering step removes areas with too much noise or incoherence to produce a recognizable deformation signal. Specifically, this study used a spectral-adaptive filter as described by Werner and Goldstein, 1998. Its job is to determine which portion of the recorded signal is from actual phase change and which is from thermal (Gaussian) noise. By using patches of the interferogram and a filter parameter that may be adjusted manually for stronger or weaker filtering. The filter reduces the standard deviation of the recorded signal in each patch by taking into account all of the pixels in that region. The basic formula is $H(u,v) = |Z(u,v)|^{\alpha}$ with H(u, v) representing the response of the filter of parameter α on the power spectrum (Z) of the patch (u, v). Function is more specifically represented by:

$$Z(u,v) = \exp\left(-\frac{\frac{u^2}{\sigma_u^2} - \frac{2uv}{\sigma_u\sigma_v} + \frac{v^2}{\sigma_v^2}}{2(1-\rho^2)}\right).$$

U and v represent the patch while σ_u and σ_v are the bandwidths of the phase values in the patch. These values are what are affected by α, the filter parameter that limits the phase bandwidth. The variable ρ represents the distance between the sensor and the ground. For very noisy images, larger patches are required. The filter parameter may also change with the fringe gradient. Regions with many fringes need a lower filter parameter so that the actual signal of topography or ground motion is not removed

accidentally. Regions with low gradient fringes can sustain being filtered by a stronger parameter because all of the actual phase difference measurements are in a smaller range. Figure 3.7 shows the effect of filtering. The coherence of each individual interferogram must be accounted for while filtering, because applying too heavy a filter on an interferogram that does not require it will result in over smooth images and a loss of some data. Insufficient filtering of an interferogram, however, will perpetuate a loss of information, such that few conclusions may be drawn from processing all of the interferograms. Filtering is also an important step before unwrapping because there is a lower chance of producing unwrapping errors if there is reduced noise and widespread accurate phase measurements.

Phase unwrapping is the process of resolving the integer ambiguity in the phase measurements. Because the phase values of the SAR data are wrapped, only the fraction of a whole cycle is known from the phase difference calculation. Using the assumption that the phase change from one pixel to the next in coherent regions will be similar and not change by more than half a cycle (pi radians), the phase is extracted from a cyclical data product to a continuous data product (Figure 3.8). Errors in unwrapping can produce sudden jumps in phase when there is none in real life, as shown in Figure 3.9. The change in phase appears abrupt and widespread, indicating that it is not a real deformation signal, but a result of improper unwrapping. Each scene with an error after initially unwrapping, was noted and either fixed or culled. Another source of unwrapping errors in interferograms, that is likely not the cause in the case of this study, is the sudden deformation on the ground that is larger scale than the wavelength of the sensor. Because

the measured phase is wrapped, a change of more than one full cycle will produce values less than the actual scale of the movement because entire cycles are unaccounted for.

Owing to small errors in the satellite orbital data, the original estimate of the baseline will need to be refined to remove topographic phase signature. Baseline refinement is the process of removing topographic effects that result in differences in viewing orientation of the sensor on each pass. Refining the baseline accounts for the location of the satellites and flattens the image by removing topography. Figure 3.10 exemplifies how much of the interferogram is a result of the baseline topography signal.

After each step of the process (filtering, unwrapping, etc.) each interferogram was monitored for quality. Interferograms were culled for extreme noise or incoherence, especially in the area of the rock glaciers. Large, interferogram-wide, unwrapping errors were also noted in order to attempt a correction or cull further through the processing. The reasons for unusable levels of coherence is often due to a poor-quality scene that affects every interferograms in which it was used, or a very long timeframe between the two scenes used in the interferogram. After identifying the interferograms which too incoherent to use, the scenes used in them were cross referenced in order to find the scene responsible for repeating poor quality. Those were removed from being used for differentiation completely. Individual scenes were also marked for culling Throughout the process, over 200 interferograms were removed to preserve data quality and produce a continuous time series of deformation. 606 interferograms remained viable sources of information through to the end and were used to produce the results.

In order to mitigate regional atmospheric signals that affect each scene individually and unevenly, electromagnetic “path delay” data products from GACOS

(Generic Atmospheric Correction Online Service for InSAR; http://ceg-research.ncl.ac.uk/v2/gacos/) were used to adjust the measurements for each scene (Figure 3.12). The GACOS data products were ingested similarly to the InSAR data in that after downloading the data for each InSAR scene used, they were georeferenced, paired into the same pairs used for InSAR, and applied to the corresponding interferogram. GACOS path delay calculations present estimates of how much the signal from the radar interferometer is slowed by proceeding through atmospheric water vapor. GACOS calculations use an ECMWF (European Center for Medium Range Weather Forecast) weather model combined with a Digital Elevation Model to produce the resulting data product. Both the effects of stratification within the atmosphere and long wavelength turbulent atmospheric signals were accounted for in the GACOS atmospheric model, which is finely correlated in space and time to the interferogram that it will be used in conjunction with (Yu, et al., 2018). Some localized signals may not be accounted for in this step of atmospheric removal. For example, there appears to be a signature over Blanca peak in the stack image (Figure 3.14), even after the atmosphere was removed, and the time series (Figure 3.15) did show some long wavelength anomalies which were removed after the GACOS data was used.

Another step before creating a time series, is removal of remaining elevation-dependent phase. Elevation correlated phase is likely the result of changes in atmospheric conditions that are not fully incorporated in the GACOS data which assumes the relationship between temperature and elevation (i.e., the atmospheric “lapse rate”) is constant on a global scale. To remove this phase the elevation and phase were plotted and any linear trends in the scatter plot were eliminated (Figure 3.13). Additionally, long

wavelength quadratic trends were also estimated and removed. Subsequently, small gaps (masked, low coherence pixels) in the interferograms were interpolated (Figure 3.11), so that there are fewer null values. Some individual interferograms with phase offset effects were also identified and manually fixed, as the phase jump was a repeating pattern that was not a measured signal from the ground but was the result of an error at some point in the processing.

Once the processing of each interferogram was finished, the amount of deformation over different time periods could be quantitatively measured. The phase values that have been used up to this point in radians are now converted to measurements of the change in the line-of-sight distance. This conversion depends on the wavelength used by the radar sensor. The equation used to make this conversion is $d = \phi * \frac{\lambda}{4\pi}$ where d is displacement, ϕ is the phase difference in radians, and λ is the wavelength of the sensor (in this case 5.6cm). The reason 4π is used instead of 2π (the usual conversion from radians to liner distance) is the fact that the signal travels from to the sensor to the ground and back. Any displacement would change both the distance from sensor to ground and from ground to sensor. The rock glacier outlines were used to identify where each feature was in the interferogram and provide an area within which to measure offset. Some rock glaciers had movement that was visually apparent on the interferograms without use of any quantitative measurement. 018 had fringes of color denoting change in phase, and therefore a change in position on many interferograms of varying time scales. This is likely due to the historically observed, relatively fast movement of that rock glacier.

One of the results of the processing is a time weighted stack (Figure 3.14) of the interferograms. This displays the total displacement over time as an image showing average rate of change. At each pixel for each interferogram, the total displacement is measured and divided by the time span of that interferogram. The rate is averaged over each of the 606 interferograms and plotted on the stacked image. The STACKING command in Gamma is able to complete this processing and produces an image displaying average rate of displacement, as opposed to the magnitude of displacement shown by a standard interferogram.

The other data product that will be used for results is a time series of displacement over each individual rock glacier (Figure 3.15). The displacement over a rock glacier is determined by comparing the movement to a known stationary point in the image. For this study a location in Walsenberg, a nearby town on a flat portion of the region, was used as a stationary reference. It is important in this step that the rock glaciers do not have points of missing data, hence the vigorous interpolation. Regions of data loss will distort the final time series. The use of a time series will also allow for the interpretation of seasonal change in the flow rate and potential increasing flow due to climate change. The output of the time series processing is a series of 65 images illustrating the changing location of various parts of the region over time. The reason for only 65 images, as opposed to the original 74 InSAR scenes is that 9 had been culled throughout the quality control process due to consistent incoherence. Each time when a Sentinal-1 scene was taken will become a new image in this portion. Looking at the collection of time series images will show the progressive movement of active rock glaciers downslope.

In order to more easily interpret the resulting stack and time series images, they were converted back into map geometry from radar geometry. The resulting deformation signals are, now, no longer in the direction of the sensor. A final high pass filter was run to remove any outlier phase values that were unreasonable to represent deformation. The high pass filter removed a significant portion of the remaining long wavelength phase anomalies due to elevation and atmosphere (Figure 3.15 b). The smaller anomalies over the active rock glaciers were not affected due to their relatively small spatial extent. The stack and time series images were converted into GeoTIFF files in order to be analyzed in Matlab with the 87 delineated rock glacier polygons as described in Chapter 2. The phase values of each pixel within the rock glacier polygons was recorded for each step of the time series

RESULTS

The first result product is the stack image (Figure 3.14a). This shows the average flow rate of each pixel, calculated from each of the 606 interferograms used in the final processing for this study. Looking more closely at specific rock glaciers, the number of fringes relates to the flow rate over the entire period of radar observation. For example, on rock glacier 02 on Mount Mestas, there is one full cycle of color fringes, beginning and ending with light blue (Figure 3.14 b). Rock glacier 18 (also on Mestas) has fewer fringes and they occur in the opposite order. Instead of changing from blue to yellow to pink with increasing phase displacement, the shift is from blue to pink to yellow. This is due to the fact that, since they are on opposite sides of the peak, they are flowing in opposite directions. 02 is flowing toward the sensor and 18 is flowing away from the

sensor, so the relative displacement is opposite. 18 is also experiencing less of a phase shift, because there are fewer fringes.

The time series produced a single image showing the cumulative displacement at each of the 65 remaining time steps of the initial Sentinel-1 data. Only 65 of the 74 remain, as nine were culled. The pixels inside each of the 87 delineated rock glaciers were averaged together and plotted on a timeline to produce a graph of the displacement over time at each individual rock glacier. Rock glaciers that are moving toward the satellite sensor will have a negative linear trend, while rock glaciers moving away from the sensor will have a positive linear trend. Rock glaciers that are moving orthogonal to the sensor will have no positive or negative slope, despite the fact that they may be moving. Examples of rock glaciers with movement and no movement that are flowing toward the sensor, away from the sensor are shown in Figures 3.17-3.20. Those figures also display rock glaciers with varying sensitivity.

Noise is present in the time series plots. The variation in apparent change in direction of motion from time step to time step as well and any large changes in phase value that are only present over a very short time span are considered to be noise. General linear trends and repeating annual variation in the phase is considered to be a signal of real displacement.

There are two peaks on the elevation histogram (Figure 3.16). The rock glaciers on Blanca Peak are over 1000 m higher than the rock glaciers on Mount Mestas. The relationship between elevation and phase displacement cannot be determined due to the effect of azimuth being more prevalent and disrupting the phase shift signal of rock

glaciers at all elevations. There are rock glaciers at a wide range of elevations displaying large phase shifts, including rock glaciers on both Mount Mestas and Blanca.

The azimuth has a strong correlation with the displacement of the rock glacier. In Figure 3.21, the sinusoidal properties of the phase value when plotted against azimuth illustrates the measurement of the rock glaciers in the look direction of the sensor. The phase offset is at the greatest magnitude when parallel to the sensor look direction and decreases to zero at an angle perpendicular to the look direction. In order to determine the efficacy of the sensor at determining phase displacement at any given rock glacier, a sensitivity coefficient is calculated by taking the dot product of the sensor look direction and the flow direction vector of the rock glacier as determined by azimuth and slope. A higher sensitivity value correlates to a greater ability of the sensor to accurately measure the amount of movement of the rock glacier, a lower value indicates that the sensor will be unable to provide an accurate phase displacement value for the specific rock glacier. Figure 5.2 depicts plot of azimuth vs. sensitivity for all 87 rock glaciers.

The number of pixels has no observed correlation with the amount of flow observed at the rock glacier, with smaller rock glaciers experiencing less flow. Both small and large rock glaciers are recorded experiencing large displacements. There are also cases in large and small rock glaciers with low displacements, but the direction of the rock glacier also influences the amount of flow observed.

The rock glacier that is recorded to be moving the fastest is 04 on the slopes of Mt. Mestas. Its average phase displacement is 3.34 radians/year away from the sensor, which equates to 1.49 cm per year linearly in the direction of the sensor. There may be another rock glacier that moves at an azimuth orthogonal to the line of sight direction that

is experiencing more displacement, which is not recorded because it is not in the line of sight direction. For example, rock glacier 81 on Blanca is flowing downhill at an azimuth of 189, nearly due south, and perpendicular to the line of sight direction of the radar sensor. However, it has a displacement of 1.06 radians/year over the three years of observation, equating to a displacement of 0.47cm away from the sensor. Because of the azimuth, the actual displacement is likely much higher than what was recorded.

Based on the flow rate and sensitivity factors, all of the rock glaciers were categorized into three categories: active, inactive, uncertain. Table 2 lists each rock glacier with its sensitivity, average flow rate, and activity classification. Active rock glaciers are those with a flow rate of over 0.2 radians per year. Even with a low sensitivity, a measured displacement indicates that there is movement, the inability of the sensor to accurately quantify displacement on the rock glacier just means that the actual amount of displacement is unknown. There are 54 rock glaciers in the active category. An inactive rock glacier is one with a sensitivity factor over 0.2 and a flow rate less than 0.2 radians per year. The flow rate must be low enough that, accounting for noise, there is no significant measurable movement. The sensor must also have a level of certainty to determine that were there any movement, it could be measured. There are 20 rock glaciers that fall into the inactive category. The final category uncertain. These are rock glaciers with a flow rate less than 0.2 and a sensitivity less than 0.2. These are rock glaciers that cannot be sensed will enough to say whether or not there is displacement and there is not enough displacement to overcome the limitation of the sensor orientation. It is unknown whether they are flowing or not, so they are separated from both certain

categories. The uncertain category likely contains both active and inactive rock glaciers but cannot be resolved. There are 13 rock glaciers in this category.

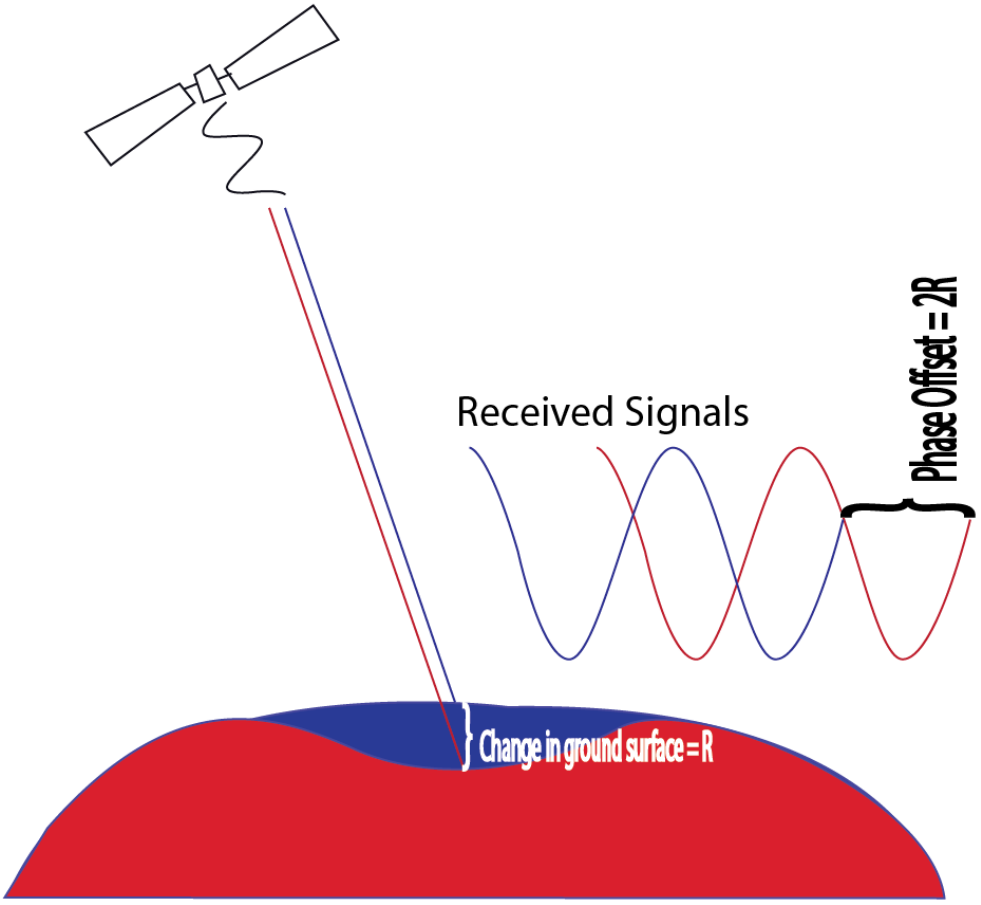

Figure 3.1: This image portrays the theory behind radar interferometry. Satellites measure the distance to Earth and back by the phase of the returning signal. The amount of phase shift in the signal over time determines the shift of the ground surface in the direction of the satellite viewing angle.

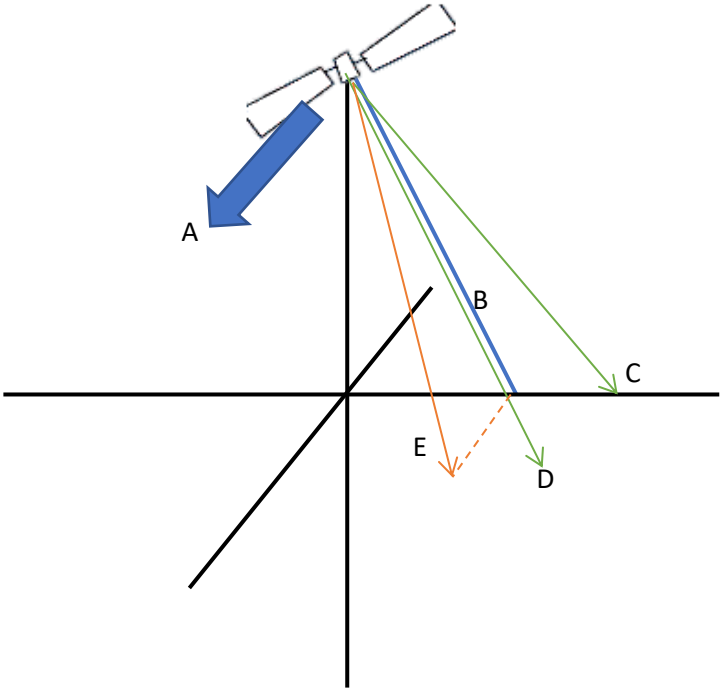

A) Sensor flight direction
B) Sensor look direction
C) X displacement: horizontal, parallel to look direction
D) Z displacement: vertical
E) Y displacement: horizontal, perpendicular to look direction

Figure 3.2: This displays the effect of different displacement directions relative to the sensor. The Green arrows represent directions in which the sensor is able to measure displacement. The red arrow represents horizontal motion perpendicular to the sensor look direction, so the sensor is unable to measure displacement.

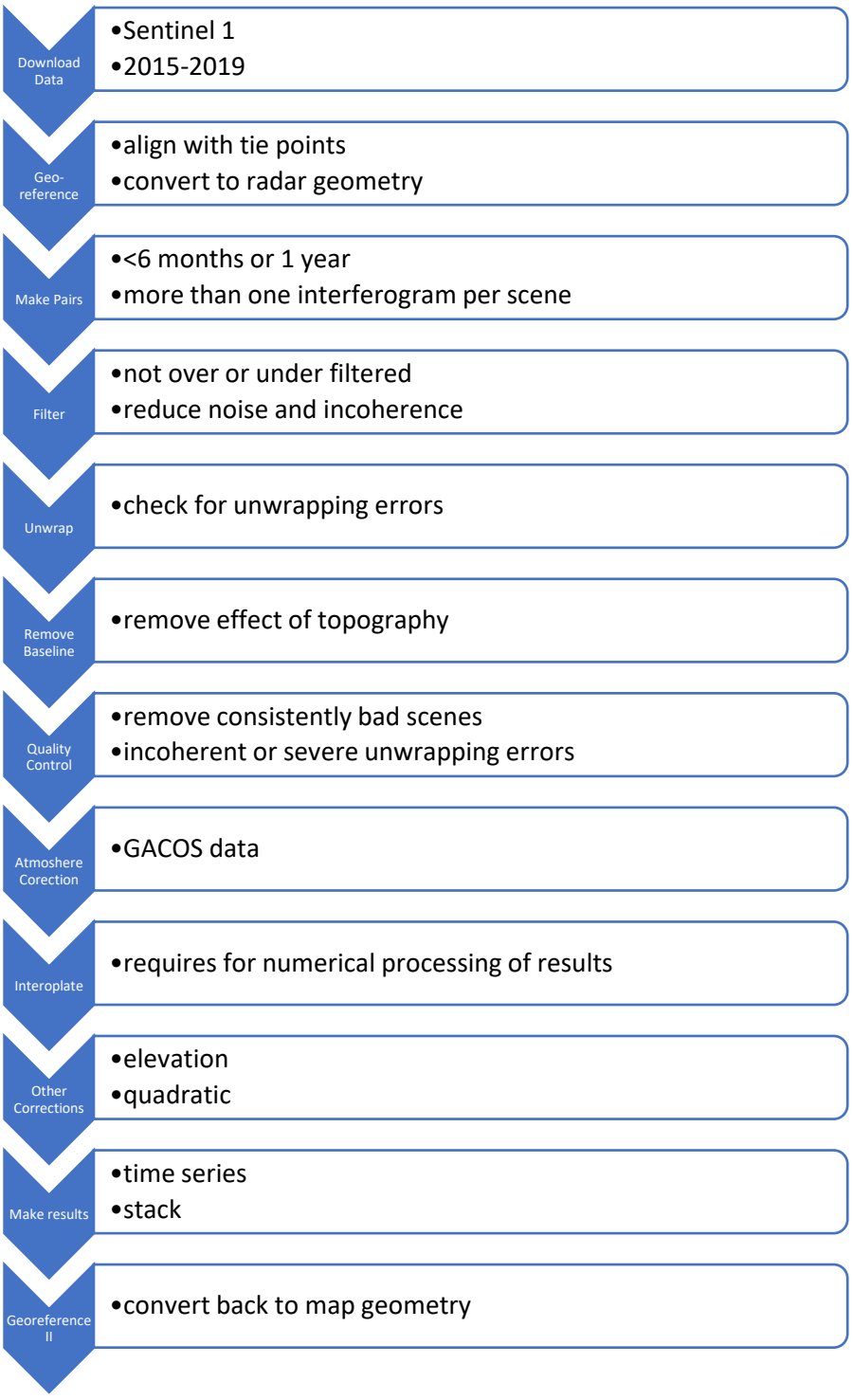

Figure 3.3: This outlines the steps completed on the InSAR data for Southern Colorado from downloading to producing result images. The order of the steps was determined so that the most original information is conserved and the greatest number of interferograms could be used for future steps.

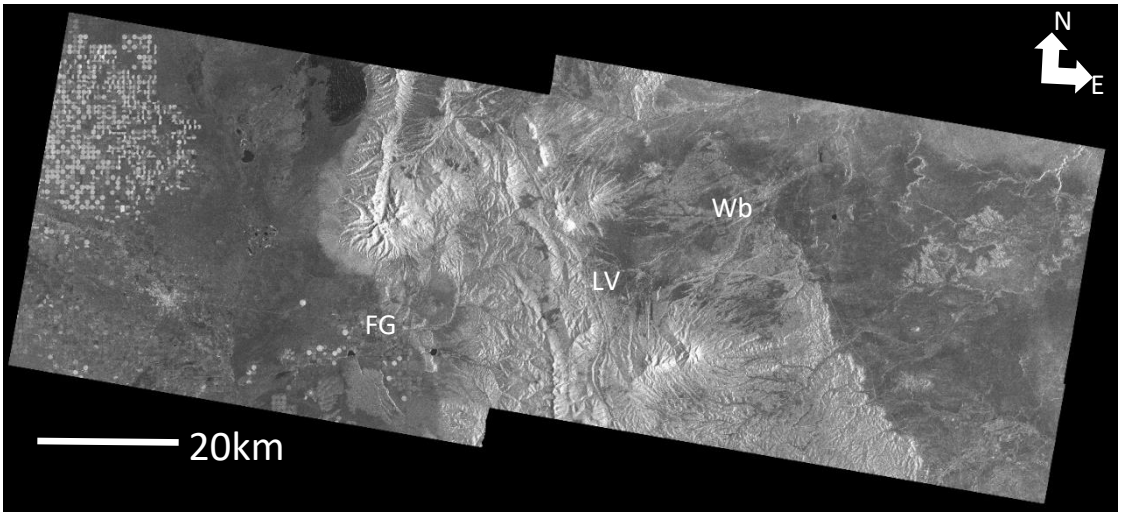

Figure 3.4: This is the initial map geometry of the radar scenes. Note that the satellite orbit track is at an angle. The bursts are also slightly misaligned, as edge is not perfectly smooth. The reason for the irregular halved shape of the image is that it is stitched together from two swaths of data that were captured. Walsenburg (Wb), La Veta (LV), and Fort Garland (FG) have been labeled for geographic context.

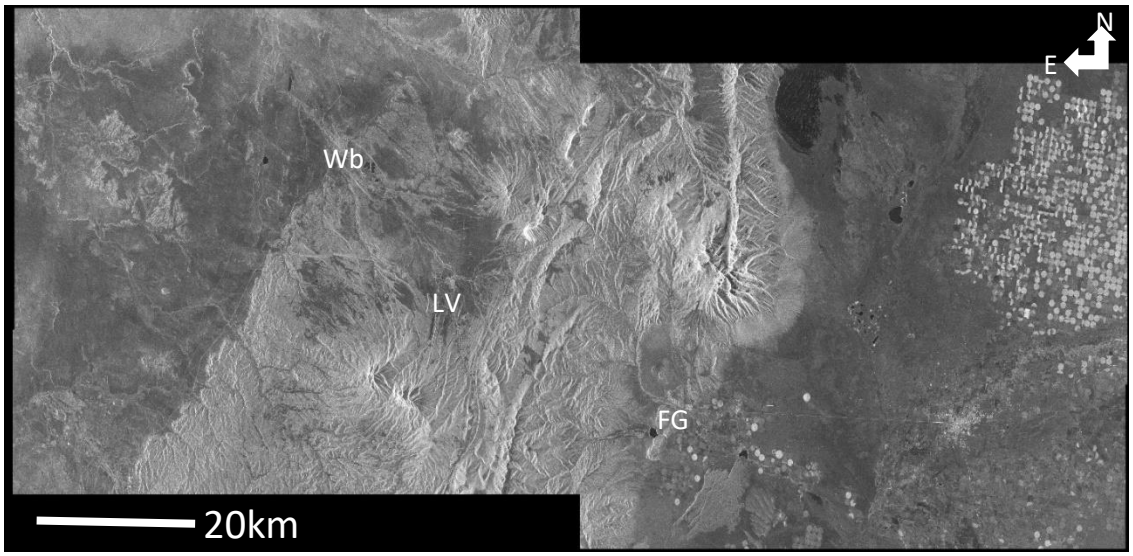

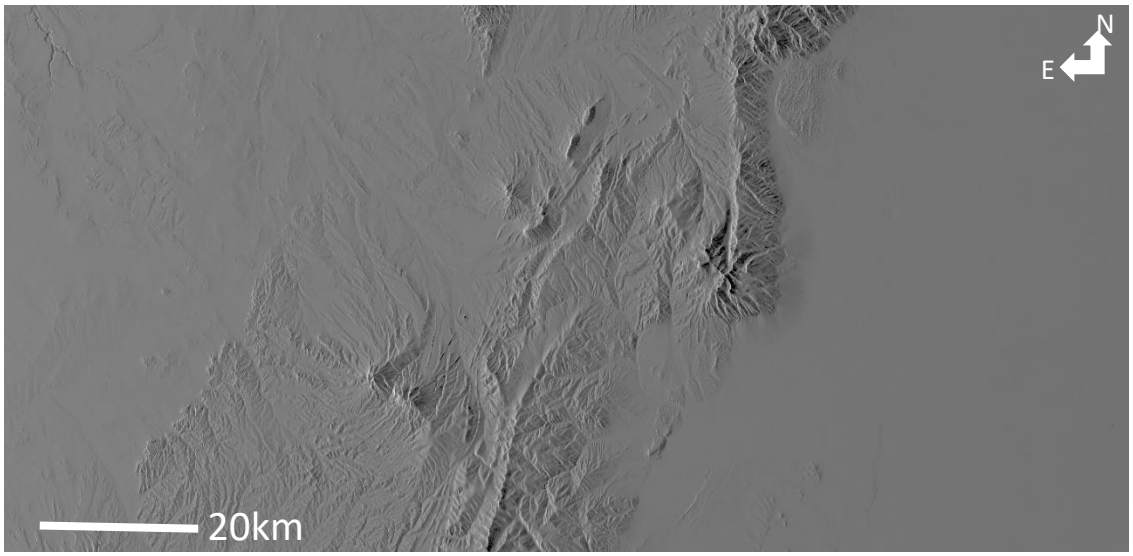

Figure 3.5a and b: The upper image (a) shows an example Sentinel-1 image in radar geometry. This image was initially made of several smaller bursts in two columns that have been stitched together through the process of geocoding. In order to get the image properly stitched and aligned, the values are compared to a simulated radar image from a DEM. This simulated scene is pictured below (b). Note the scenes become mirrored when measured by the satellite. The North direction remains loyal to the map geometry but East and West have been inverted. Walsenburg (Wb), La Veta and Fort Garland are labeled in a for geographic context.

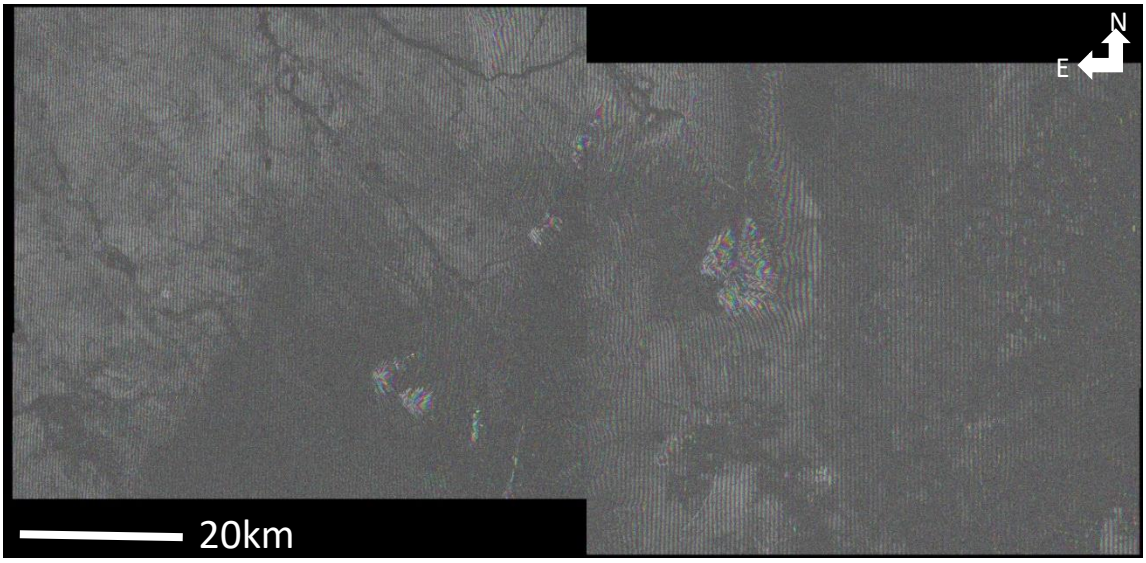

Figure 3.6: This image shows the initial outcome of the differencing of two SAR scenes. There is a strong ramp of fringes all across the scene perpendicular to the sensor line of sight. Pixels farther away from the sensor with have a different phase from pixels closer to the sensor and that is signified by the interferogram-wide pattern. It is inconsistent due to topography (especially noticeable on Blanca peak) as well as surface deformation over the time period of the interferogram. This is interferogram number 575 from 1-4-2018 to 6-9-2018 and will be used to demonstrate all steps of processing unless otherwise specified.

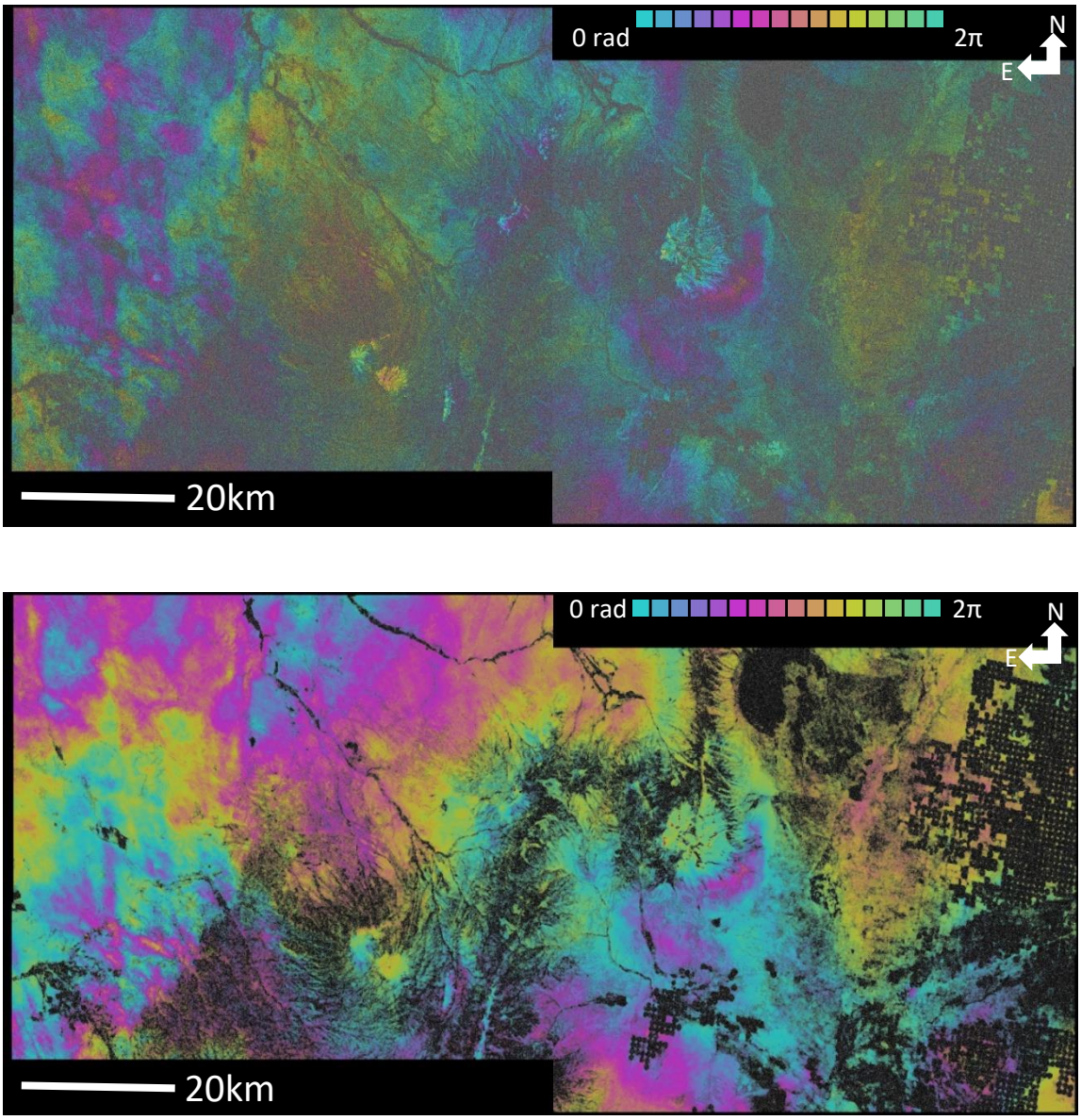

Figure 3.7: Filtering was applied to this interferogram (575 from 1-4-2018 to 6-9-2018). Filtering smoothed the data by removing noise and filled in some incoherent areas. The topographic background has been removed from the filtered image and the black locations represent areas that were masked due to low coherence.

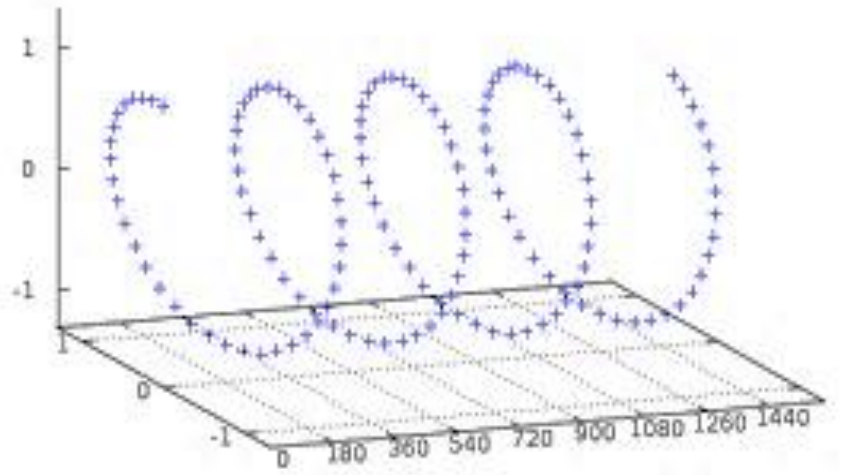

Figure 3.8: This image depicts the reason for phase unwrapping. The phase is displayed along the x axis in degrees. When there is a phase displacement, the measured value in the y and z directions changes in a cyclical pattern so two different phase displacements could show the same value in the x and z axes because entire cycles have been passed. Unwrapping adds those whole cycles back in, so the actual phase displacement can be measured.

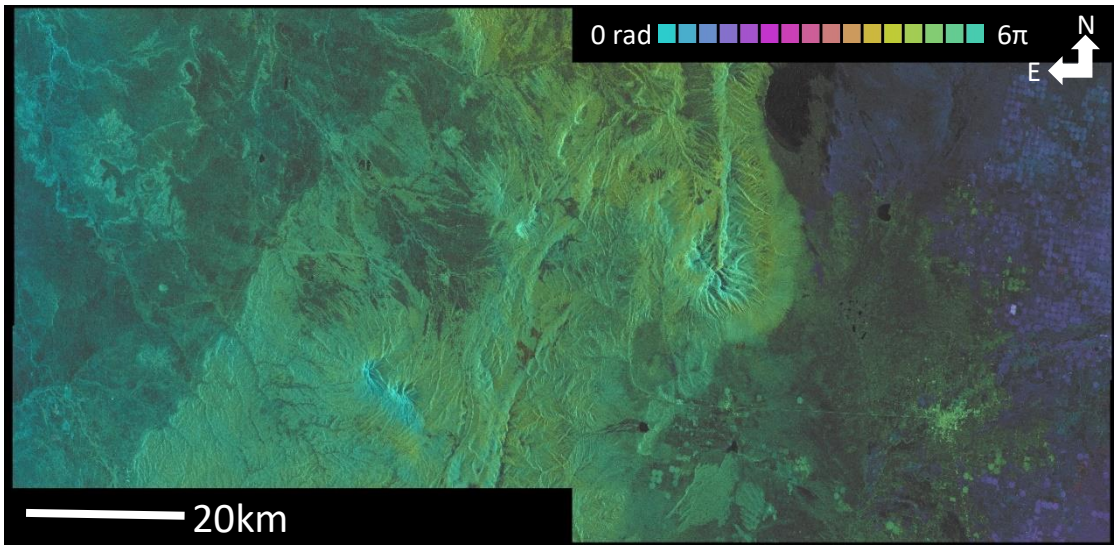

Figure 3.9: Unwrapping is the process of converting cyclical phase values into continuous phase values. This step can sometimes create errors with large phase jumps where the program does not recognize which cycle the phase is in and chooses incorrectly. This interferogram (537 from 12-11-2017 to 1-4-2018) displays a large error in unwrapping on the right side of the image as shown by the sudden widespread change in color from light greed to dark blue.

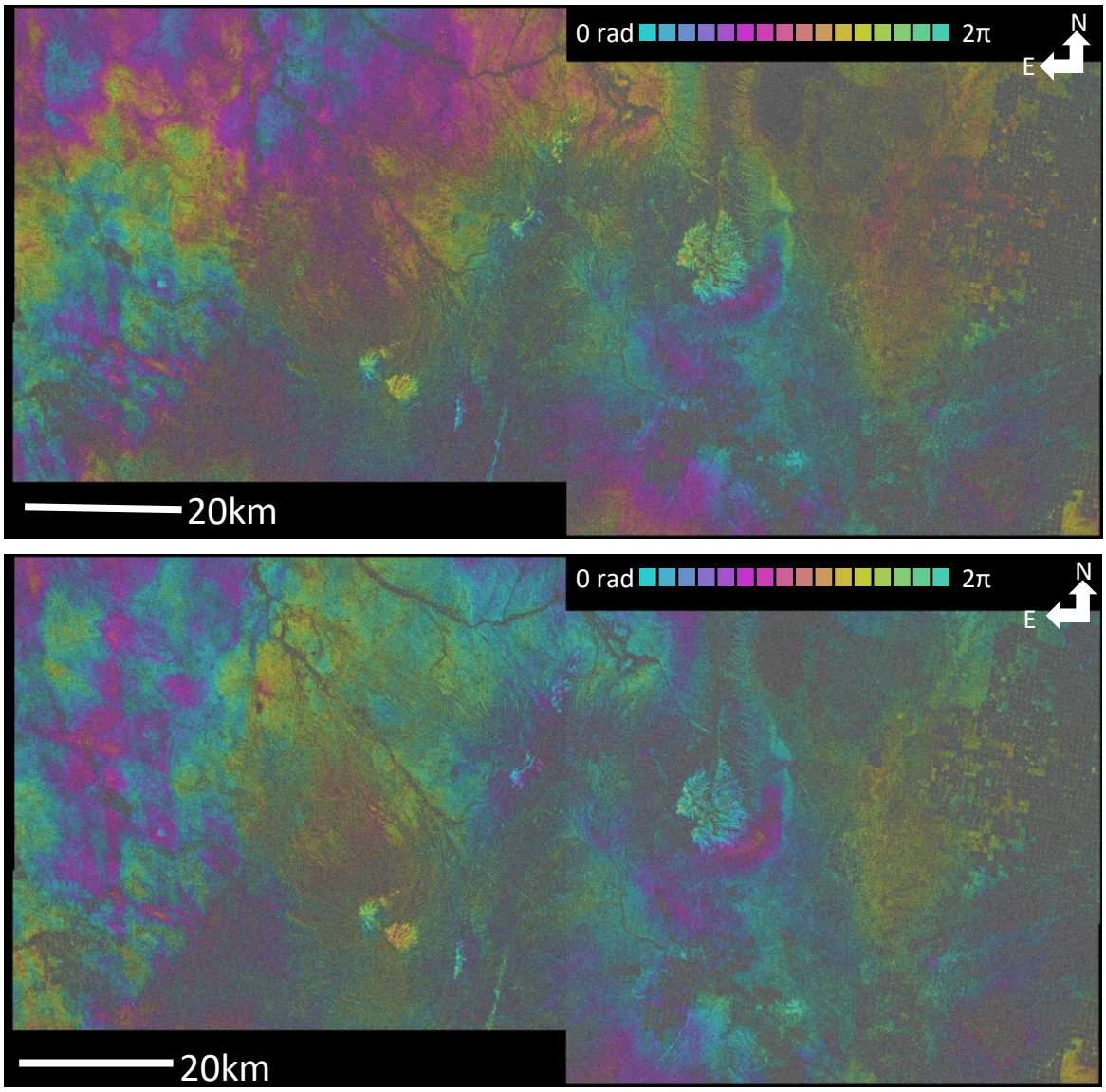

Figure 3.10: Baseline removal is the process of accounting for the distance between the satellites when the initial SAR images were taken. The greatest effect of this is to reduce the contribution of topography. That is shown by the extension of the fringes in this images after baseline removal. Higher numbers of fringes indicate a greater displacement over time, but a portion of that displacement is due to topography appearing differently from different locations.

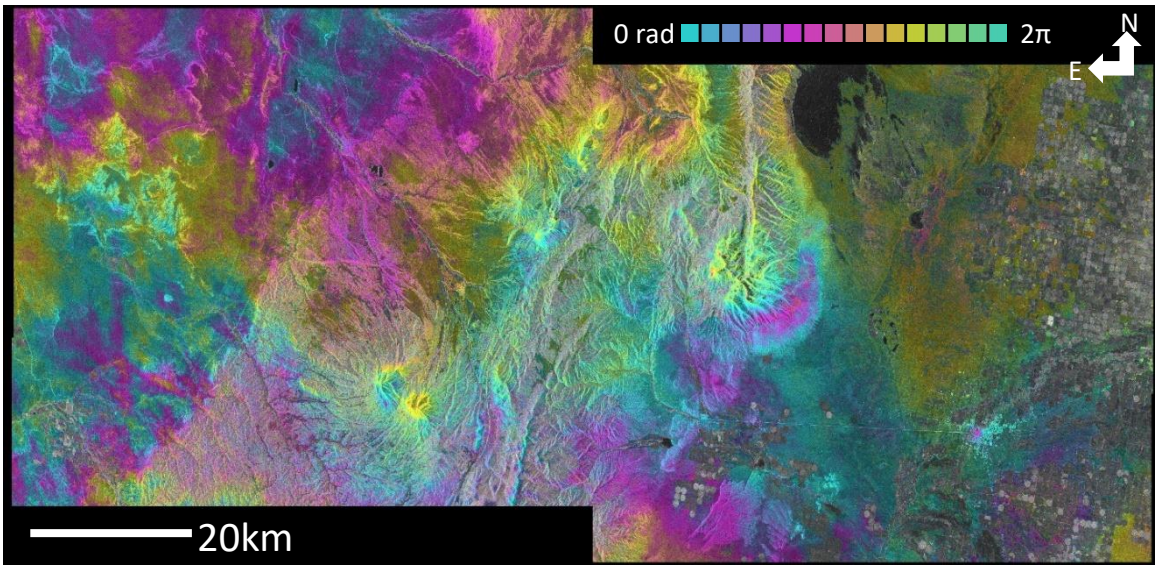

Figure 3.11: Interpolation is important because it fills in regions where there is no data. A lack of data could be due to the removal of noise through filtering or just an initial incoherent region. Having a high rate of data fill is important for creating a stack and time series for results. This interferogram is number 575.

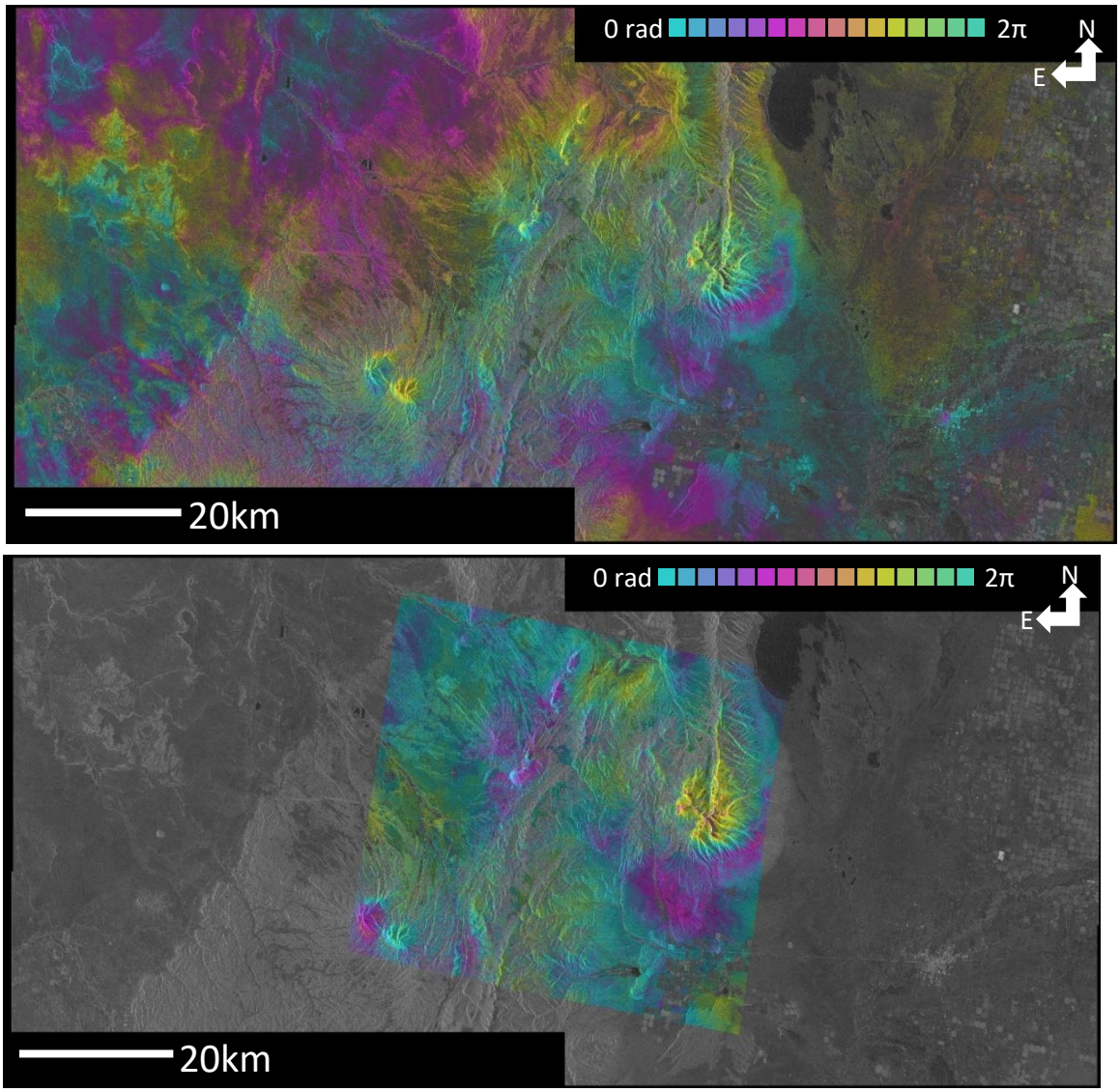

Figure 3.12: This shows the effects of removing the atmosphere using the GACOS data. Note the irregular patches of fringe that do not correspond to ground movement. After applying the GACOS data, the patches, which were due to clouds have been removed and the scene is much smoother and does not have false indicators of deformation. The GACOS data downloaded was limited to the extent of the study area.

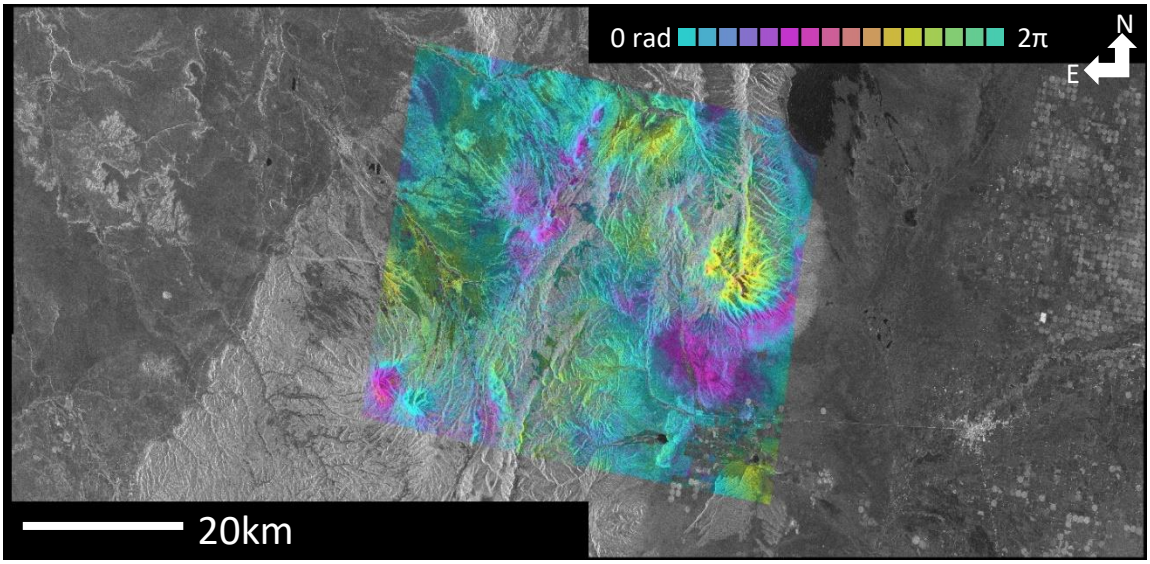

Figure 3.13: This is the resulting image from elevation signal removal. The algorithm used to remove the elevation finds a linear relationship between phase and altitude and removes it, but it does this on a large scale from the entire scene. It will not always match the elevation signal on a local scale so some elevation effects may remain, as is visible on Blanca peak.

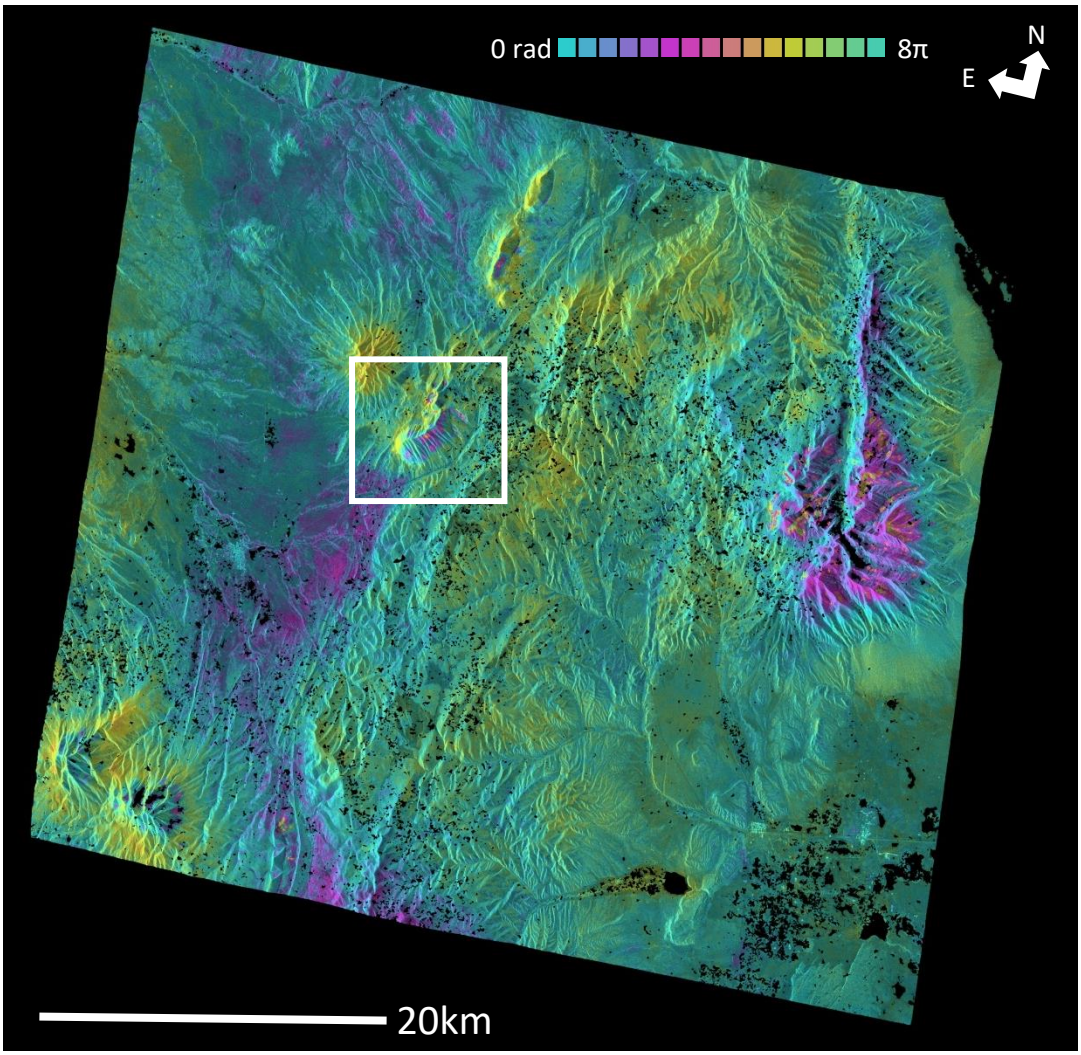

Figure 3.14a: The stack image here shows the average rate of motion as calculated at each pixel on each of the 606 fully processed interferograms. The overall solid color indicates that large parts of the image are not moving. However, the streaks of color down the sides of the peaks are moving features, for example, an active rock glacier. The average rate of movement on several rock glaciers can be determined quantitatively form this figure based on the number of colored fringes. A close up of the white square is on the next page.

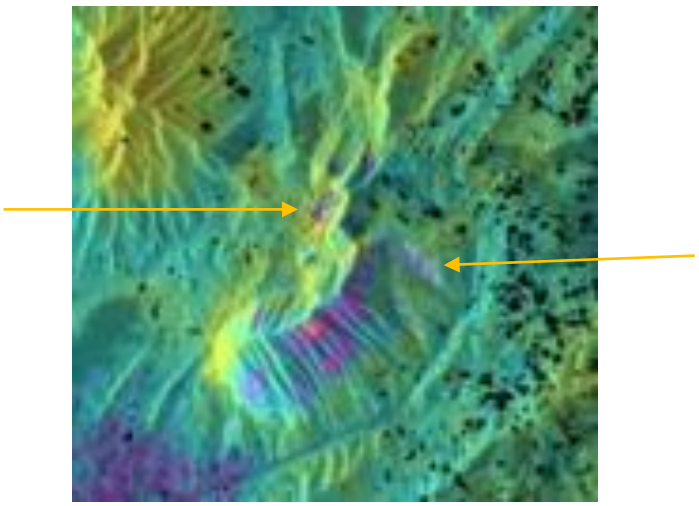

Figure 3.14b: This close up of the stack on Mount Mestas portrays the different directions of flow with fringes. The arrow on the left shows a rock glacier with several colors of fringes while the arrow on the right shows a rock glacier with fewer fringes and, therefore, less flow. The fringes on the right rock glacier are also in a different color order (blue to pink instead of blue to yellow), indicating a different flow direction.

Figure 3.15a-c: This images on the next two pages show several dates (from top to bottom 04-26-2015, 18-08-2016, 10-12-2017) of time series images. The first date is the first time step which the other scenes are measured in comparison to, so there is no movement within it. Over time with more movement away from time step 1, fringes appear on the active rock glaciers displaying flow. There were 65 time steps remaining after the InSAR processing, so there were 65 of these images, showing the slow progression of movement. These images have also been smoothed with a high pass filter to eliminate long wavelength displacement signals that are not the result of rock glacier movement. The time series before the filter is shown in the inset next to time 08-18-2016. The final image of the time series is very similar to the stack result because it represents the total displacement that happened over the time period, which should be directly proportional to the average displacement over the entire period of study. The data from each rock glacier may be extracted to produce a customized plot of displacement vs. time in a graph format.

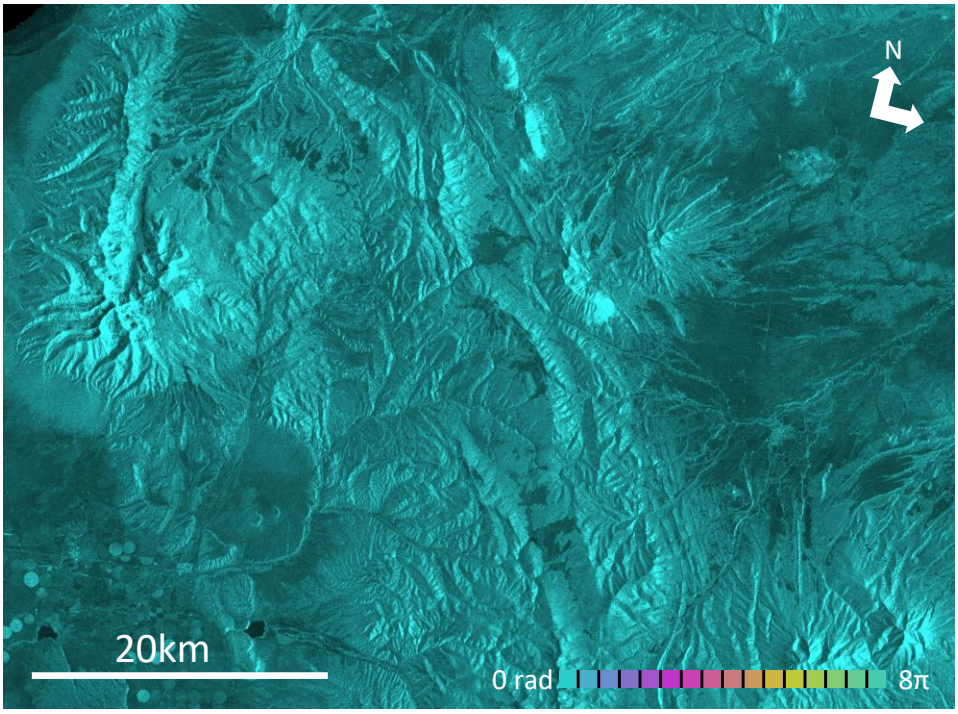

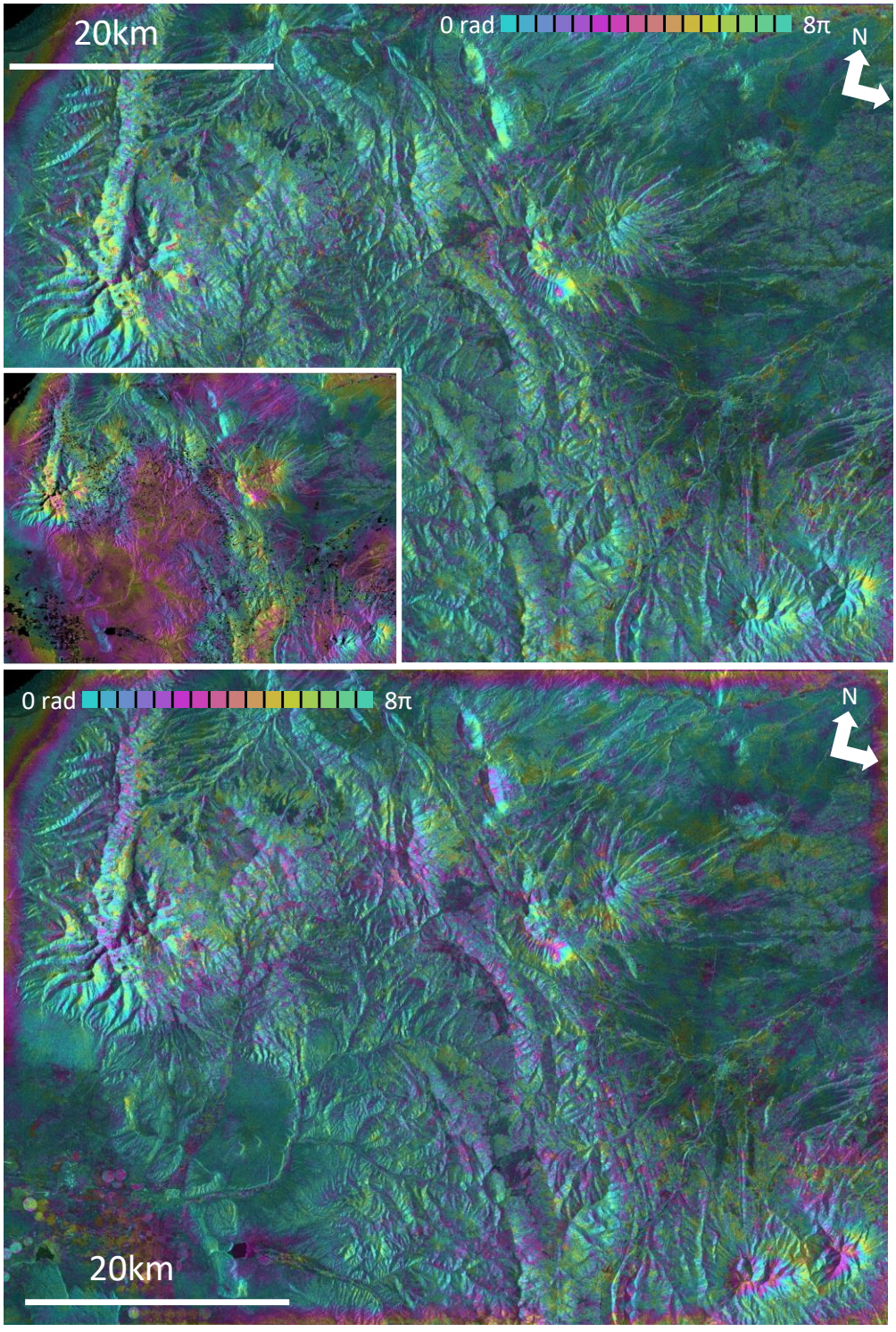
20km
0 rad
8π
N
0 rad
8π
N
20km

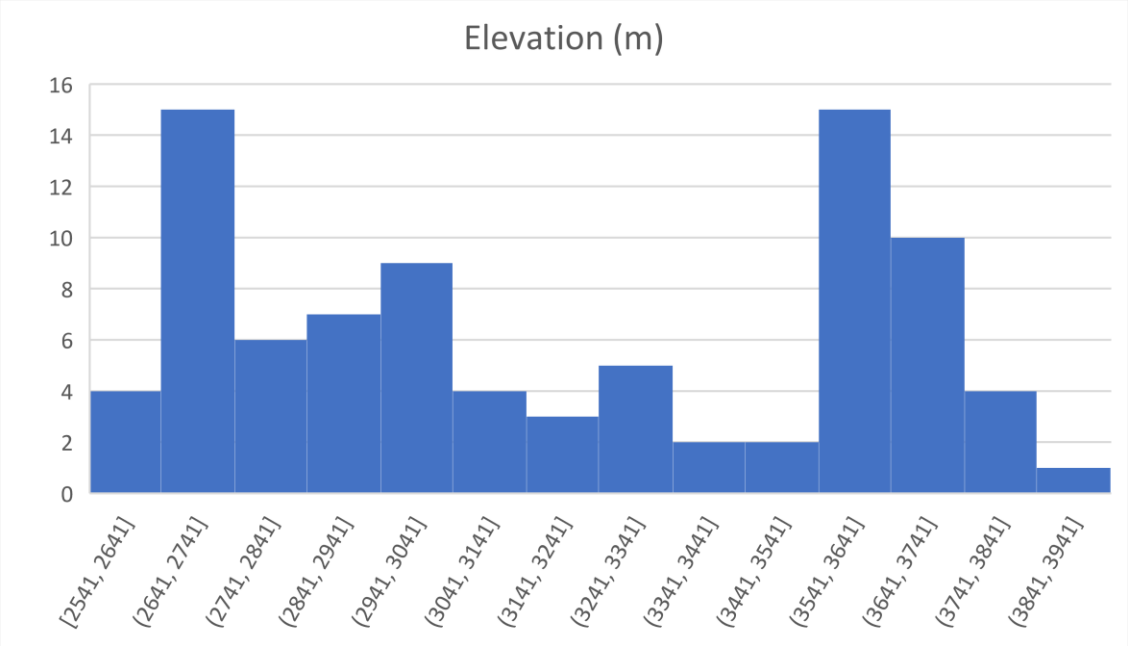

Figure 3.16: Histogram of average rock glacier elevations. Note that there are two peaks in the distribution of rock glacier elevation. The rock glaciers at the lower elevation are on peaks with no history of glaciation, while those at the higher elevation occur on previously or currently glaciated peaks.

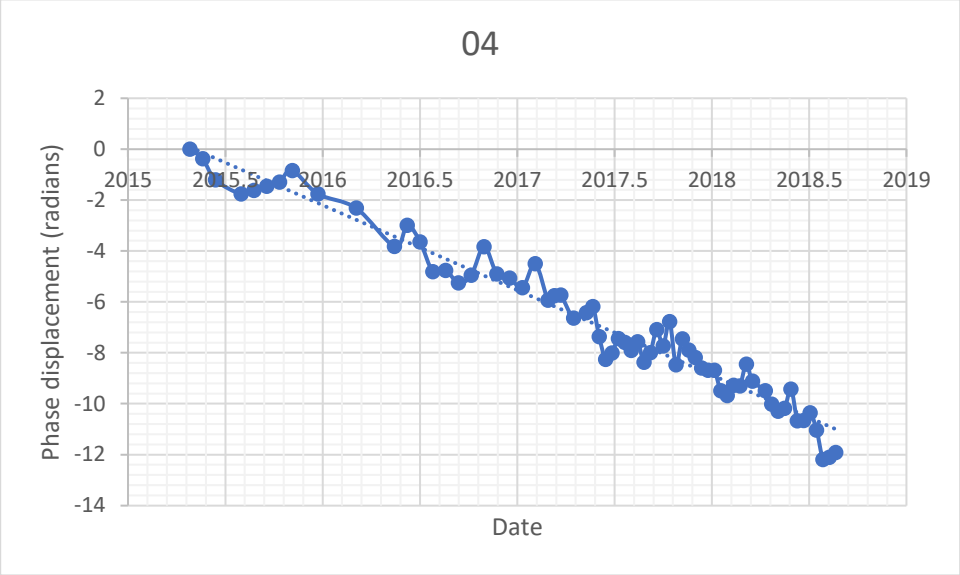

Figure 3.17: This graph shows the phase displacement of rock glacier 004 over time. It is significant because this is the fastest moving rock glacier recorded out of the 87 rock glaciers. The slope of the dotted linear fit represents the average flow rate.

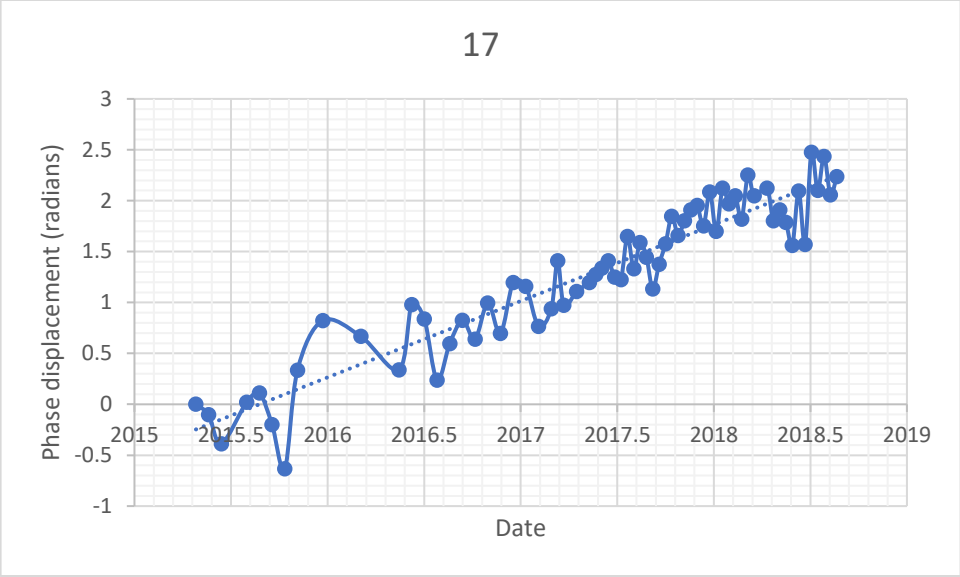

Figure 3.18: This graph shows the phase displacement of rock glacier 17 over time. This rock glacier is moving in the opposite direction as the previous rock glacier (04). This is evident in the positive slope of this displacement time series, as opposed to the negative slope of 04. Both of these rock glaciers are active because of the magnitude of flow rate, regardless of direction.

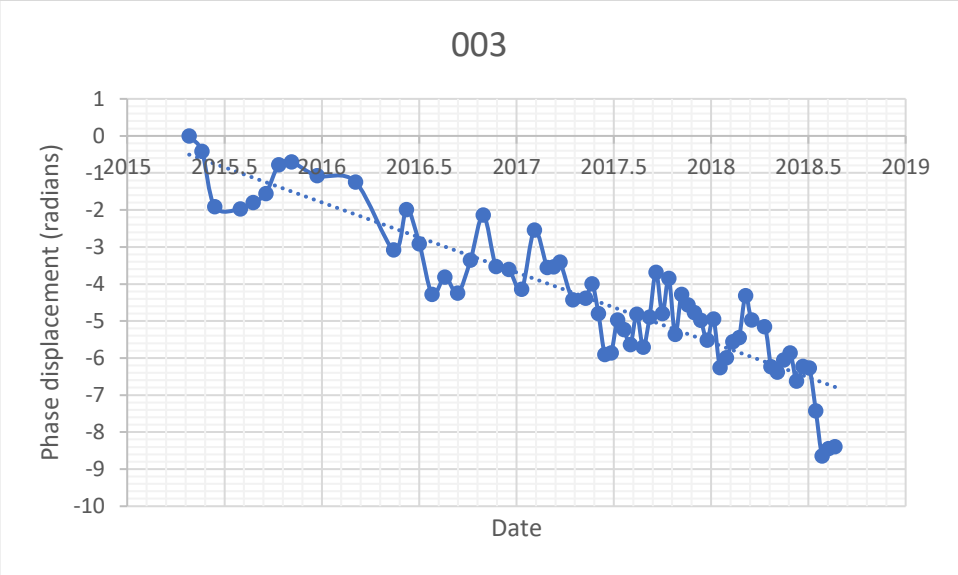

Figure 3.19: This graph shows the phase displacement of rock glacier 03 over time. The sensitivity of this rock glacier is very low (0.057 in magnitude). Even though the sensor is not able to measure displacement well on this rock glacier, there is a strong displacement signal with a relatively small amount of noise. This rock glacier is certainly flowing and likely at a greater rate than is measured here, it is therefore, classified as active.

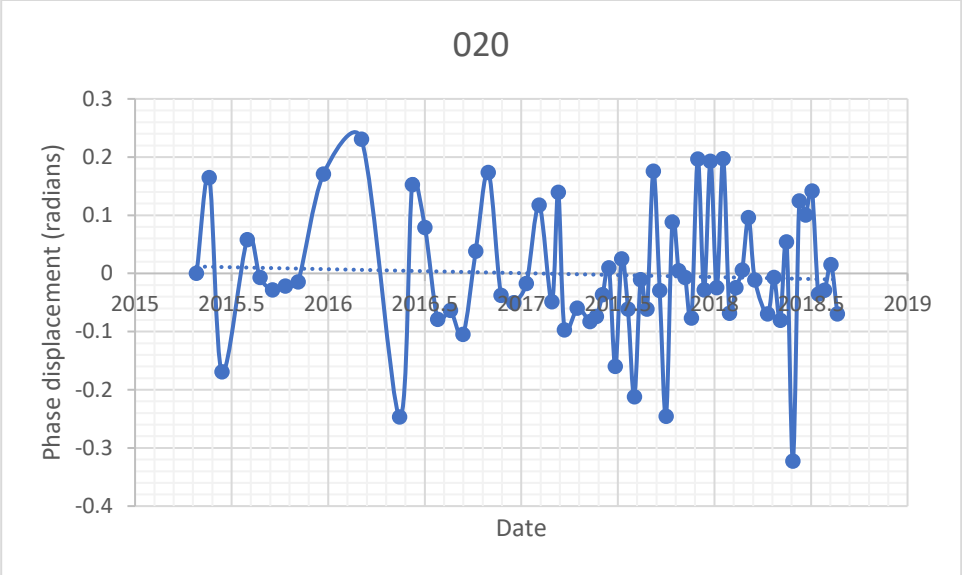

Figure 3.20: This graph shows the phase displacement of rock glacier 20 over time. The sensitivity of this rock glacier is very high (0.778 in magnitude). The sensor is able to measure any displacement on this rock glacier, but it has not measured any. This rock glacier is certainly inactive, therefore.

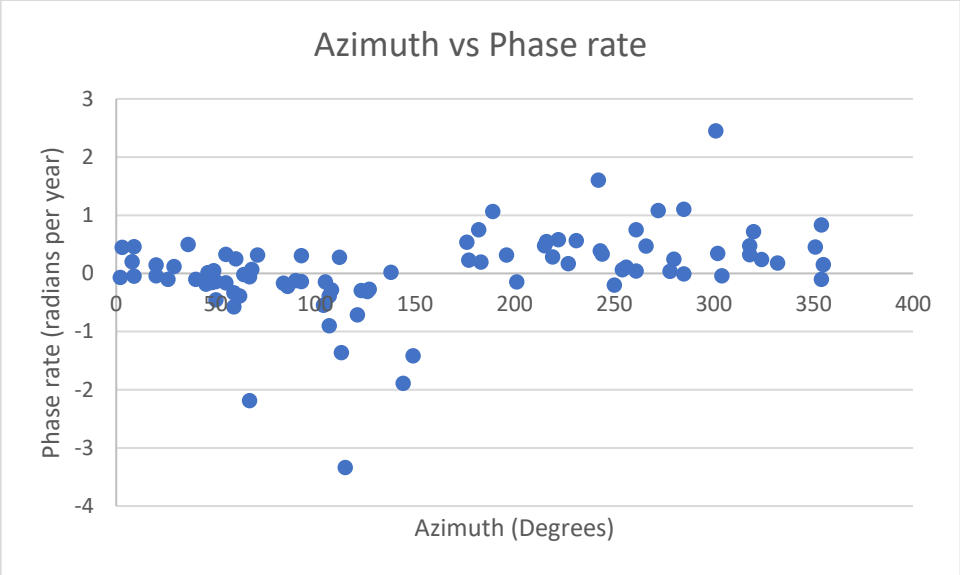

Figure 3.21: The azimuth is related to the measured flow rate due to the effect of sensitivity. Rock glaciers in an azimuth away from the sensor will have a negative flow rate, while rock glaciers moving toward the sensor will have a positive flow rate. Rock glaciers flowing perpendicular to the sensor will not exhibit a strong flow signal because the sensor is insensitive to them.

Chapter 4: Thermal Analysis

BACKGROUND

The ice within the rock glacier is maintained when the interior of the talus body remains at a temperature below the melting point of water for an extended period of time. The debris acts as an insulator for the ice, keeping the interior at a cooler, more stable temperature than the surface (Brenning et al., 2012). Over time, however, the ice content within the rock glacier will decay, if the temperature is not well below 0C (Martin and Whalley, 1992). As the ice content decays, the thickness of the ice-free talus layer is increased in thickness, while the ice saturated debris layer and massive internal ice block will decrease in thickness.

Because the ice is below the surface, the ice content cannot be directly measured. As a result, thermal properties must be measured and correlated to ice content (Brenning et al., 2012). Cyclical changes in air temperature over diurnal and seasonal time scales will cause the temperature of the rock glacier to change. Thermal inertia, which is the ability of a material to change temperature when the temperature of its surroundings have changed (Brenning et al., 2012), and thermal skin depth, which is the depth to which surface temperature changes affect the subsurface, are two properties that can be used to estimate the ice content of a rock glacier. A rock glacier with a large amount of internal ice will have a higher thermal inertia because a large portion of the inside of the rock glacier is at a constant cold temperature in order to maintain the ice. Similarly, if the layer containing ground ice is above the thermal skin depth, the rock glacier will experience the exchange of heat between the ground ice and surface. During the warm season, the

ice will cool the surface from below, while in the cold season, if the air temperature is below freezing, the ice could have a warming effect.

Thermal inertia and skin depth may vary over the surface of a rock glacier due to variation in particle size, and depth to ice, characteristics that are affected by movement. The sorting of debris, which varies across the rock glacier due to different flow speeds in the center and the edges of the rock glacier, has a greater effect on thermal inertia than the ice content. The insulating effect of the talus varies with the size of the talus, so thermal inertia would be different depending of the different size of the debris across the rock glacier (Piatek, 2009). Other factors including the density, iron content, and silica content of the substrate, as well as the moisture content of the air all affect thermal inertia (Brenning et al., 2012). With high enough resolution remote sensing imagery, the thermal inertia of different parts of the rock glacier could be measured, however, it may not have a direct correlation to the ice content of the rock glacier because of the plethora of variables that affect thermal inertia. Whether or not the ice is interstitial or there are massive ice lenses within the rock glacier could also not be determined (Piatek, et al., 2013).

Using remote sensing to determine thermal inertia is challenging due to the temporal resolution of remote sensing data. Ideally, the daily maximum and minimum temperature of the rock glacier surface would be used to calculate the thermal inertia (Piatek, 2009). With satellite-based imagery, however, it is impossible to acquire these values because it would require two images over the same location in the same day. The time when the maximum and minimum temperatures occur also changes daily (Piatek, 2009).

Measuring land surface temperature (LST)with a satellite-based sensor introduces several variables into thermal inertia variations, as well (Brenning et al., 2012). Even in higher resolution thermal band sensors, a rock glacier will only be a few pixels. Within each pixel, there may be a range of debris clast sizes, partial vegetation cover, or differences in exposure to solar radiation. The amount of variation that could be expected in thermal inertia in ice filled versus ice free rock glaciers is likely less than the error associated with thermal inertia calculations and inherent limitations on satellite based remote sensing (Brenning et al., 2012).

The thermal skin depth of the rock glacier also changes with ice content due to the difference in geothermal gradient. The thermal inertia of a rock glacier with a high ice content would be higher due to the decreased variation in temperature on the rock glacier. The ice acts as a heat sink, preventing the surface of the rock glacier from reaching the same high temperature as an ice-free rock glacier on a diurnal timeframe (Brenning et al., 2012).

Seasonally, the temperature gradient with depth is more affected than the thermal inertia (Brenning et al., 2012). Temperature gradient is related to thermal skin depth since the ice in a rock glacier provides a constant low temperature that does not vary. Only the surface temperature would change. The skin depth could also provide a better estimate of ice content because it would indicate the depth of ice beneath the surface of the rock glacier.

METHODOLOGY

The source of all the thermal infrared imagery used were from the thermal bands of Landsat7 (10.4-12.5 micrometers) and Landsat8 (10.6-11.19 micrometers) thermal bands. The daytime images are all in the GeoTIFF format, with a mask filter that automatically removed the clouded portions of the scene. The online user interface from the Remote Sensing Lab, was used to select the data source and time frame. All thermal infrared scenes from 2000 to 2019 were selected in order to have a long-term coverage within which to find seasonal trends, as well as long term differences between ice-filled and ice-free groundmass or changes in rock glacier temperature.

The method that produced the LST values is outlined in the paper "Online Global Land Surface Temperature Estimation from Landsat" by Parastatidis, et al (2017). The calculations were performed using a single channel approach with the radiative transfer equation. This method uses the radiance at the sensor as well as inputs of atmospheric transmissivity thermal path radiance, downwelling irradiance, and surface emissivity to calculate the land surface temperature (LST) as a variable in the Planck function. A cloud mask, based on reflected visible and near-infrared light, was applied to the scenes before being made available for download through the RS Lab interface. An Fmask, based on approach detailed in Zhu and Woodcock (2012) for detecting clouds, and water in Landsat images was the source of this data. Several options for emissivity source data are available through this service. The ASTER emissivity data product was chosen to be applied in this study,because of the similar spatial resolution and its superiority compared to an NDVI or MODIS based emissivity value on bare rock and non-vegetated surfaces. While the other sources for emissivity have a higher temporal resolution, the resolution is

better for ASTER and there is no need to make multiple observations of emissivity for rock glaciers over the entire time series. The emissivity of rock glacier surfaces should remain constant due to the bare rock surface with little seasonal change and consistent composition of talus throughout time on each rock glacier. The atmospheric corrections were comprised from the MODTRAN (MODerate resolution atmospheric TRANsmission).

Advantages of using LST data from the RS Lab LST estimator include the high accuracy, simplicity, and speed of acquisition. The accuracy of the resulting thermal image files is less than 2 degrees Celsius for any point, but the value may be lowered by using the correct emissivity source (ASTER). This study utilized 537 LST images, 134 of originating from Landsat 8 data, ranging from 2013-2019 and 403 originating from Landsat 7 data, ranging from 2000-2019. Not all of the scenes will be used in the temperature time series due to the cloud mask producing null values over specific parts of the image at different times, but the large quantity of data and the long time frame will produce high temporal resolution and seasonal analysis of thermal characteristics of active and inactive rock glaciers. Figure 4.1 shows an example LST data product for the region with the cloud mask.

Landsat 7 data has lines of data loss on each side of the image, as can be seen in Figure 4.1. This is the result of the failure of the scan line corrector on the satellite in 2003. While there is some data loss on the peaks, Mestas, both Sheep Mountains, White Ridge, and a portion of West Spanish Peak are unaffected by it because they are in the central region of the scene that does not have data loss. The presence of clouds poses a much greater source of data loss than the scan line corrector failure.

Nighttime thermal imagery was not used for this study. It is not available from RS Lab. Though the same procedure used on the other data could be carried out on nighttime observations, one step cannot. The cloud mask is produced from the radiance from a visible band, only available in daytime observations. Without the clouds automatically removed, the clouded pixels would have to be removed manually or with an algorithm trained to identify clouds. Neither of those options would have the same precision as the cloud mask already used in the RS lab data products, and the noise introduced by including night time data would interfere with future steps, including curve fitting.

Rock glacier pixels were extracted from the imagery in Matlab using the 87 rock glacier polygons created in Google Earth. Because the downloaded images are in a format that can be immediately used, the next step is to import them and the rock glacier polygons into Matlab in order to produce a time series. The LST of each pixel within each of the 87 rock glaciers was averaged together, after the pixels with a recorded value of zero due to the cloud mask were removed. The temperature of each rock glacier was plotted on a time series graph, for the entire 20 years of LST measurements.

Owing to the sparse, irregular time sampling of LST for each rock glacier, spectral analysis of periodic signals (e.g., FFT and power spectra) did not seem feasible. Instead, recognizing that key climatic periodicities will be annual and multiples thereof, sinusoidal functions were fit for periodicities of 1-10 years using non-linear regression. To improve the fit, peak/trough values were weighted more heavily than temperatures near the mean (which were more numerous). Specifically, data were weighted as $(LST - \langle LST \rangle)^2$ where $\langle LST \rangle$ is the mean value for an individual time series. The best fit took the form of a 10 term sinusoidal function, with each term representing a different period

of cyclical temperature variation was plotted as well (Figure 4.3 shows an example rock glacier) (Appendix A shows the time series plots for all of the rock glaciers).

For comparison, air temperature time series were created using weather observation data from the NOAA Daily Summary data product at the stations Ute Creek, CO and Walsenburg, CO (Figure 4.2). The same approach was used to fit 1-10 year periodic functions to these data. These represent average air temperature measurements, not ground surface temperatures which are also affected by incoming solar radiation. The ability of the exposed rock to retain heat better than the air also produces differences in the temperature of the rock glacier surface and air temperature. The amplitude of the fit curve for each period is the dataset that will be used to calculate the results and determine the viability of thermal observation in activity classification.

RESULTS

The amplitude of the fit curve for each period was plotted for both the weather and the LST datasets at each rock glacier. An example of the plot of amplitude vs period for the rock glacier and the weather can be found in Figure 4.4. In order to determine the distinguishing characteristics between the ice filled rock glaciers and ice free rock glaciers, thermally, the amplitudes of both were compared to the weather data. The comparison was made by subtracting the amplitude of the weather data from the amplitude of the LST data. This produces a number that represents how much more the LST varies than the daily air temperature and will be referred to as comparative amplitude. Figure 4.5 contains a diagram illustrating the concept of comparative amplitude.

Histograms of the frequency of the comparative amplitude at active and passive rock glaciers was produced at each period. Figure 4.6 contains the 20 histograms (10 different length periods each for active and inactive rock glaciers). The general trend in distribution of comparative amplitude was similar in each period histogram, except the 1 year. In the one year period histogram, the inactive rock glaciers had an overall higher comparative amplitude than the active rock glaciers. The average comparative amplitude for the 16 inactive rock glaciers was 5.76, while for the 43 active rock glaciers it was 4.97. The standard deviation for both active and inactive comparative 1-year amplitudes is 2.46.

The comparative amplitudes diverge at a period of 1 year, suggesting that the presence of ground ice may be modulating the land surface temperature. The skin depth represents the thickness of the active layer which does vary in temperature. Below the active layer, the temperature does not vary. In this case the active layer ends at the ice layer boundary. Compared to the talus which heats and cools daily and annually, the ground ice in a rock glacier is at a constant temperature of 0 degrees C. The skin depth, or depth to the ground ice, can be calculated using the method described in Fowler, 2004

$$z^* = \sqrt{\frac{2\kappa}{\omega \rho c_p}}$$

Where z* is the thermal skin depth, κ is the thermal conductivity of the material, ρ is the density, ω is the frequency of temperature oscillation, and c_p is the specific heat. The values used for the material were taken from Robertson, 1988 for granite, as that is the closest standard igneous rock composition to the rock glacier talus. This function depends on the periodicity of thermal variation, as the inverse of frequency. Because it was

determined that ice filled (active) rock glaciers vary from ice free (inactive) rock glaciers on the one-year period, the resulting skin depth ranges from 4.8 to 6.9m depth depending of the exact composition of the rock. This was calculated using thermal property values for a range of granites, which is the most similar to the generally felsic igneous rock. Because Blanca Peak is partially composed of hornblende gneiss and amphibolite, the skin depth calculations were repeated with thermal property values more similar to rocks of that composition. Accounting for the anisotropy of gneiss, the skin depth values would be in the range of 4.4 and 7.3 meters.

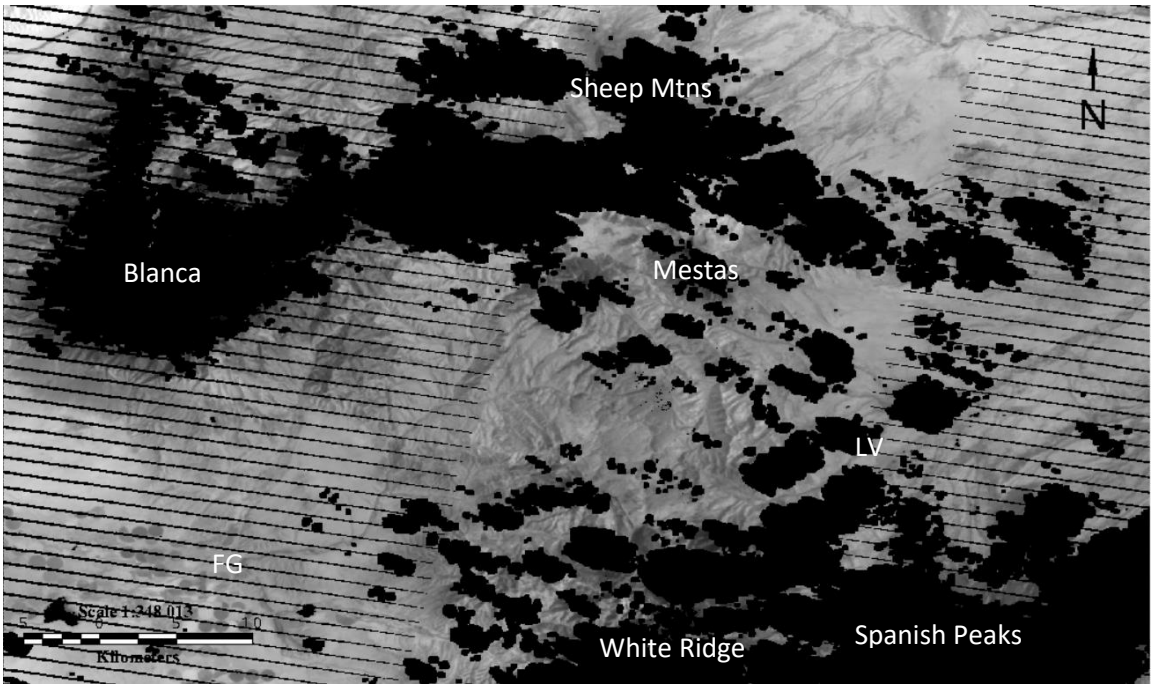

Figure 4.1: This image displays an example of a downloaded LST file. This is a Landsat7 image from 6-15-2019. The horizontal stripes around the edges are the result of a problem with the scan line corrector, the black splotches throughout the entire image are the result of the cloud mask. The extent of the image is exactly the same as the study region. The peaks are mostly covered by clouds, causing the data loss seen in the time series. The locations of the peaks and the towns La Veta (LV) and Fort Garland (FG) have been labeled for context.

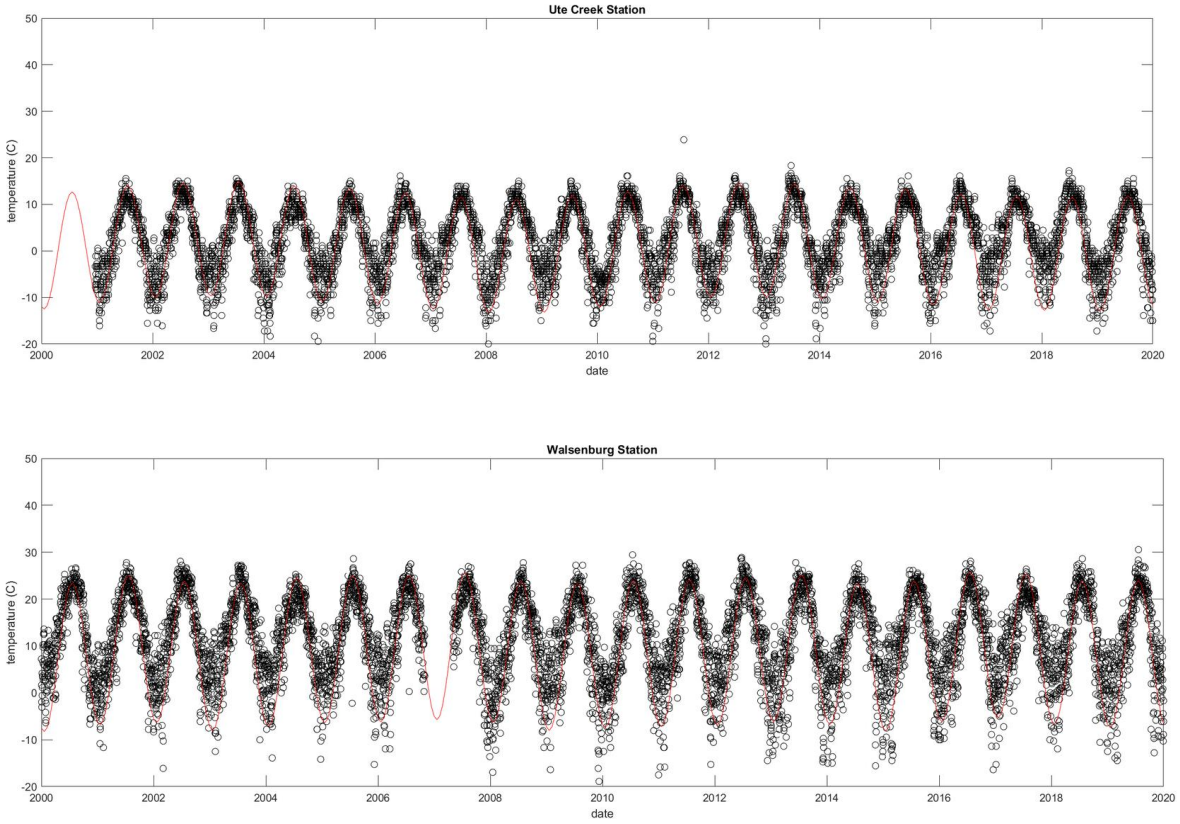

Figure 4.2: These are the time series for the weather data. There are a lot of data observation points, allowing for a very good fit line to be generated. The Ute Creek station is at a higher elevation than the Walsenburg station which was used to calculate the local temperature/elevation lapse rate.

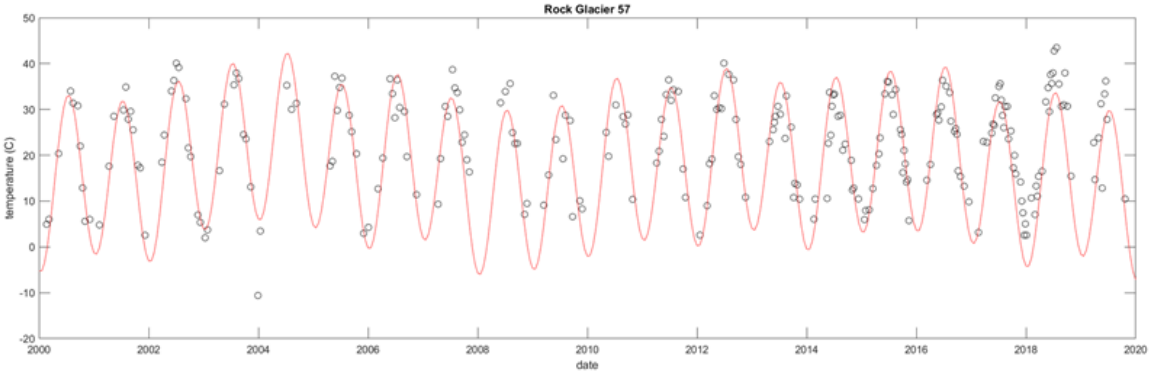

Figure 4.3: This is the time series from the LST data over rock glacier 57. There are far fewer datapoints in this time series than the weather time series, though they cover the same time span. The fit function is a 10 component sinusoid. Each component represents a period of variation of 1 to 10 years.

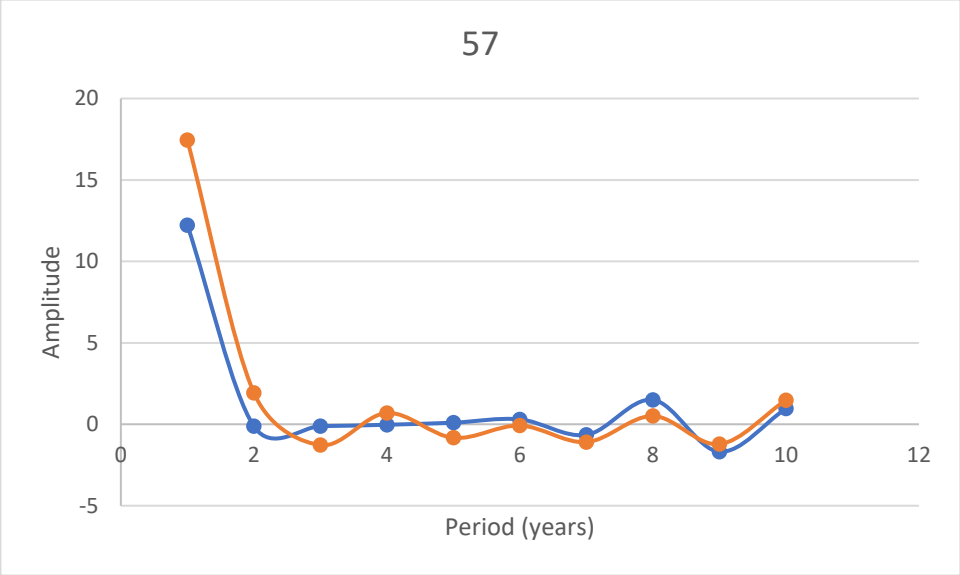

Figure 4.4: This plot compares the period of each of the 10 components of the fit for the rock glacier (orange) with the weather time series (blue) . The higher amplitude of the rock glacier over a 1 year period indicates that the land surface temperature varies more than the air temperature by approximately 5C. The fit curve for this rock glacier has more long period variation than the weather measurements on the 3,4,5,7, and 10 year periods as well. There are only 10 components to the fit line because the 20 year observation period only allows for repeating patterns to be established over a maximum of 10 years.

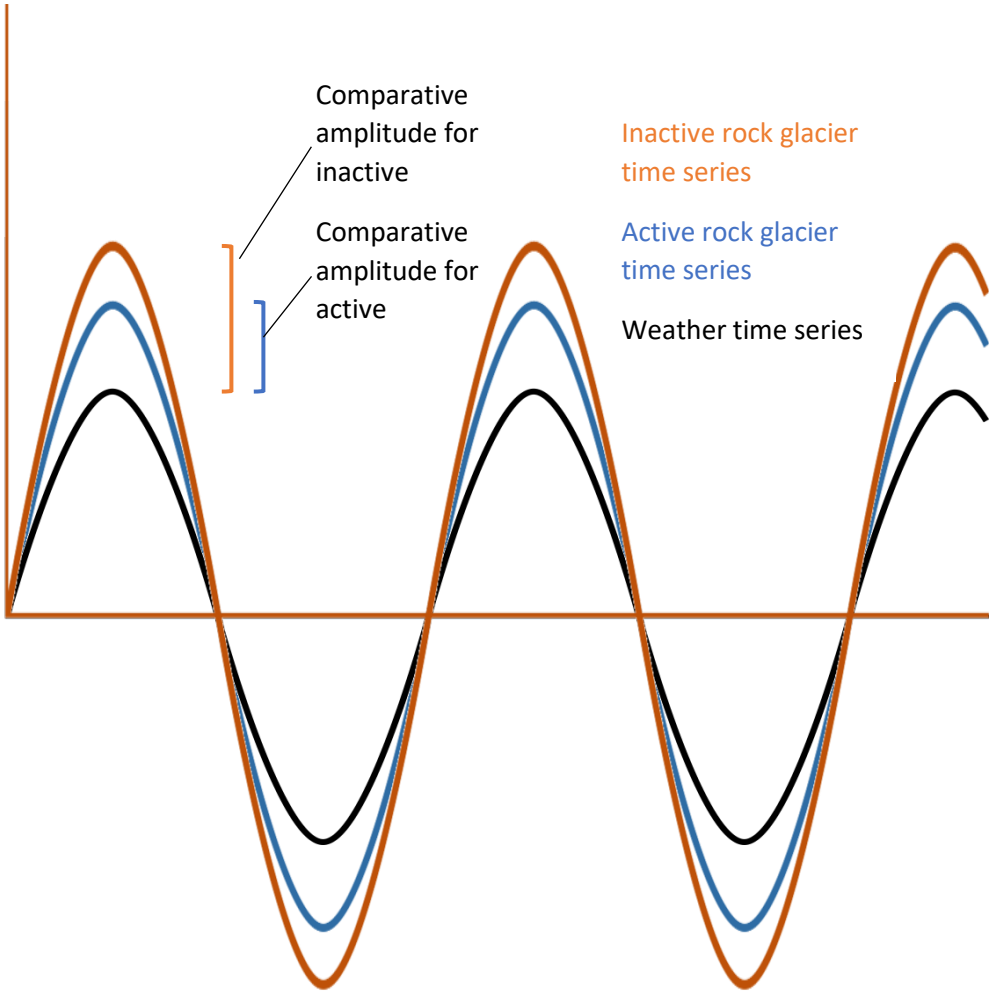

Figure 4.5: This figure illustrates the idea behind comparative amplitude. Axes represent a standard time series with the y representing temperature, and the x representing time. The amplitude of temperature variation for the two groups of rock glaciers was compared to the amplitude of variation of the weather data. A positive value of comparative amplitude means that the temperature of the rock glaciers reaches higher highs and lower lows than the weather. A negative value of comparative amplitude means that the rock glacier temperature varies less than the air temperature.

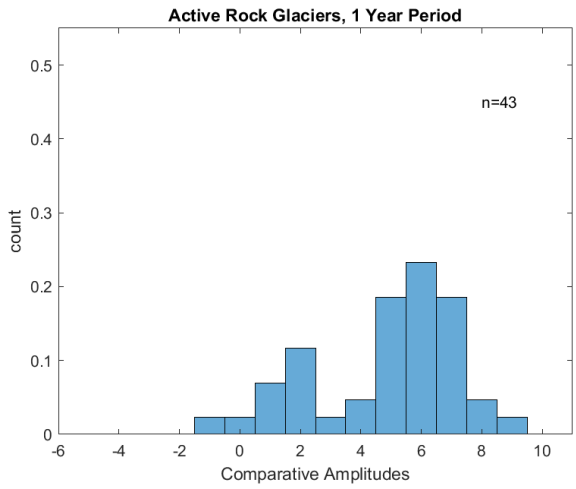
Active Rock Glaciers, 1 Year Period
n=43
count
Comparative Amplitudes

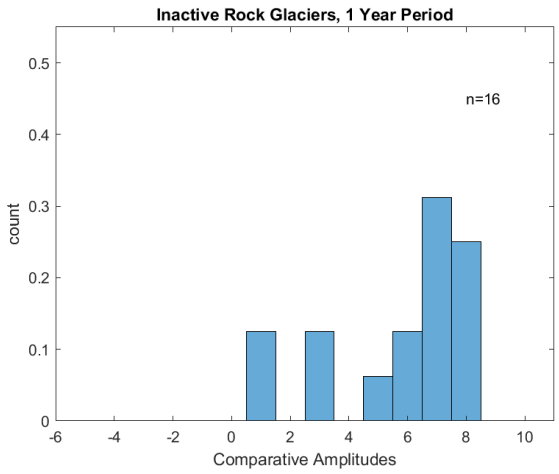
Inactive Rock Glaciers, 1 Year Period
n=16
count
Comparative Amplitudes

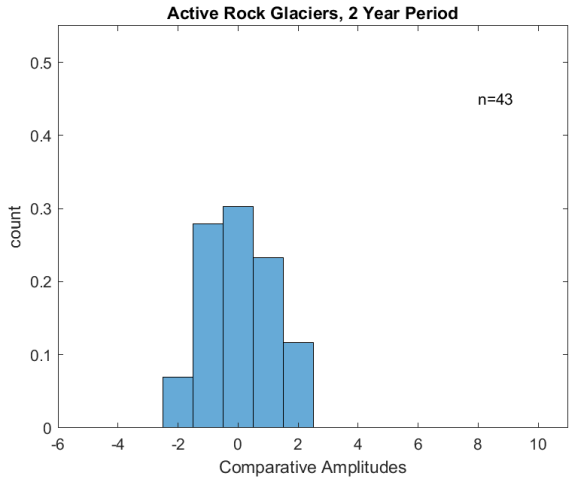
Active Rock Glaciers, 2 Year Period
n=43
count
Comparative Amplitudes

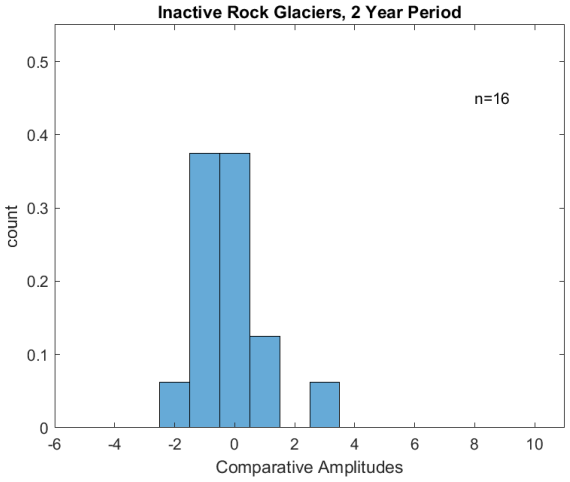
Inactive Rock Glaciers, 2 Year Period
n=16
count
Comparative Amplitudes

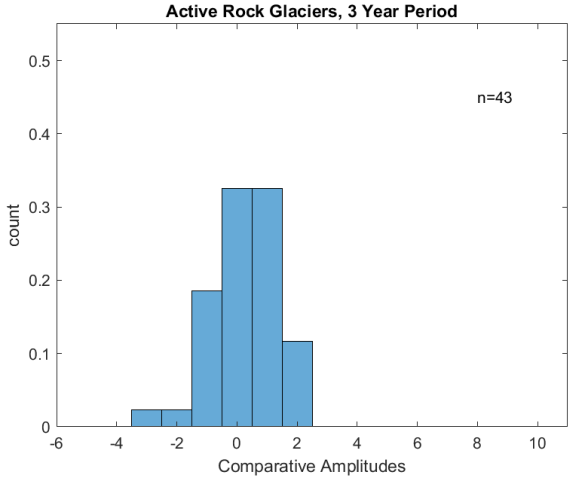
Active Rock Glaciers, 3 Year Period
n=43
count
Comparative Amplitudes

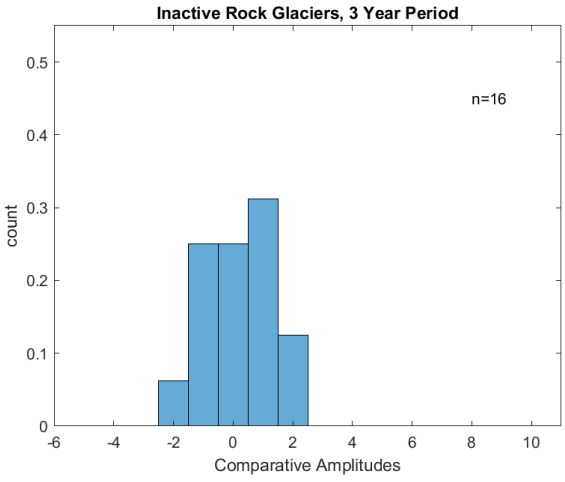
Inactive Rock Glaciers, 3 Year Period
n=16
count
Comparative Amplitudes

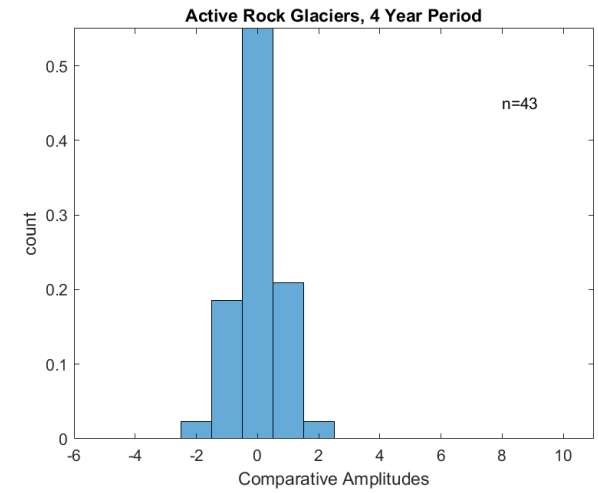
Active Rock Glaciers, 4 Year Period
n=43
count
Comparative Amplitudes

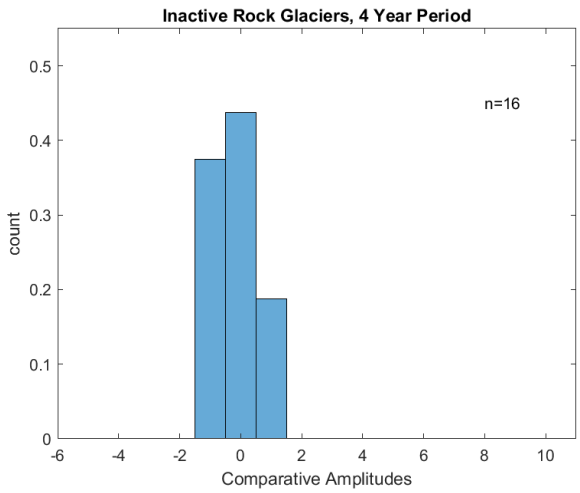
Inactive Rock Glaciers, 4 Year Period
n=16
count
Comparative Amplitudes

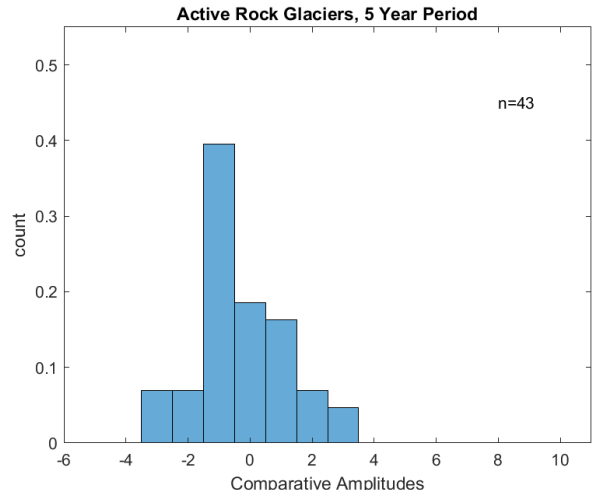
Active Rock Glaciers, 5 Year Period
n=43
count
Comparative Amplitudes

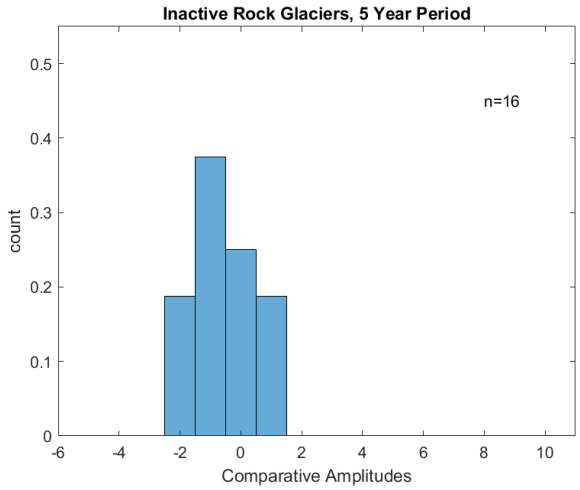
Inactive Rock Glaciers, 5 Year Period
n=16
count
Comparative Amplitudes

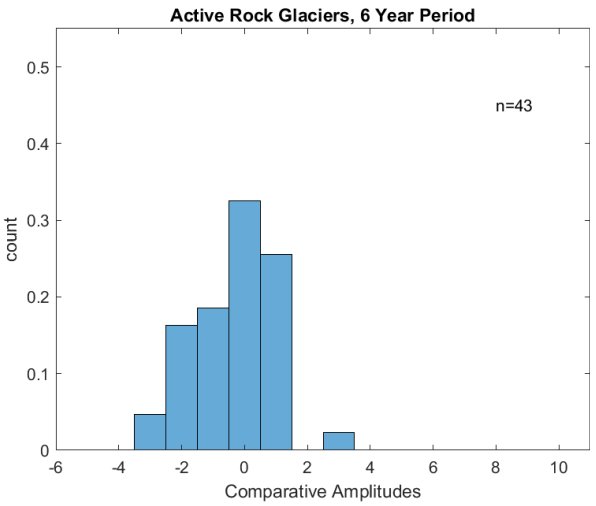
Active Rock Glaciers, 6 Year Period
n=43
count
Comparative Amplitudes

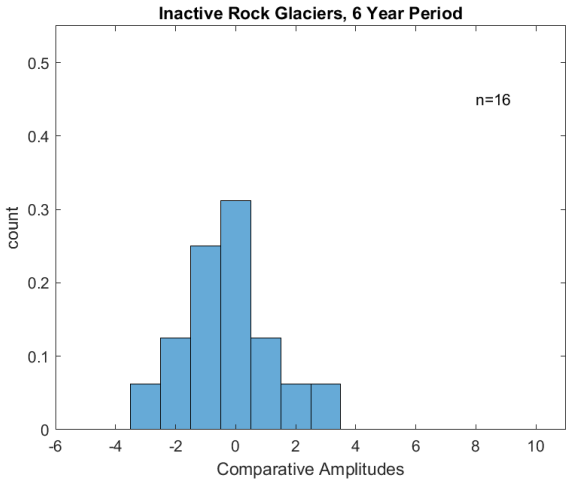
Inactive Rock Glaciers, 6 Year Period
n=16
count
Comparative Amplitudes

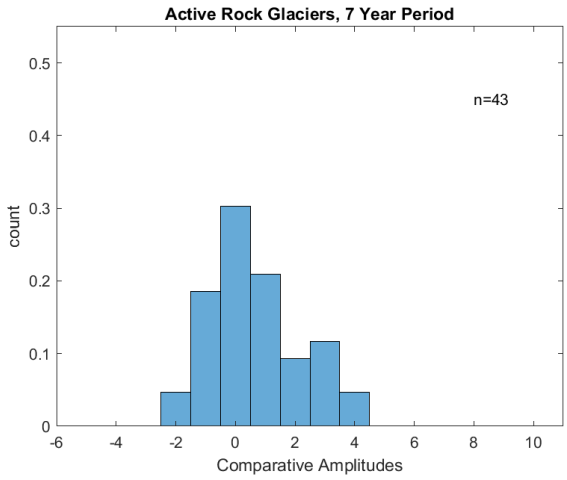
Active Rock Glaciers, 7 Year Period
n=43
count
Comparative Amplitudes

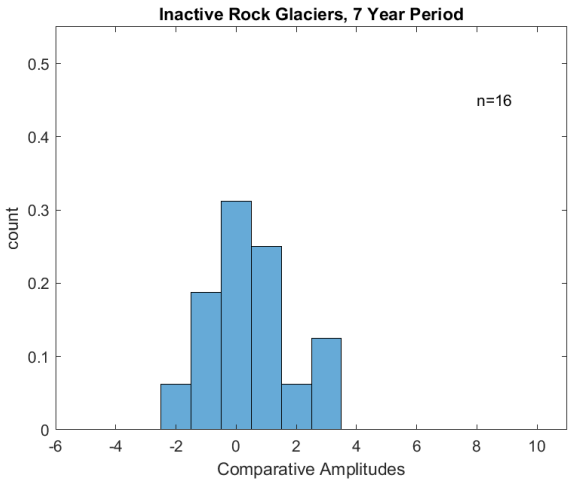
Inactive Rock Glaciers, 7 Year Period
n=16
count
Comparative Amplitudes

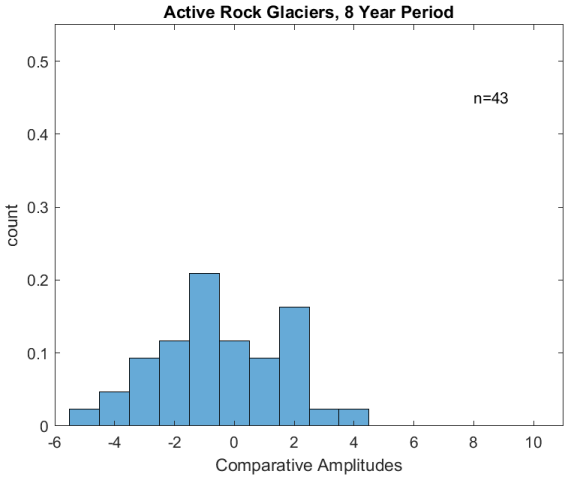
Active Rock Glaciers, 8 Year Period
n=43
count
Comparative Amplitudes

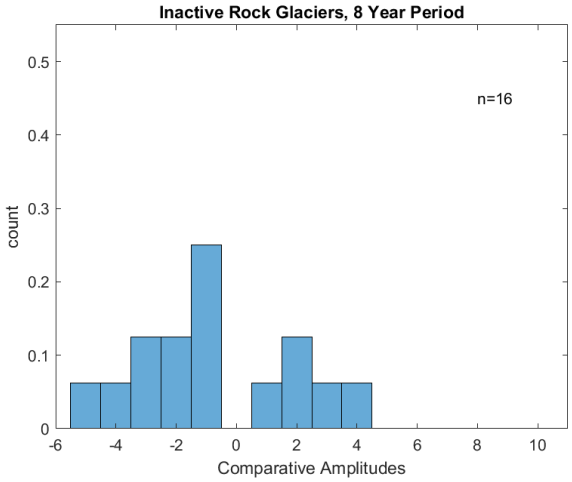
Inactive Rock Glaciers, 8 Year Period
n=16
count
Comparative Amplitudes

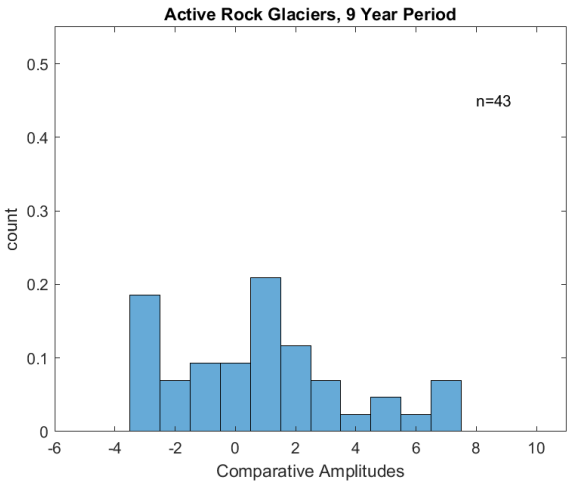
Active Rock Glaciers, 9 Year Period
n=43
count
Comparative Amplitudes

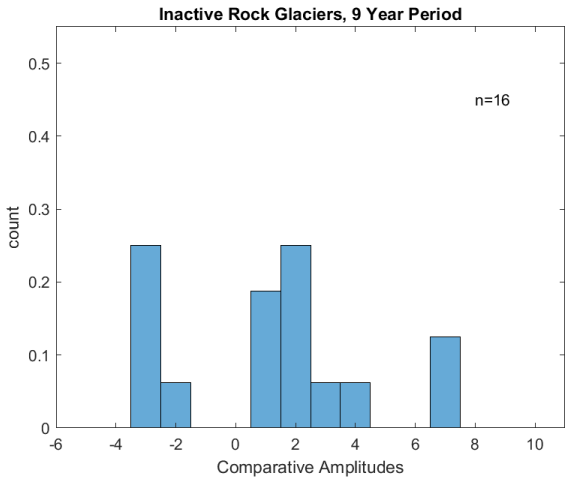
Inactive Rock Glaciers, 9 Year Period
n=16
count
Comparative Amplitudes

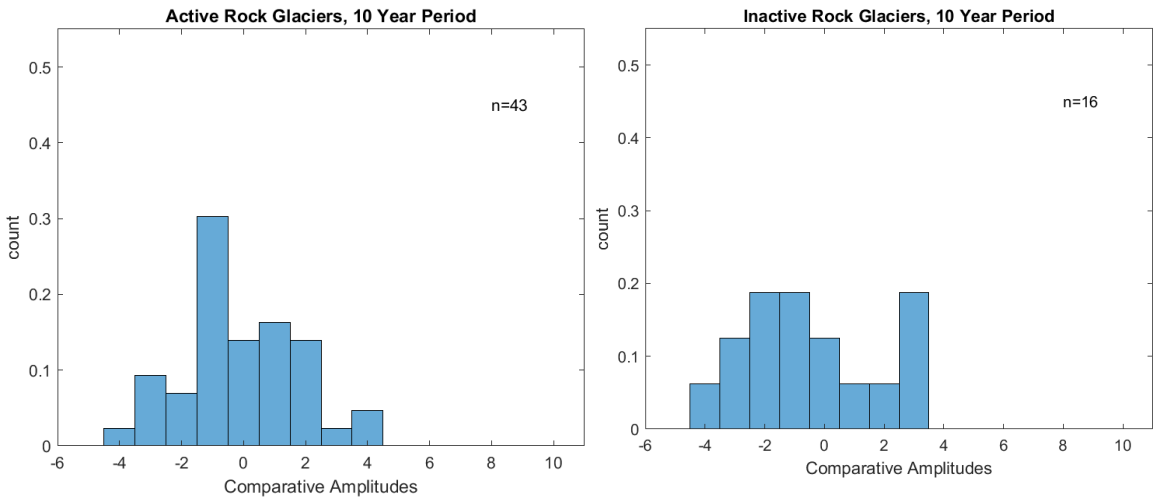

Figure 4.6: These 20 histograms show the comparative amplitudes of the active (left) versus the inactive (right) rock glacier fit functions. The axes on all the histograms are the same with the count being measured in percent. The average comparative amplitudes is the same for active and inactive rock glaciers at all periods except the one year histograms, in which the inactive rock glaciers had an overall higher comparative amplitude than the active rock glaciers, meaning that it varies in temperature more annually. The plots become less similar at longer periods but the fit function is less accurate for longer period signatures because of the lack of regular wintertime data.

Chapter 5: Discussion and Conclusions

DISCUSSION OF RADAR INTERFEROMETRY

Based on the radar interferometric analysis, the rock glaciers were classified into categories: active, inactive, and uncertain. The active rock glaciers (54 rock glaciers in the study area) have an InSAR derived phase rate of at least 0.2 radians per year in magnitude, regardless of sensitivity. An inactive rock glacier (20 rock glaciers in the study area) is a rock glacier with a phase rate of less than 0.2 rad/yr and a sensitivity of greater than 0.2. The sensor is able to detect displacement on these rock glaciers, but it does not, indicating that there is no movement. The third category is composed of uncertain activity rock glaciers (13 rock glaciers in the study area). These are rock glaciers with a low sensitivity (<0.2) and a low apparent phase rate. Because the sensor is unable to accurately measure these, even if there is movement, it would not be measured so it cannot be determined from just the radar interferometric data whether they are active or not. Radar interferometry is unable to determine the difference between inactive and relict rock glaciers because neither category is able to flow downslope. For the purpose of this portion of the study, inactive and fossil rock glaciers are both grouped in the category inactive because they do not contain sufficient ice to flow. Radar Interferometry can only determine activity based on flow, not on ice content, so inactive and fossil rock glaciers are the same in terms of activity as characterized by radar interferometry. Thermal analysis would be a better method to determine ice content in non-moving rock glaciers. Figure 5.4 shows maps of the distribution of the three categories of rock glaciers.

Noise is present in the time series, taking the form of apparent movement back and forth at each observation. The rock glacier does not have actual displacements of that magnitude over such short time spans, so the effect of noise was reduced in the classification process by using the average flow rate, instead of total displacement over time. Noise could also be reduced using a stronger filter, however, that could interfere with the actual movement signal and reduce the amount of movement observed. A longer observation period would allow increase the amount of displacement away from the original position and could help to reduce the role of noise in the final displacement values. Extending the time series would also provide more evidence of seasonal variation in flow. Changes in the flow patter on the rock glaciers would be visible in a longer time series, as well. Gradual slowing of the rock glacier could indicate a loss of ice and could be a warning of a gradual reduction in the water resource that rock glacier provides.

There is a seasonal variation in the flow of rock glaciers as measured by the interferometric time series. During the summer months, the displacement of rock glaciers trends toward the negative direction (away from the sensor). This happens in both flow directions, toward and away from the sensor (positive phase rate toward the satellite, negative phase rate away) (Figure 5.1). For a rock glacier flowing toward the sensor, the displacement goes toward zero, away from the sensor, while for a rock glacier flowing away from the sensor, the displacement increases in magnitude during the summer, implying more movement away from the sensor. Because the direction of seasonal displacement in the summer is always away from the sensor, regardless of rock glacier azimuth, the seasonal signal likely indicates vertical displacement. It is also unlikely to be in a horizontal direction because that would indicate the rock glacier would have to have

seasonal upslope flow. Vertical displacement seasonally means there is a relative subsidence in the rock glacier surface in the summer and a relative uplift of the rock glacier surface in the winter.

One possible cause of winter uplift is the expansion of the ice layer below the surface of the rock glacier. The top of the internal ice layer will experience some warming and cooling seasonally. This may be referred to the active ice layer because it changed annually. The active layer of the internal ice, like other permafrost features, freezes and thaws seasonally with seasonal temperature variations. Permafrost can cause mass movement and sediment transport due to the frost wedging and the annual expansion and contraction of the ice (Easterbrook, 1999). The depth to the ground ice is affected by ambient air temperature, which varies seasonally, so the ground ice would be deeper in the summer, when the temperature is warmer. The winter expansion and summer melting of the active layer could produce vertical displacement at the surface by pushing the surface up toward the sensor in the winter and subsiding away from the sensor in the summer, producing the signals seen in the rock glaciers. Figure 5.1 depicts displacement with seasonal signatures in rock glaciers that flow both toward and away from the sensor. The presence of seasonal uplift and subsidence, even on rock glaciers that are not flowing downslope could indicate the presence of ground ice and help to identify potential water resources, without using thermal imagery. Seasonal signals are distinguished from noise because they are larger in amplitude and in wavelength. The reoccurrence of the away-from-sensor movement in only the summer months and the movement being on a scale greater than 0.2 radians, indicates that this signal is not simply noise.

Two peaks in the elevation distribution of each of the rock glaciers correspond to the genesis of the rock glaciers. The rock glaciers at higher elevations (higher than 3100m) are the ones found on peaks with glacial history including Blanca and W Spanish Peak. Rock glaciers at lower elevations (lower than 3100m) are found on peaks with no glacial history including the Sheep Mountains and Mount Mestas. This indicates that rock glaciers are glacially derived while at lower elevations they are periglacially derived, but the genetic classification has little bearing on the flow of the rock glacier, since flow is found on both types of rock glacier. There is no correlation between elevation and flow rate, as there are rock glaciers at all elevations with high and low rates of phase displacement. This indicates that rock glacier genetic classification does control the movement of the rock glacier or the ice content.

The strong influence of rock glacier flow azimuth on apparent phase displacement (Figure 5.3) is a challenge to overcome when identifying the activity classification of a rock glacier. The quantification of sensitivity and imposition of minimum prerequisites to be considered can help to reduce the limitations. Another way to eliminate the azimuth is to combine interferograms produced from the descending orbit radar sensor, as was used in this study, with interferograms produced from scenes taken on the ascending orbit. The different look directions, when combined would produce actual ground displacement, as opposed to measuring only the component of displacement in the look direction. In order to determine the actual displacement, as well as determine any displacement on the rock glaciers that flow orthogonal to the sensor, the combination should be used. Being able to sense movement at any angle will increase the sample size of rock glaciers that can be analyzed and contribute to present and past climate models. It will also fill in the

distribution of data on north and south facing rock glaciers, instead of focusing on only the east and west flanks of peaks. Due to the near polar path of the satellite orbit (12-13 degrees from N/S), this approach is less sensitive to flow in the N/S direction (Wright, 2004). Being able to sense rock glacier flow in every direction would eliminate the need for an uncertain category of rock glaciers, so all of the rock glaciers in the area could be sorted into active (flowing) or inactive (nonflowing) categories.

Based on the sensitivity coefficient derived from the look direction and the flow direction of the rock glacier, two azimuths are the least able to be recorded are approximately 40 and 160 (Figure 5.2). The look direction vector is at an azimuth of 283, so, on a horizontal plane, the least sensitive azimuths would be perpendicular (193 and 13). Since the rock glaciers flow downslope, a direction inherently away from the sensor in the vertical direction, the sinusoidal relationship between azimuth and sensitivity is shifted. The sensor points toward the west and is most sensitive in directions away from the sensor because the vertical component contributes to the away-from-sensor sensitivity. In rock glaciers with an azimuth toward the sensor, the sensitivity is lower because the away-from-sensor vertical component is in opposition to the toward-sensor horizontal component.

DISCUSSION OF THERMAL ANALYSIS

Amplitudes of periodic fits were differenced with those from the weather data (ambient air temperature) for all periodicites. The inactive rock glaciers showed a greater deviation from the air temperature than the active rock glaciers on a one year periodicity. The average comparative amplitude for the 1-year periodic fit of the active rock glaciers and the weather data was 4.0, while for the inactive rock glaciers it was 5.8. Longer

periodicities (2 or more years) had similar trends of difference to the weather data in both active and inactive. Thus, inactive rock glaciers had a larger variation in temperatures on a yearly scale overall than the active rock glaciers. This suggests that the ice within the active rock glaciers may modulate the surface temperature, keeping the temperature of the surface cooler during the warm months than the inactive rock glaciers, decreasing the amount of temperature fluctuation. One active rock glacier had a negative comparative amplitude, indicating that it varied less than the air temperature throughout the year.

The standard deviation in comparative amplitude for all of the rock glaciers is 2.46. This is high, relative to the comparative amplitude values, but there are several reasons for this. The active rock glaciers had a bimodal distribution of comparative amplitude that was related to elevation. Higher elevation rock glaciers had, on average, lower comparative amplitudes, meaning that temperature varied less on rock glaciers at higher elevations. This could be due to the fact that at higher elevations, like the Ute Creek weather station, the air temperature varied less than at lower elevations, like the Walsenburg weather station (Figure 4.2). The standard deviation may be raised in the inactive rock glacier comparative amplitude because of the smaller sample size, as well as the inclusion of inactive and relict rock glaciers in the inactive category for this study. Some rock glaciers that were not observed to move and were therefore classified as inactive may contain ice, and therefore would have different thermal properties than the fossil rock glaciers that contain no ice. Based on the results of this study, the inactive rock glaciers would have lower comparative amplitudes than the relict rock glaciers because they contain ice to modulate the temperature.

The reliability of these trends could be improved using a larger sampling of rock glaciers, so that there are more than 20 inactive rock glaciers with which to identify trends. The smaller number of inactive rock glaciers could create random biases in the trend and confirm the reliability of observed greater comparative periodicity in inactive rock glaciers. Including more rock glaciers would also allow for better quantification of the differences between the two categories and may help to identify rock glaciers of unknown activity classes.

This study classified rock glacier activity, initially, based on movement, not based on ice content. The results indicate that moving and non-moving rock glaciers are different thermally, but the rock glaciers have not been classified thermally. Producing a thermal model to refine the distinguishing characteristics of ice filled rock glaciers from ice free rock glaciers is a future step that could be used to classify rock glaciers by ice content remotely. The ice content is the more important factor in determining the water resource potential of a rock glacier.

Movement is a proxy for ice content because movement occurs within the ice portion of the rock glacier. Inactive rock glaciers may contain ice, but do not flow, so the ice could be detected using thermal methods, though they would not be identified as a water resource by radar interferometry because they do not move. Thermal analysis could find water resources in inactive rock glaciers that could not be identified by other methods. At extremely low temperatures, when rock glacier flow may be slowed, the thermal method of identifying ground ice could be more useful because it does not rely on the proxy of surface movement to identify ground ice. This could be especially important on Mars, as the surface temperatures are colder than on Earth, so flow may not

be a reliable way to classify rock glaciers. The use of thermal imagery, which is already available on Mars, could allow for more accurate classification of rock glaciers, and other landforms containing ground ice.

While there are differences in the short term periods, there may also be differences on a time scale that is longer than can be measured over the timespan of this study. With 20 year coverage, the longest period cycle is 10 years. Quasi-decadal process like sunspot cycles (solar flares) would not be accounted for in the fitting curve but may have an effect on the measured temperature data. Temporally more extensive observation would also allow the fit function to be refined to fit the data better, both in the time span used in the study and the frequency of observation.

The lack of winter data is a challenge in this specific study, but future studies could use multiple sources of thermal data to attempt to have increased temporal resolution or use frequent ground based land surface temperature measurements to refine the curve fitting model. Landsat 5 could easily be used to supplement the existing thermal imagery on the same spatial and temporal resolution. It is also available from RS Lab and would extend the time series by over a decade. Extending the time series, while it may introduce long term signatures, like sun-spot cycles, it could also increase the accuracy of long period fit functions. A thirty-year thermal time series would also create the potential to monitor the change in ice content over time. If the amplitude of the one-year temperature variation on an active rock glacier increases over time, this may indicate that the rock glacier is becoming more inactive, and losing ground ice. The loss of ground ice is important to monitor; people use water from the rock glaciers to survive and the loss of

ground ice over time puts their access to water in danger. Monitoring the rate of ice loss provides an estimate of how long the water would be available to those who need it.

Differences between the rock glacier fit curves and the weather fit curve also occur in the longer periods, but they depict similar frequency distributions between active and inactive rock glaciers and have mean values near zero. Additionally, the distributions present much wider spread of values in each category, suggesting the fit curve may not be able to measure with accuracy the longer period functions as the short period function components. More data is needed to establish longer period trends because, with the randomness associated with short term observation, more is needed to know what the general trends are. A low temperature measurement in one year can help establish the fit line for that specific year, but low temperature measurements would be needed over the entire 10 year period to fit a 10 year period curve.

SOURCES OF UNCERTAINTY

The Radar Interferometry time series have some sources of error that should be noted. In the creation of the time series plots, the phase displacement values of every pixel within the rock glaciers was averages together. Each rock glacier was a different size and contained a different number of pixels. The entirety of each pixel may not have been inside the rock glacier, with some extending out of the boundary being included in the average. The location of the pixel was calculated from the center of the pixel, so if the center of the pixel was within the boundary, more than half of the pixel was contained as well. The presence of other ground coverings within the pixel could skew the calculation of average phase displacement. This would be a larger issue for smaller rock glaciers as the ratio of perimeter to area is larger, so a larger percentage of the rock glacier pixels

would extend outside the boundary. The inclusion of vegetation, in particular, could provide a large source of noise, as vegetation growth would be a seasonal displacement on a larger scale than the potential movement of the rock glacier.

Averaging all the pixels together may present a source of error in that the rock glacier does not flow at a constant spatial rate. The greatest flow speed would be found in the center, with ice thinning toward the edges of the rock glacier. This is the very process that produces the distinctive ridges and furrows on the surface of the rock glacier, but it means that, even though part of the rock glaciers is flowing, another part may not be. The presence of displacement does indicate flow, but the maximum amount of flow may not be exactly the same amount as the phase displacement of the averaged pixels.

A similar challenge is found in the thermal data used in this study. Due to the cloud mask used on the land surface temperature images, many of the pixel values are 0, despite the actual ground surface temperature not matching that value. The greater number of observation scenes and longer time span does allow for the emergence of seasonal patterns in the time series, but the actual measurements are more temporally sparse than the number of scenes initially suggests. While it is easy to disregard any values that are 0 in the time series due to cloud cover, a greater challenge is when the rock glacier is only partially covered by clouds. The pixels were averaged together without accounting for those pixels with a value of 0 that were the result of the cloud mask. Decreasing the number of pixels in a rock glacier increases the magnitude of uncertainty. Because clouds are the source of this error, the magnitude of error would also be seasonally dependent, as winter months generally have a higher frequency of

cloud cover than summer months. The lack of winter data could worsen the numerical periodic fit of the temperature data,

There are also fewer pixels in each rock glacier in the thermal data due to the greater pixel size (90m as opposed to 15m for Sentinel). The smaller number of pixels would exacerbate the same issues of averaging that were present in the radar interferometric data. An error in one pixel, or presence of a cloud mask, would have a much greater effect on the average for the entire rock glacier because there are fewer other pixels to average with. The pixels are larger, so they cover a larger area outside the rock glacier, if they are only partially contained within the boundary. This also means that each pixel would contain a wider variety of land covers that could interfere with the temperature measurement.

The modelling of thermal skin depth from the land surface temperature function is based on several assumptions. The first assumption is that the structure of the rock glacier consists of an upper layer of solid rock and below that is a layer of solid perennial ground ice. The depth to the boundary between the two layers is the skin depth. The rock glacier in reality may have seasonal melting in the upper portions of the ice layer, and the ice layer may contain talus and debris. The upper portion is also not only composed of rock, but pores may be filled with air and portions of interstitial ice. All of these assumptions produce uncertainty in the skin depth calculation, and the actual depth to the ice would vary on each rock glacier. Daily temperature fluctuations only have a skin depth that is much lower than the depth to the ice, so the daily temperature fluctuations have very little effect on the ice within the rock glaciers. Annual variations, however, would have a much greater skin depth and would interact with the ice layer. Longer term changes, like

climate change or sun-spot cycles, may even cause changes in the ice layer, by melting or freezing the upper active ice layer.

In order to calculate skin depth, the period at which the LST fit function diverges from the regional air temperature data is related to how much the interior ice affects thermal fluctuations over long time scales. Plots of the periodicity and the amplitude for each rock glacier were compared to the weather station data from NOAA's Ute Creek, Colorado station. The difference between the Ute Creek Weather station and the rock glacier amplitude for all of the rock glaciers at each of the 10 period timeframes.

The skin depth calculation based on periodic variation determined that the rock glacier skin depth is likely 4.4-7.3m. Previous studies have observed the depth to the ice within rock glaciers to be on a similar scale. Observations do vary, however. Easterbrook, 1999, claims that rock glaciers have ice within 1 meter of the surface. Potter, 1972 made observations of 1 meter of debris at the surface of a rock glacier and a solid ice core at a depth on a scale of 10s of meters. Fisch, 1979 drilled 10m into a rock glacier to find a solid mix of ice and debris. Evin, 1983 observed ice at the bottom of a 4m crevasse. There is a wide range of depths of ice within rock glaciers, and it will vary from rock glacier to rock glacier because rock glaciers have different activity classifications and ice contents. Each rock glacier in the study area likely has a different depth to the ice, so the skin depth calculation shows whether or not the ice, at a depth of 1-10m of depth based on observation, would affect the surface temperature. Because the skin depth calculation for all compositions is within the range of observed ice depth, it indicates that variation in surface temperature would reach the depth of the ice, as well as the ice having an influence on the surface temperature on a one year scale. The fact that on a one year scale

ice within a few meters of the surface would have an affect on temperature lends credence to the use of comparative amplitude for distinguishing ice filled and ice free rock glaciers.

Not all of the rock glaciers had sufficient temporal coverage of thermal imagery, therefore they could not all be fit accurately. 21 rock glaciers (the vast majority on Blanca Peak) were culled from the temperature time series after fitting periodic functions, before plotting the periodic comparisons. Reasons for culling included a fit line that did not seem to account for the temperature extremes and large gaps in the measured bad surface temperature data, especially in the low temperature winter (Figure 5.5). Rock glacier 74 is an example of poor winter temperature coverage. The fit line seems to fit the data that is present well, but there are no measured points around the troughs of the sinusoid throughout the entire timeline. Rock glacier 79 is an example where the fit line does seem to fit the data, especially where there is a large number of measurements in the alter portion of the time series. These were removed in order to reduce the uncertainty in comparative amplitude.

CONCLUSIONS

This study has demonstrated that thermal remote sensing, particularly LST calculations, may distinguish active and inactive rock glaciers. The use of thermal data to characterize rock glaciers could be a useful tool because of the wide availability of the data and simplicity of data processing. Thermal processing looks at ice content, rather than the proxy value of flow rate. It also has broader implications to Martian exploration and water resource monitoring. There is currently no radar interferometry system on Mars, however there is a multispectral imager with thermal infrared capabilities.

Identifying landforms that contain ice would be invaluable to organizing Martian exploration. In order to characterize ice content of rock glaciers, a long-term high frequency observation of land surface temperature would be necessary. The issue of cloud cover would be reduced for Martian observation, but other problems could arise from the extreme low temperatures and diurnal variations. The difference in periodicity of solar radiation daily, seasonally, and annually may change the way in which the periodicity of rock-ice bodies can be compared.

Radar interferometry is a better option for determining the activity of rock glaciers over a short time period, but only observes movement, which is not directly linked to the amount of ice contained within the rock glacier. Thermal analysis, with high temporal resolution, could provide an estimate of the quantity of ice contained within the landform, which is more important in resource management. Future studies could carry out thermal modelling of rock glaciers and conduct studies on a larger sample set of rock glaciers to establish distinguishing characteristics, as well as conducting ground truth studies to monitor temperature in a highly localized survey.

The goal of this study was to determine the ability of remote sensing methods to categorize rock glaciers into activity classifications. The rock glaciers were successfully classified based on flow using radar interferometry, which was then used to test the ability of thermal infrared imagery to establish differences between categories. While the thermal processing completed in this study did identify differences in active, ice filled, rock glaciers and inactive, ice free, rock glaciers, the methodology could be further refined to work independently of radar confirmation. Based on the thermal skin depth, ice within rock glaciers does have an effect on the surface temperature on an annual scale, so

that effect may be measured and quantified. The thermal methodology has more wide-reaching implications because of its potential application to Martian rock glaciers and ice resource surveying on Mars and Earth.

Revisiting the hypotheses for this study, the movement of rock glaciers was successfully determines using radar interferometry, both over a three-year period, and seasonally. Using the movement distinguished using radar interferometry, the activity of rock glaciers was determined and the active and inactive rock glaciers were found to have different comparative amplitudes of temperature variation. Rock glaciers with ice did behave thermally differently than the rock glaciers without ice. The depth to the ice within the active rock glaciers could not be precisely determined, however a general estimate of skin depth could be calculated from the annual temperature variations and was found to be at a shallow enough depth that the presence of ice would affect the temperature of the land surface.

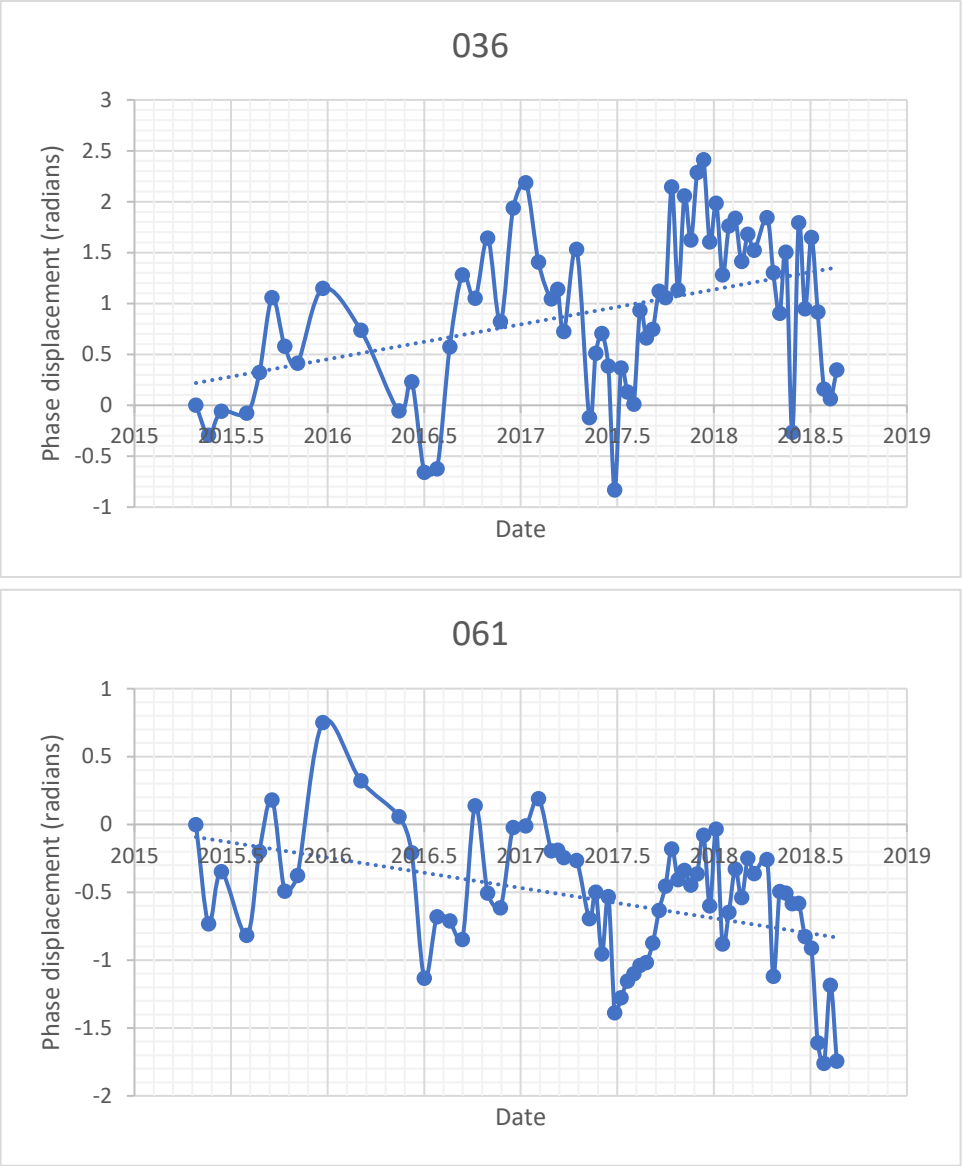

Figure 5.1: These two rock glacier displacement time series display seasonal behavior. The first time series flows toward the sensor in general, but in summer months, the motion changes to away from the sensor. The second time series is a rock glacier that flows away from the sensor generally, but in the summer the rate of displacement away from the sensor increases.

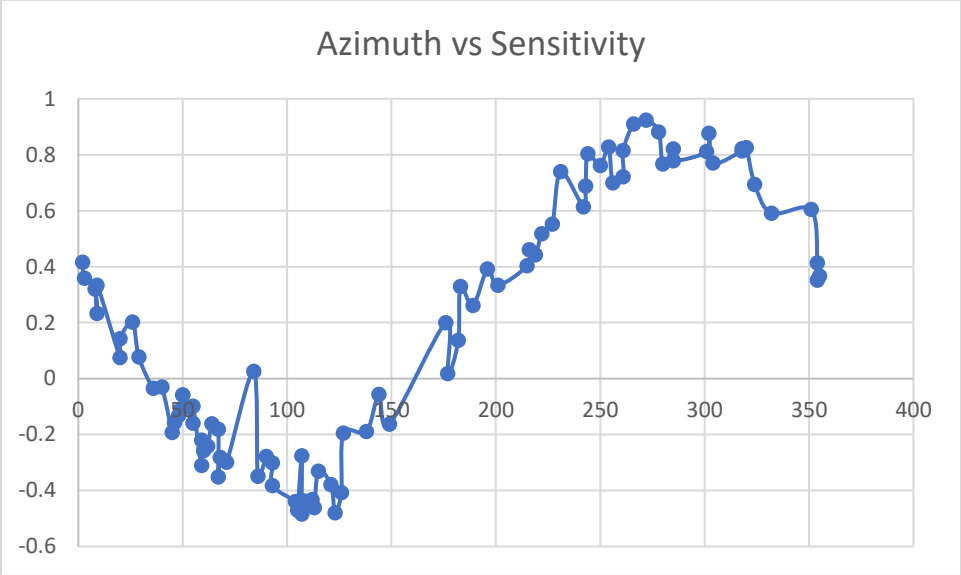

Figure 5.2: The sensitivity is directly related to the azimuth, with flow directions parallel to the sensor look direction having a higher sensitivity, than a perpendicular flow direction. The vertical component of flow causes the away-from-sensor direction of flow to have a higher sensitivity, and creates the vertical shift away from zero on this plot.

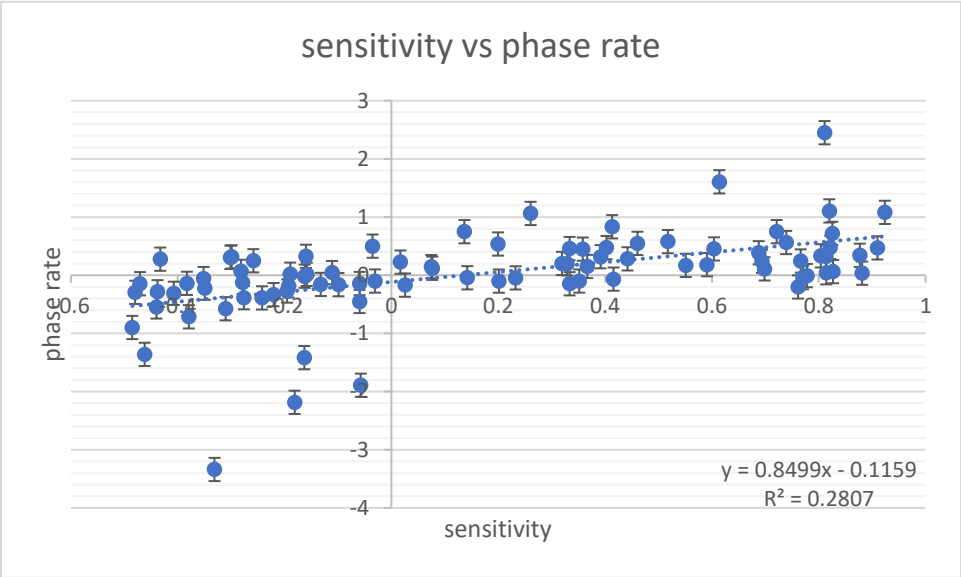

Figure 5.3: The sensitivity has a generally linear relationship to the amount of displacement that can be measured on the sensor over the three year period. This is because lower magnitude sensitivity rock glaciers, even if they are moving, cannot be measured by the sensor. The higher the magnitude of sensitivity, the more accurately the sensor will be able to distinguish displacement.

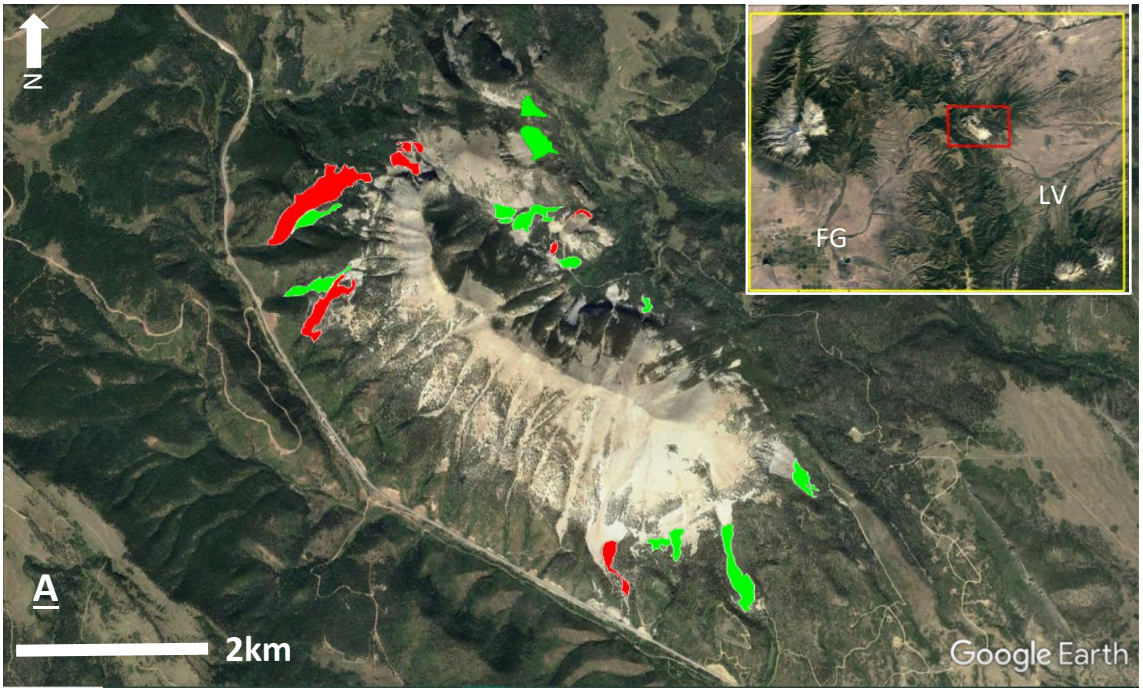
N
LV
FG
A
2km
Google Earth

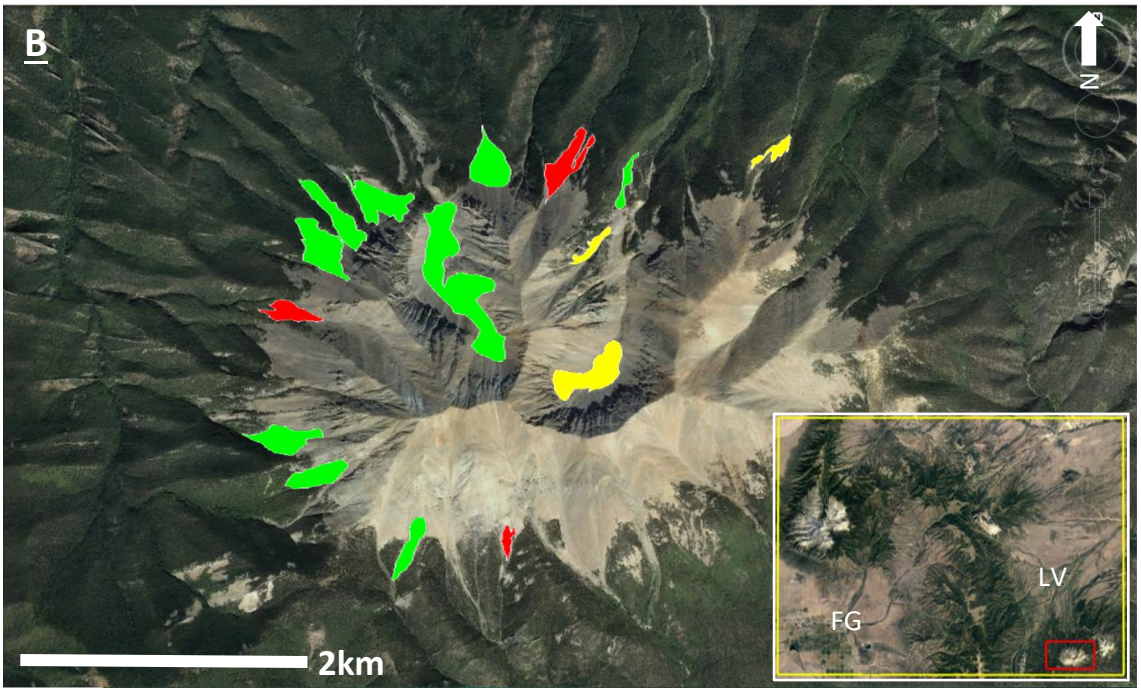
B
N
LV
FG
2km

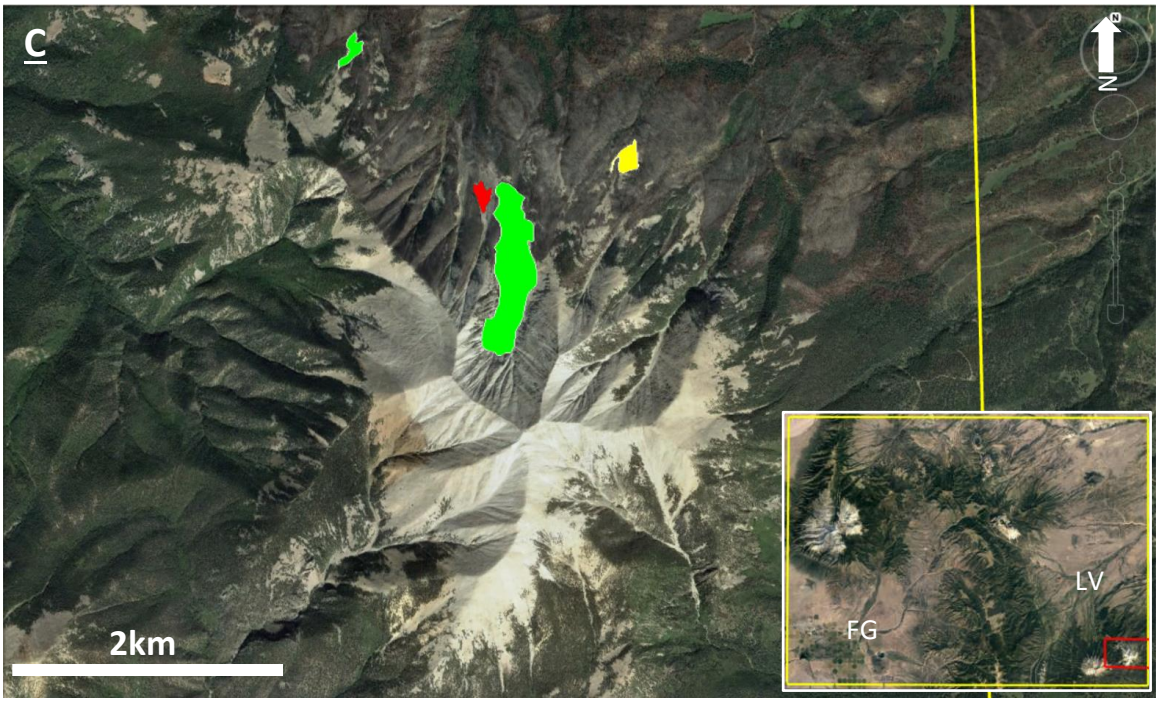
C
N
2km
LV
FG

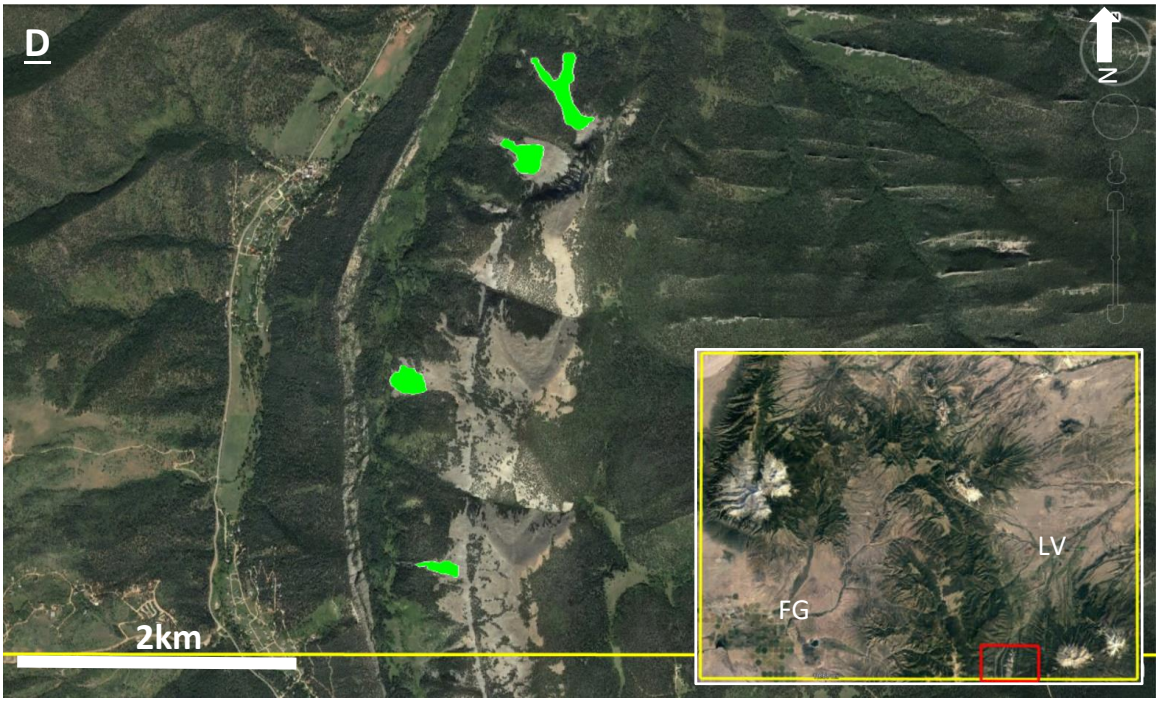
D
N
2km
LV
FG

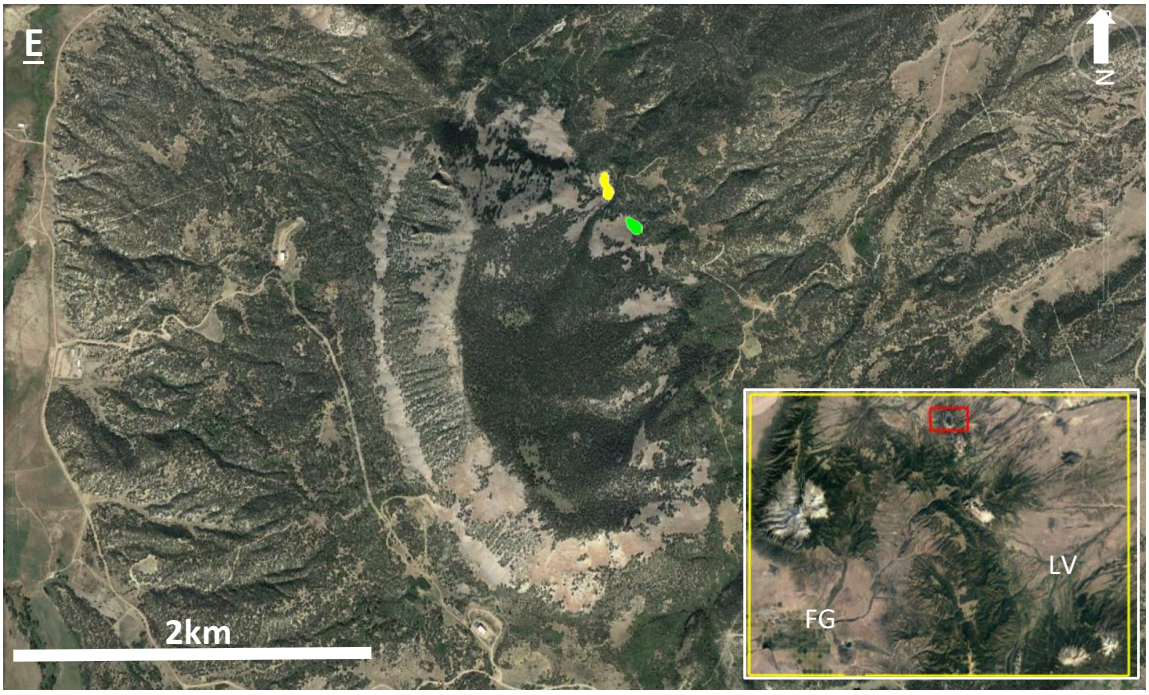
E
N
2km
LV
FG

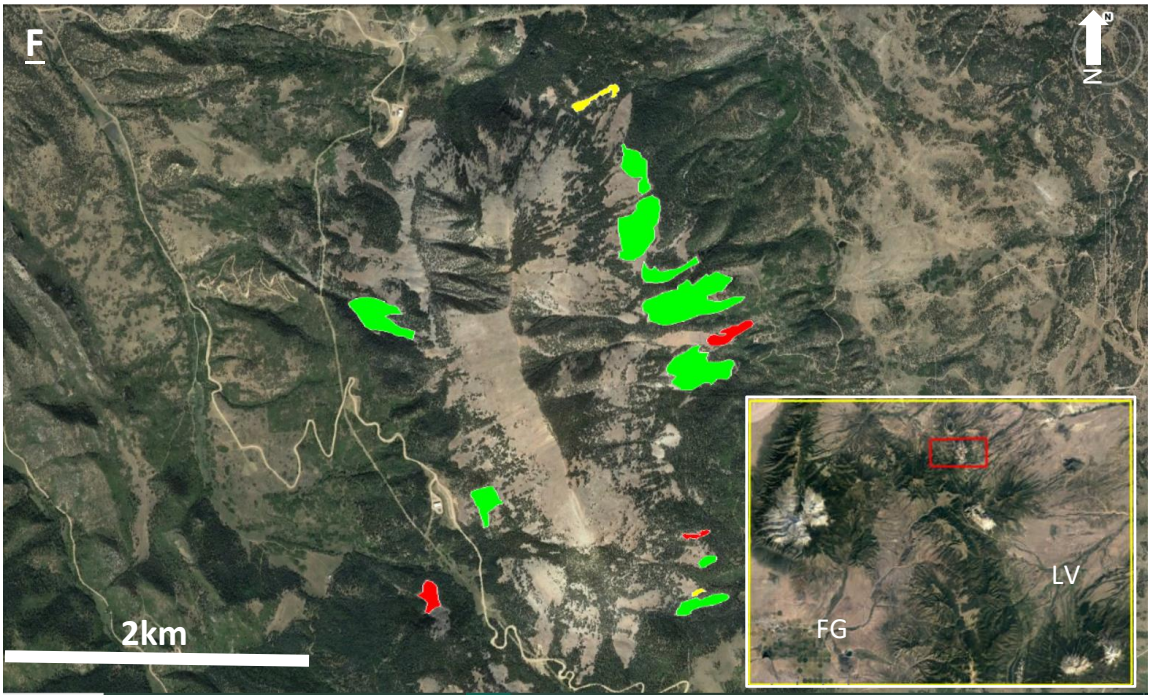
F
N
2km
LV
FG

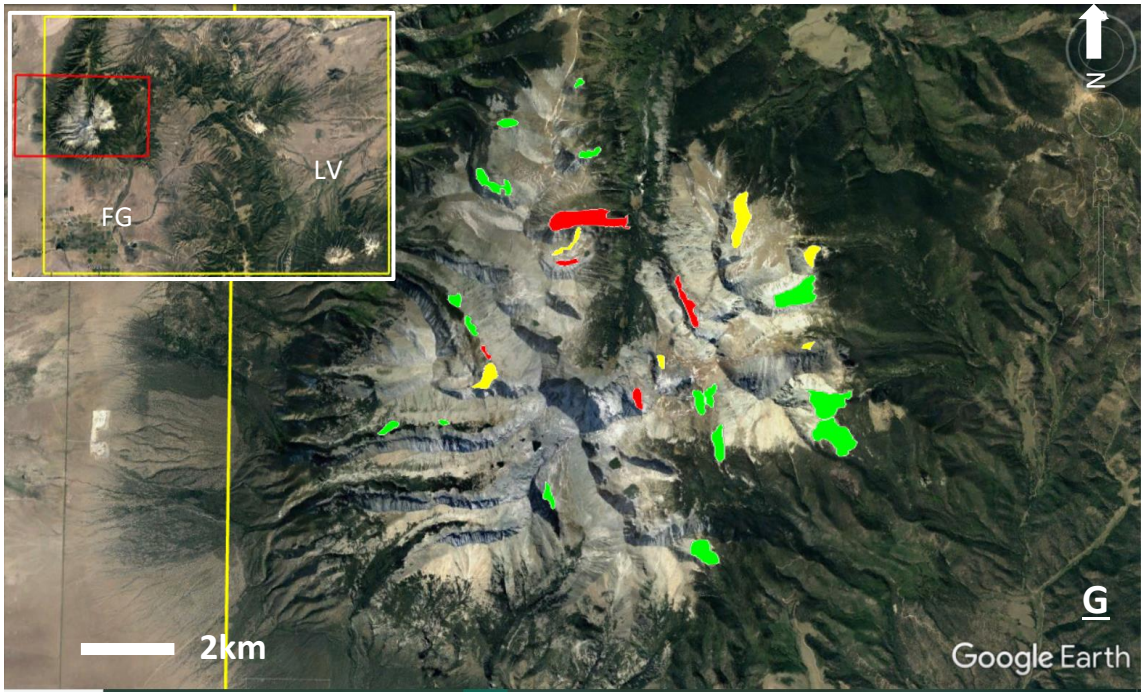

Figure 5.4: maps A-G show the exact same views of the rock glaciers as depicted in 2.4 in Chapter two, but the rock glaciers have been colored to match the activity as determined by radar interferometry. A is Mount Mestas. B is West Spanish Peak. C is East Spanish Peak. D is White Ridge. E is North Sheep Mountain. F is South Sheep Mountain. G is Blanca Peak. Red represents inactive rock glaciers. Green represents active rock glaciers. Yellow represents rock glaciers with an uncertain activity classification.

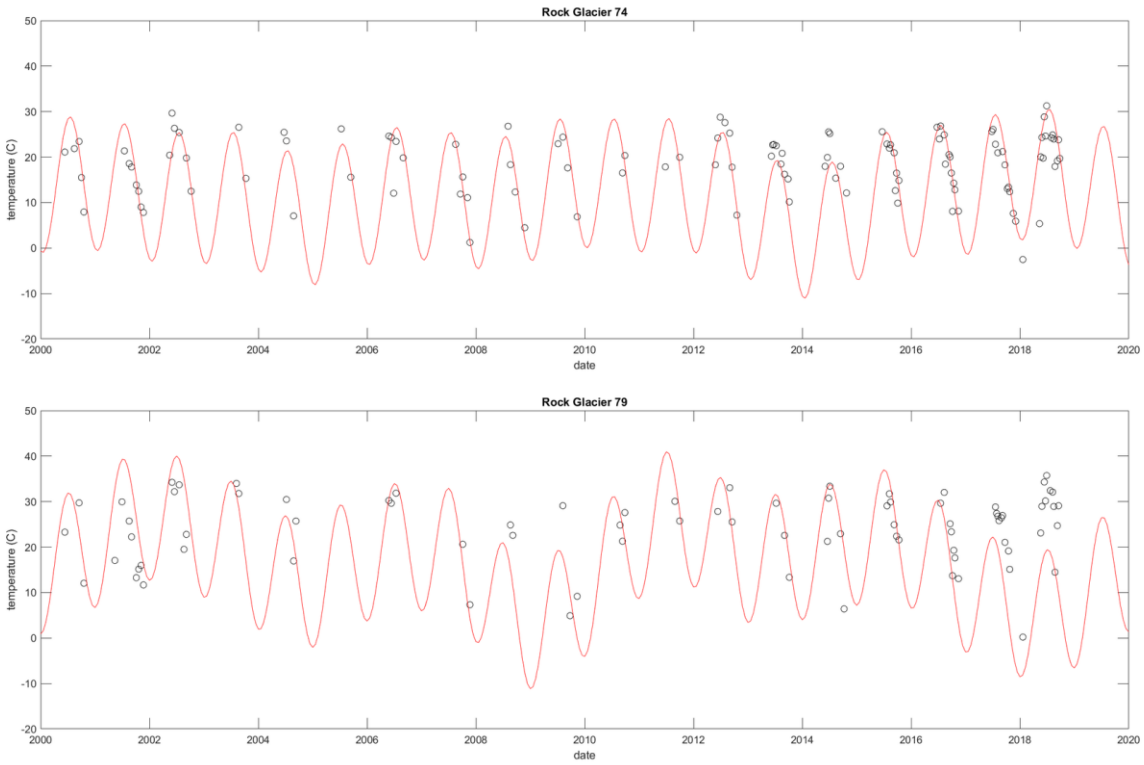

Figure 5.5: These two land surface temperature time series represent the two groups that were culled from the time series amplitude analysis. The first time series (74) does not have consistent wintertime observations, so the low values to fit the line to don't exist and, over increasing periods, cannot be accurately determined. The second time series shows a rock glacier with some timespans of good coverage, but the line does not fit them well. This is especially apparent in the last two years of the time series with several points underestimated by the fit line.

Appendix A

This portion contains all of the plotted time InSAR displacement timeseries. Each rock glacier has its own graph of phase displacement over time with a linear trendline. Attached to the graph is an information bank for each rock glacier with the peak that the rock glacier lies on, the mean elevation of the rock glacier, the azimuth of the rock glacier, the sensitivity coefficient magnitude representing the ability of the satellite based sensor to determine the displacement in the look direction. It also contains the slope of the trendline, representing average flow rate. The activity classification is based on the average flow rate, so as to minimize the effects of noise. Any rock glacier with an average flow rate of magnitude greater than 0.2 is considered active. The sign of the slope represents the direction of rock glacier flow whether that is toward (-) or away from the sensor (+). In order to convert the phase displacement to sensor line of sight displacement, the phase value may be multiplied by 0.445634cm/rad ($\lambda/4\pi$ where λ is the wavelength of the sensor, 5.6cm).

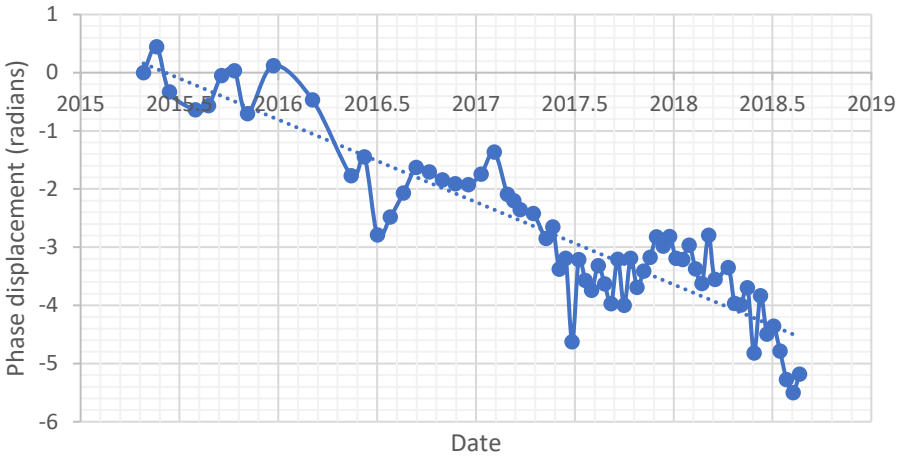

Peak: Mestas

Mean Elevation: 3016

Azimuth: 149

Average flow rate: -1.41675

Sensitivity: 0.16307

ACTIVE

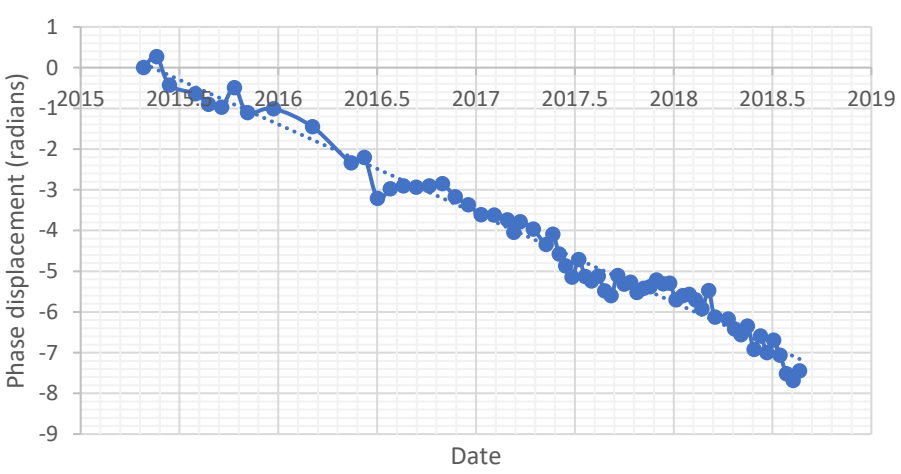

Peak: Mestas

Mean Elevation: 2986

Azimuth: 67

Average flow rate: -2.1849

Sensitivity: 0.18117

ACTIVE

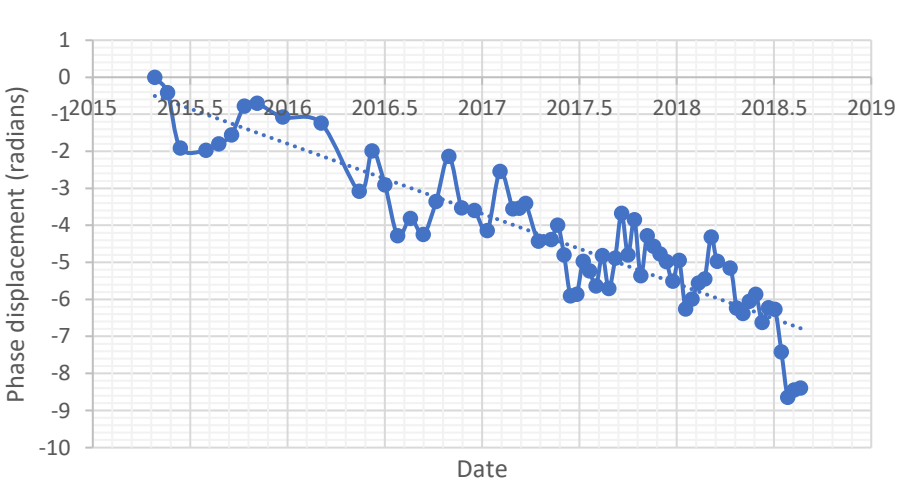

Peak: Mestas

Mean Elevation: 3037

Azimuth:144

Average flow rate: -1.89121

Sensitivity: 0.05721

ACTIVE

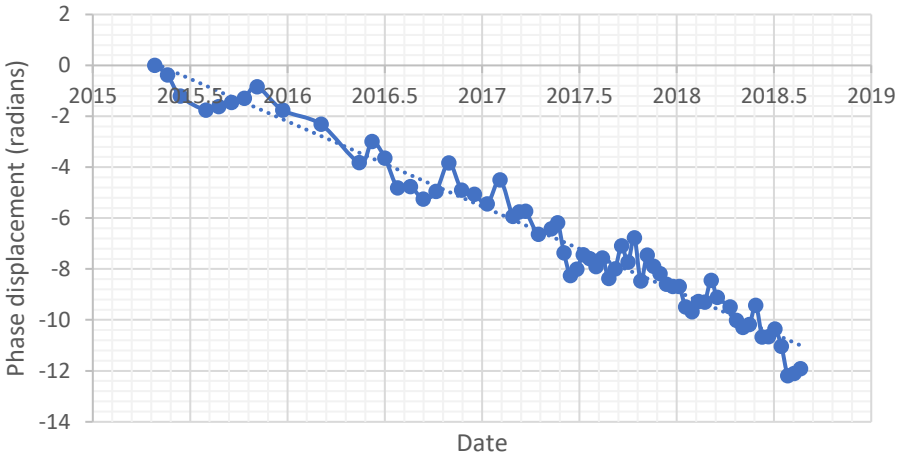

Peak: Mestas

Mean Elevation: 3016

Azimuth: 115

Average flow rate: -3.33917

Sensitivity: 0.33106

ACTIVE

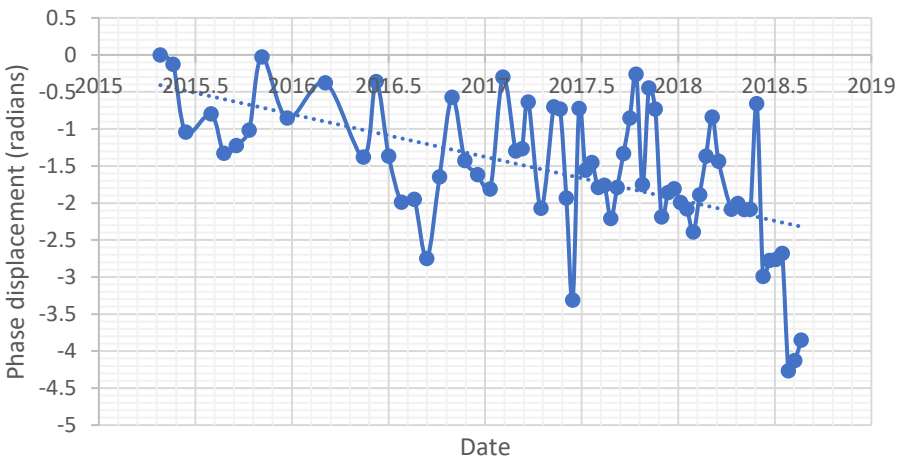

Peak: Mestas

Mean Elevation: 2960

Azimuth: 59

Average flow rate: -0.576

Sensitivity: 0.31052

ACTIVE

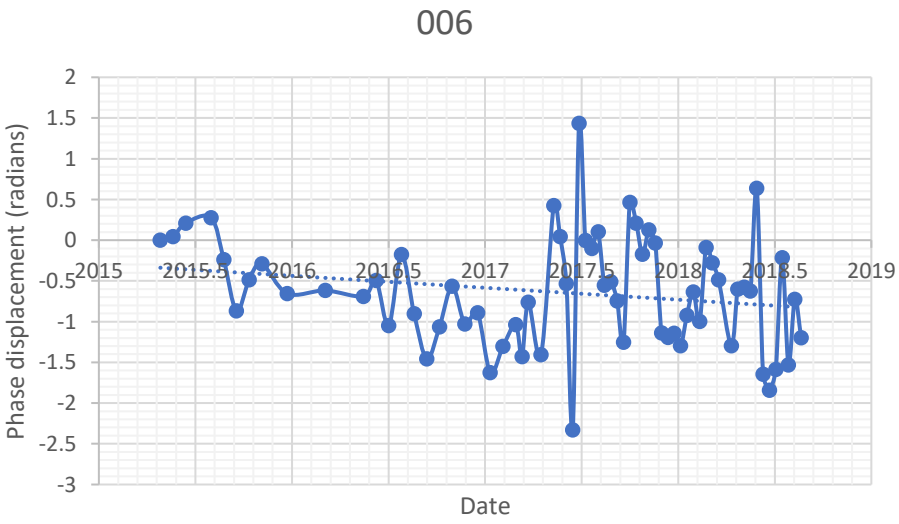

Peak: Mestas

Mean Elevation: 2865

Azimuth: 105

Average flow rate: -0.14632

Sensitivity: 0.4707

INACTIVE

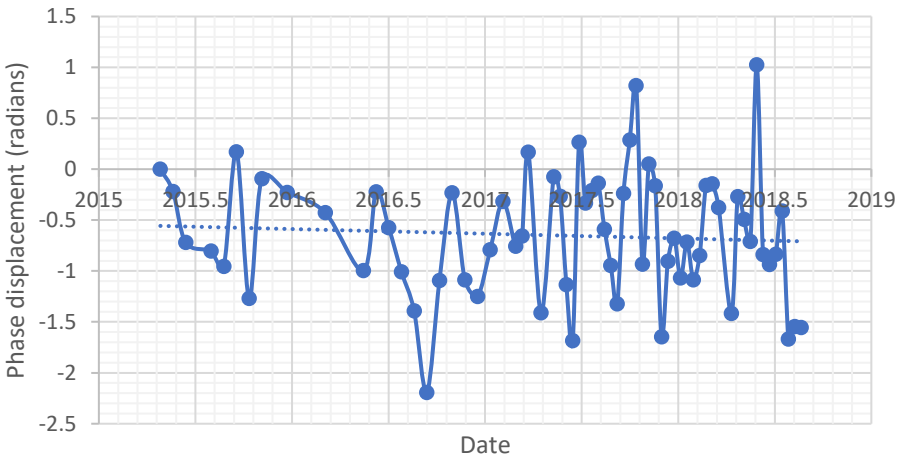

Peak: Mestas

Mean Elevation: 2963

Azimuth: 9

Average flow rate: -0.04569

Sensitivity: 0.232536

INACTIVE

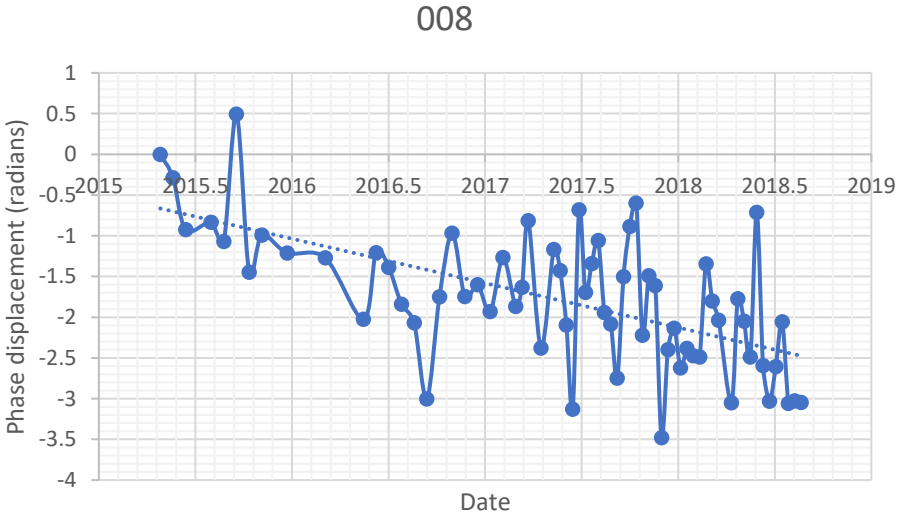

Peak: Mestas

Mean Elevation: 2948

Azimuth: 104

Average flow rate: -0.54534

Sensitivity: 0.43987

ACTIVE

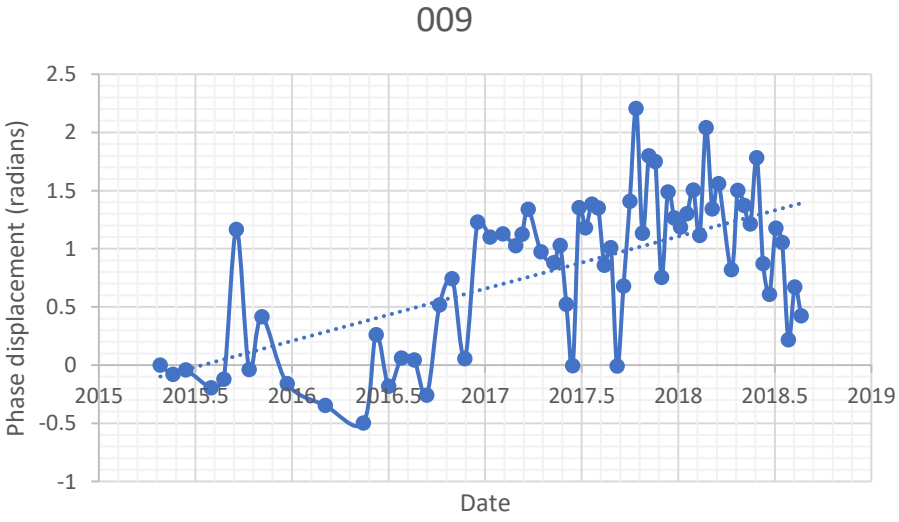

Peak: Mestas

Mean Elevation: 2954

Azimuth: 3

Average flow rate: 0.448804

Sensitivity: 0.358225

ACTIVE

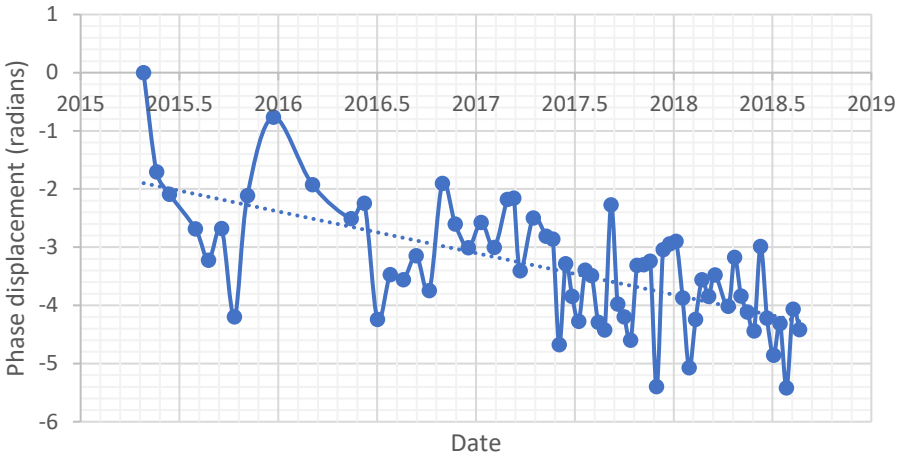

Peak: Mestas

Mean Elevation: 2738

Azimuth: 121

Average flow rate: -0.71518

Sensitivity: 0.37916

ACTIVE

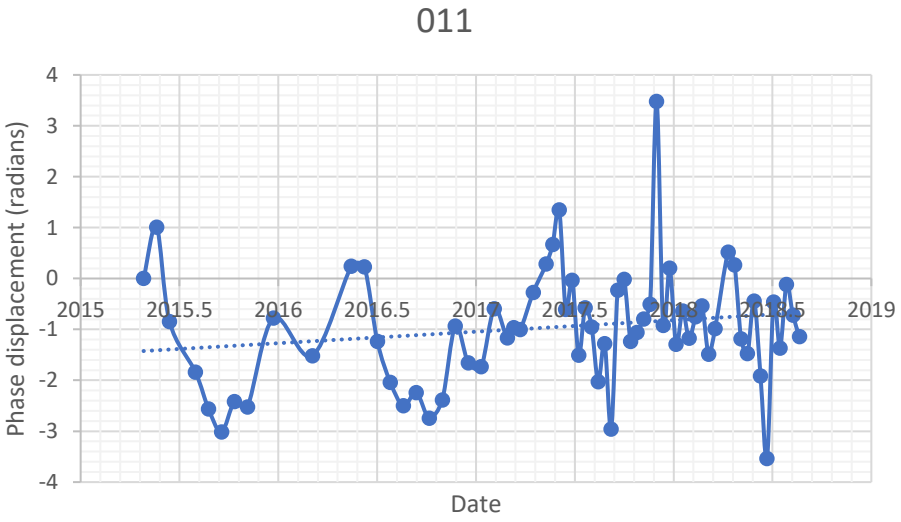

Peak: Mestas

Mean Elevation: 2656

Azimuth: 177

Average flow rate: 0.225878

Sensitivity: 0.017021

INACTIVE

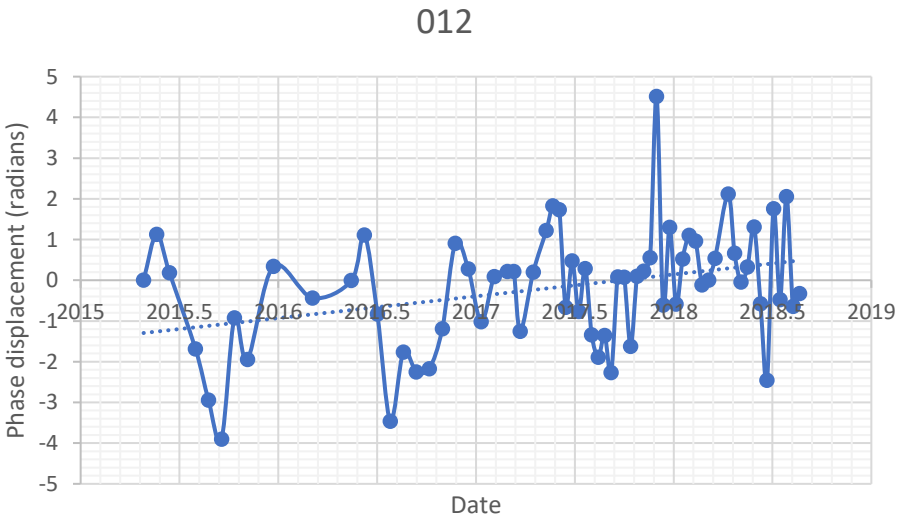

Peak: Mestas

Mean Elevation: 2757

Azimuth: 176

Average flow rate: 0.536559

Sensitivity: 0.199658

ACTIVE

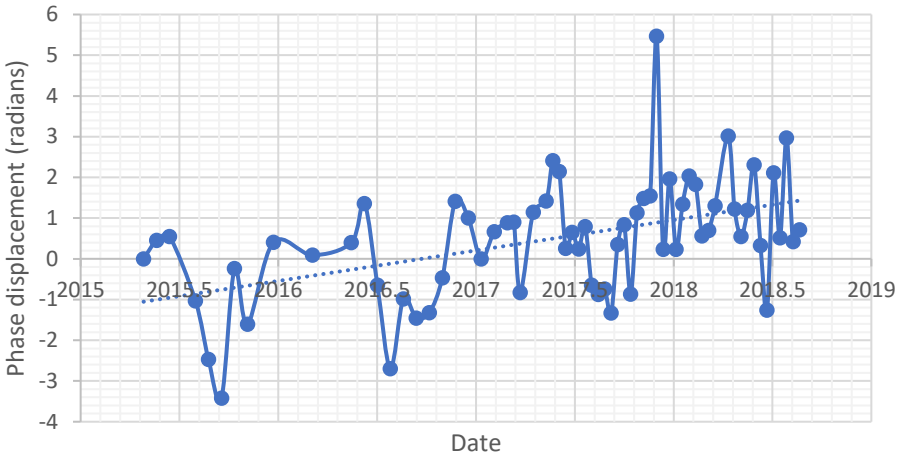

Peak: Mestas

Mean Elevation: 2765

Azimuth: 182

Average flow rate: 0.748401

Sensitivity: 0.13683

ACTIVE

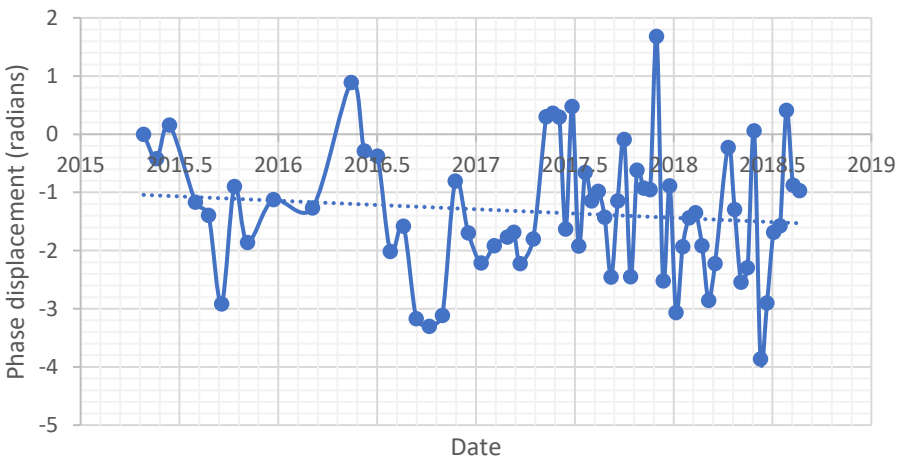

Peak: Mestas

Mean Elevation: 2660

Azimuth: 201

Average flow rate: -0.14693

Sensitivity: 0.333579

INACTIVE

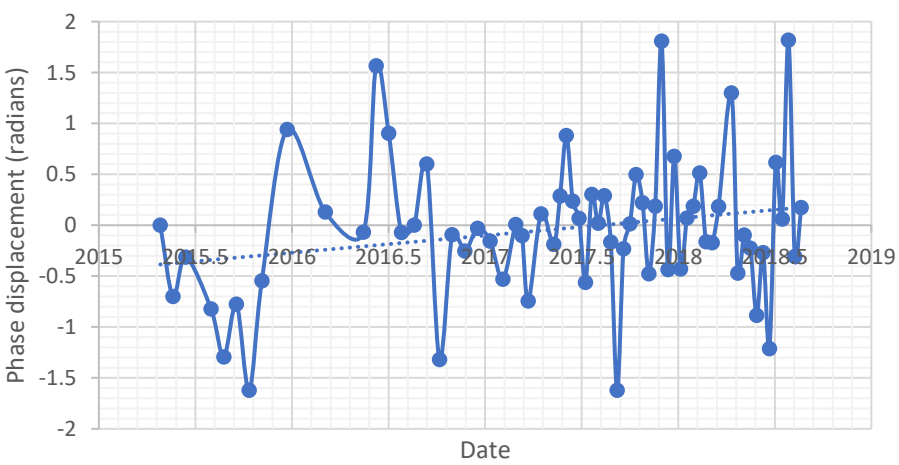

Peak: Mestas

Mean Elevation: 2882

Azimuth: 227

Average flow rate: 0.168631

Sensitivity: 0.551147

INACTIVE

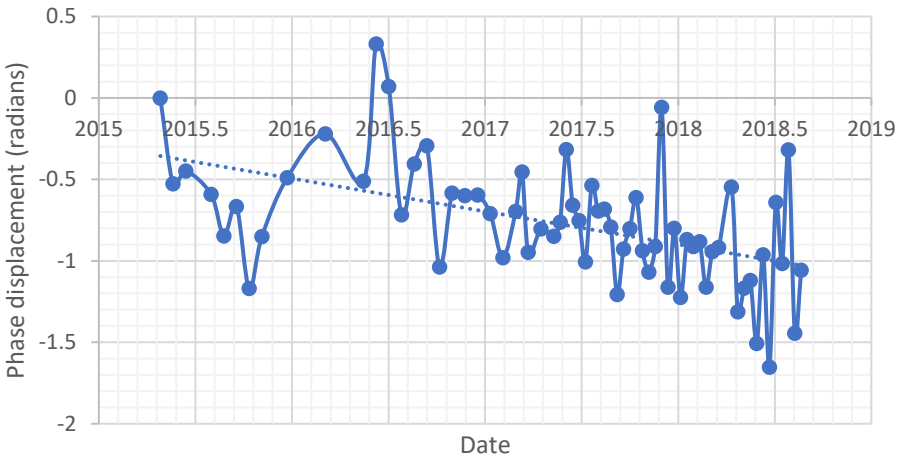

Peak: Mestas

Mean Elevation: 2879

Azimuth: 250

Average flow rate: -0.20228

Sensitivity: 0.761303

ACTIVE

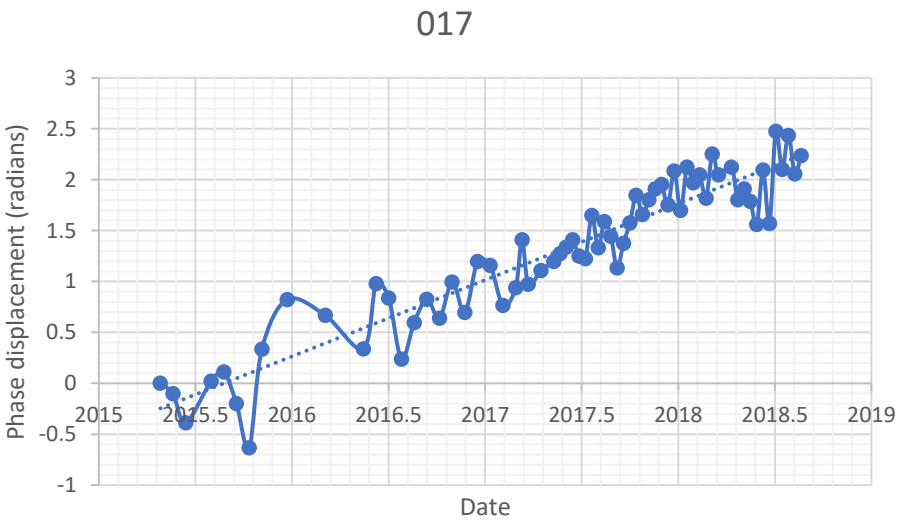

Peak: Mestas

Mean Elevation: 2892

Azimuth: 261

Average flow rate: 0.749598

Sensitivity: 0.721254

ACTIVE

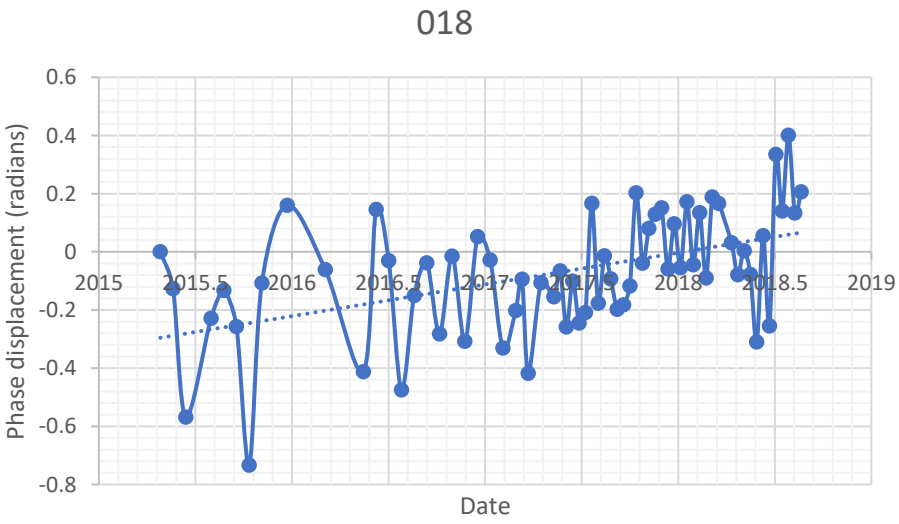

Peak: Mestas

Mean Elevation: 2915

Azimuth: 256

Average flow rate: 0.109001

Sensitivity: 0.698687

INACTIVE

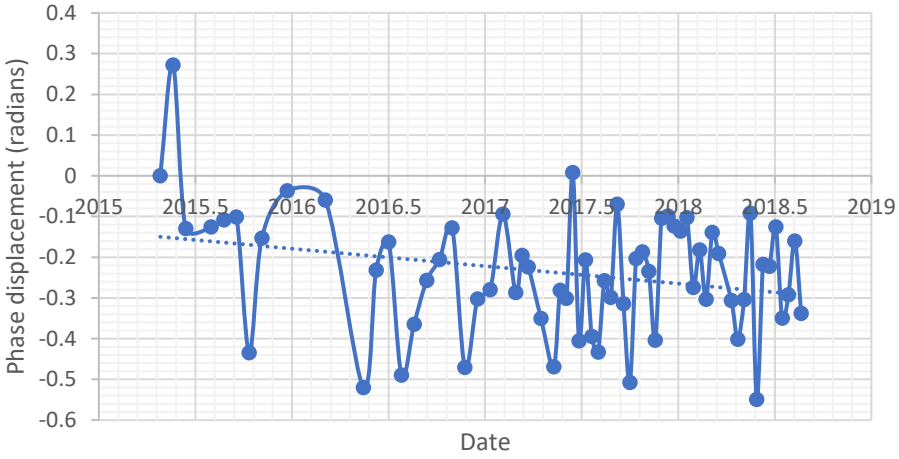

Peak: Mestas

Mean Elevation: 3078

Azimuth: 304

Average flow rate: -0.04285

Sensitivity: 0.770308

INACTIVE

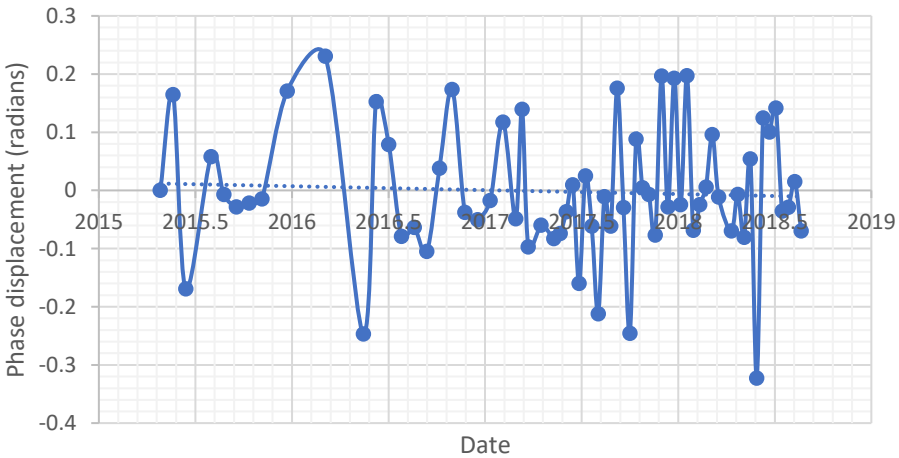

Peak: Mestas

Mean Elevation: 3069

Azimuth: 285

Average flow rate: -0.00674

Sensitivity: 0.777913

INACTIVE

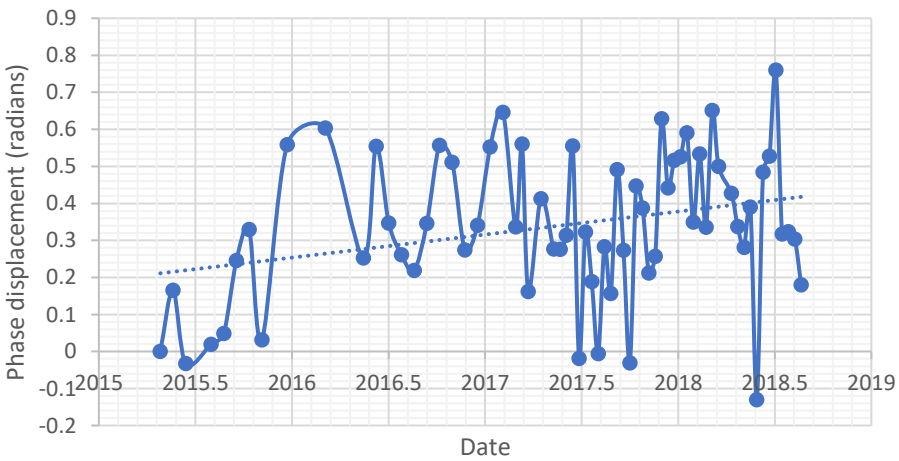

Peak: Mestas

Mean Elevation: 3104

Azimuth: 254

Average flow rate: 0.062226

Sensitivity: 0.826895

INACTIVE

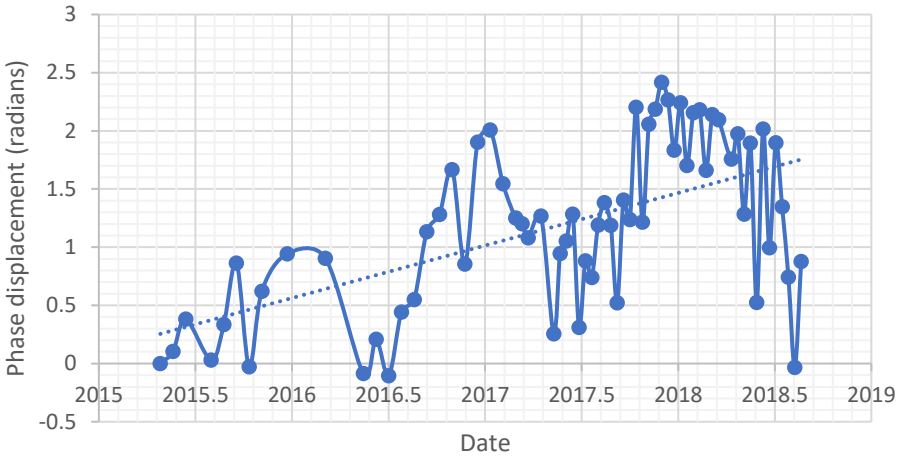

Peak: W Spanish

Mean Elevation: 3257

Azimuth: 351

Average flow rate: 0.451711

Sensitivity: 0.603914

ACTIVE

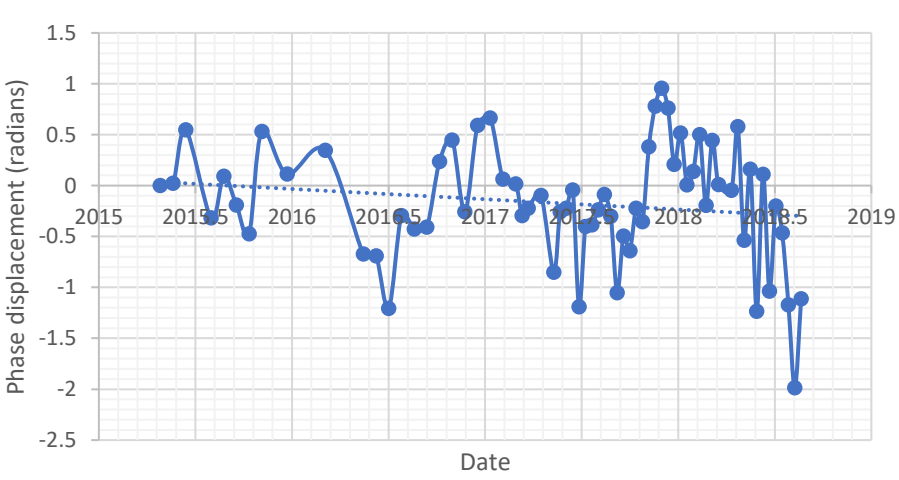

Peak: W Spanish

Mean Elevation: 3229

Azimuth: 26

Average flow rate: -0.10075

Sensitivity: 0.20131

INACTIVE

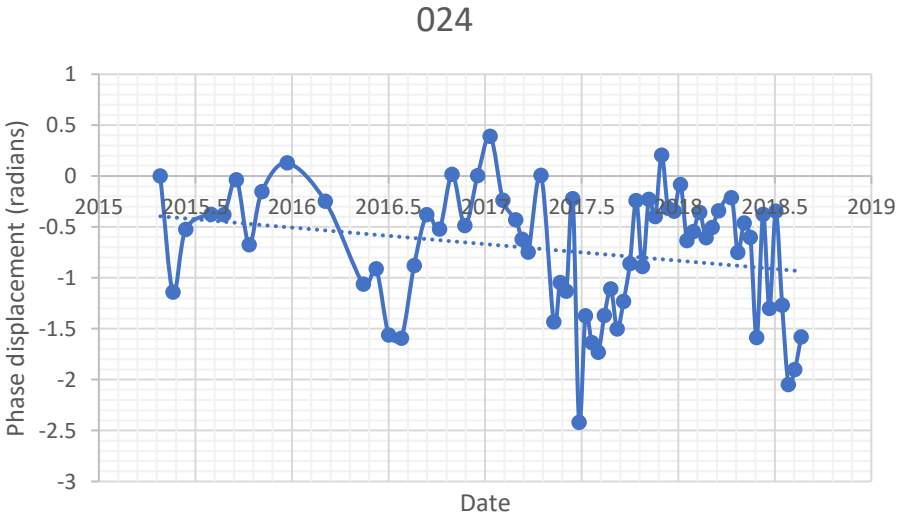

Peak: W Spanish

Mean Elevation: 3647

Azimuth: 55

Average flow rate: -0.1625

Sensitivity: 0.09906

INACTIVE

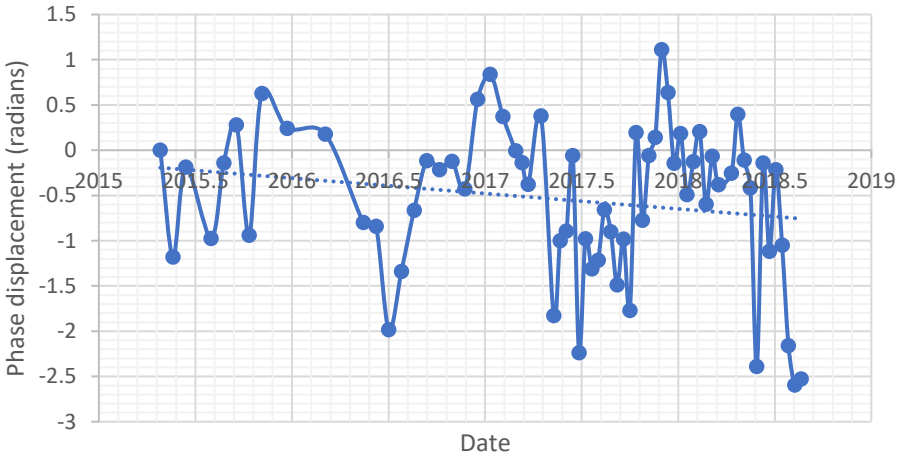

Peak: W Spanish

Mean Elevation: 3438

Azimuth: 84

Average flow rate: -0.16997

Sensitivity: 0.025497

INACTIVE

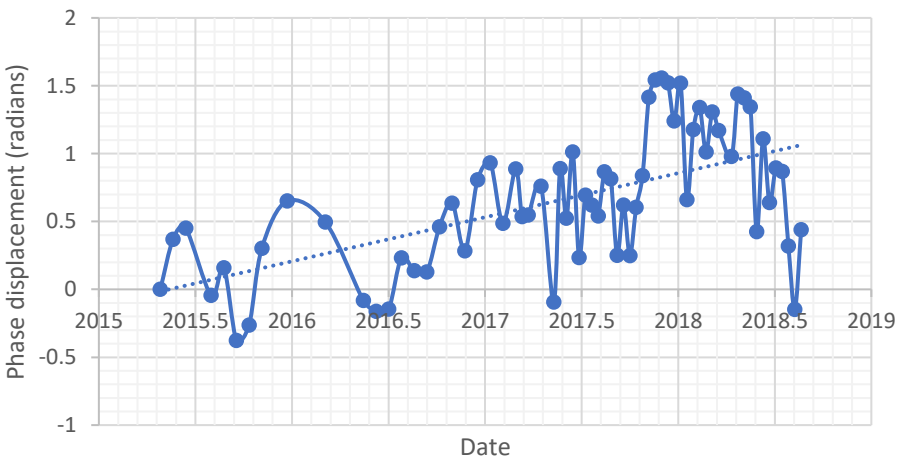

Peak: W Spanish

Mean Elevation: 3217

Azimuth: 55

Average flow rate: 0.32477

Sensitivity: 0.15999

ACTIVE

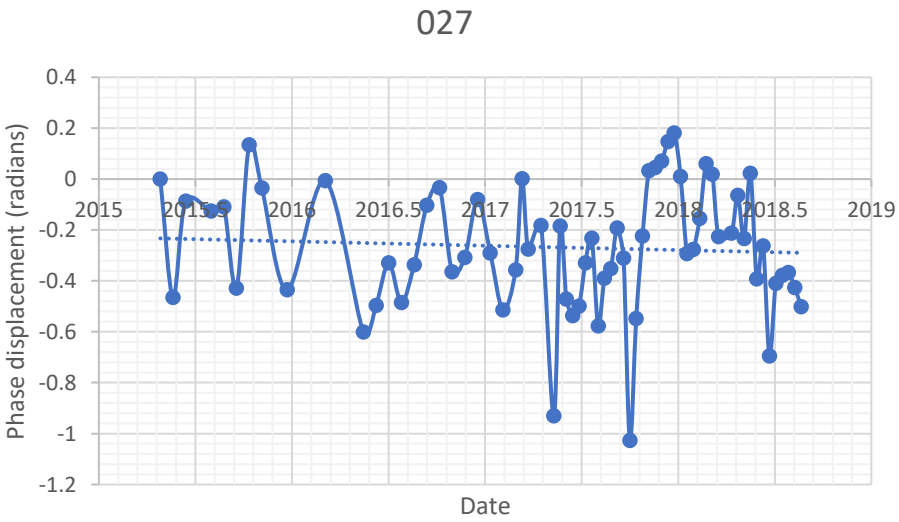

Peak: W Spanish

Mean Elevation: 3088

Azimuth: 64

Average flow rate: -0.01716

Sensitivity: 0.16245

INACTIVE

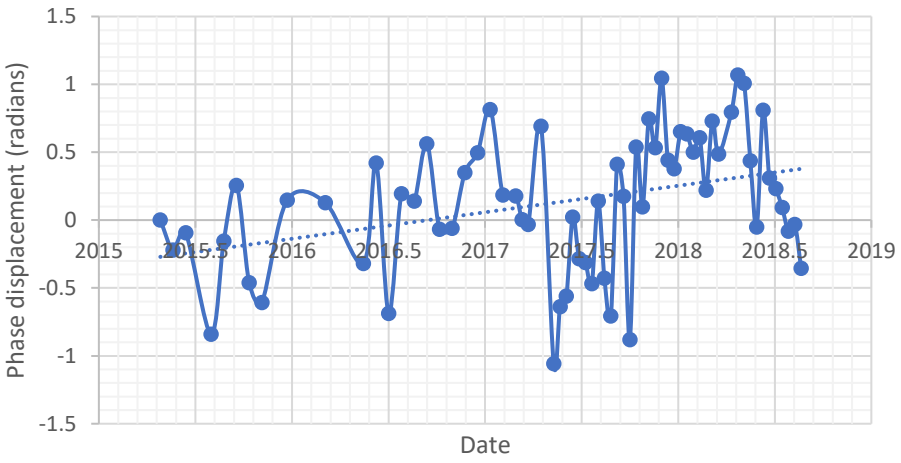

Peak: W Spanish

Mean Elevation: 3584

Azimuth: 183

Average flow rate: 0.19538

Sensitivity: 0.328987

INACTIVE

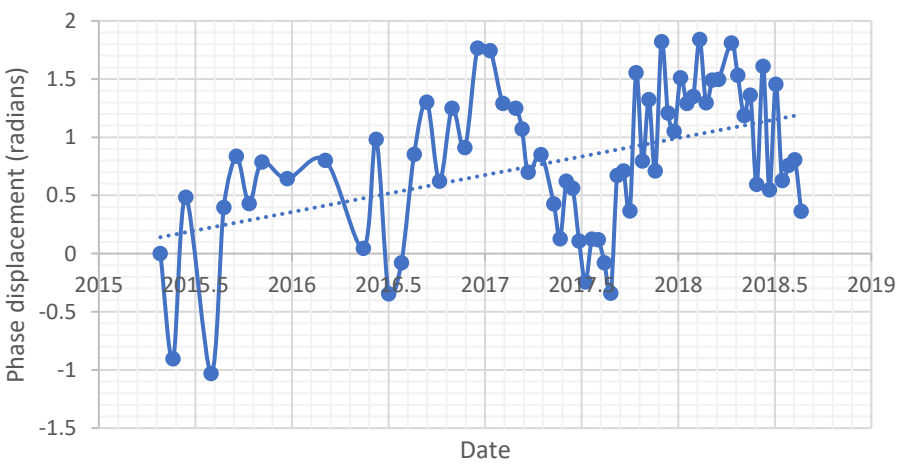

Peak: W Spanish

Mean Elevation: 3607

Azimuth: 196

Average flow rate: 0.317892

Sensitivity: 0.391522

ACTIVE

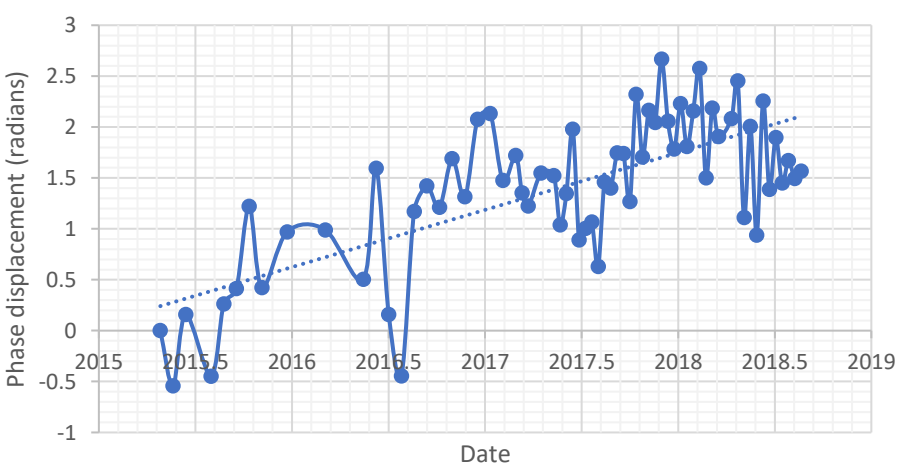

Peak: W Spanish

Mean Elevation: 3539

Azimuth: 231

Average flow rate: 0.5622

Sensitivity: 0.739027

ACTIVE

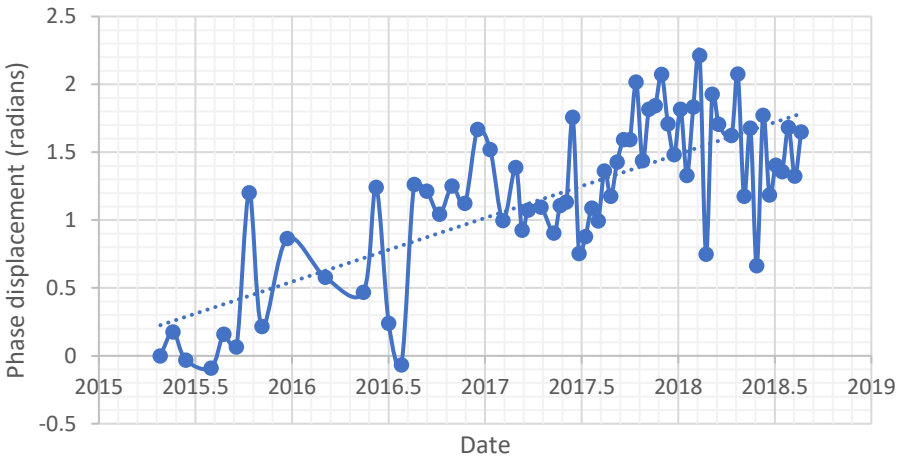

Peak: W Spanish

Mean Elevation: 3425

Azimuth: 266

Average flow rate: 0.469782

Sensitivity: 0.909745

ACTIVE

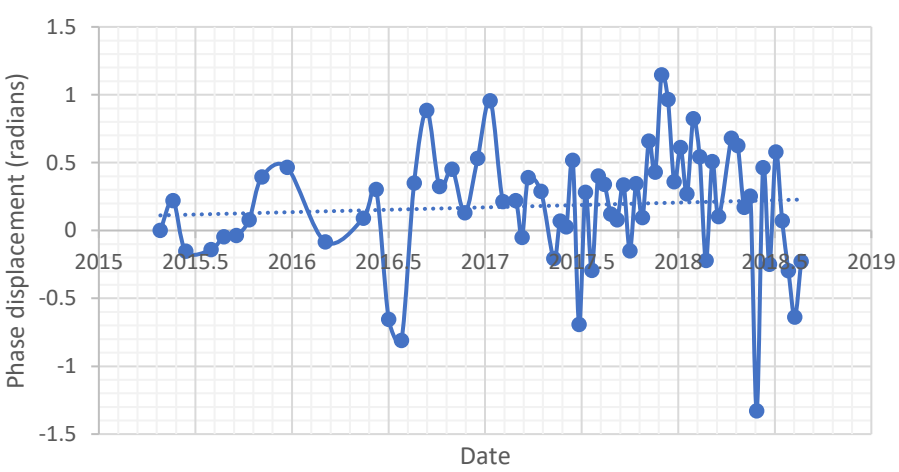

Peak: W Spanish

Mean Elevation: 3337

Azimuth: 278

Average flow rate: 0.03515

Sensitivity: 0.881345

INACTIVE

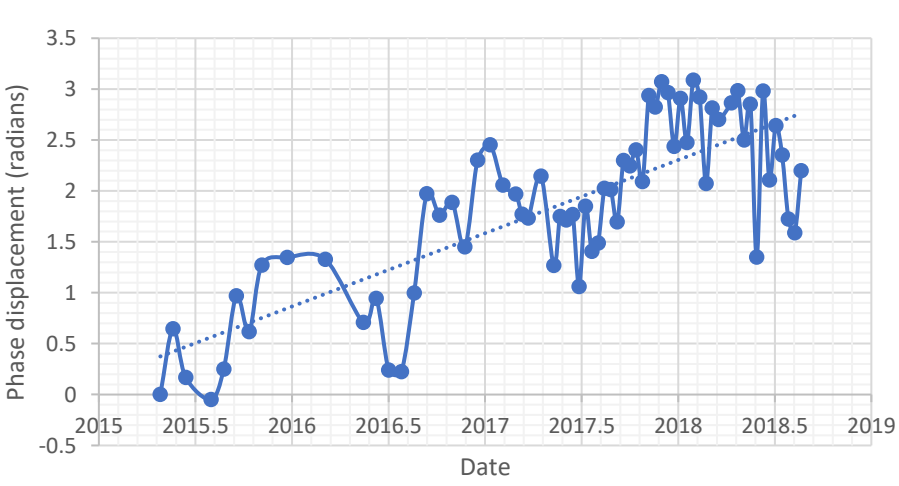

Peak: W Spanish

Mean Elevation: 3322

Azimuth: 320

Average flow rate: 0.719528

Sensitivity: 0.825327

ACTIVE

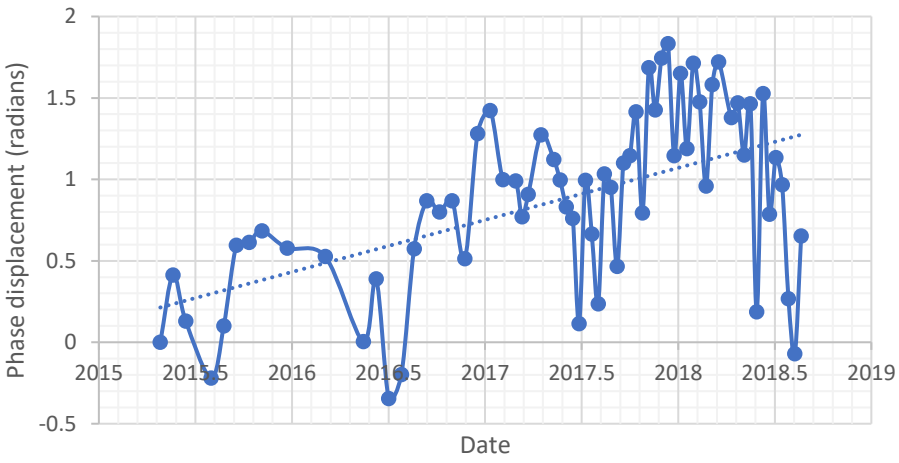

Peak: W Spanish

Mean Elevation: 3255

Azimuth: 318

Average flow rate: 0.319535

Sensitivity: 0.813712

ACTIVE

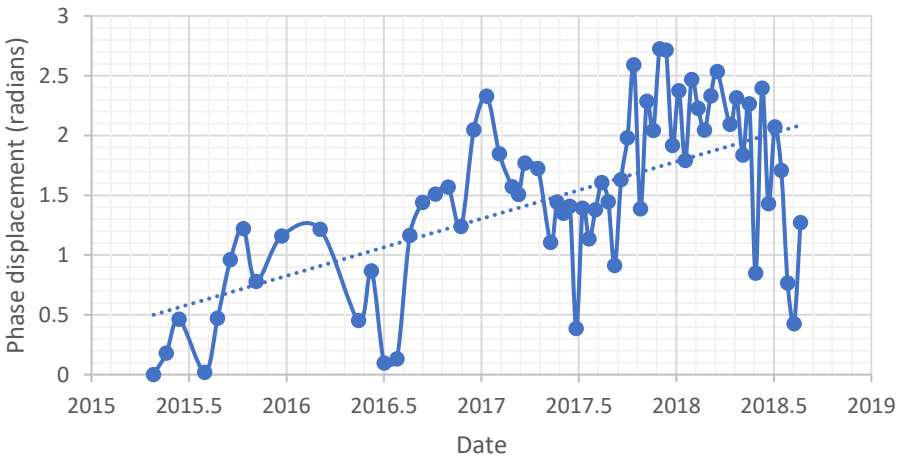

Peak: W Spanish

Mean Elevation: 3287

Azimuth: 318

Average flow rate: 0.477808

Sensitivity: 0.821552

ACTIVE

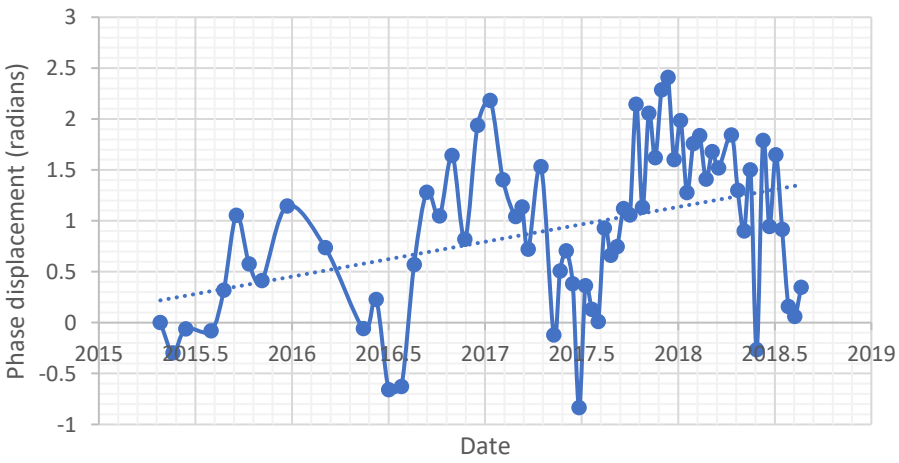

Peak: W Spanish

Mean Elevation: 3542

Azimuth: 302

Average flow rate: 0.342131

Sensitivity: 0.876765

ACTIVE

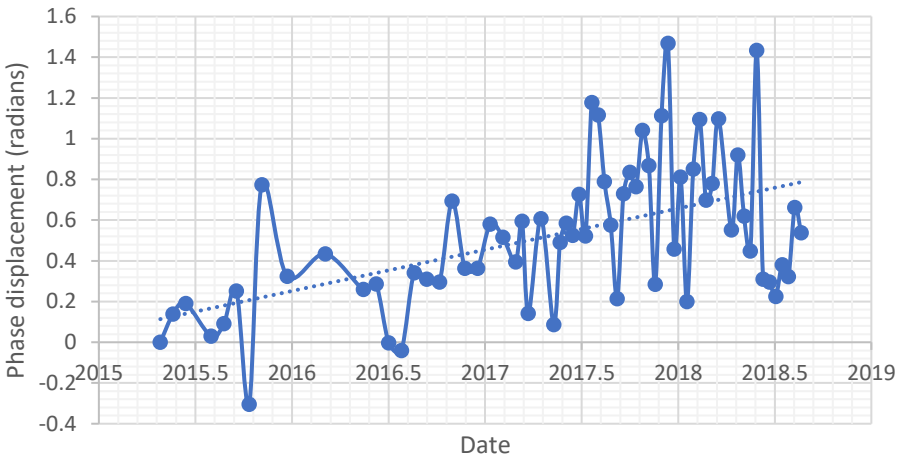

Peak: E Spanish

Mean Elevation: 2792

Azimuth: 8

Average flow rate: 0.202768

Sensitivity: 0.319108

ACTIVE

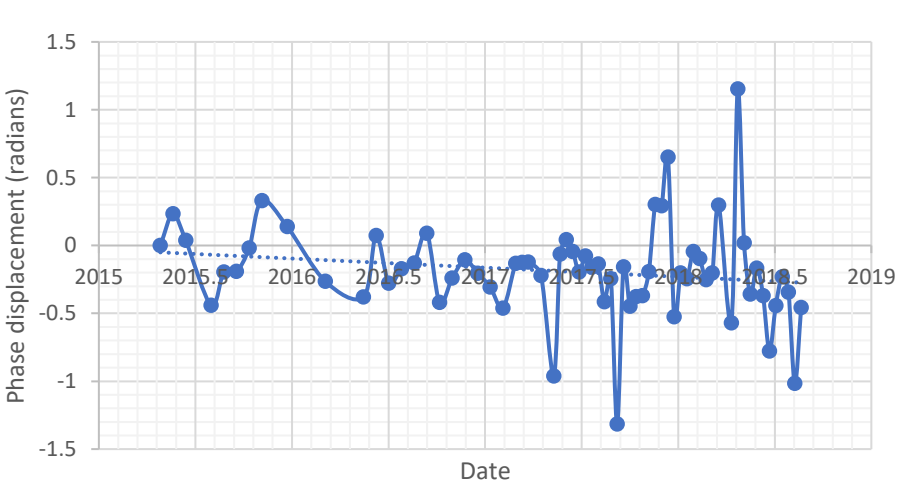

Peak: E Spanish

Mean Elevation: 2996

Azimuth: 2

Average flow rate: -0.06718

Sensitivity: 0.415954

INACTIVE

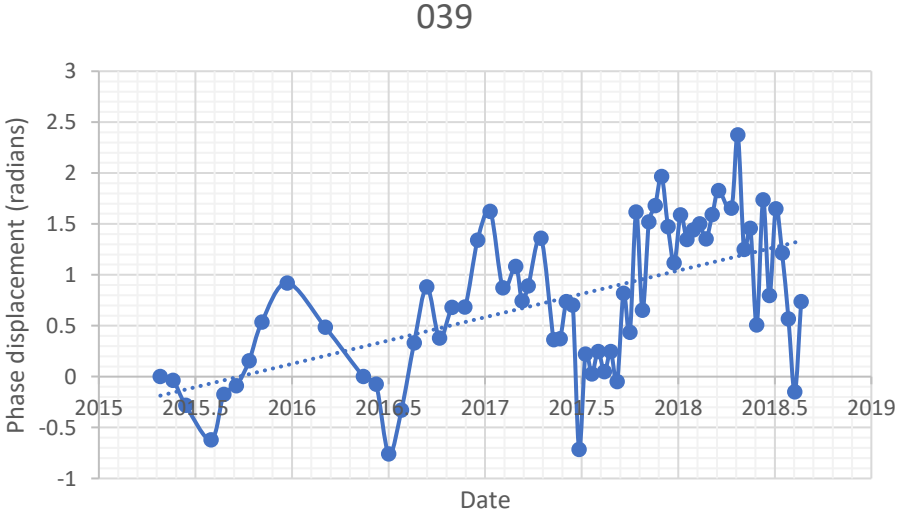

Peak: E Spanish

Mean Elevation: 3236

Azimuth: 9

Average flow rate: 0.458053

Sensitivity: 0.333509

ACTIVE

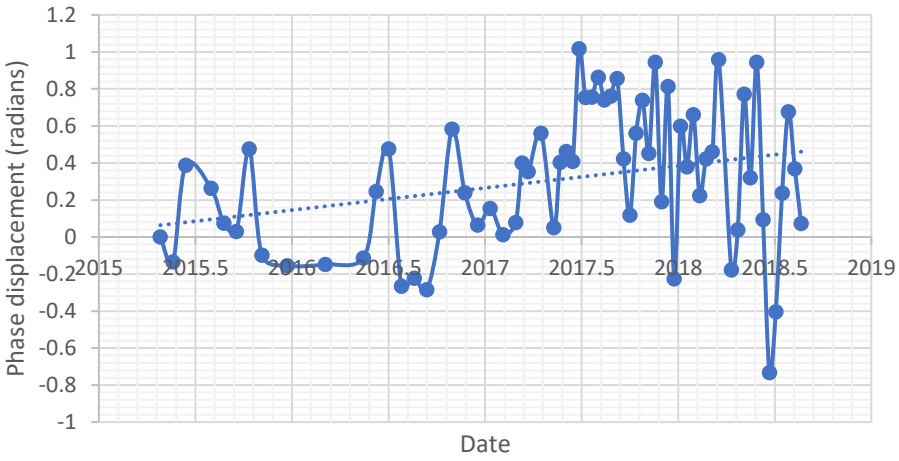

Peak: E Spanish

Mean Elevation: 2836

Azimuth: 29

Average flow rate: 0.119731

Sensitivity: 0.076474

INACTIVE

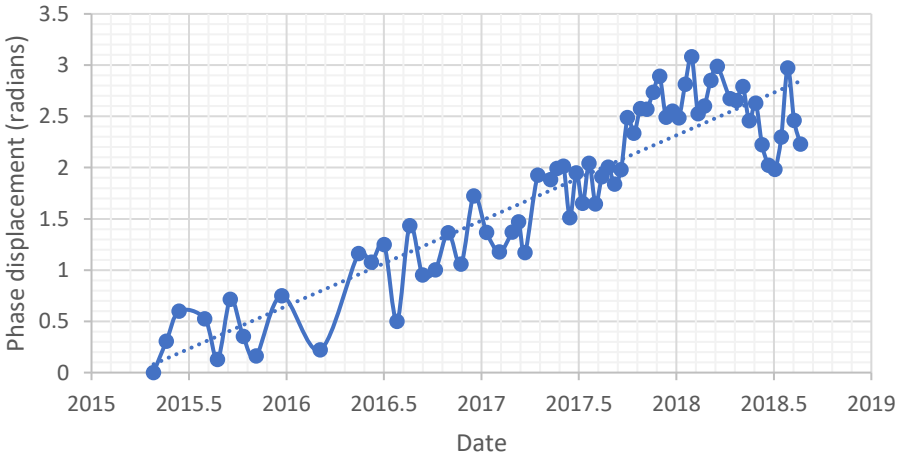

Peak: White

Mean Elevation: 2678

Azimuth: 354

Average flow rate: 0.832938

Sensitivity: 0.413252

ACTIVE

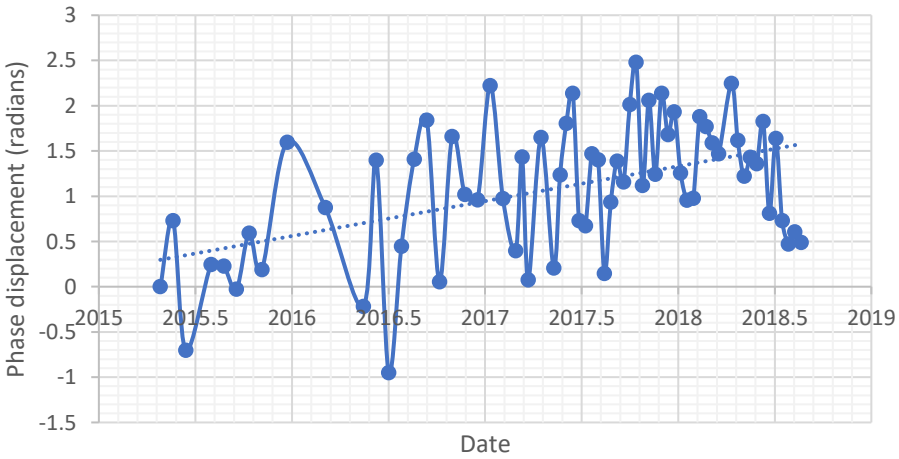

Peak: White

Mean Elevation: 2874

Azimuth: 243

Average flow rate: 0.385762

Sensitivity: 0.687536

ACTIVE

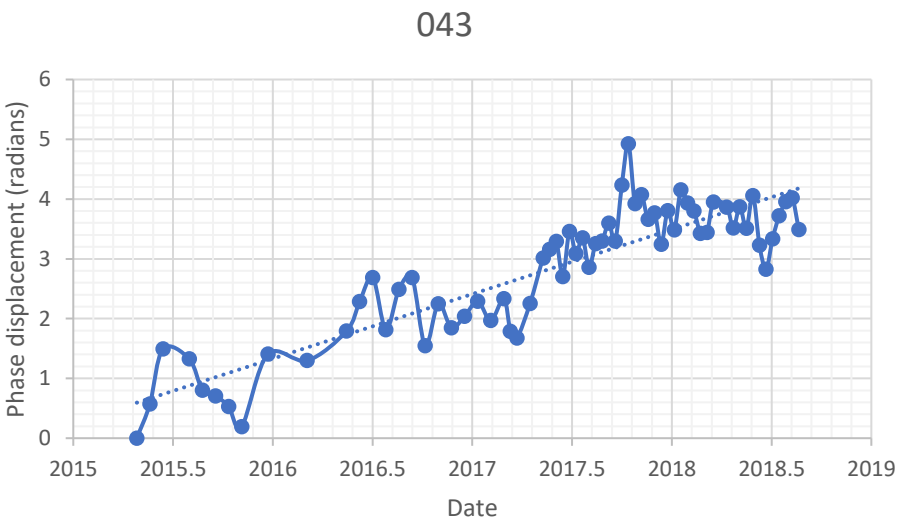

Peak: White

Mean Elevation: 2720

Azimuth: 272

Average flow rate: 1.080516

Sensitivity: 0.923768

ACTIVE

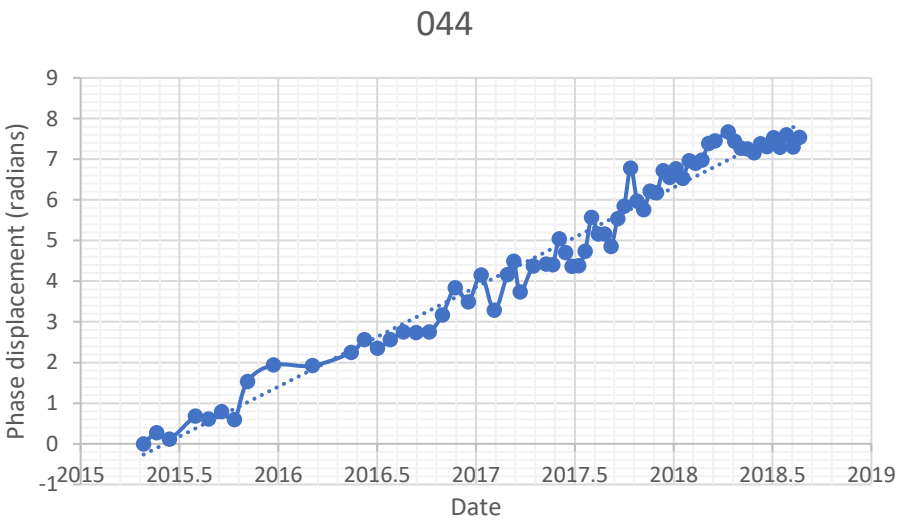

Peak: White

Mean Elevation: 2717

Azimuth: 301

Average flow rate: 2.449899

Sensitivity: 0.811874

ACTIVE

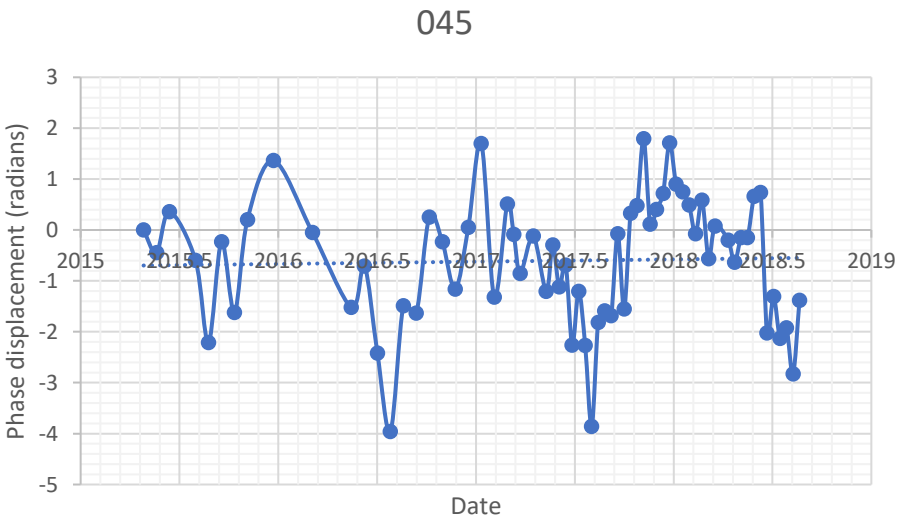

Peak: N Sheep

Mean Elevation: 2541

Azimuth: 49

Average flow rate: 0.044839

Sensitivity: 0.11107

INACTIVE

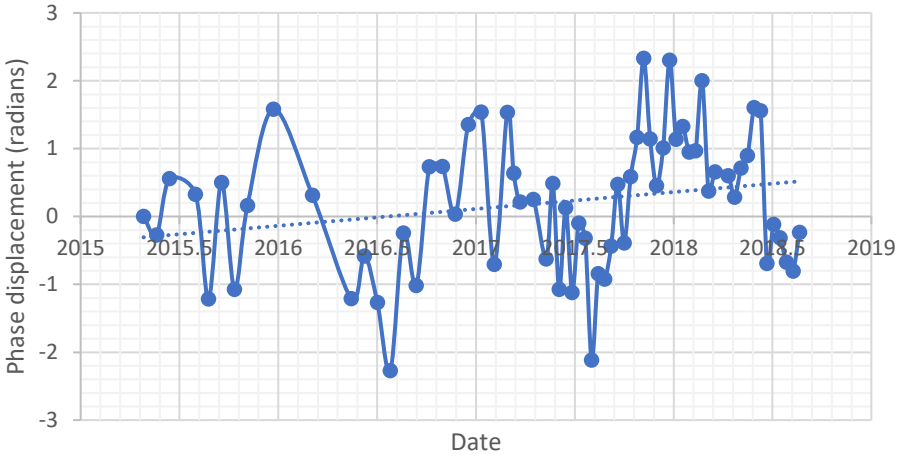

Peak: N Sheep

Mean Elevation: 2544

Azimuth: 60

Average flow rate: 0.248593

Sensitivity: 0.25835

ACTIVE

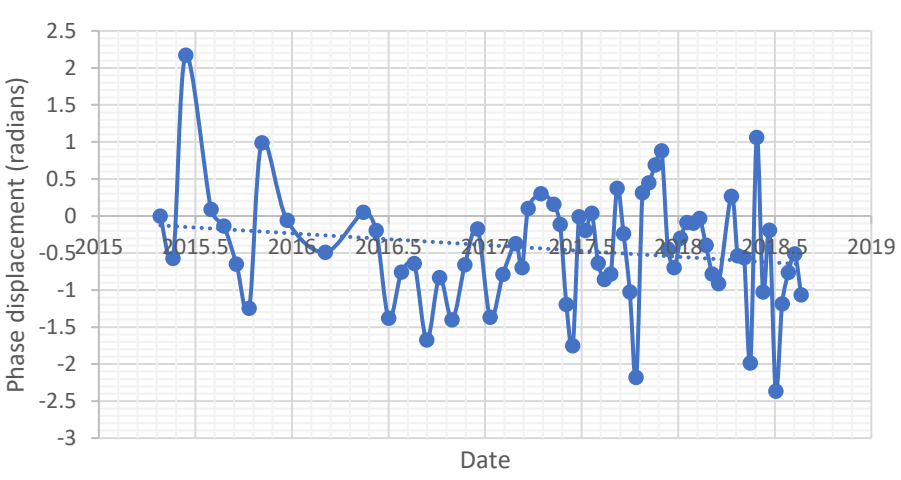

Peak: S Sheep

Mean Elevation: 2582

Azimuth: 48

Average flow rate: -0.15784

Sensitivity: 0.1321

INACTIVE

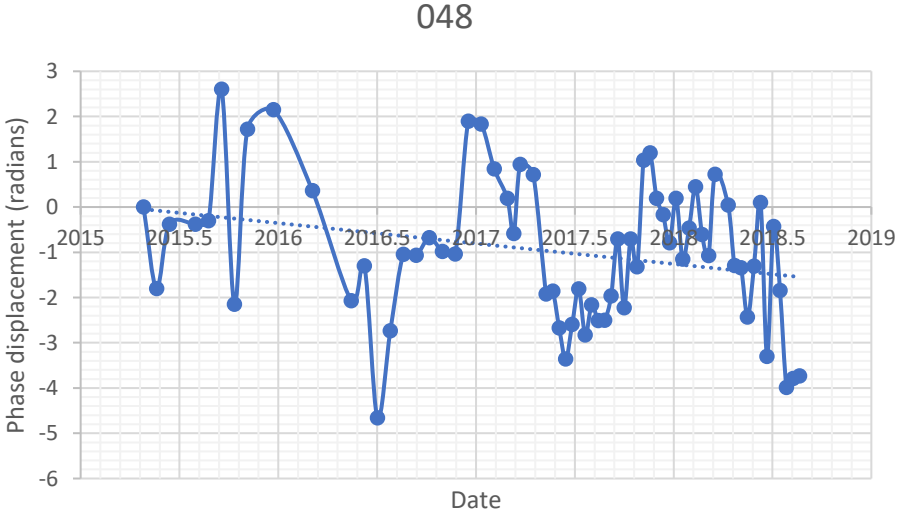

Peak: S Sheep

Mean Elevation: 2664

Azimuth: 50

Average flow rate: -0.45132

Sensitivity: 0.05959

ACTIVE

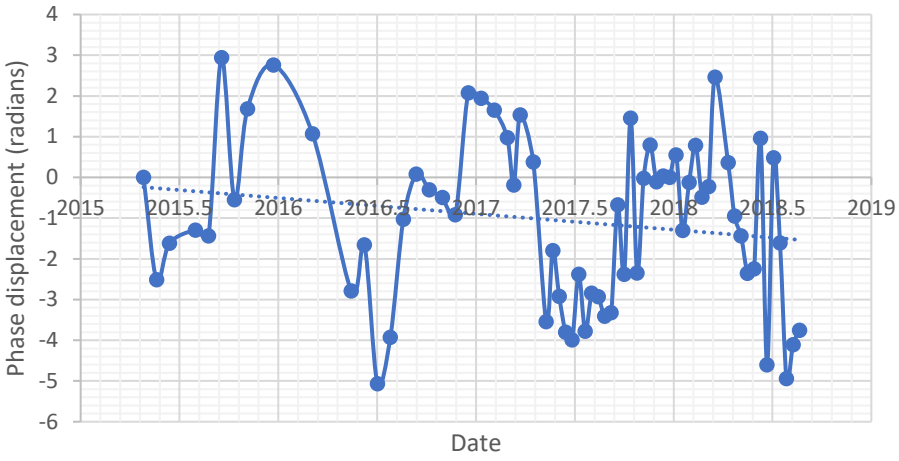

Peak: S Sheep

Mean Elevation: 2736

Azimuth: 62

Average flow rate: -0.38978

Sensitivity: 0.24225

ACTIVE

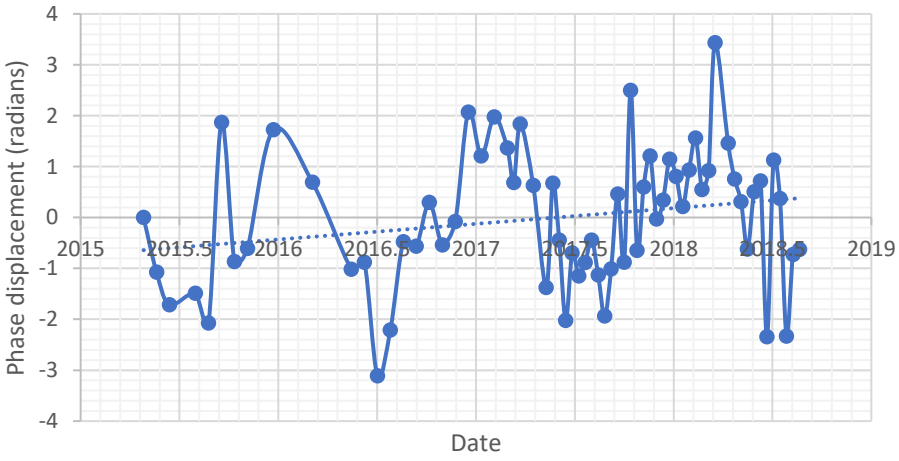

Peak: S Sheep

Mean Elevation: 2672

Azimuth: 93

Average flow rate: 0.307502

Sensitivity: 0.30138

ACTIVE

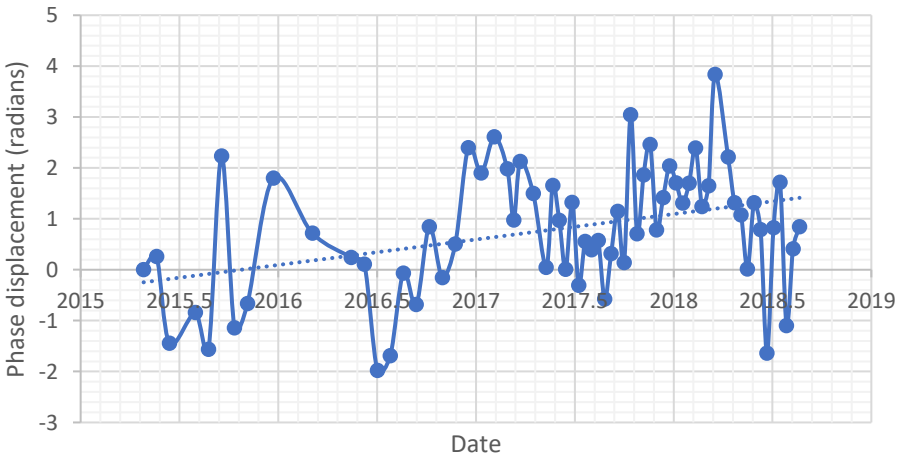

Peak: S Sheep

Mean Elevation: 2658

Azimuth: 36

Average flow rate: 0.499935

Sensitivity: 0.03523

ACTIVE

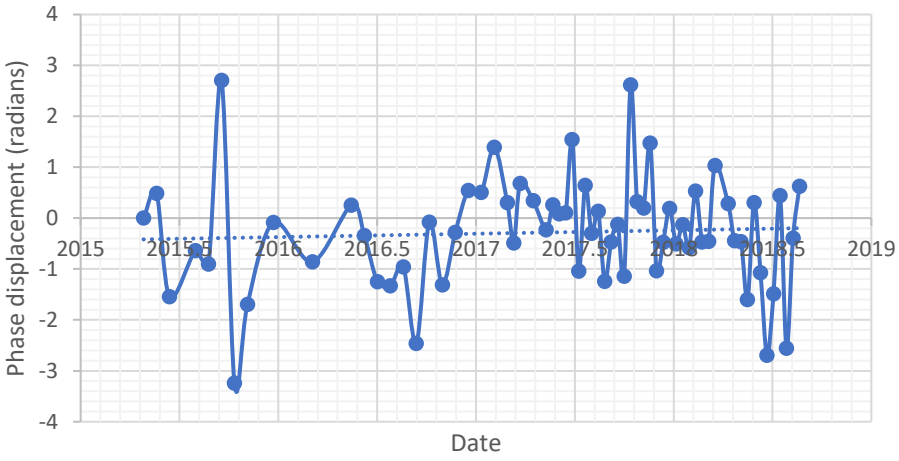

Peak: S Sheep

Mean Elevation: 2615

Azimuth: 68

Average flow rate: 0.066381

Sensitivity: 0.28149

INACTIVE

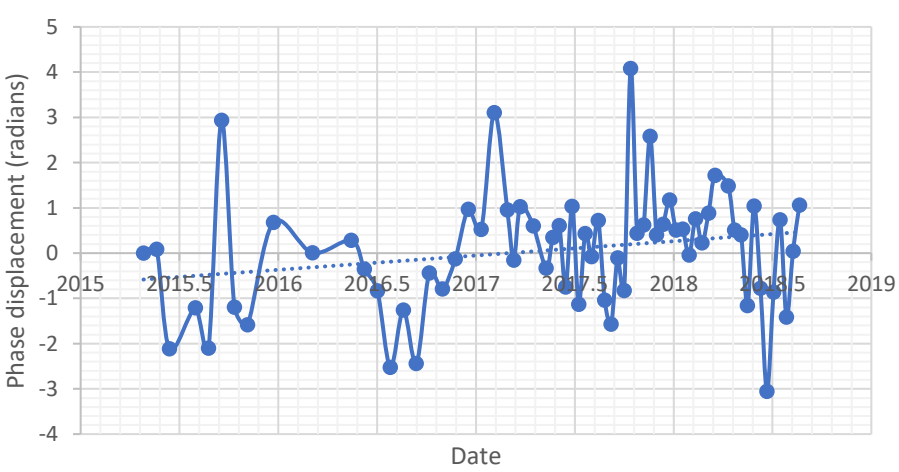

Peak: S Sheep

Mean Elevation: 2673

Azimuth: 71

Average flow rate: 0.3135745

Sensitivity: 0.2991

ACTIVE

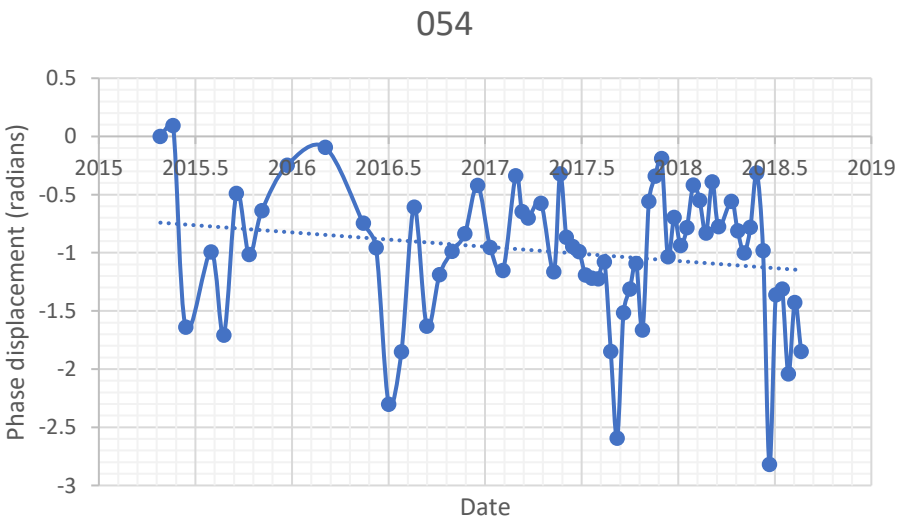

Peak: S Sheep

Mean Elevation: 2708

Azimuth: 90

Average flow rate: -0.12283

Sensitivity: 0.2786

INACTIVE

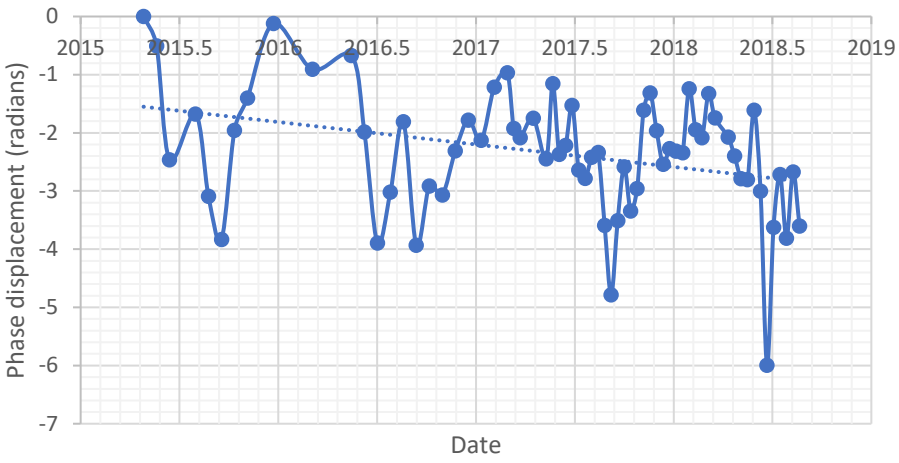

Peak: S Sheep

Mean Elevation: 2679

Azimuth: 107

Average flow rate: -0.38609

Sensitivity: 0.27604

ACTIVE

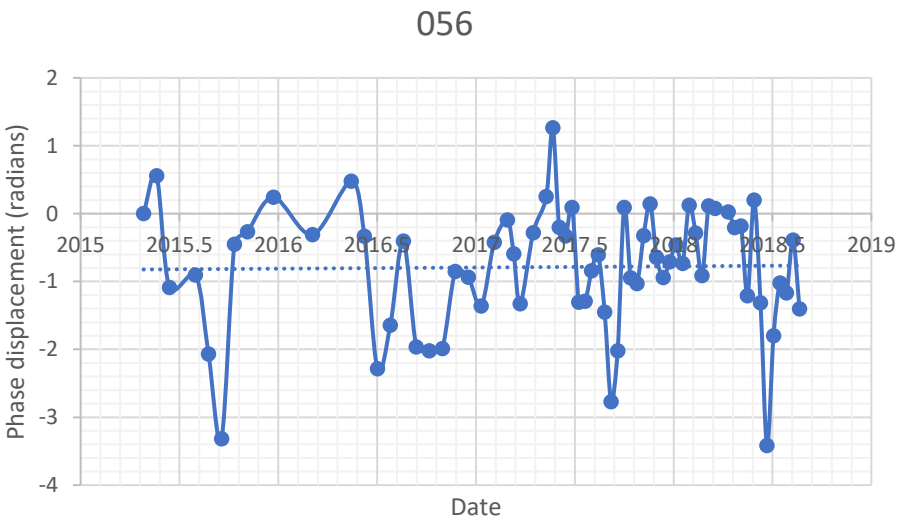

Peak: S Sheep

Mean Elevation: 2673

Azimuth: 138

Average flow rate: 0.017569

Sensitivity: 0.18946

INACTIVE

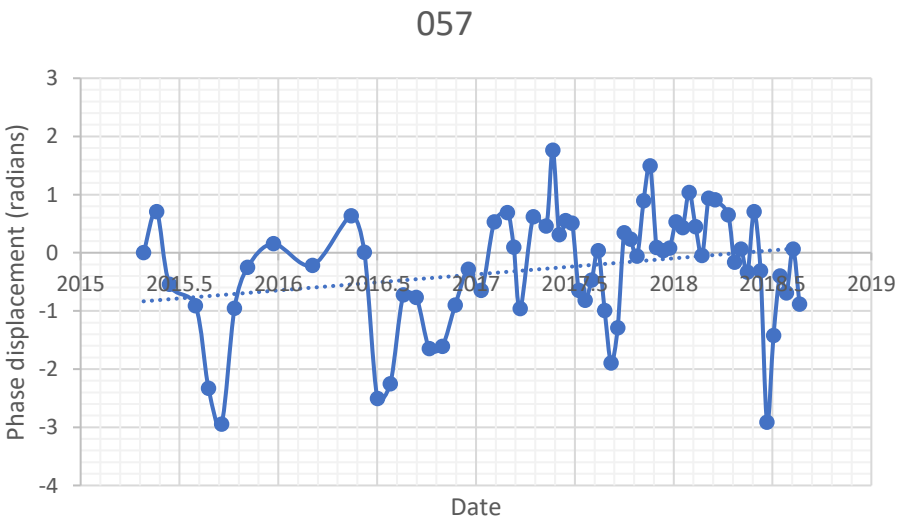

Peak: S Sheep

Mean Elevation: 2657

Azimuth: 112

Average flow rate: 0.275577

Sensitivity: 0.4327

ACTIVE

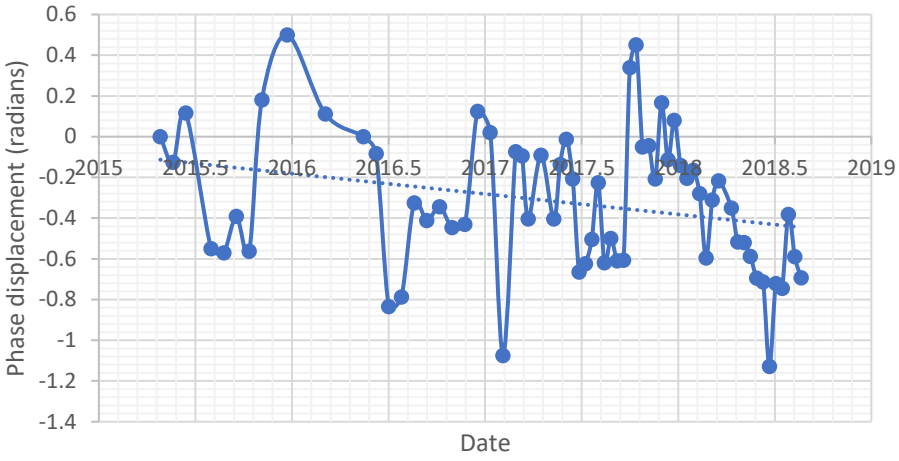

Peak: S Sheep

Mean Elevation: 2761

Azimuth: 354

Average flow rate: -0.10014

Sensitivity: 0.351649

INACTIVE

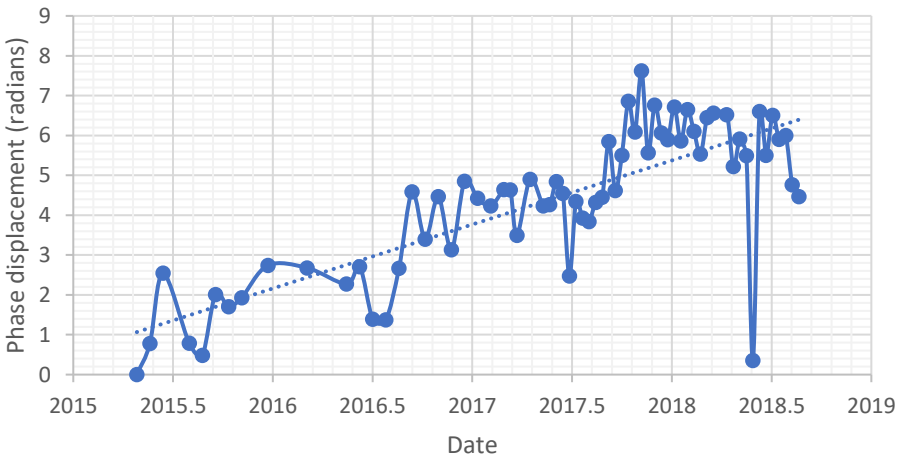

Peak: S Sheep

Mean Elevation: 2864

Azimuth: 242

Average flow rate: 1.605697

Sensitivity: 0.613875

ACTIVE

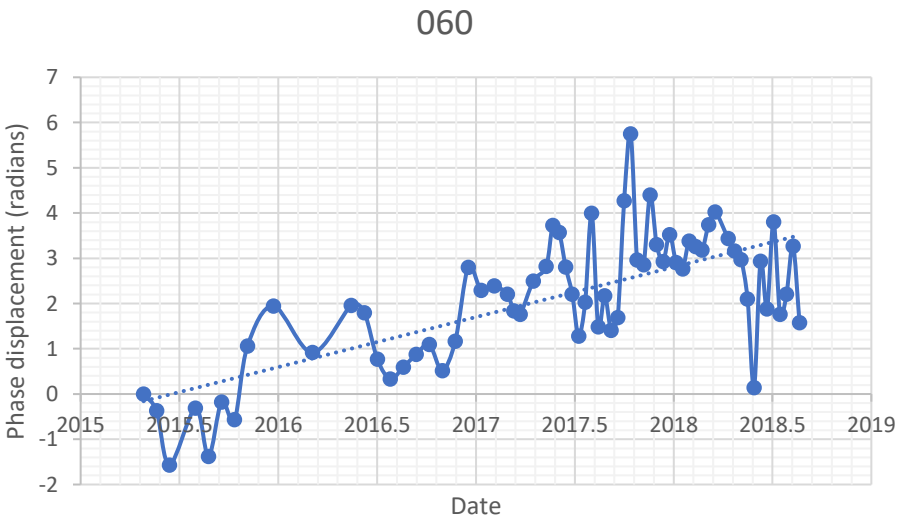

Peak: S Sheep

Mean Elevation: 2744

Azimuth: 285

Average flow rate: 1.105421

Sensitivity: 0.819824

ACTIVE

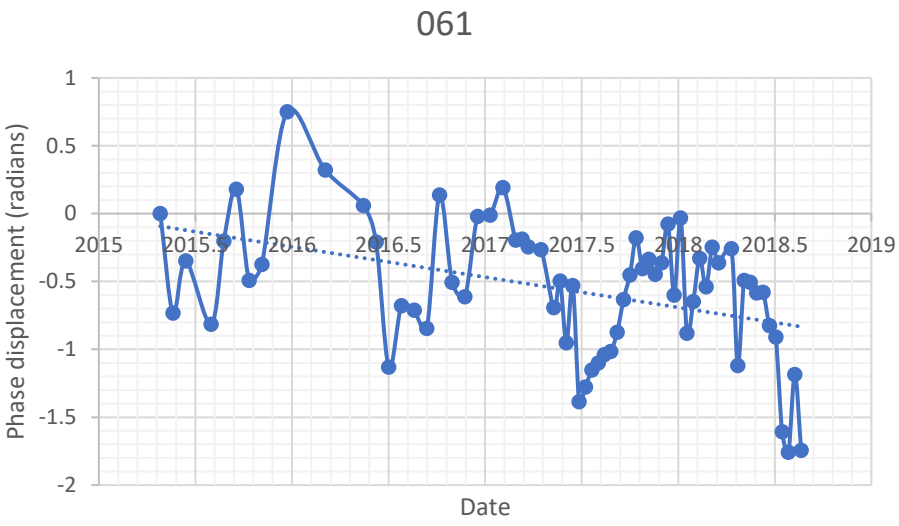

Peak: Blanca

Mean Elevation: 3583

Azimuth: 86

Average flow rate: -0.22308

Sensitivity: 0.34925

ACTIVE

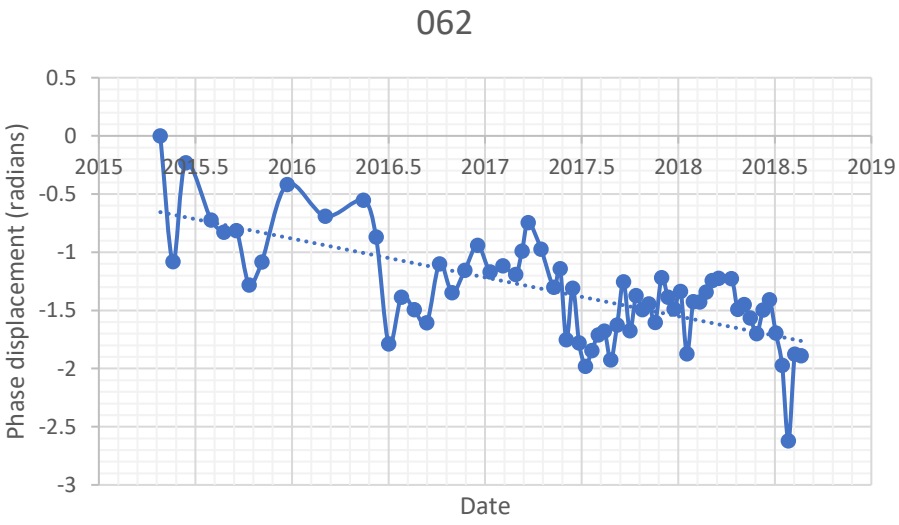

Peak: Blanca

Mean Elevation: 3605

Azimuth: 59

Average flow rate: -0.33361

Sensitivity: 0.22073

ACTIVE

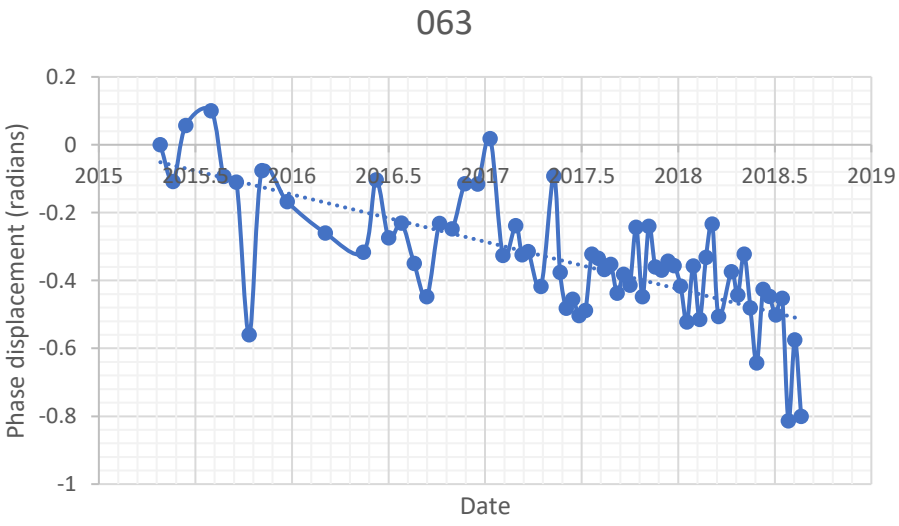

Peak: Blanca

Mean Elevation: 3596

Azimuth: 93

Average flow rate: -0.13932

Sensitivity: 0.38276

INACTIVE

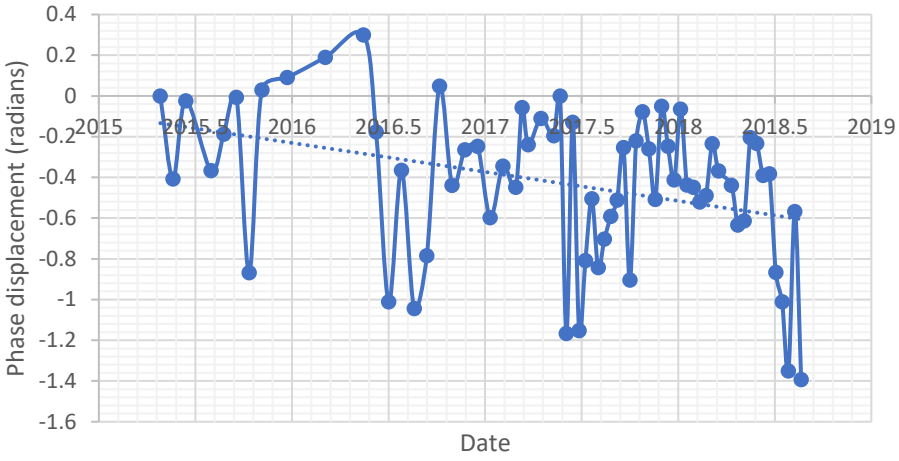

Peak: Blanca

Mean Elevation: 3765

Azimuth: 50

Average flow rate: -0.14226

Sensitivity: 0.05959

INACTIVE

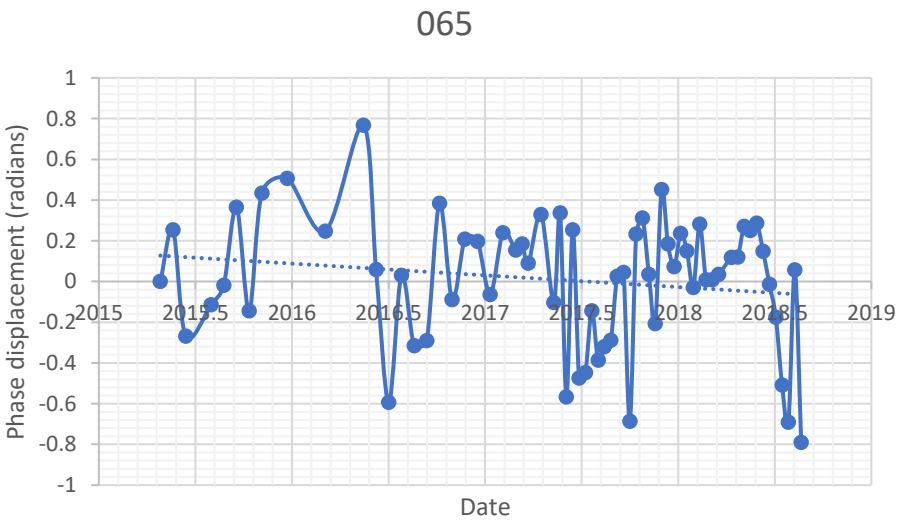

Peak: Blanca

Mean Elevation: 3820

Azimuth: 67

Average flow rate: -0.05761

Sensitivity: 0.35151

INACTIVE

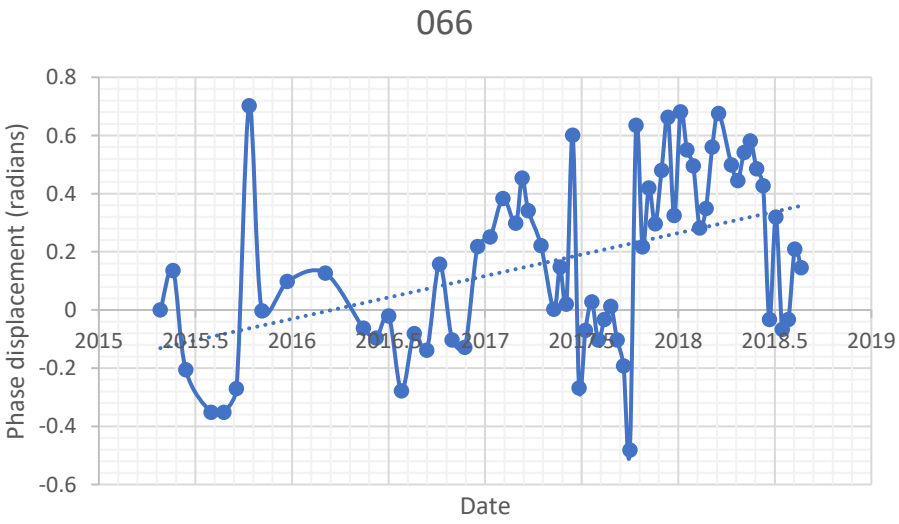

Peak: Blanca

Mean Elevation: 3684

Azimuth: 20

Average flow rate: 0.147492

Sensitivity: 0.074755

INACTIVE

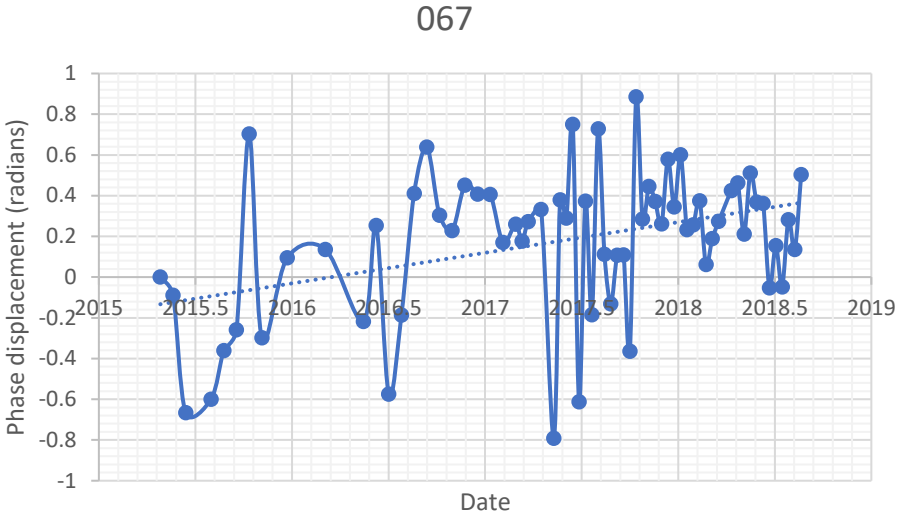

Peak: Blanca

Mean Elevation: 3666

Azimuth: 355

Average flow rate: 0.150232

Sensitivity: 0.366479

INACTIVE

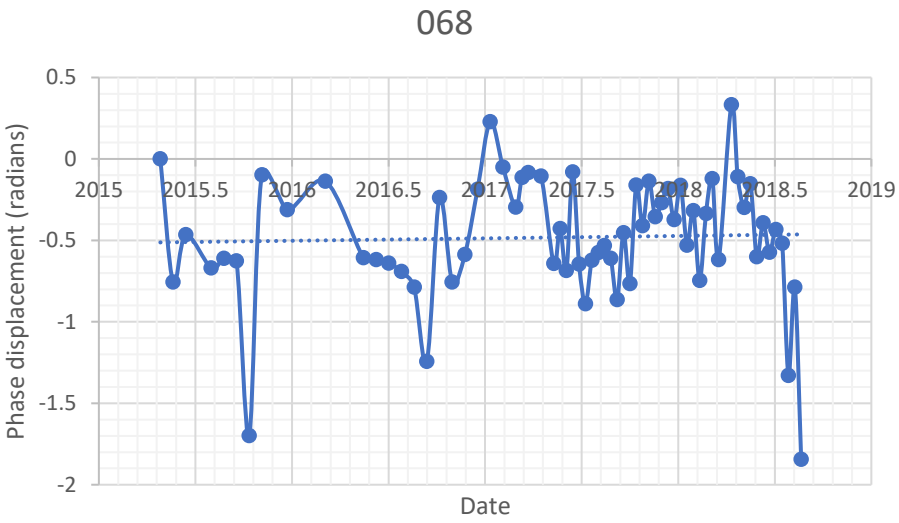

Peak: Blanca

Mean Elevation: 3597

Azimuth: 46

Average flow rate: 0.01479

Sensitivity: 0.15833

INACTIVE

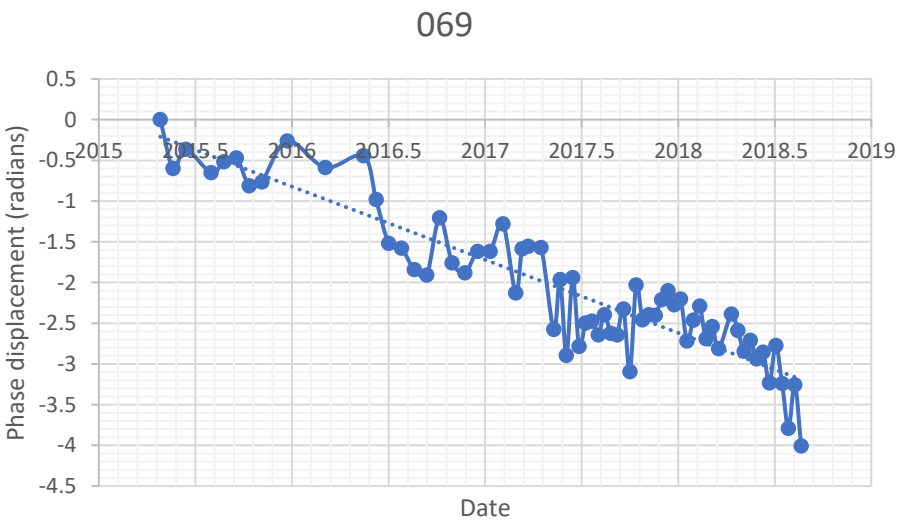

Peak: Blanca

Mean Elevation: 3736

Azimuth: 107

Average flow rate: -0.89818

Sensitivity: 0.48496

ACTIVE

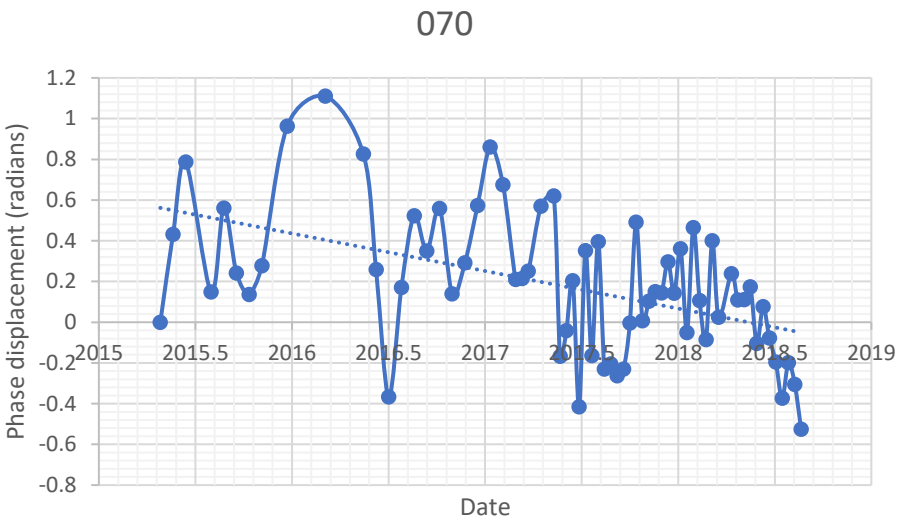

Peak: Blanca

Mean Elevation: 3671

Azimuth: 45

Average flow rate: -0.18442

Sensitivity: 0.19254

INACTIVE

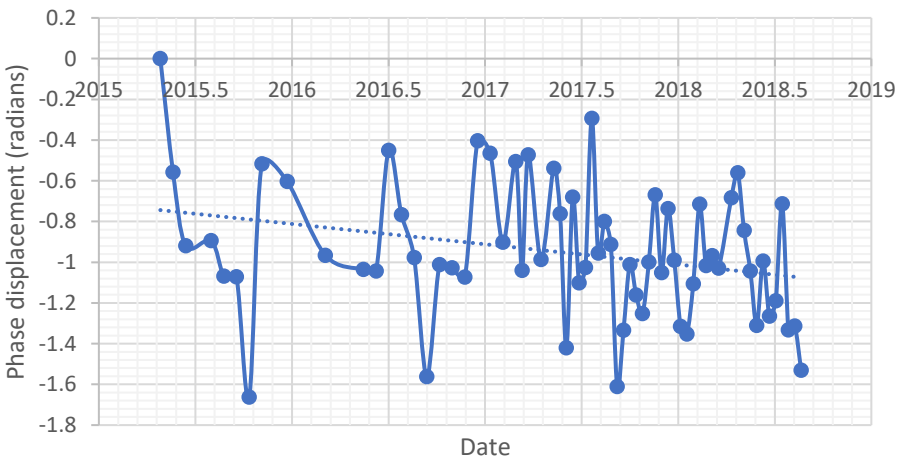

Peak: Blanca

Mean Elevation: 3566

Azimuth: 40

Average flow rate: -0.0998

Sensitivity: 0.03065

INACTIVE

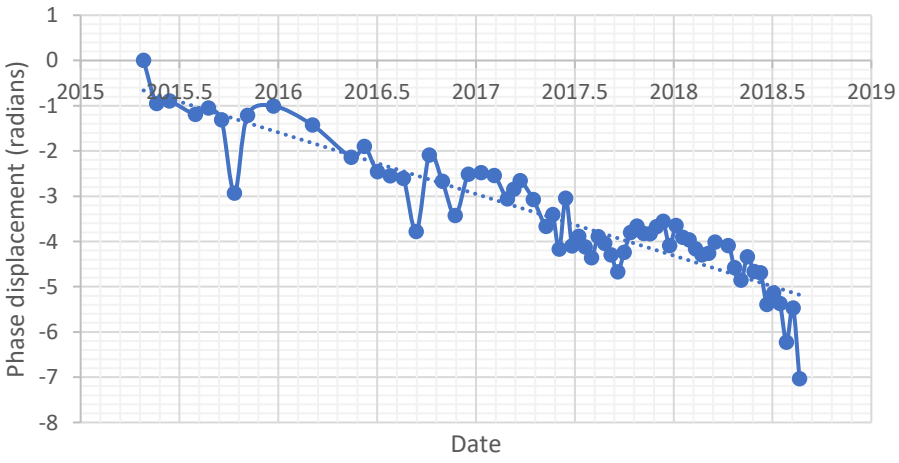

Peak: Blanca

Mean Elevation: 3651

Azimuth: 113

Average flow rate: -1.36103

Sensitivity: 0.46197

ACTIVE

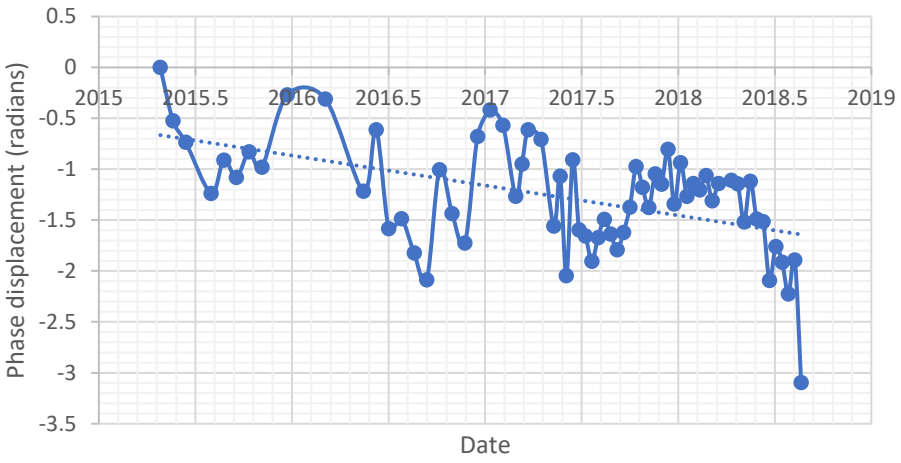

Peak: Blanca

Mean Elevation: 3556

Azimuth: 123

Average flow rate: -0.2942

Sensitivity: 0.4796

ACTIVE

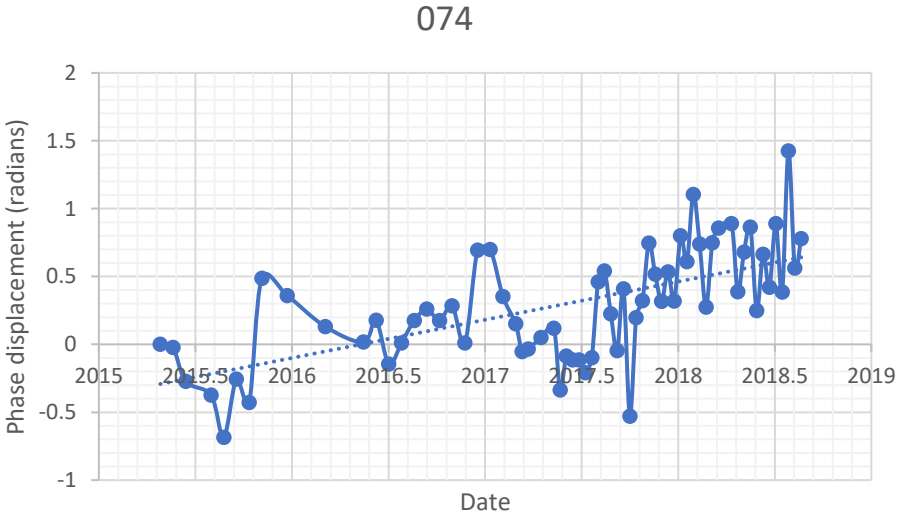

Peak: Blanca

Mean Elevation: 3617

Azimuth: 219

Average flow rate: 0.281268

Sensitivity: 0.44202

ACTIVE

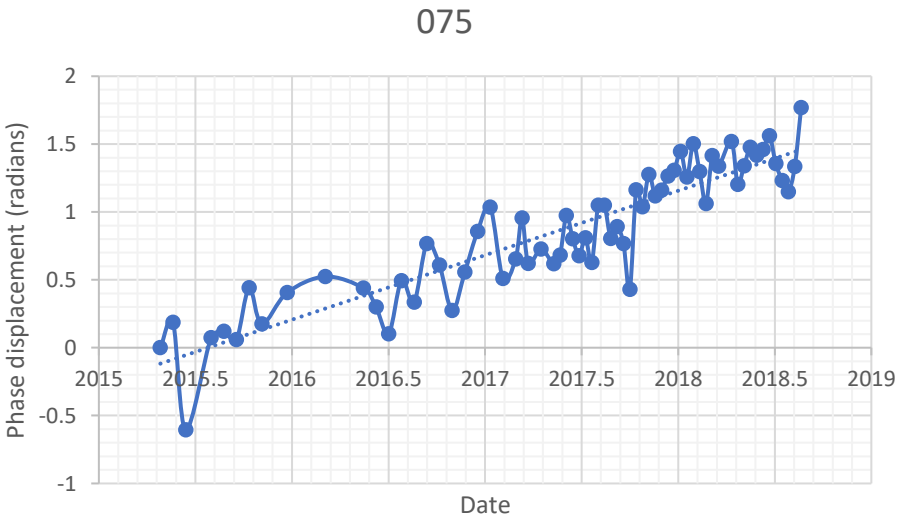

Peak: Blanca

Mean Elevation: 3771

Azimuth: 215

Average flow rate: 0.475098

Sensitivity: 0.402777

ACTIVE

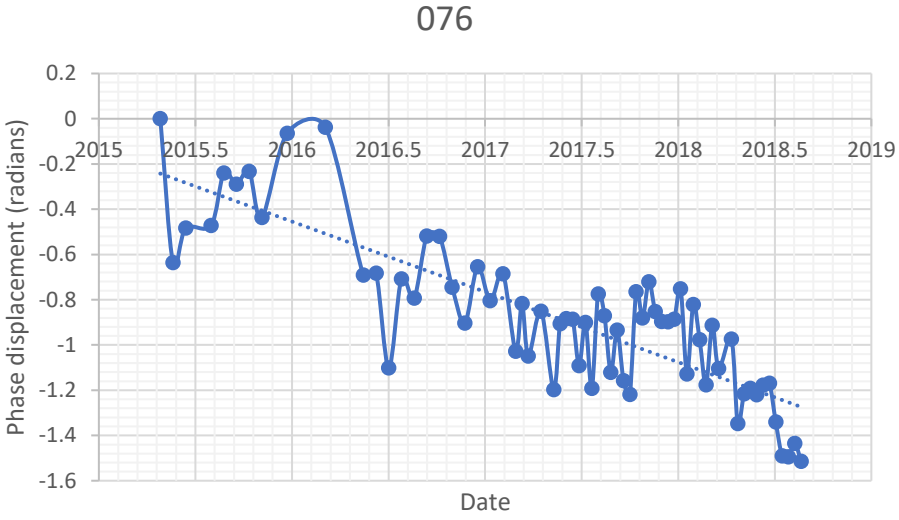

Peak: Blanca

Mean Elevation: 3759

Azimuth: 126

Average flow rate: -0.31082

Sensitivity: 0.40733

ACTIVE

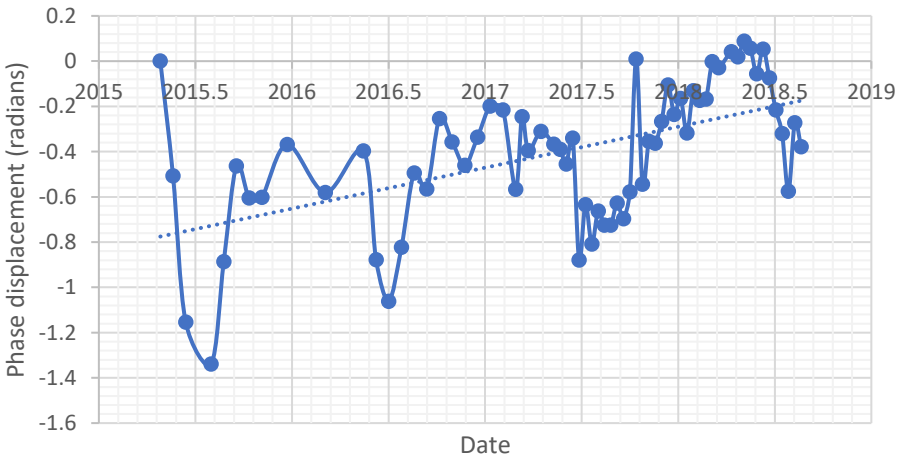

Peak: Blanca

Mean Elevation: 3701

Azimuth: 332

Average flow rate: 0.181009

Sensitivity: 0.590792

INACTIVE

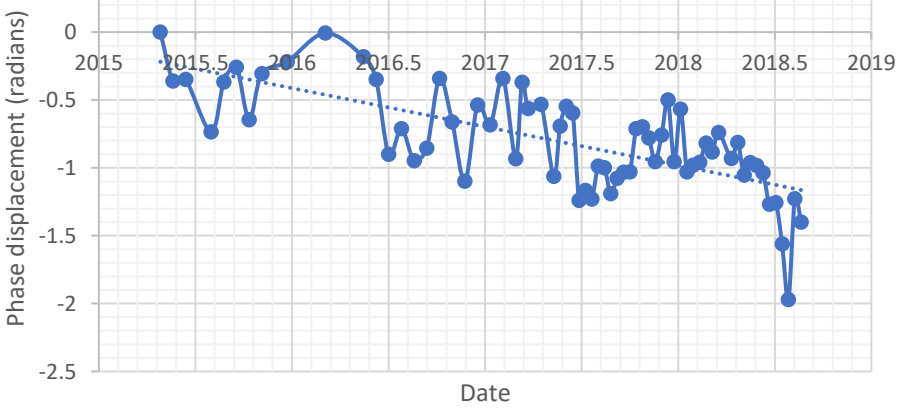

Peak: Blanca

Mean Elevation: 3589

Azimuth: 108

Average flow rate: -0.28467

Sensitivity: 0.43778

ACTIVE

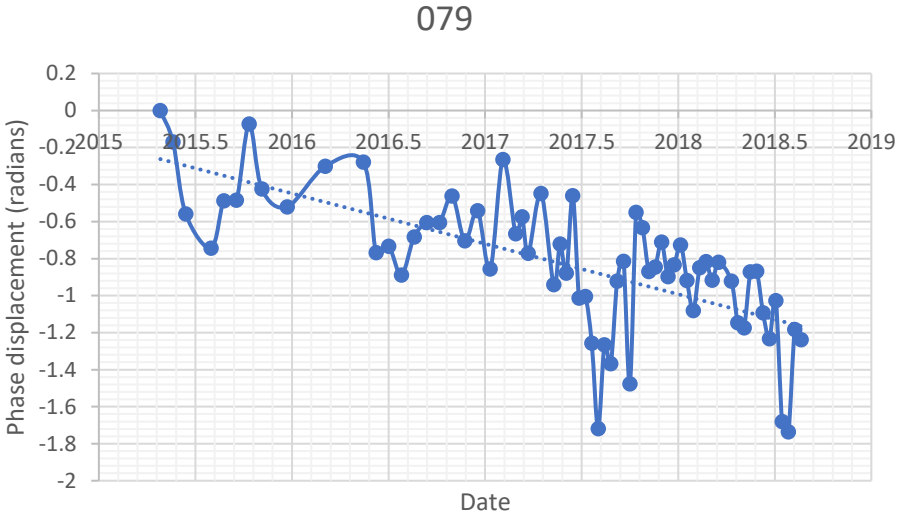

Peak: Blanca

Mean Elevation: 3882

Azimuth: 127

Average flow rate: -0.27223

Sensitivity: 0.19501

ACTIVE

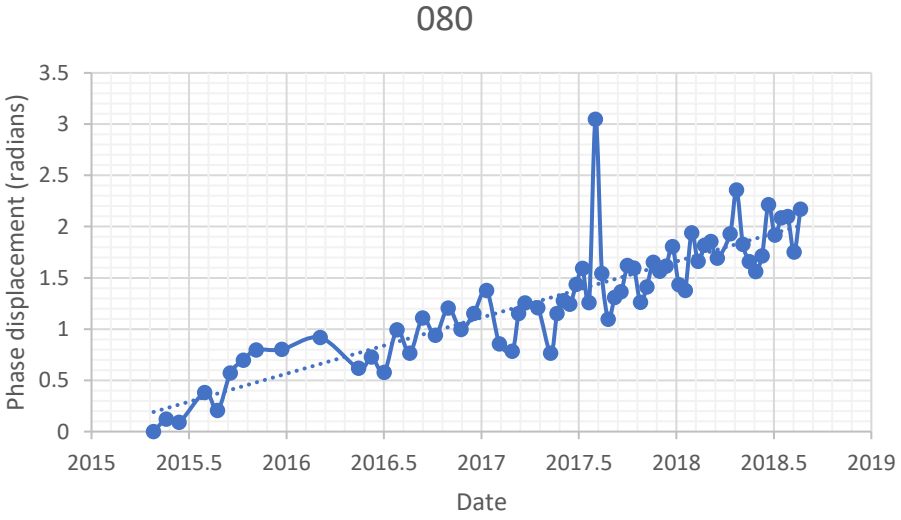

Peak: Blanca

Mean Elevation: 3517

Azimuth: 216

Average flow rate: 0.547723

Sensitivity: 0.460603

ACTIVE

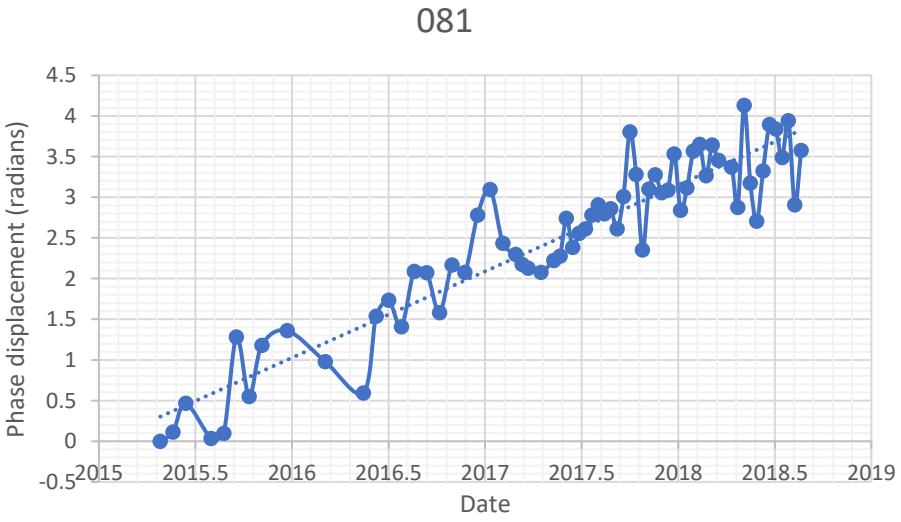

Peak: Blanca

Mean Elevation: 3636

Azimuth: 189

Average flow rate: 1.06222

Sensitivity: 0.260702

ACTIVE

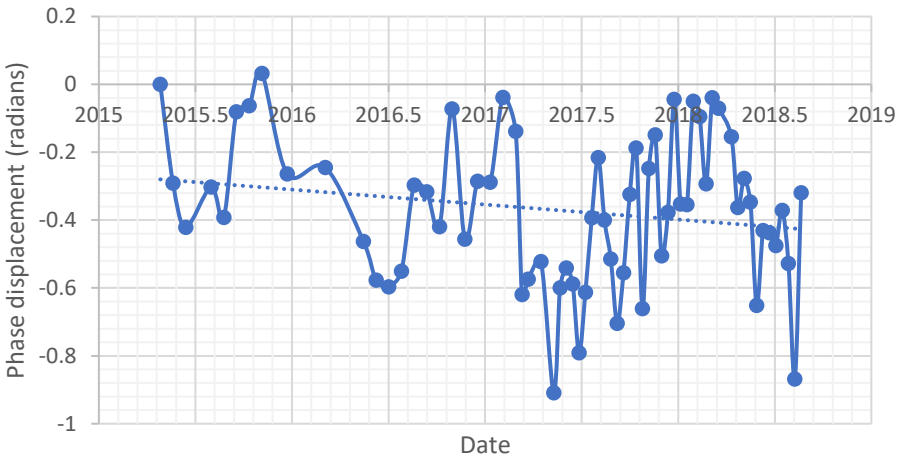

Peak: Blanca

Mean Elevation: 3693

Azimuth: 20

Average flow rate: -0.0441

Sensitivity: 0.142103

INACTIVE

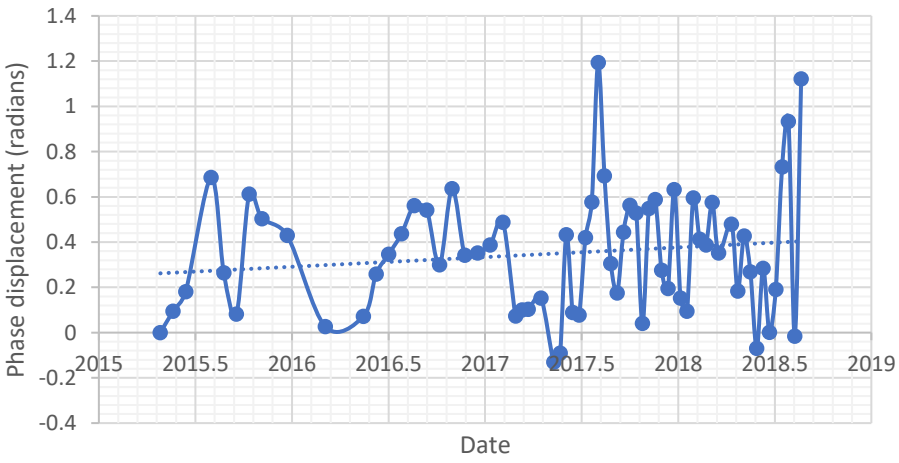

Peak: Blanca

Mean Elevation: 3643

Azimuth: 261

Average flow rate: 0.042694

Sensitivity: 0.814107

INACTIVE

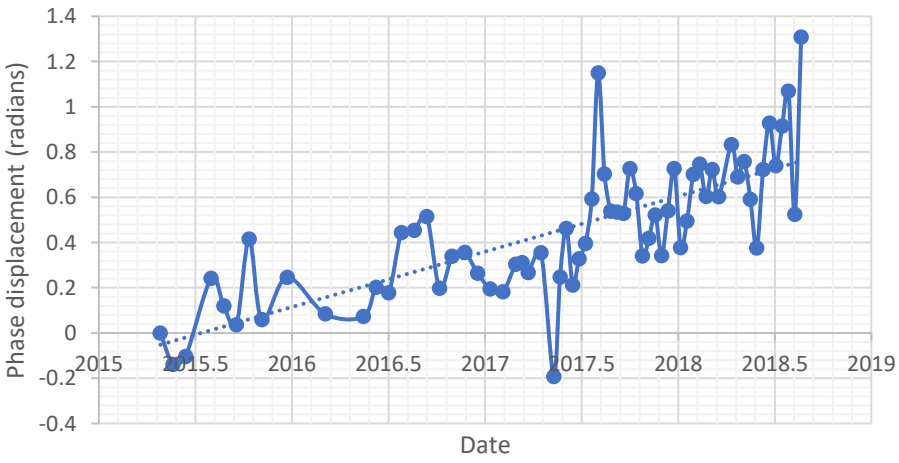

Peak: Blanca

Mean Elevation: 3612

Azimuth: 280

Average flow rate: 0.244756

Sensitivity: 0.766176

ACTIVE

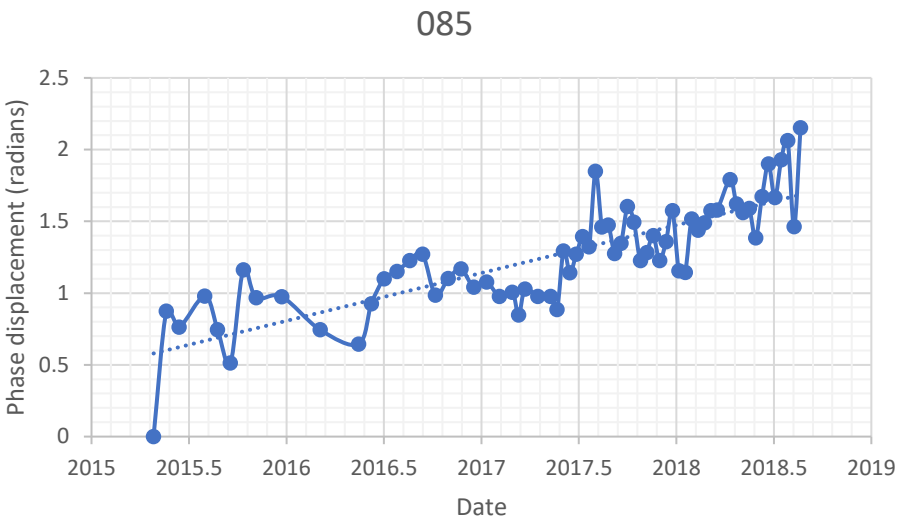

Peak: Blanca

Mean Elevation: 3552

Azimuth: 244

Average flow rate: 0.333373

Sensitivity: 0.803669

ACTIVE

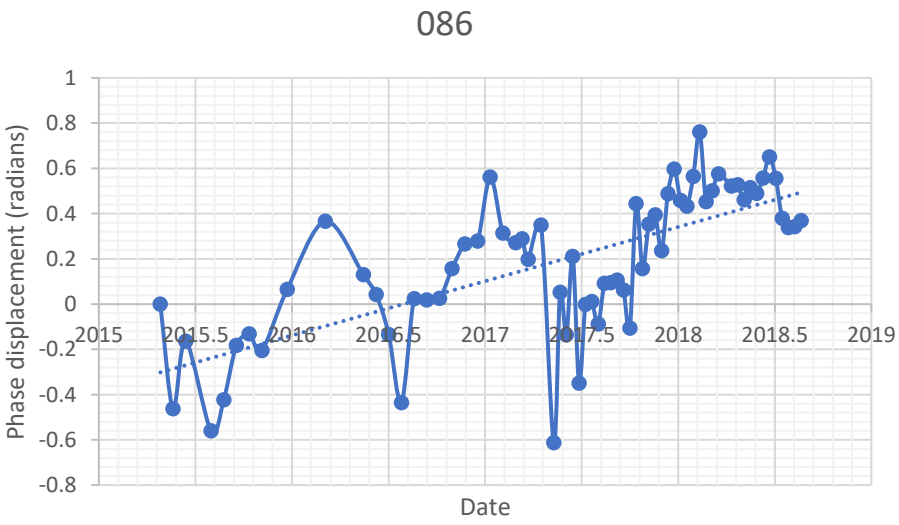

Peak: Blanca

Mean Elevation: 3701

Azimuth: 324

Average flow rate: 0.239702

Sensitivity: 0.69383

ACTIVE

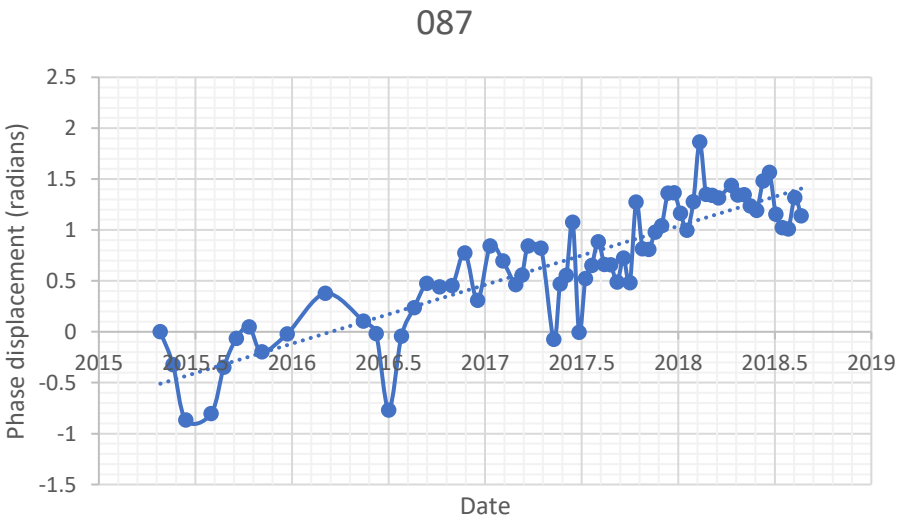

Peak: Blanca

Mean Elevation: 3619

Azimuth: 222

Average flow rate: 0.577596

Sensitivity: 0.517438

ACTIVE

Appendix B

This chapter contains the time series of Land Surface Temperatures for each rock glacier. The data source was Landsat 7 and 8. The best fit line was produced in Matlab using a 10 term sinusoidal function, with each term representing a different period function from a 1 year period to a 10 year period. The amplitude of the one year period component, representing annual variation in temperature, is stated below the time series along with the vertical shift representing average annual temperature, the R^2 value to display the fit of the function and the root mean square error. The activity classification as obtained from the displacement time series, as produced from InSAR, is also listed. All of the time series cover a period from 2000 to 2019 and a temperature range of -20 to 50 degrees Celsius is used for the y axis on all of them.

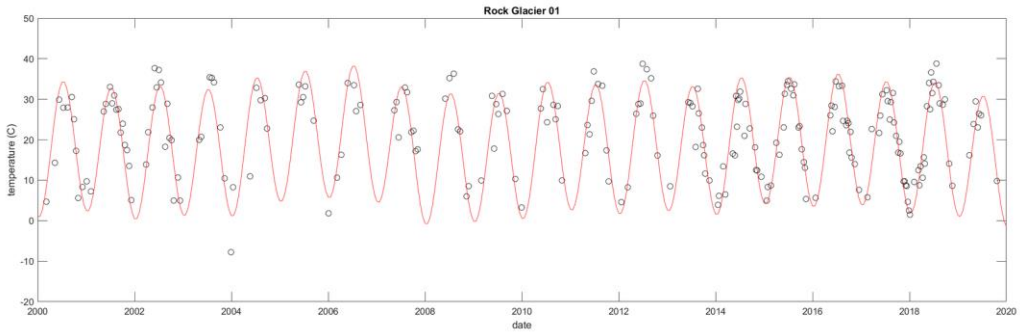

A1: 15.948 T0: 18.063 R^2: 0.91106 RMSE: 41.719 ACTIVE

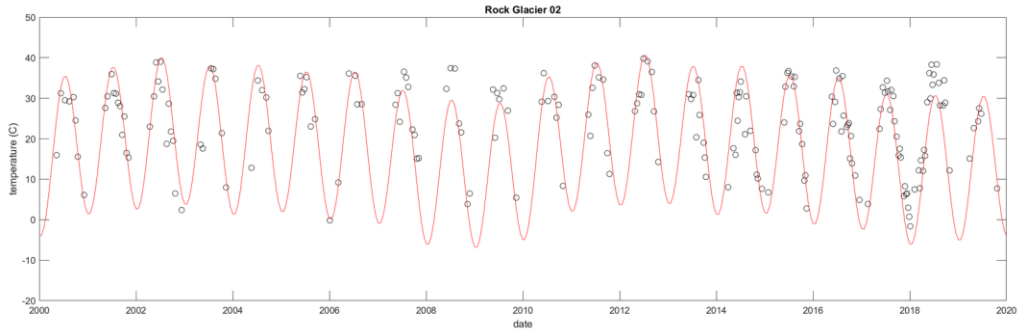

A1: 13.206 T0: 18.372 R^2: 0.87 RMSE: 53.951 ACTIVE

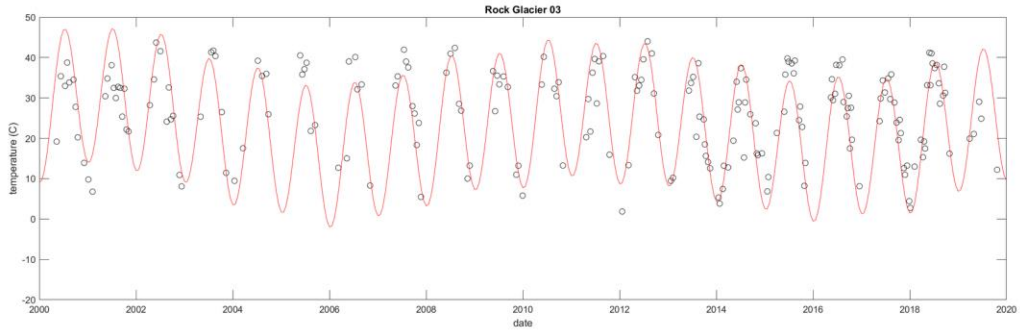

A1: 17.182 T0: 22.233 R^2: 0.91559 RMSE: 46.404 ACTIVE

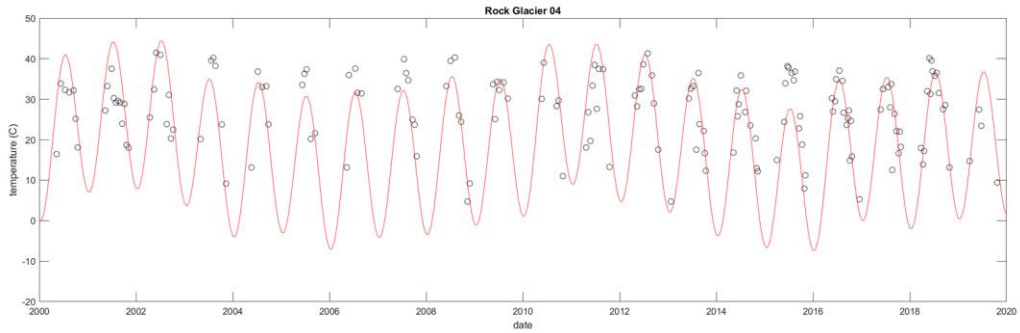

A1: 18.512 T0: 17.852 R^2: 0.83004 RMSE: 49.531 ACTIVE

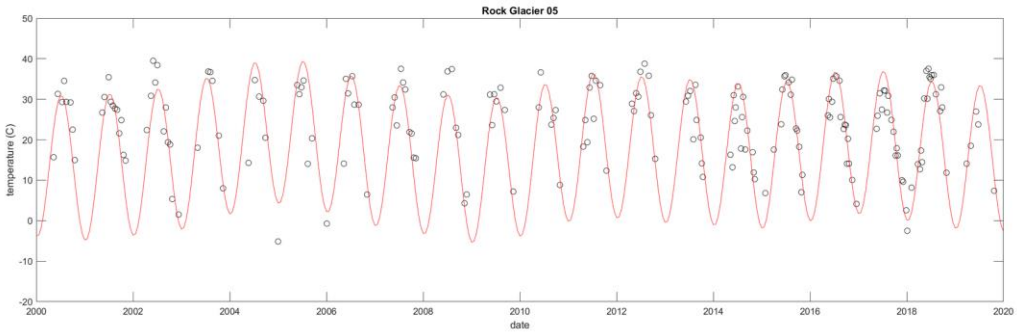

A1: 17.972 T0: 16.58 R^2: 0.9146 RMSE: 42.44 ACTIVE

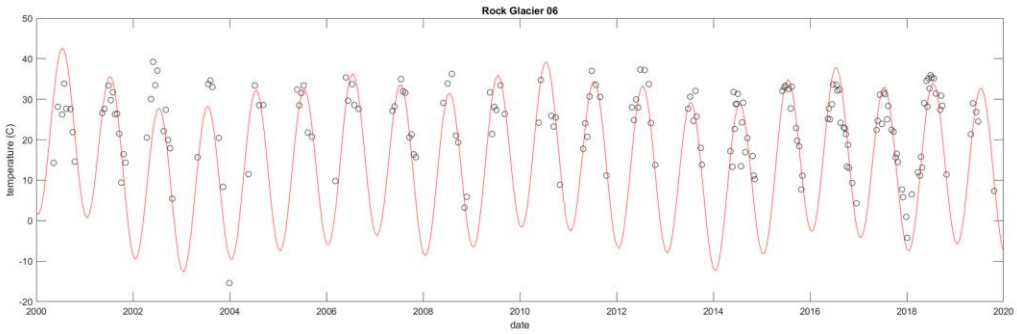

A1: 20.317 T0: 13.223 R^2: 0.90896 RMSE: 46.857 INACTIVE

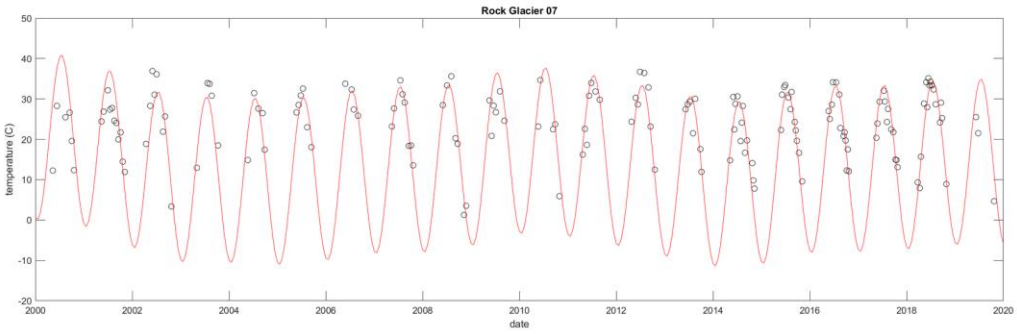

A1: 20.14 T0: 13.089 R^2: 0.89944 RMSE: 32.101 INACTIVE

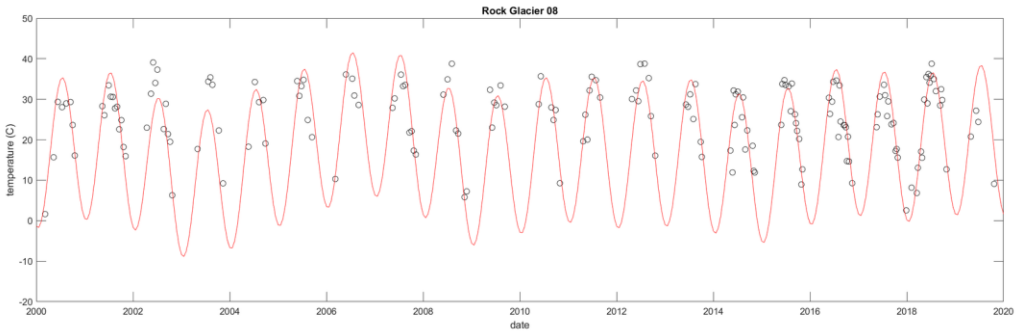

A1: 18.314 T0: 16.63 R^2: 0.8918 RMSE: 36.26 ACTIVE

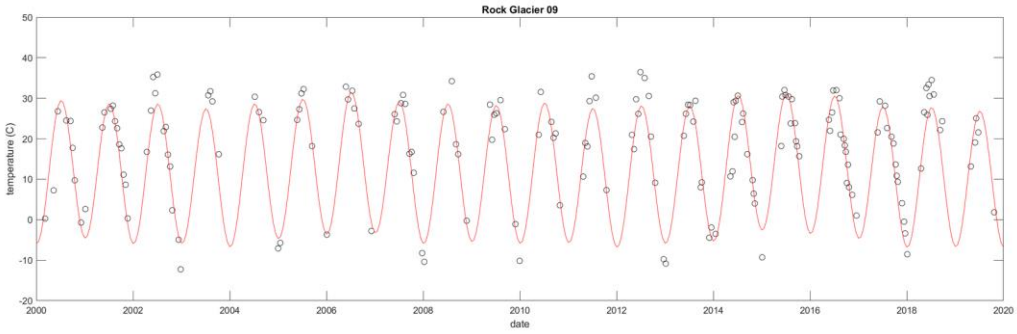

A1: 20.199 T0: 12.21 R^2: 0.96168 RMSE: 43.08 ACTIVE

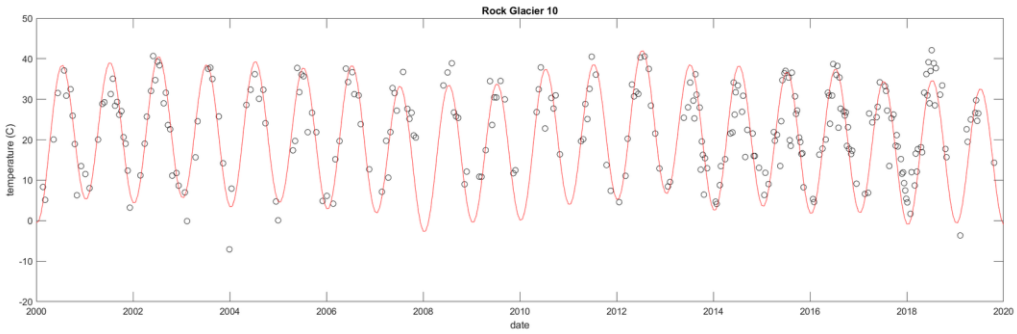

A1: 17.347 T0: 19.976 R^2: 0.9195 RMSE: 45.976 ACTIVE

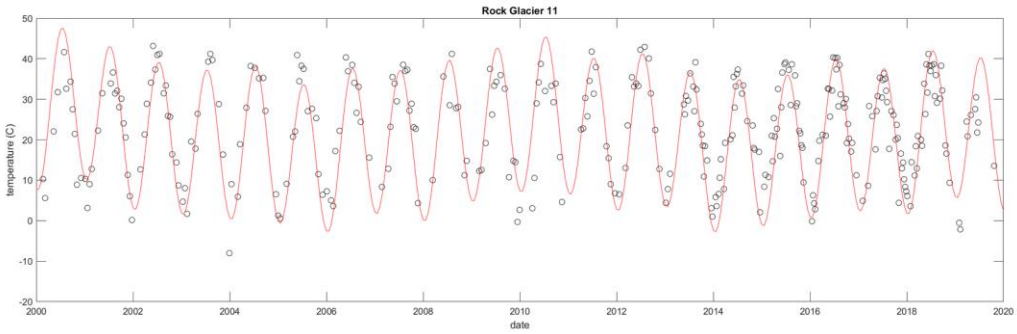

A1: 18.462 T0: 20.842 R^2: 0.92838 RMSE: 52.033 INACTIVE

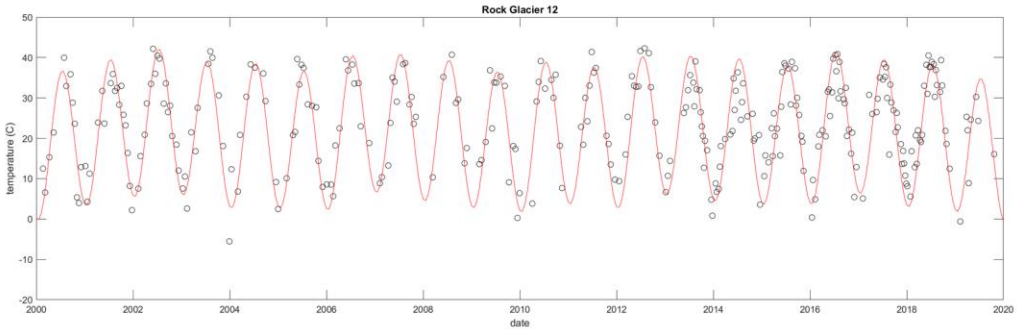

A1: 17.712 T0: 21.388 R^2: 0.90969 RMSE: 52.213 ACTIVE

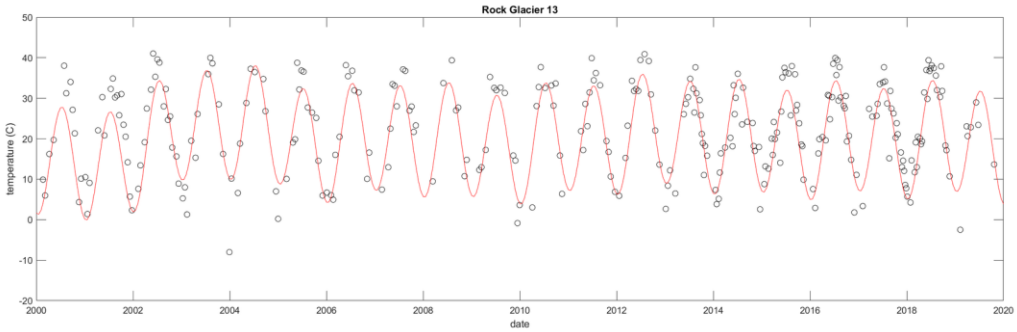

A1: 17.892 T0: 20.216 R^2: 0.9185 RMSE: 49.883 ACTIVE

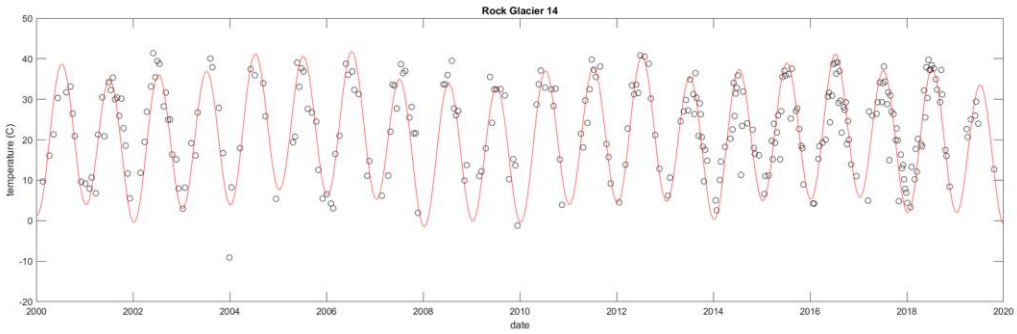

A1: 17.262 T0: 20.162 R^2: 0.89941 RMSE: 52.063 INACTIVE

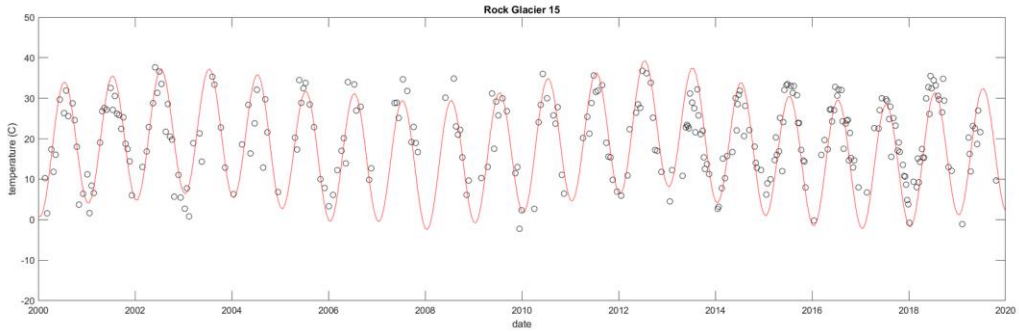

A1: 15.638 T0: 17.658 R^2: 0.9057 RMSE: 39.701 INACTIVE

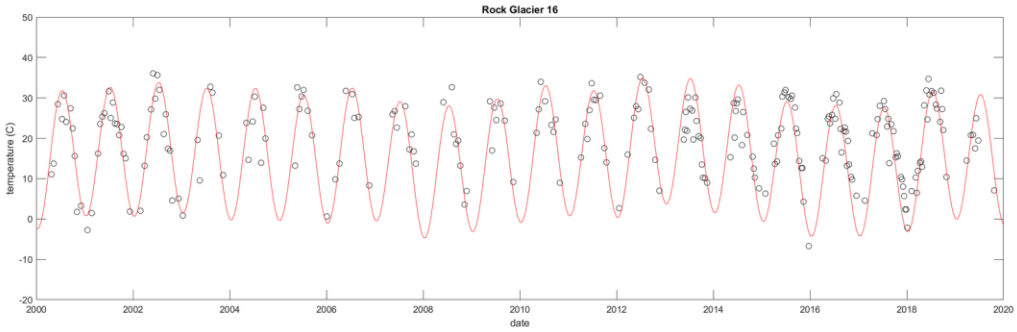

A1: 16.147 T0: 15.422 R^2: 0.9173 RMSE: 35.712 ACTIVE

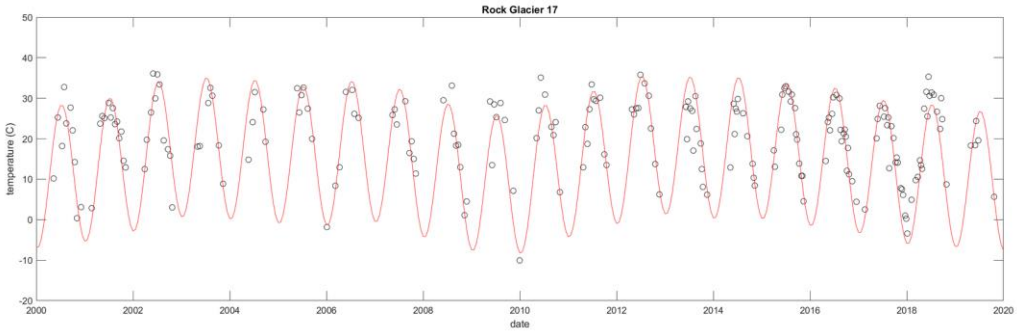

A1: 17.347 T0: 14.399 R^2: 0.92327 RMSE: 37.425 ACTIVE

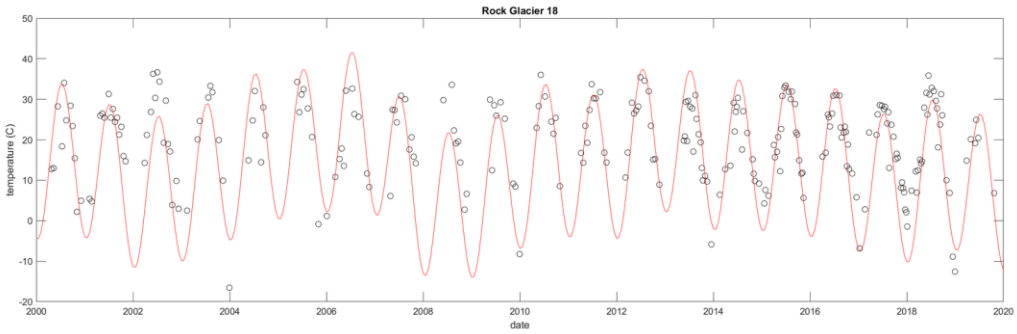

A1: 18.811 T0: 14.368 R^2: 0.8978 RMSE: 55.147 INACTIVE

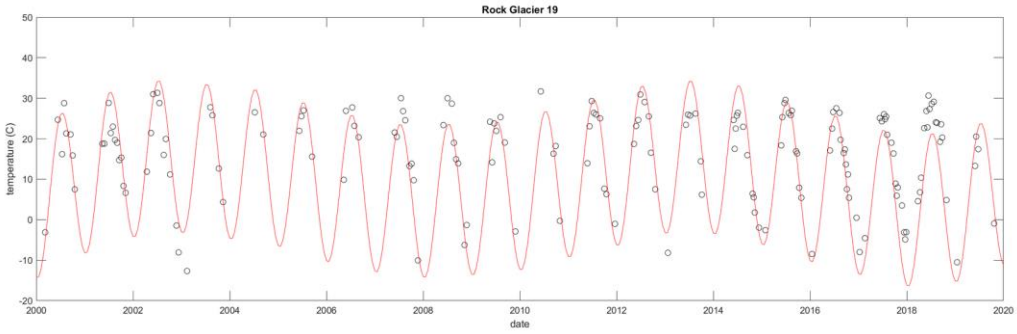

A1: 18.766 T0: 9.6638 R^2: 0.9511 RMSE: 38.641 INACTIVE

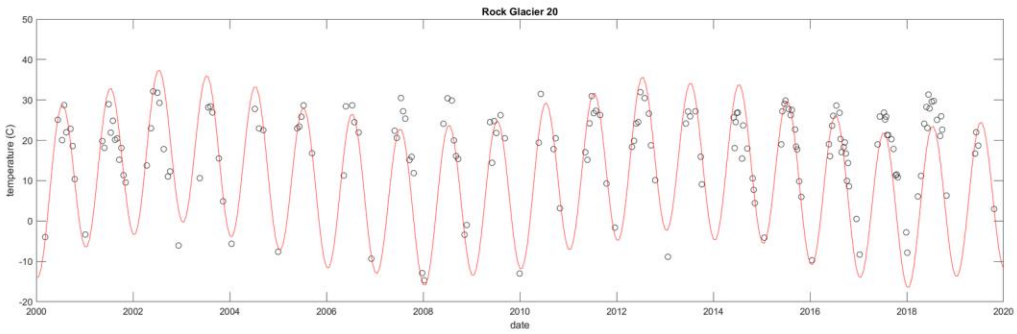

A1: 12.873 T0: 7.8427 R^2: 0.8452 RMSE: 72.925 INACTIVE

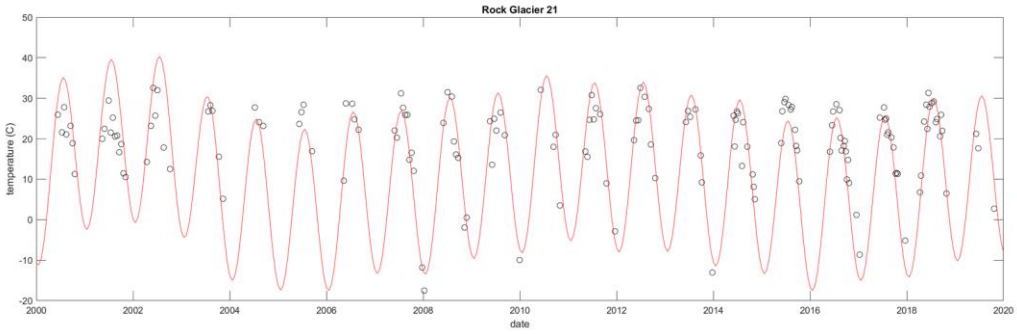

A1: 20.536 T0: 9.5775 R^2: 0.96179 RMSE: 33.506 INACTIVE

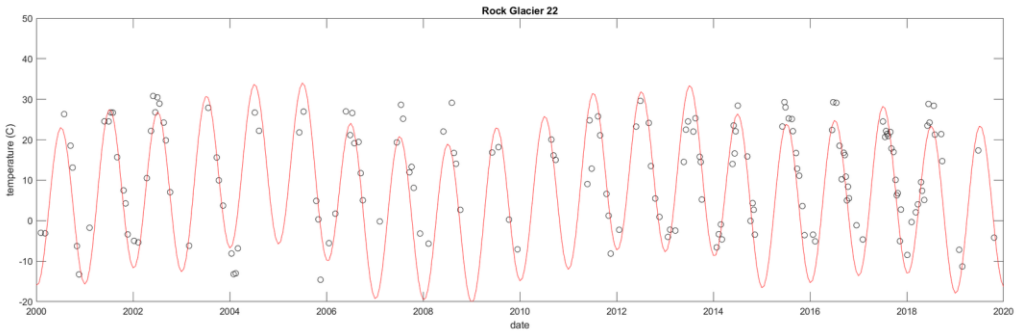

A1: 13.77 T0: 6.2789 R^2: 0.84304 RMSE: 92.954 ACTIVE

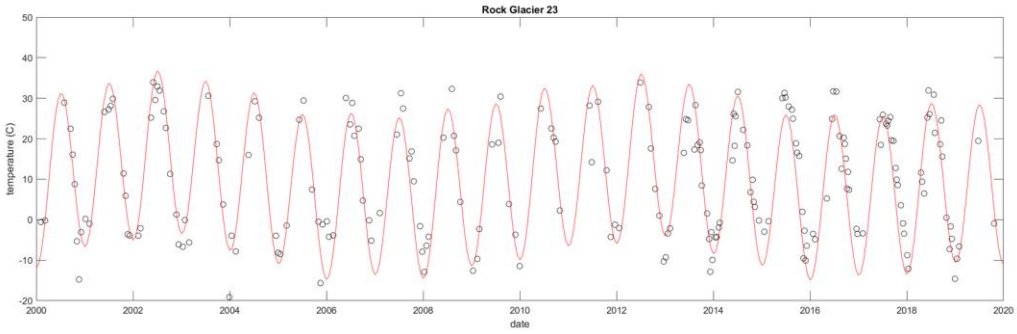

A1: 19.954 T0: 10.27 R^2: 0.94219 RMSE: 62.905 INACTIVE

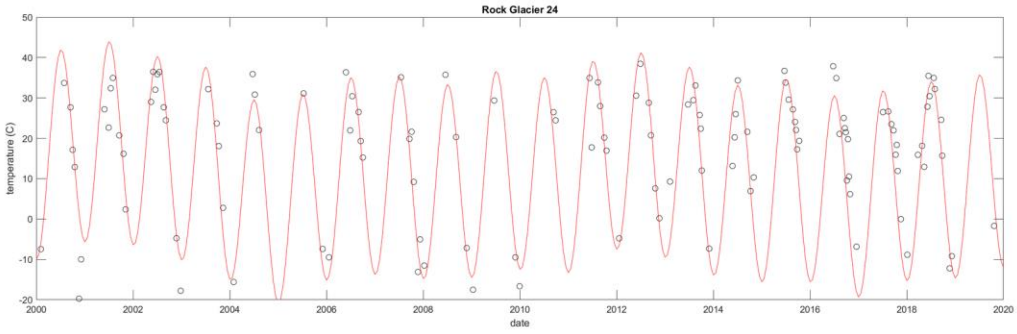

A1: 24.696 T0: 11.098 R^2: 0.95817 RMSE: 71.407 INACTIVE

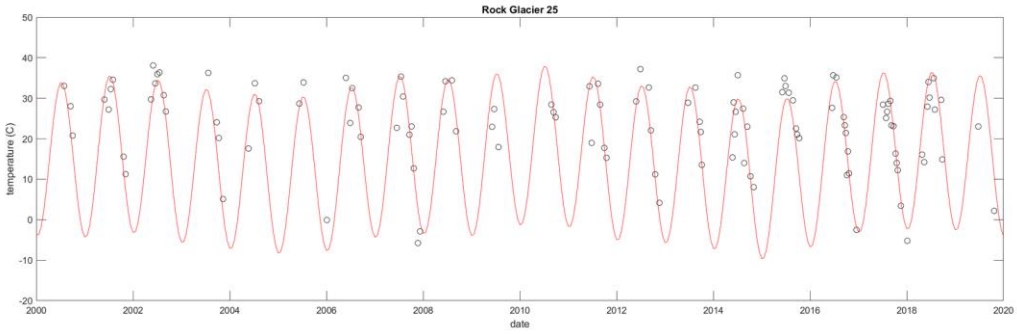

A1: 19.602 T0: 13.698 R^2: 0.95242 RMSE: 36.774 INACTIVE

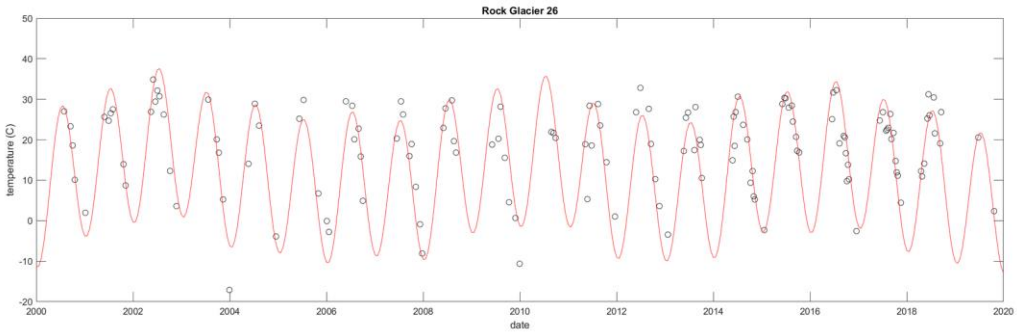

A1: 14.166 T0: 10.80 R^2: 0.89132 RMSE: 58.868 ACTIVE

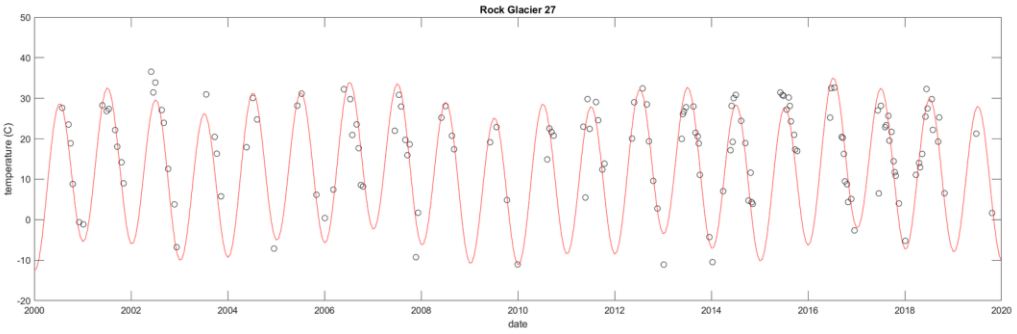

A1: 18.42 T0: 11.467 R^2: 0.92068 RMSE: 53.507 INACTIVE

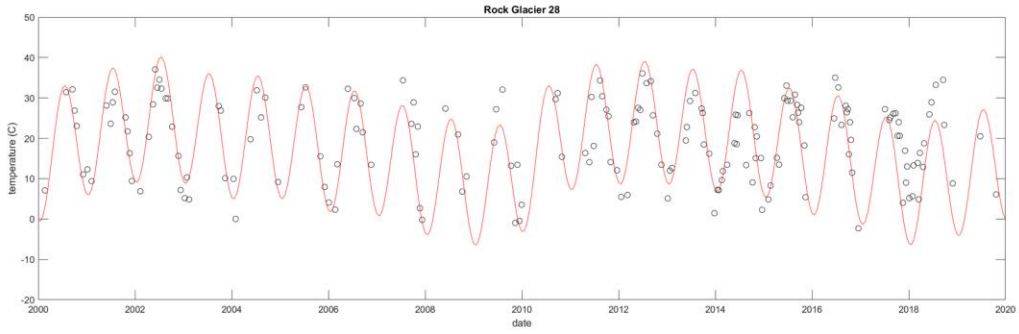

A1: 15.434 T0: 17.41 R^2: 0.89016 RMSE: 45.286 INACTIVE

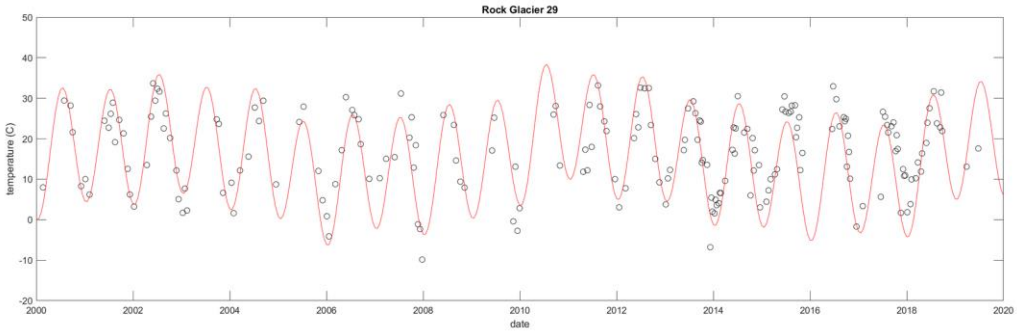

A1: 14.697 T0: 15.409 R^2: 0.89231 RMSE: 45.924 ACTIVE

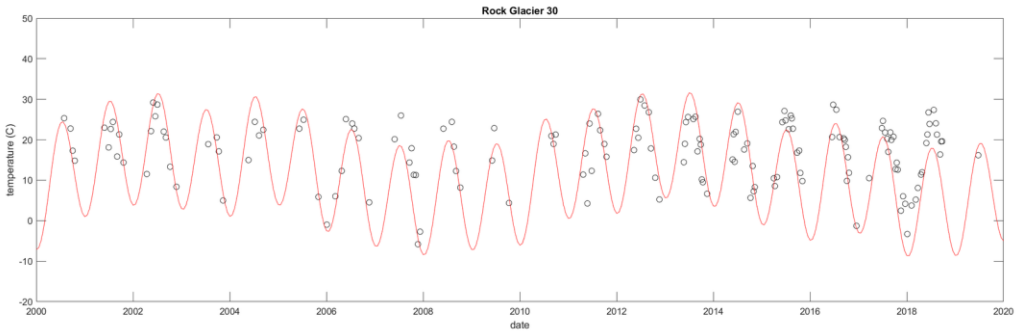

A1: 14.429 T0: 9.9445 R^2: 0.91693 RMSE: 26.718 ACTIVE

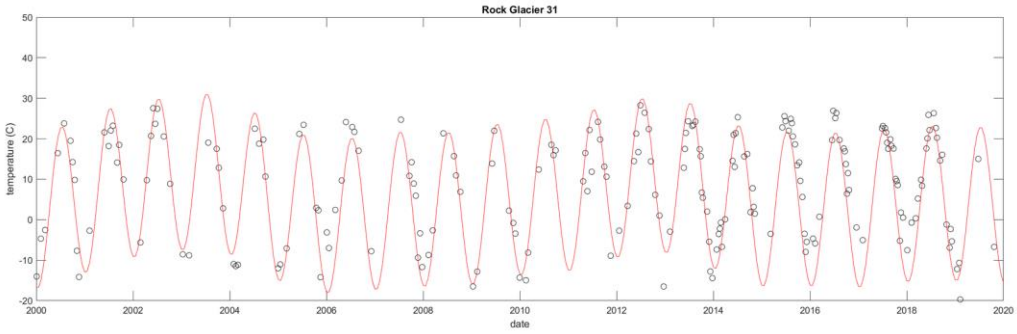

A1: 17.142 T0: 5.1776 R^2: 0.92143 RMSE: 63.76 ACTIVE

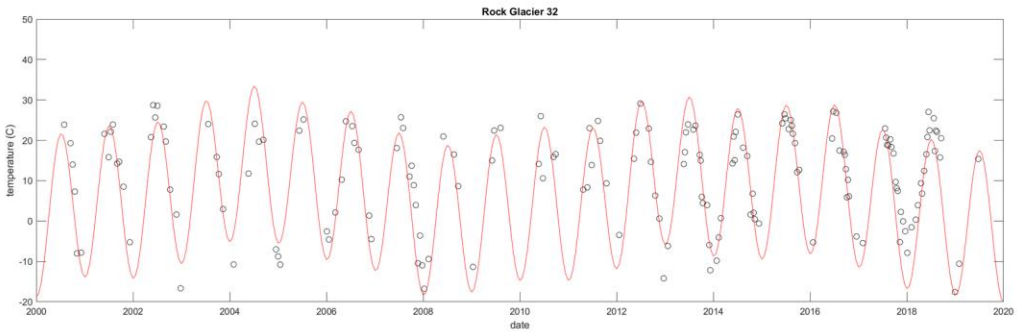

A1: 18.474 T0: 7.0843 R^2: 0.94801 RMSE: 48.369 INACTIVE

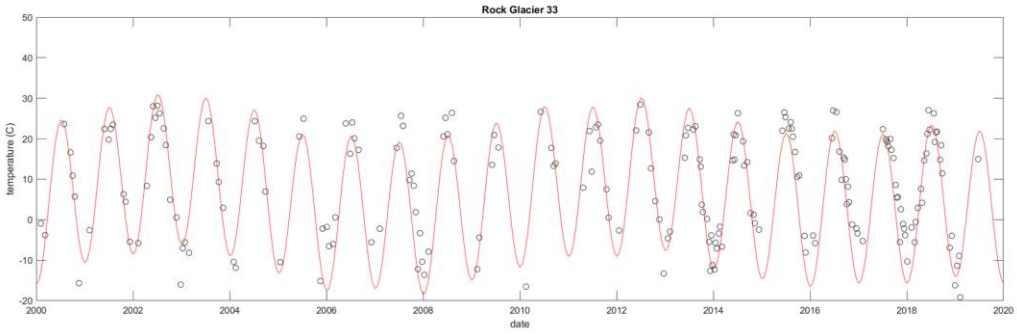

A1: 18.793 T0: 5.8557 R^2: 0.93868 RMSE: 56.546 ACTIVE

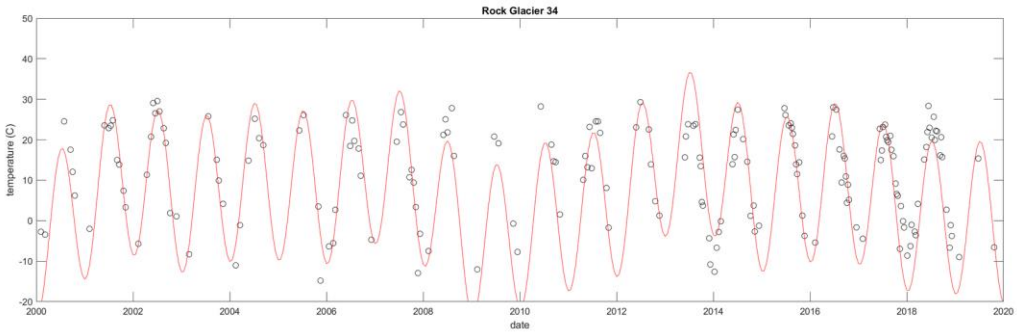

A1: 13.921 T0: 5.8476 R^2: 0.85067 RMSE: 83.445 ACTIVE

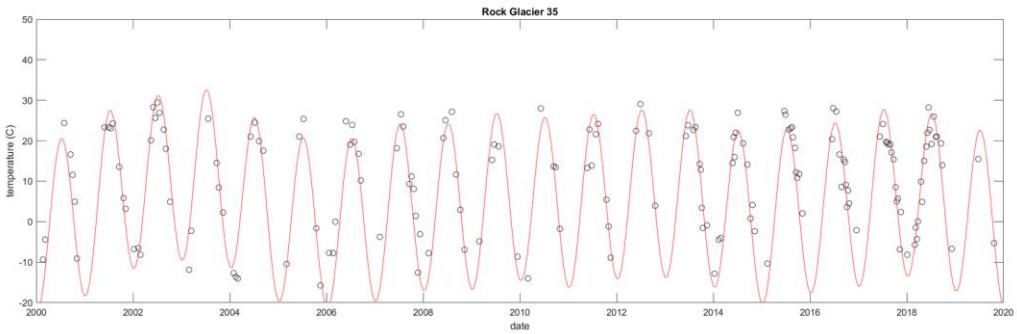

A1: 18.103 T0: 4.487 R^2: 0.90989 RMSE: 72.468 ACTIVE

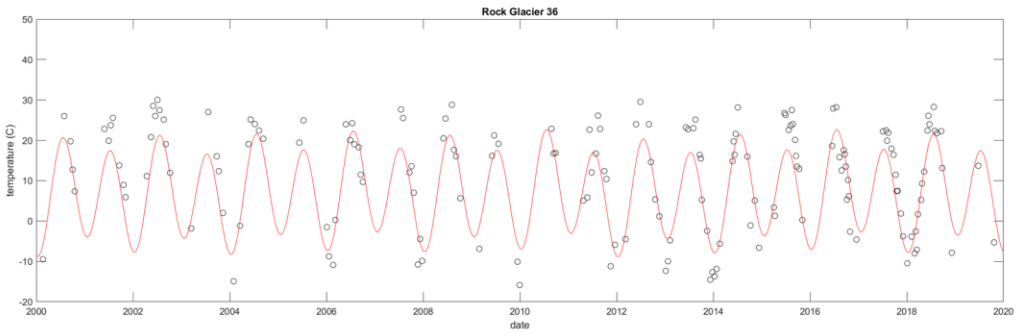

A1: 13.159 T0: 6.093 R^2: 0.87038 RMSE: 78.276 ACTIVE

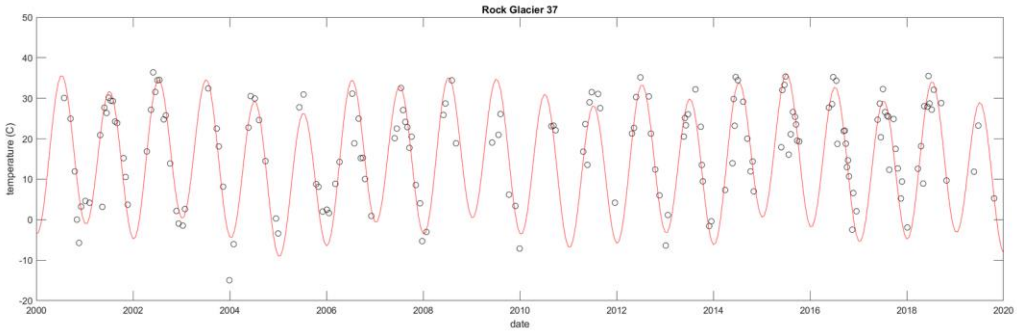

A1: 18.101 T0: 13.802 R^2: 0.92633 RMSE: 53.656 ACTIVE

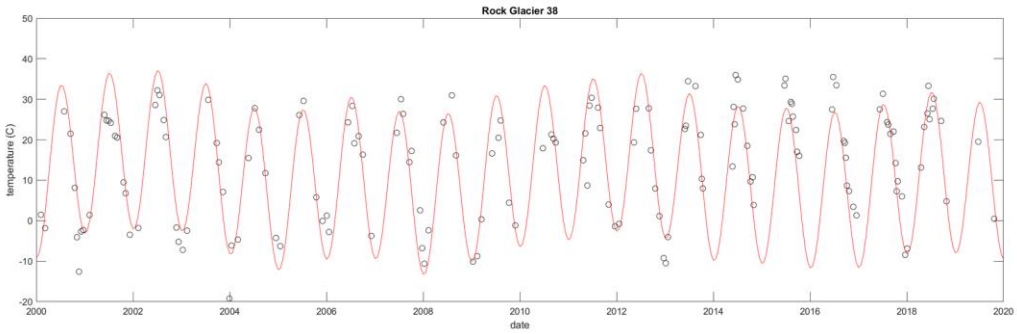

A1: 19.649 T0: 11.419 R^2: 0.94301 RMSE: 59.778 INACTIVE

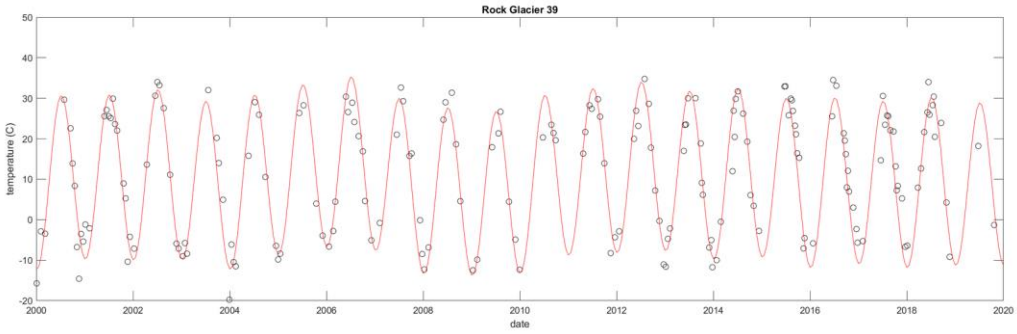

A1: 20.742 T0: 9.8991 R^2: 0.95825 RMSE: 58.839 ACTIVE

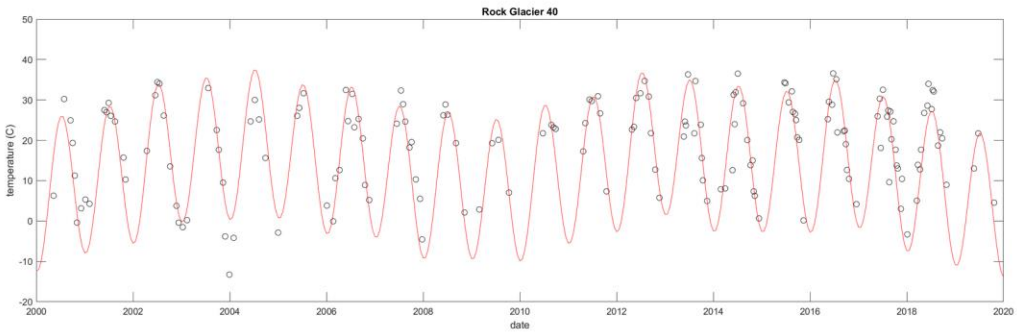

A1: 15.219 T0: 14.305 R^2: 0.91048 RMSE: 53.969 INACTIVE

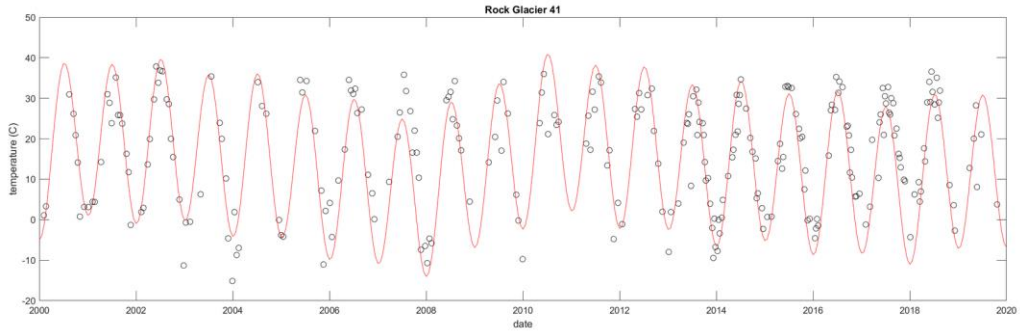

A1: 19.597 T0: 14.04 R^2: 0.94153 RMSE: 58.282 ACTIVE

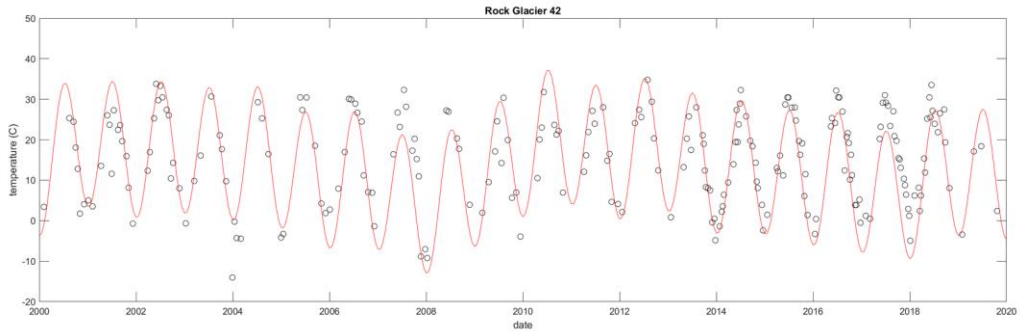

A1: 10.915 T0: 12.666 R^2: 0.82448 RMSE: 72.916 ACTIVE

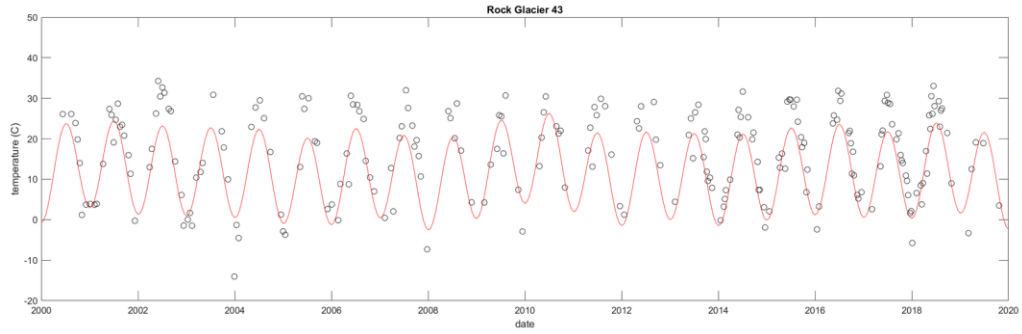

A1: 16.413 T0: 13.411 R^2: 0.9368 RMSE: 39.576 ACTIVE

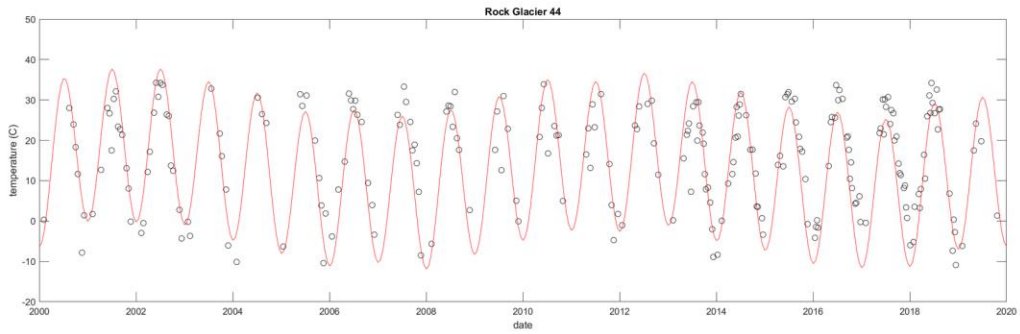

A1: 18.853 T0: 12.364 R^2: 0.94669 RMSE: 48.042 ACTIVE

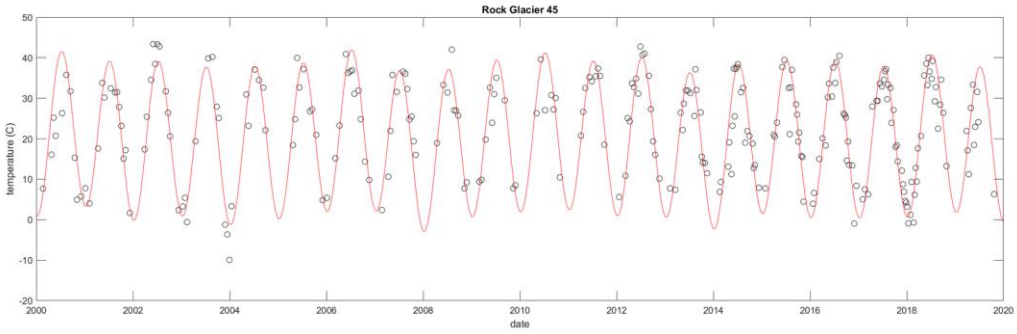

A1: 14.062 T0: 19.575 R^2: 0.86819 RMSE: 72.394 INACTIVE

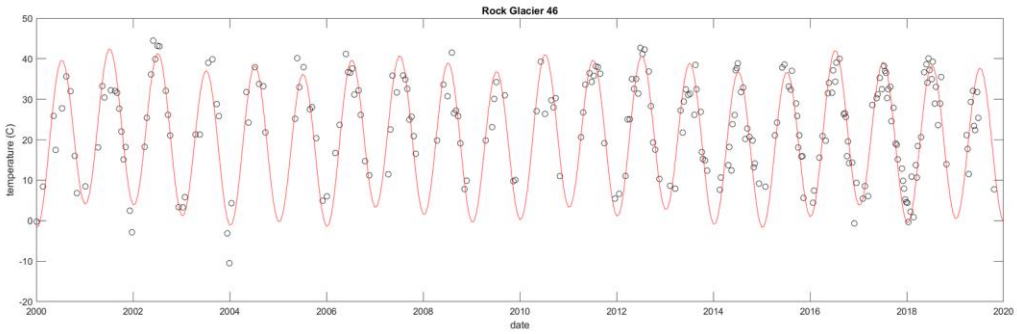

A1: 19.181 T0: 19.984 R^2: 0.92829 RMSE: 52.759 ACTIVE

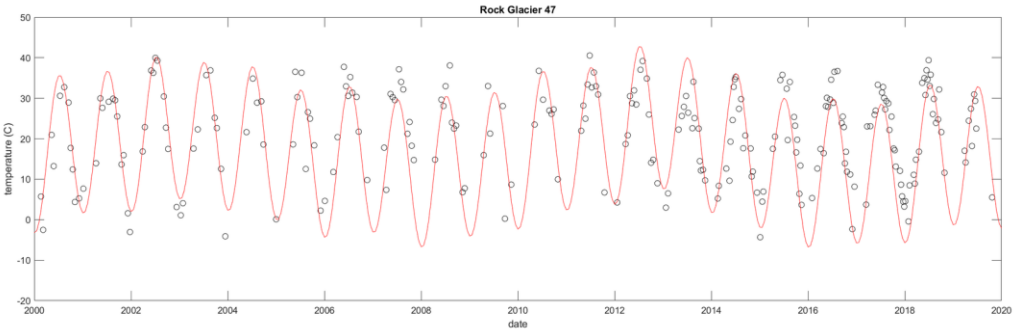

A1: 17.596 T0: 17.165 R^2: 0.89603 RMSE: 55.936 INACTIVE

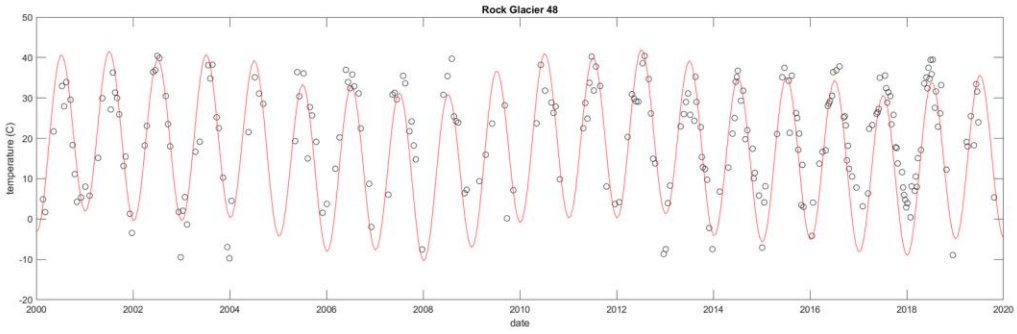

A1: 20.117 T0: 16.751 R^2: 0.9265 RMSE: 63.864 INACTIVE

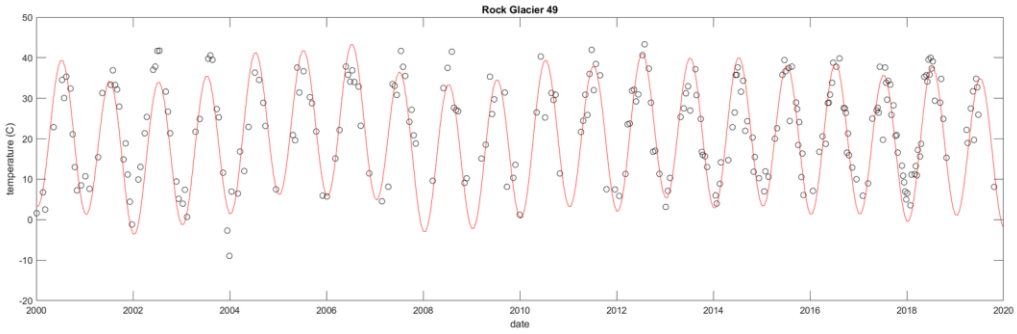

A1: 18.314 T0: 20.006 R^2: 0.92814 RMSE: 50.241 ACTIVE

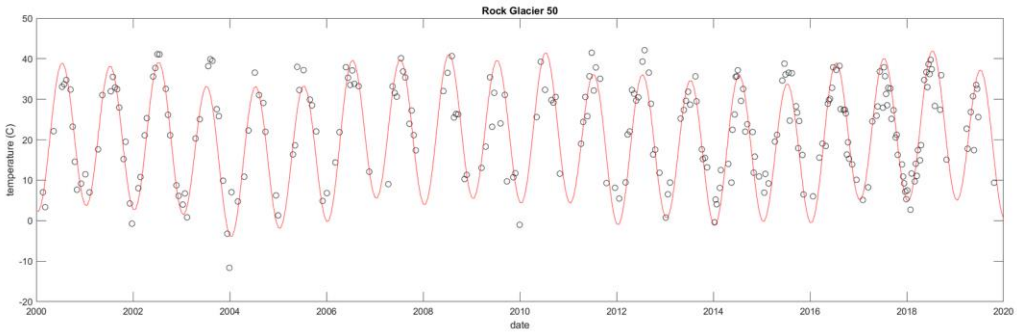

A1: 17.929 T0: 19.886 R^2: 0.91598 RMSE: 54.89 ACTIVE

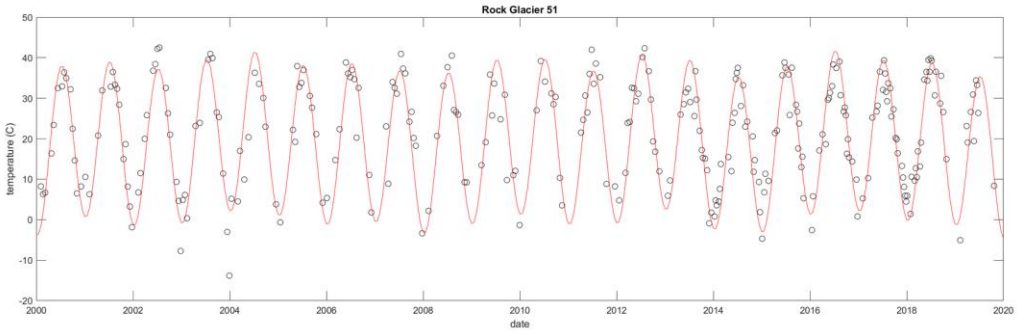

A1: 19.54 T0: 19.231 R^2: 0.92761 RMSE: 59.791 ACTIVE

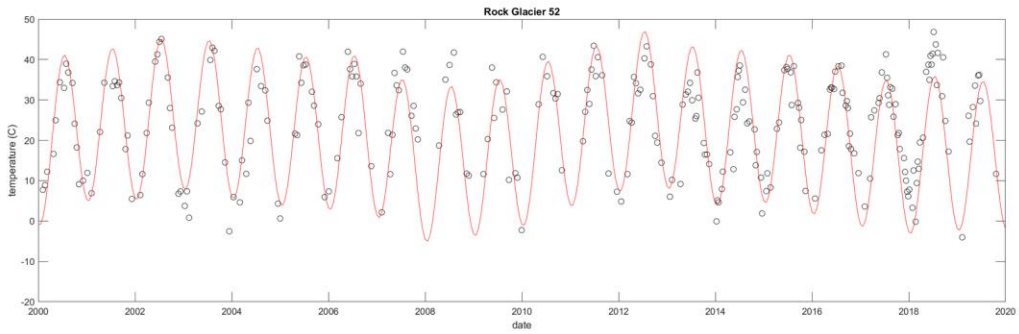

A1: 19.024 T0: 21.28 R^2: 0.92686 RMSE: 54.822 INACTIVE

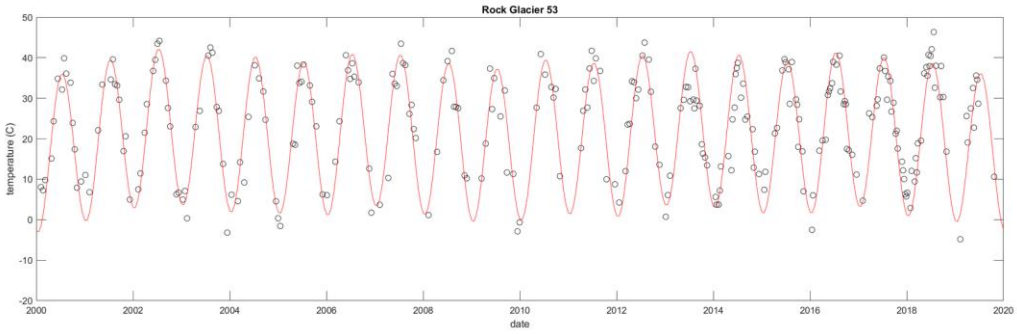

A1: 19.162 T0: 20.499 R^2: 0.94207 RMSE: 51.178 ACTIVE

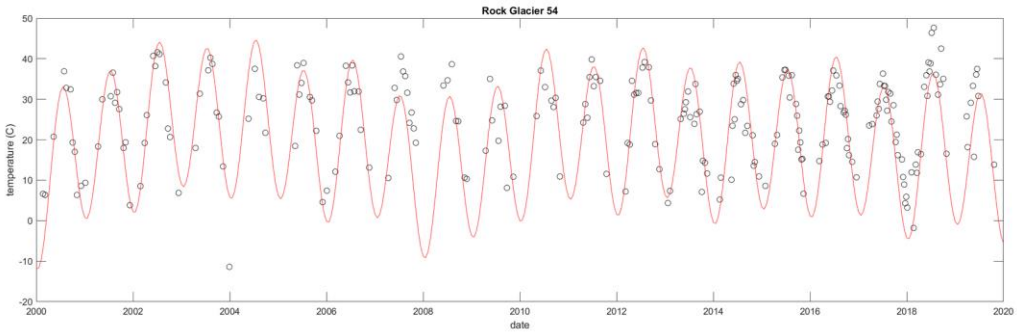

A1: 18.538 T0: 18.707 R^2: 0.88969 RMSE: 57.889 INACTIVE

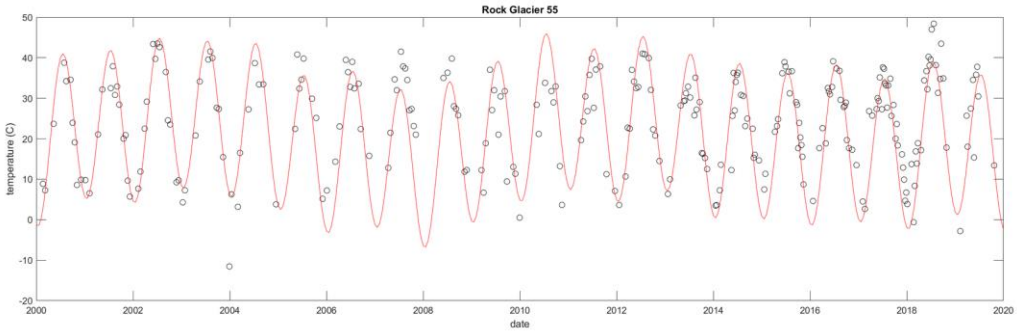

A1: 18.66 T0: 20.939 R^2: 0.90445 RMSE: 61.265 ACTIVE

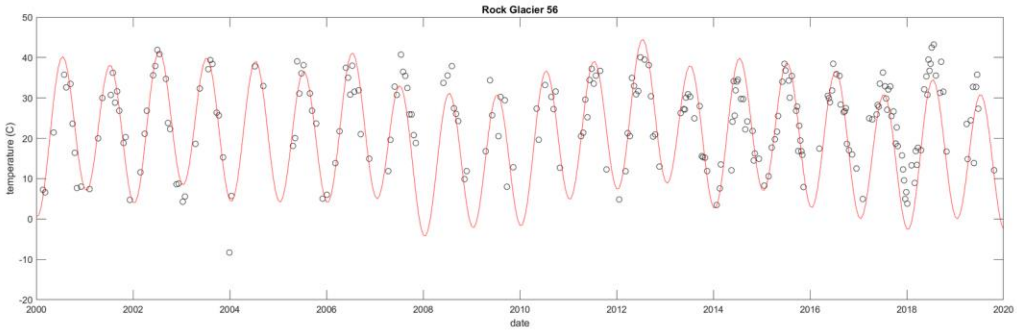

A1: 17.05 T0: 19.947 R^2: 0.91276 RMSE: 46.333 INACTIVE

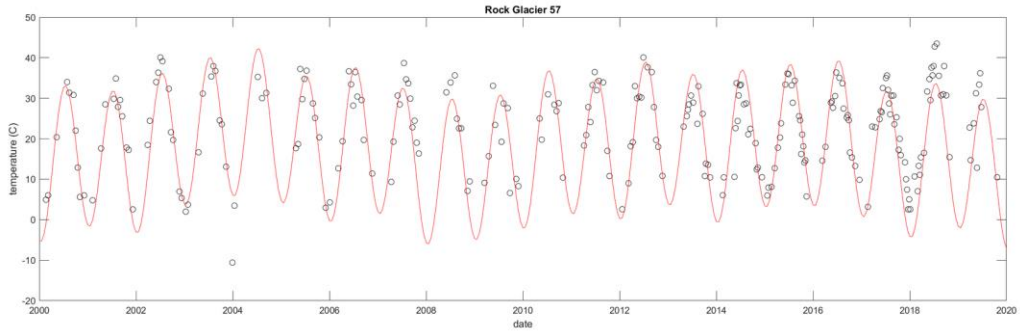

A1: 17.446 T0: 18.621 R^2: 0.90992 RMSE: 48.9 ACTIVE

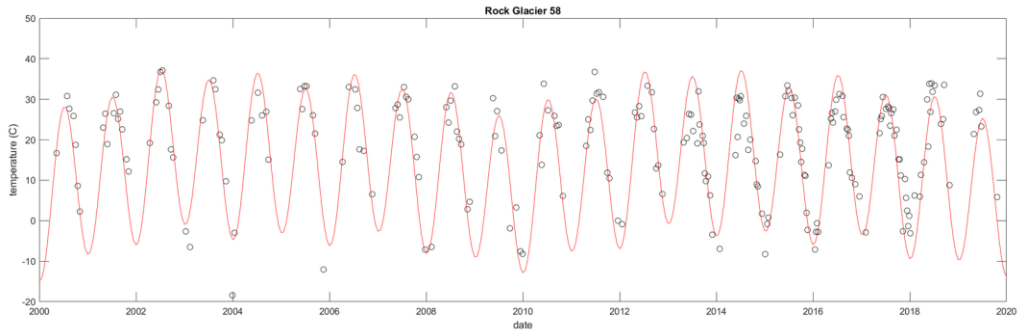

A1: 19.381 T0: 13.62 R^2: 0.91021 RMSE: 63.731 INACTIVE

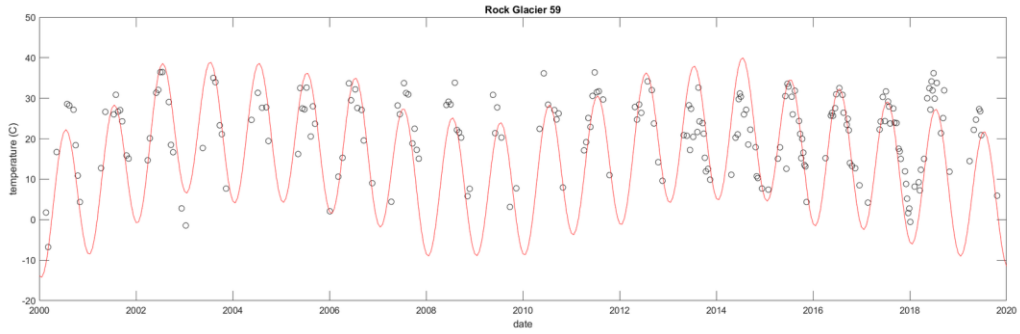

A1: 16.949 T0: 15.024 R^2: 0.89446 RMSE: 42.122 ACTIVE

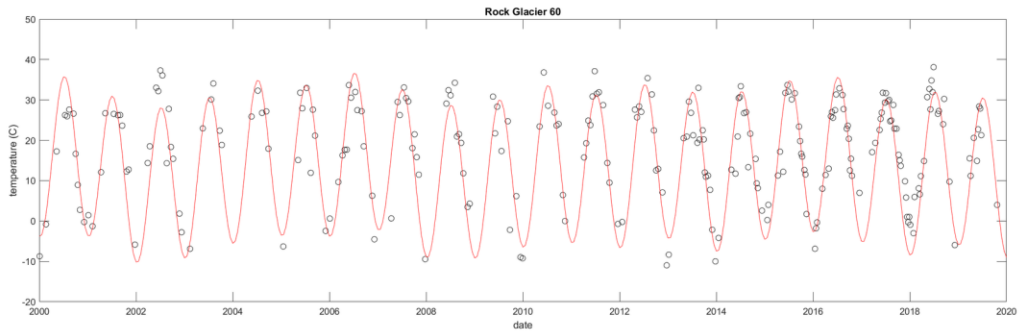

A1: 19.333 T0: 13.46 R^2: 0.93306 RMSE: 54.799 ACTIVE

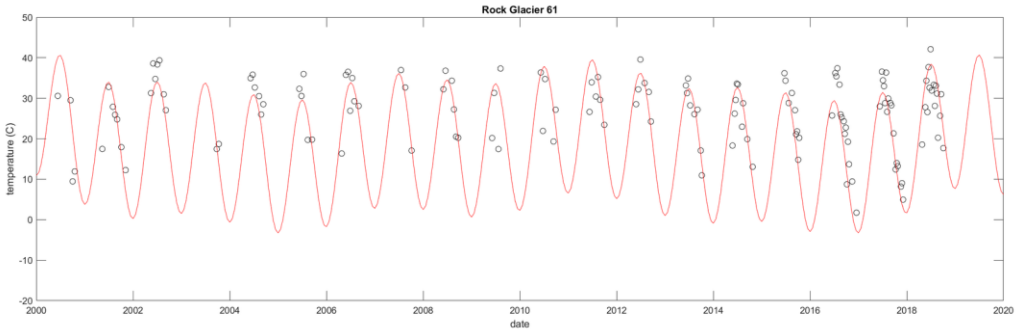

A1: 16.819 T0: 17.499 R^2: 0.89655 RMSE: 35.717 ACTIVE

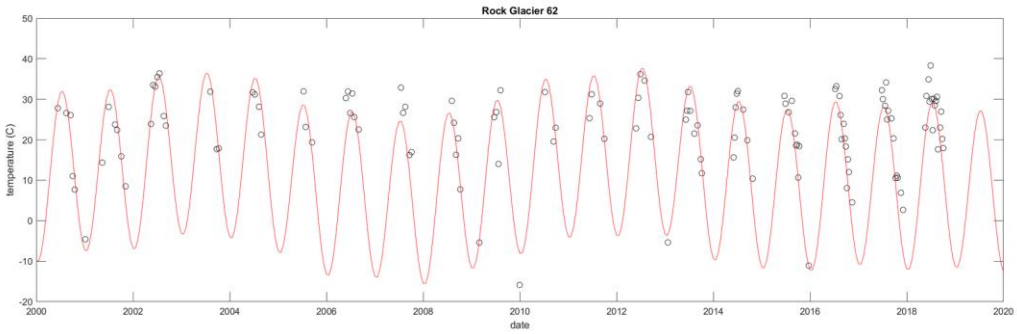

A1: 12.611 T0: 11.783 R^2: 0.87042 RMSE: 67.623 ACTIVE

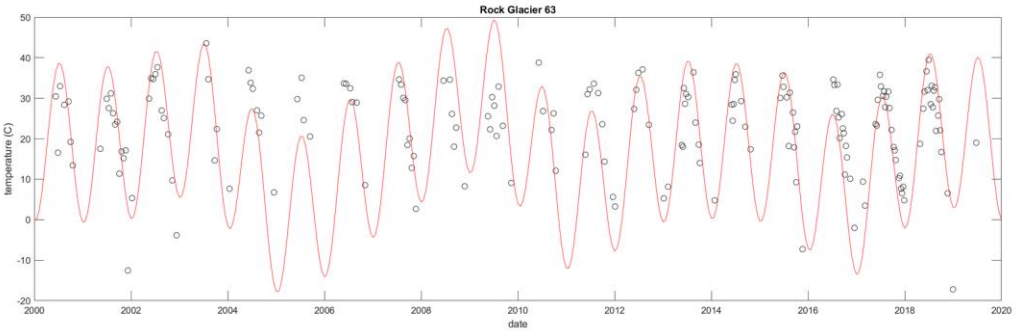

A1: 19.69 T0: 15.215 R^2: 0.89221 RMSE: 66.092 ACTIVE

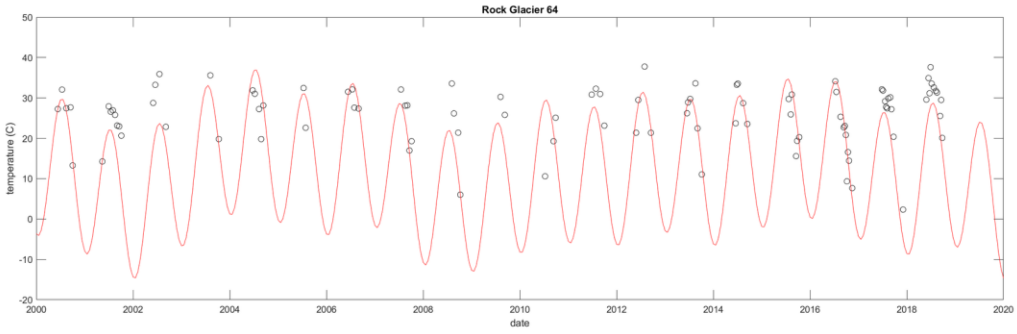

A1: 17.649 T0: 11.602 R^2: 0.86438 RMSE: 32.785 INACTIVE

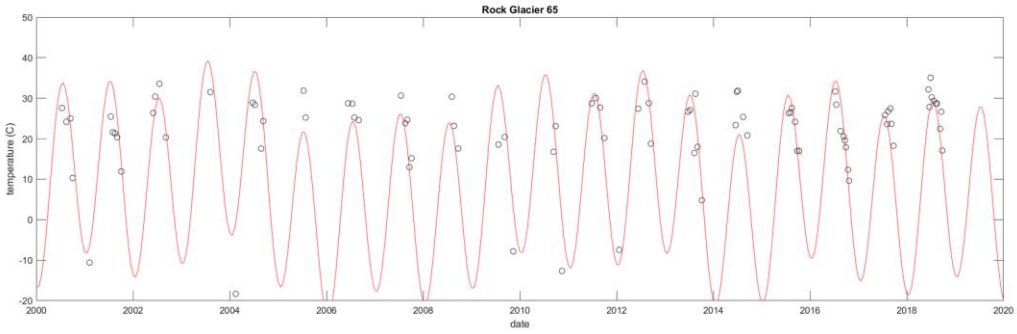

A1: 11.056 T0: 5.4739 R^2: 0.83312 RMSE: 83.518 INACTIVE

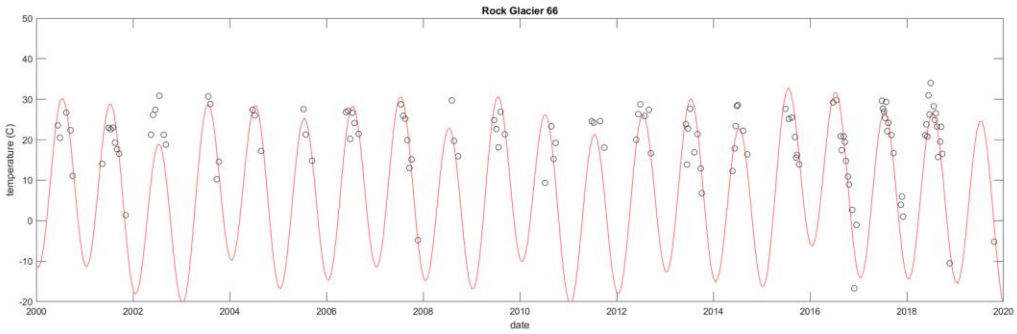

A1: 20.794 T0: 6.296 R^2: 0.91289 RMSE: 44.73 INACTIVE

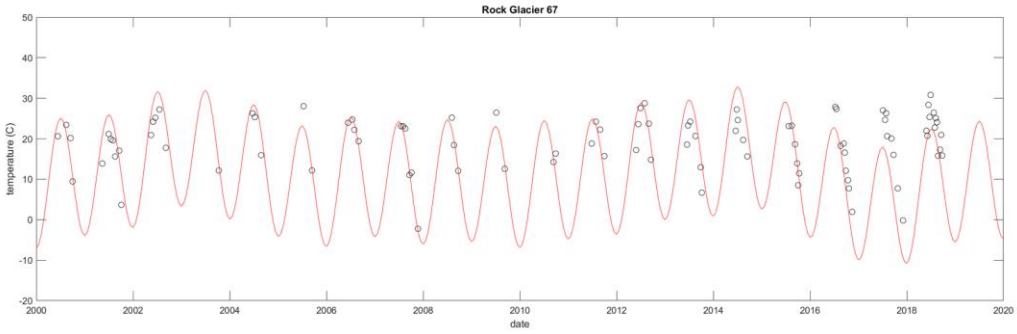

A1: 15.398 T0: 10.605 R^2: 0.97869 RMSE: 11.845 INACTIVE

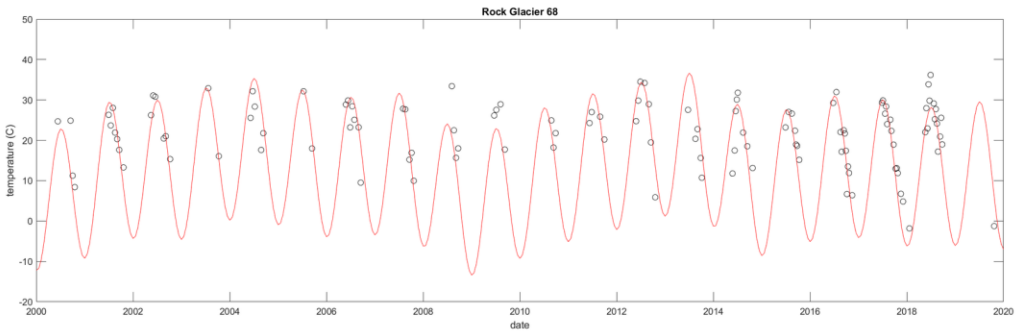

A1: 17.065 T0: 13.448 R^2: 0.89815 RMSE: 32.969 INACTIVE

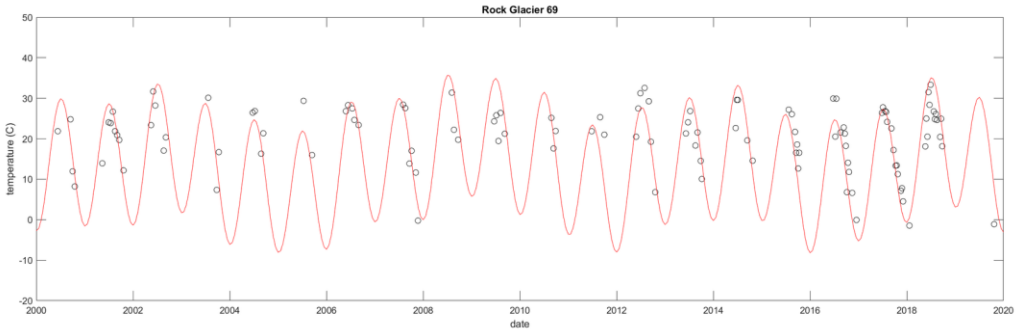

A1: 15.81 T0: 12.94 R^2: 0.91962 RMSE: 28.675 ACTIVE

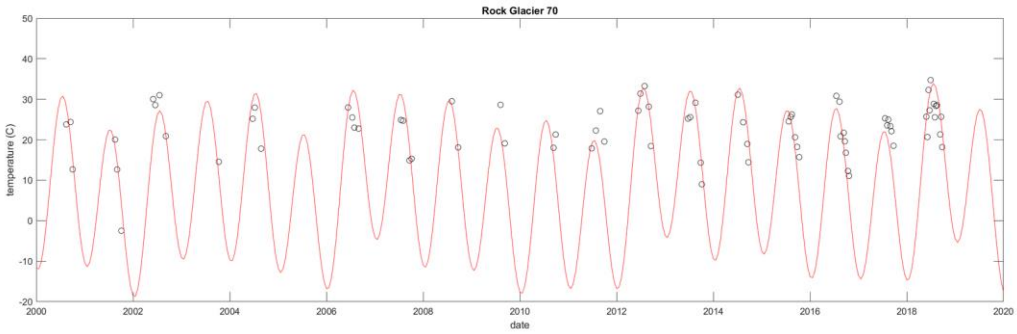

A1: 18.625 T0: 10.83 R^2: 0.92901 RMSE: 23.124 INACTIVE

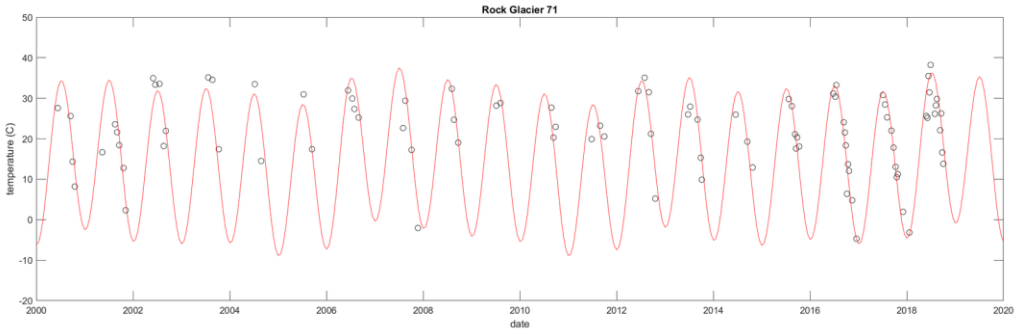

A1: 19.515 T0: 14.21 R^2: 0.95463 RMSE: 32.578 INACTIVE

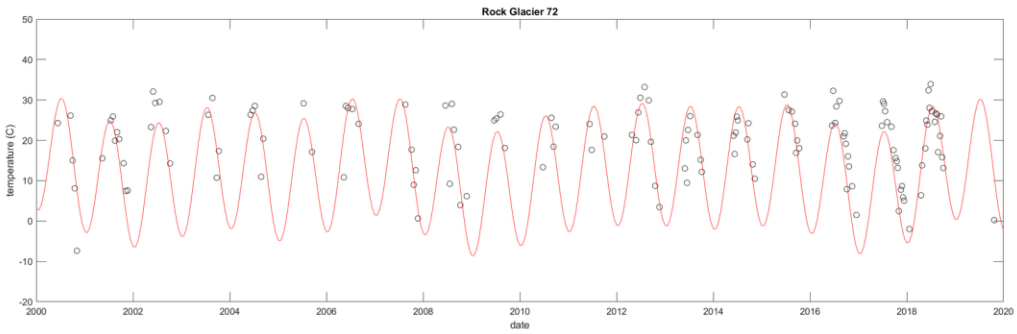

A1: 15.164 T0: 11.864 R^2: 0.83038 RMSE: 48.048 ACTIVE

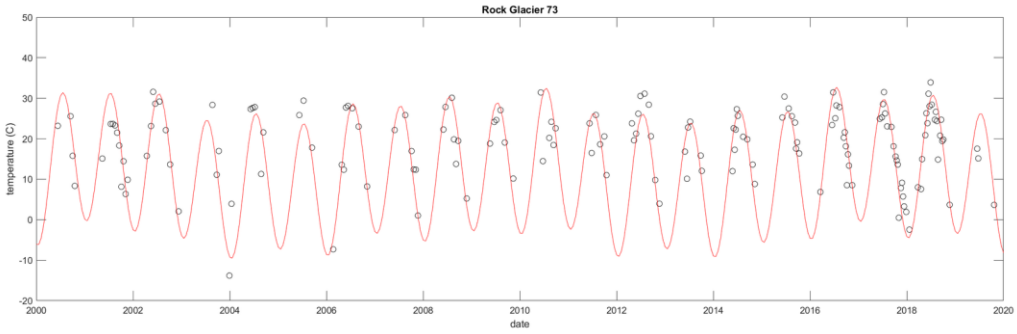

A1: 16.796 T0: 11.179 R^2: 0.9039 RMSE: 40.826 ACTIVE

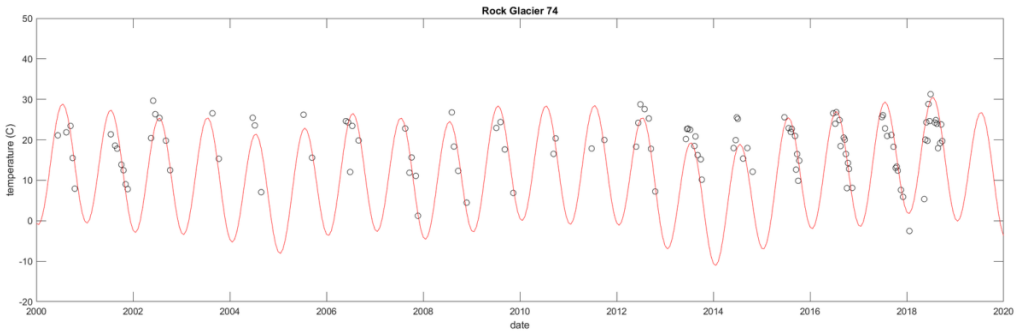

A1: 14.936 T0: 9.9439 R^2: 0.83594 RMSE: 29.942 ACTIVE

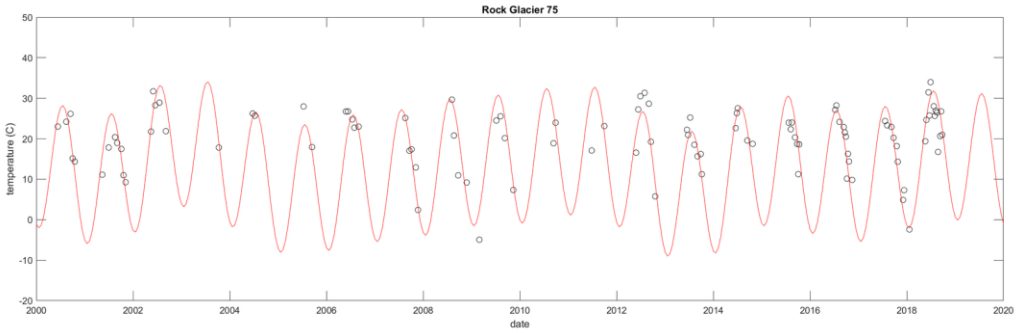

A1: 17.768 T0: 10.372 R^2: 0.91596 RMSE: 29.077 ACTIVE

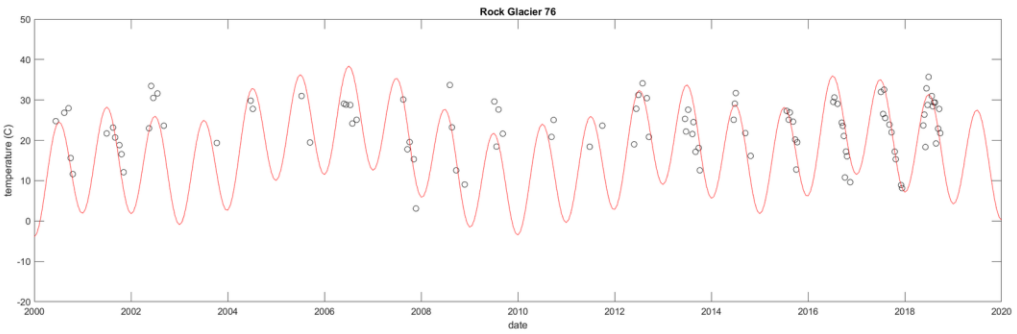

A1: 12.848 T0: 17.285 R^2: 0.89567 RMSE: 24.557 ACTIVE

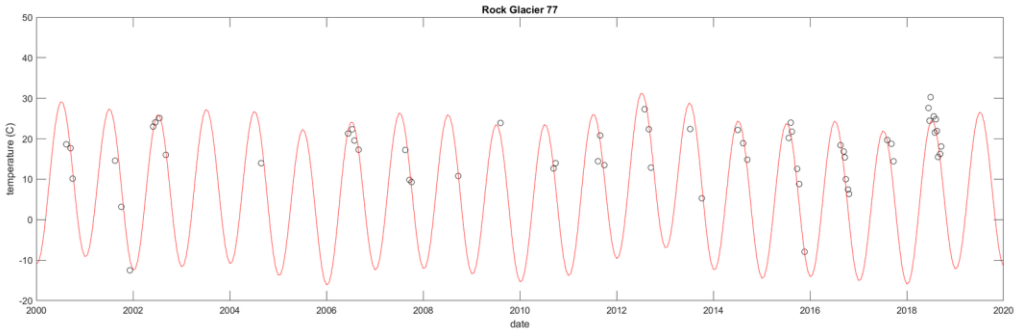

A1: 19.216 T0: 6.4613 R^2: 0.98924 RMSE: 14.336 INACTIVE

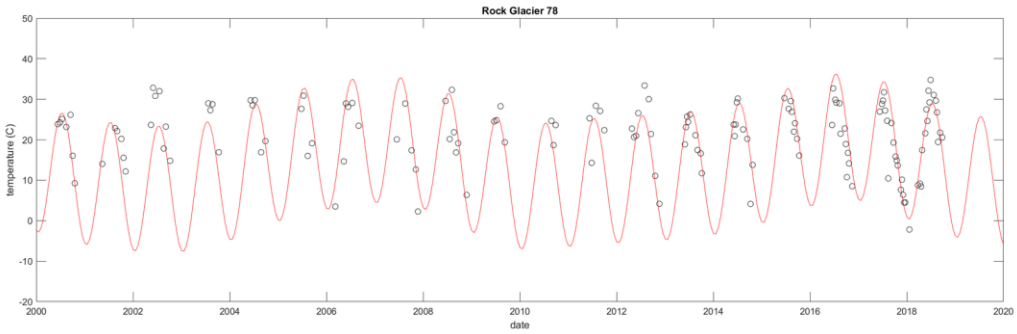

A1: 15.662 T0: 13.443 R^2: 0.87426 RMSE: 34.736 ACTIVE

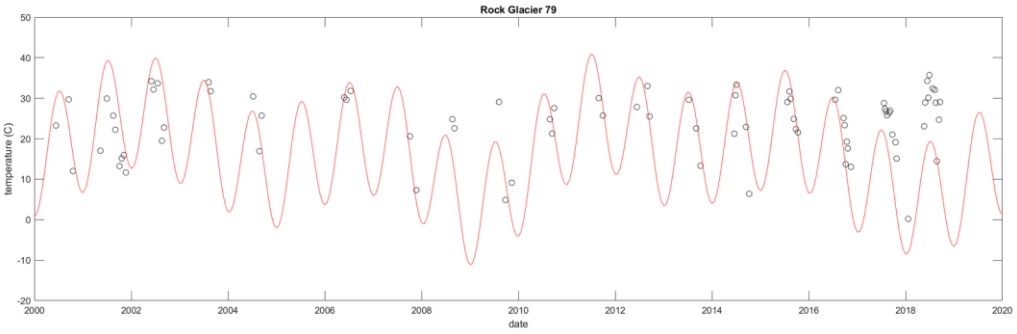

A1: 15.0 T0: 17.002 R^2: 0.85233 RMSE: 38.758 ACTIVE

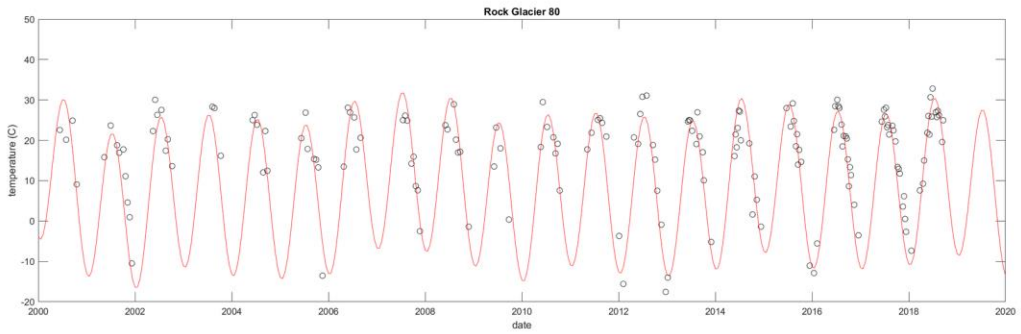

A1: 13.508 T0: 6.0661 R^2: 0.83698 RMSE: 77.193 ACTIVE

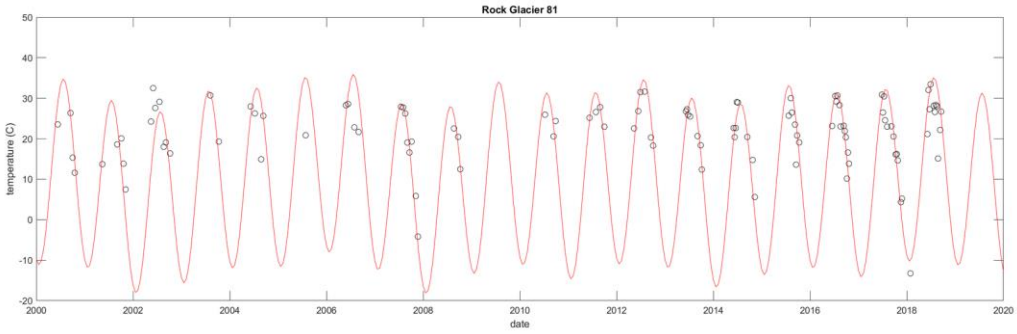

A1: 22.382 T0: 9.0271 R^2: 0.95042 RMSE: 29.125 ACTIVE

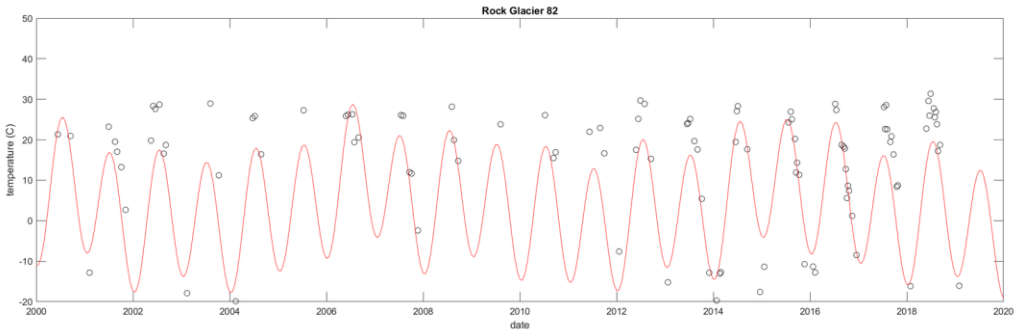

A1: 22.763 T0: 4.5011 R^2: 0.97118 RMSE: 55.873 INACTIVE

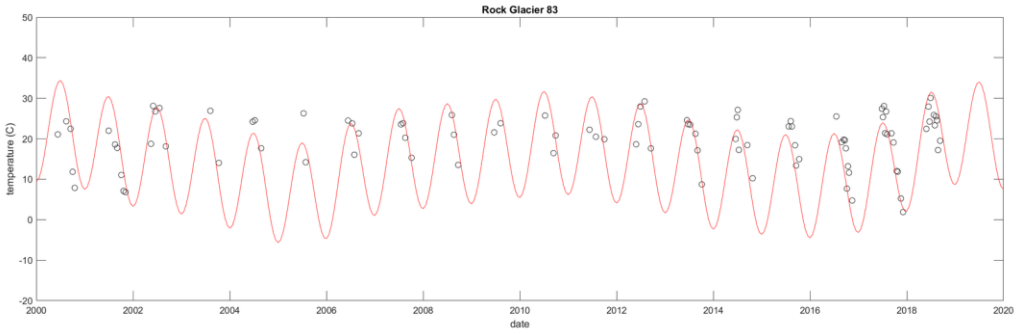

A1: 13.038 T0: 12.718 R^2: 0.94795 RMSE: 14.456 INACTIVE

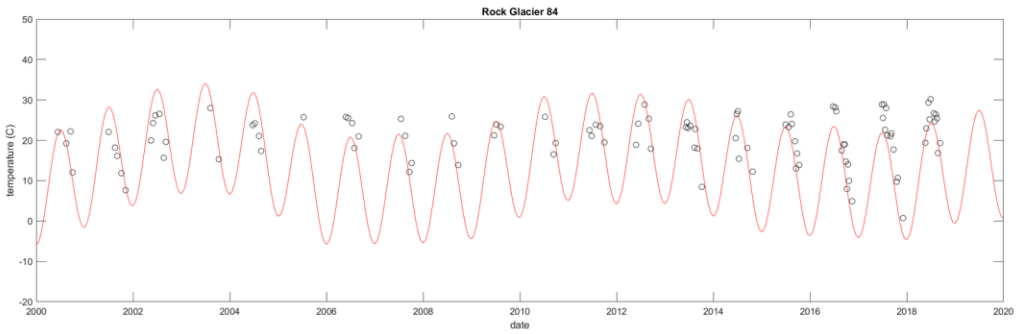

A1: 13.461 T0: 13.862 R^2: 0.93489 RMSE: 15.357 ACTIVE

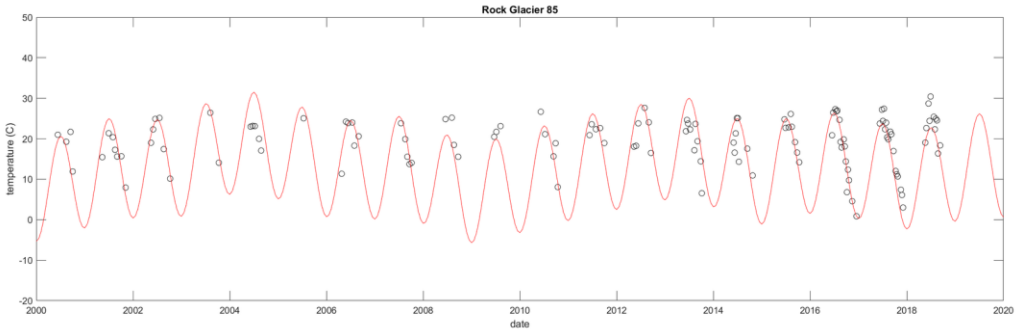

A1: 12.693 T0: 12.169 R^2: 0.93556 RMSE: 14.801 ACTIVE

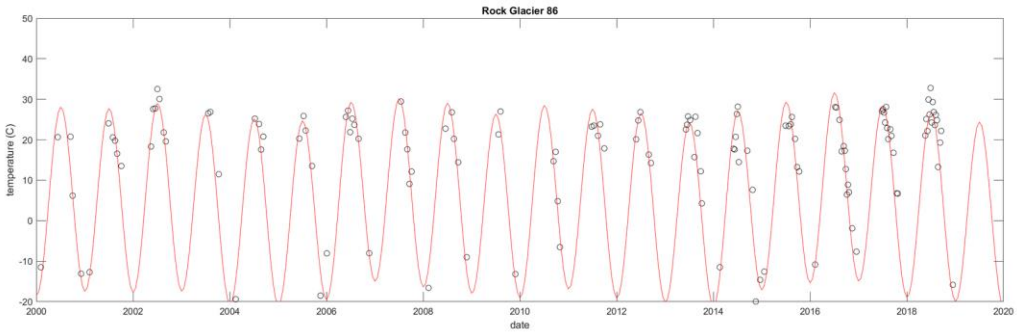

A1: 22.397 T0: 4.3881 R^2: 0.94581 RMSE: 60.35 ACTIVE

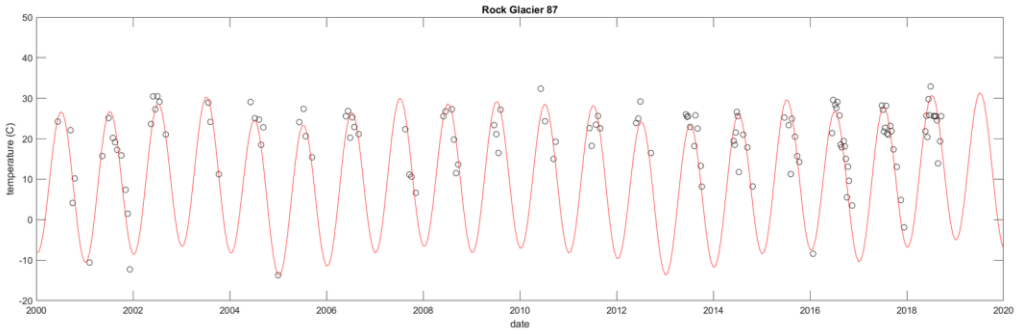

A1: 18.909 T0: 8.4895 R^2: 0.94279 RMSE: 35.745 ACTIVE

APPENDIX C: Tables

Table 1: Sentinel-1 Scenes and how many interferograms they were used in

Culled	**Scene Date (yyyymmdd)**	**Number of Interferograms using the scene**
	20150426	7
	20150520	9
	20150613	6
*	20150707	4
	20150731	8
	20150824	12
	20150917	11
	20151011	14
	20151104	14
*	20151128	10
	20151222	14
*	20160115	12
	20160303	15
*	20160327	16
*	20160420	17
	20160514	14
	20160607	17
	20160701	16
	20160725	14
	20160818	18
	20160911	20
	20161005	21
	20161029	18
	20161122	24
	20161216	17
	20170109	24
	20170202	26
*	20170214	26
	20170226	25
	20170310	27
	20170322	16
*	20170403	26
	20170415	30
*	20170427	29
	20170509	23
	20170521	30
	20170602	26

	20170614	29
	20170626	32
	20170708	33
	20170720	30
	20170801	34
	20170813	33
	20170825	34
	20170906	34
	20170918	28
	20170930	32
	20171012	30
	20171024	31
	20171105	23
	20171117	31
	20171129	31
	20171211	29
	20171223	30
	20180104	30
	20180116	19
	20180128	32
	20180209	32
	20180221	29
	20180305	31
	20180317	27
*	20180329	28
	20180410	26
	20180422	13
	20180504	24
	20180516	24
	20180528	24
	20180609	23
	20180621	22
	20180703	17
	20180715	22
	20180727	21
	20180808	18
	20180820	16

Table 2: Classification of Rock Glaciers Based on Phase Rate and Sensitivity

Rock Glacier	**Peak**	**Sensitivity**	**Phase Rate (radians/yr)**	**Classification**
1	Mestas	-0.16	-1.42	Active

2	Mestas	-0.18	-2.18	Active
3	Mestas	-0.06	-1.89	Active
4	Mestas	-0.33	-3.34	Active
5	Mestas	-0.31	-0.58	Active
6	Mestas	-0.47	-0.15	Inactive
7	Mestas	0.23	-0.05	Inactive
8	Mestas	-0.44	-0.55	Active
9	Mestas	0.36	0.45	Active
10	Mestas	-0.38	-0.72	Active
11	Mestas	0.02	0.23	Active
12	Mestas	0.20	0.54	Active
13	Mestas	0.14	0.75	Active
14	Mestas	0.33	-0.15	Inactive
15	Mestas	0.55	0.17	Inactive
16	Mestas	0.76	-0.20	Active
17	Mestas	0.72	0.75	Active
18	Mestas	0.70	0.11	Inactive
19	Mestas	0.77	-0.04	Inactive
20	Mestas	0.78	-0.01	Inactive
21	Mestas	0.83	0.06	Inactive
22	W Spanish	0.60	0.45	Active
23	W Spanish	0.20	-0.10	Inactive
24	W Spanish	-0.10	-0.16	Uncertain
25	W Spanish	0.03	-0.17	Uncertain
26	W Spanish	-0.16	0.32	Active
27	W Spanish	-0.16	-0.02	Uncertain
28	W Spanish	0.33	0.20	Inactive
29	W Spanish	0.39	0.32	Active
30	W Spanish	0.74	0.56	Active
31	W Spanish	0.91	0.47	Active
32	W Spanish	0.88	0.04	Inactive
33	W Spanish	0.83	0.72	Active
34	W Spanish	0.81	0.32	Active
35	W Spanish	0.82	0.48	Active
36	W Spanish	0.88	0.34	Active
37	E Spanish	0.32	0.20	Active
38	E Spanish	0.42	-0.07	Inactive
39	E Spanish	0.33	0.46	Active
40	E Spanish	0.08	0.12	Uncertain
41	White	0.41	0.83	Active
42	White	0.69	0.39	Active
43	White	0.92	1.08	Active
44	White	0.81	2.45	Active

45	Little (N) Sheep	-0.11	0.04	Uncertain
46	Little (N) Sheep	-0.26	0.25	Active
47	Big (S) Sheep	-0.13	-0.16	Uncertain
48	Big (S) Sheep	-0.06	-0.45	Active
49	Big (S) Sheep	-0.24	-0.39	Active
50	Big (S) Sheep	-0.30	0.31	Active
51	Big (S) Sheep	-0.04	0.50	Active
52	Big (S) Sheep	-0.28	0.07	Inactive
53	Big (S) Sheep	-0.30	0.32	Active
54	Big (S) Sheep	-0.28	-0.12	Inactive
55	Big (S) Sheep	-0.28	-0.39	Active
56	Big (S) Sheep	-0.19	0.02	Uncertain
57	Big (S) Sheep	-0.43	0.28	Active
58	Big (S) Sheep	0.35	-0.10	Inactive
59	Big (S) Sheep	0.61	1.61	Active
60	Big (S) Sheep	0.82	1.11	Active
61	Blanca	-0.35	-0.22	Active
62	Blanca	-0.22	-0.33	Active
63	Blanca	-0.38	-0.14	Inactive
64	Blanca	-0.06	-0.14	Uncertain
65	Blanca	-0.35	-0.06	Inactive
66	Blanca	0.07	0.15	Uncertain
67	Blanca	0.37	0.15	Inactive
68	Blanca	-0.16	0.01	Uncertain
69	Blanca	-0.48	-0.90	Active
70	Blanca	-0.19	-0.18	Uncertain
71	Blanca	-0.03	-0.10	Uncertain
72	Blanca	-0.46	-1.36	Active
73	Blanca	-0.48	-0.29	Active
74	Blanca	0.44	0.28	Active
75	Blanca	0.40	0.48	Active
76	Blanca	-0.41	-0.31	Active
77	Blanca	0.59	0.18	Inactive
78	Blanca	-0.44	-0.28	Active
79	Blanca	-0.20	-0.27	Active
80	Blanca	0.46	0.55	Active
81	Blanca	0.26	1.06	Active
82	Blanca	0.14	-0.04	Uncertain
83	Blanca	0.81	0.04	Inactive
84	Blanca	0.77	0.24	Active
85	Blanca	0.80	0.33	Active
86	Blanca	0.69	0.24	Active
87	Blanca	0.52	0.58	Active

CITATIONS

Benedict, J. B. (1967). Recent Glacial History of an Alpine Area in the Colorado Front Range, U.S.A.: I. Establishing a Lichen-Growth Curve. Journal of Glaciology. https://doi.org/10.3189/s0022143000020128

Benedict, J. B. (1968). Recent Glacial History of an Alpine Area in the Colorado Front Range, U.S.A.: II. Dating the Glacial Deposits. Journal of Glaciology. https://doi.org/10.3189/s0022143000020414

Berthling, I. (2011). Beyond confusion: Rock glaciers as cryo-conditioned landforms. Geomorphology. https://doi.org/10.1016/j.geomorph.2011.05.002

Brenning, A., Grasser, M., & Friend, D. A. (2007). Statistical estimation and generalized additive modeling of rock glacier distribution in the San Juan Mountains, Colorado, United States. Journal of Geophysical Research: Earth Surface, 112(F2). https://doi.org/10.1029/2006JF000528

Brenning, A., Peña, M. A., Long, S., & Soliman, A. (2012). Thermal remote sensing of ice-debris landforms using ASTER: an example from the Chilean Andes. The Cryosphere, 6(2), 367–382. https://doi.org/10.5194/tc-6-367-2012

Bürgmann, R., Rosen, P. A., & Fielding, E. J. (2000). Synthetic Aperture Radar Interferometry to Measure Earth's Surface Topography and Its Deformation. Annual Review of Earth and Planetary Sciences. https://doi.org/10.1146/annurev.earth.28.1.169

Cicoira, A., Beutel, J., Faillettaz, J., Gärtner-Roer, I., & Vieli, A. (2019). Resolving the influence of temperature forcing through heat conduction on rock glacier dynamics: A numerical modelling approach. Cryosphere. https://doi.org/10.5194/tc-13-927-2019

Colaprete, A., & Jakosky, B. M. (1998). Ice flow and rock glaciers on Mars. Journal of Geophysical Research: Planets, 103(E3), 5897–5909. https://doi.org/10.1029/97JE03371

Colucci, R. R., Forte, E., Žebre, M., Maset, E., Zanettini, C., & Guglielmin, M. (2019). Is that a relict rock glacier? Geomorphology. https://doi.org/10.1016/j.geomorph.2019.02.002

Easterbrook, D. J. (1999). Surface processes and landforms. Pearson College Division.

Evin, M. (1983). Structure et mouvement des glaciers rocheux des Alpes du Sud (Doctoral dissertation, Université de Grenoble I).

Fergason, R. L., Christensen, P. R., & Kieffer, H. H. (2006). High-resolution thermal inertia derived from the Thermal Emission Imaging System (THEMIS): Thermal model

and applications. Journal of Geophysical Research E: Planets. https://doi.org/10.1029/2006JE002735

Fisch, W., & Sen, F. W. Electrical DC resistivity soundings with long profiles on rock glaciers and moraines in the alps of Switzerland. (1979). International Journal of Rock Mechanics and Mining Sciences & Geomechanics Abstracts. https://doi.org/10.1016/0148-9062(79)90470-4

Fowler, C. M. R. (2004). The solid earth: An introduction to global geophysics: Cambridge Univ.

François, C., & Ottlé, C. (1996). Atmospheric corrections in the thermal infrared: global and water vapor dependent split-window algorithms - applications to atsr and avhrr data. IEEE Transactions on Geoscience and Remote Sensing. https://doi.org/10.1109/36.485123

Giardino, J. R., & Vitek, J. D. (1988). The significance of rock glaciers in the glacial-periglacial landscape continuum. Journal of Quaternary Science, 3(1), 97–103. https://doi.org/10.1002/jqs.3390030111

Giardino, J. R., Jr., J. F. S., & Lawson, M. P. (1984). Tree-Ring Analysis of Movement of A Rock-Glacier Complex on Mount Mestas, Colorado, U.S.A. Arctic and Alpine Research, 16(3), 299–309. https://doi.org/10.1080/00040851.1984.12004419

Gillespie, A., Rokugawa, S., Matsunaga, T., Steven Cothern, J., Hook, S., & Kahle, A. B. (1998). A temperature and emissivity separation algorithm for advanced spaceborne thermal emission and reflection radiometer (ASTER) images. IEEE Transactions on Geoscience and Remote Sensing. https://doi.org/10.1109/36.700995

Haberle, R. M., & Jakosky, B. M. (1991). Atmospheric effects on the remote determination of thermal inertia on mars. Icarus. https://doi.org/10.1016/0019-1035(91)90100-8

Harris, S. A. (1994). Climatic zonality of periglacial landforms in mountain areas. Arctic. https://doi.org/10.14430/arctic1288

Hoffman, Matt. "Glaciers of Colorado." Glaciers of the American West, Portland State University, 31 Aug. 2011, glaciers.research.pdx.edu/Glaciers-Colorado.

Jakosky, B. M., Mellon, M. T., Kieffer, H. H., Christensen, P. R., Varnes, E. S., & Lee, S. W. (2000). The thermal inertia of Mars from the Mars Global Surveyor Thermal Emission Spectrometer. Journal of Geophysical Research E: Planets. https://doi.org/10.1029/1999JE001088

Janke, J. R. (2005). Modeling past and future alpine permafrost distribution in the Colorado Front Range. Earth Surface Processes and Landforms. https://doi.org/10.1002/esp.1205

Janke, J. R. (2007). Colorado front range rock glaciers: Distribution and topographic characteristics. Arctic, Antarctic, and Alpine Research. https://doi.org/10.1657/1523-0430(2007)39[74:CFRRGD]2.0.CO;2

Jorgensen, W. R. (2007) A Validation of Ground Penetrating Radar for Reconstructing the Internal Structure of a Rock Glacier: Mount Mestas, Colorado, USA (Master's Thesis) Texas A&M University.

Kääb, A. (2013). Rock Glaciers and Protalus Forms. In Encyclopedia of Quaternary Science: Second Edition. https://doi.org/10.1016/B978-0-444-53643-3.00104-7

Kääb, A., Frauenfelder, R., & Roer, I. (2007). On the response of rockglacier creep to surface temperature increase. Global and Planetary Change. https://doi.org/10.1016/j.gloplacha.2006.07.005

Kealy, P. S., & Hook, S. J. (1993). Separating Temperature and Emissivity in Thermal Infrared Multispectral Scanner Data: Implications for Recovering Land Surface Temperatures. IEEE Transactions on Geoscience and Remote Sensing. https://doi.org/10.1109/36.317447

Li, F., Jackson, T. J., Kustas, W. P., Schmugge, T. J., French, A. N., Cosh, M. H., & Bindlish, R. (2004). Deriving land surface temperature from Landsat 5 and 7 during SMEX02/SMACEX. Remote Sensing of Environment. https://doi.org/10.1016/j.rse.2004.02.018

Liang, S. (2001). An optimization algorithm for separating land surface temperature and emissivity from multispectral thermal infrared imagery. IEEE Transactions on Geoscience and Remote Sensing. https://doi.org/10.1109/36.905234

Liu, L., Millar, C. I., Westfall, R. D., & Zebker, H. A. (2013). Surface motion of active rock glaciers in the Sierra Nevada, California, USA: Inventory and a case study using InSAR. Cryosphere. https://doi.org/10.5194/tc-7-1109-2013

Mahaney, W. C., Miyamoto, H., Dohm, J. M., Baker, V. R., Cabrol, N. A., Grin, E. A., & Berman, D. C. (2007). Rock glaciers on Mars: Earth-based clues to Mars' recent paleoclimatic history. Planetary and Space Science, 55(1–2), 181–192. https://doi.org/10.1016/J.PSS.2006.04.016

Marker, M. E. (1990). Minimum Altitudes for Former Periglacial Landforms Adjacent to Longitude 106°W in Colorado and New Mexico, USA, Between Latitudes 33°N and 40°N. Arctic and Alpine Research, 22(4), 366–374. https://doi.org/10.1080/00040851.1990.12002802

Martin, H. E., & Whalley, W. B. (1987). Rock glaciers: Part 1: Rock glacier morphology: Classification and distribution. Progress in Physical Geography. https://doi.org/10.1177/030913338701100205

Mellon, M. T., & Jakosky, B. M. (1993). Geographic variations in the thermal and diffusive stability of ground ice on Mars. Journal of Geophysical Research. https://doi.org/10.1029/92JE02355

Mellon, M. T., Jakosky, B. M., Kieffer, H. H., & Christensen, P. R. (2000). High-Resolution Thermal Inertia Mapping from the Mars Global Surveyor Thermal Emission Spectrometer. Icarus. https://doi.org/10.1006/icar.2000.6503

Morris, S. E. (1981). Topoclimatic Factors and the Development of Rock Glacier Facies, Sangre de Cristo Mountains, Southern Colorado. Arctic and Alpine Research, 13(3), 329–338. https://doi.org/10.1080/00040851.1981.12004253

National Elevation Dataset, . (1978). Blanca Peak. In USGS Geographic Names Information System. Retrieved from https://geonames.usgs.gov/apex/f?p=gnispq:3:0::NO::P3_FID:192735

Parastatidis, D., Mitraka, Z., Chrysoulakis, N., & Abrams, M. (2017). Online global land surface temperature estimation from landsat. Remote Sensing. https://doi.org/10.3390/rs9121208

Potter Jr, N. (1972). Ice-cored rock glacier, Galena Creek, northern Absaroka Mountains, Wyoming. Geological Society of America Bulletin, 83(10), 3025-3058.

Price, J. C. (1985). On the analysis of thermal infrared imagery: The limited utility of apparent thermal inertia. Remote Sensing of Environment, 18(1), 59–73. https://doi.org/10.1016/0034-4257(85)90038-0

Robertson, E. C. (1988). Thermal properties of rocks. https://pubs.usgs.gov/of/1988/0441/report.pdf

Schmidt, D. A., & Bürgmann, R. (2003). Time-dependent land uplift and subsidence in the Santa Clara valley, California, from a large interferometric synthetic aperture radar data set. Journal of Geophysical Research: Solid Earth, 108(B9). https://doi.org/10.1029/2002JB002267

Siebenthal, C. E. (1907). Notes on Glaciation in the Sangre De Cristo Range, Colorado. The Journal of Geology. https://doi.org/10.1086/621366

Watson, K. (1992). Two-temperature method for measuring emissivity. Remote Sensing of Environment. https://doi.org/10.1016/0034-4257(92)90095-2

Whalley, Brian. "Rock glaciers: their ice and debris balances." Vignettes: Key concepts in geomorphology, Carleton College, 15 Nov. 2016, serc.carleton.edu/vignettes/collection/68182.html.

Whalley, W. B., & Martin, H. E. (1992). Rock glaciers : II models and mechanisms. Progress in Physical Geography. https://doi.org/10.1177/030913339201600201

Wright, T. J., Parsons, B. E., & Lu, Z. (2004). Toward mapping surface deformation in three dimensions using InSAR. Geophysical Research Letters, 31(1).

Yu, C., Li, Z., Penna, N. T., & Crippa, P. (2018). Generic atmospheric correction model for interferometric synthetic aperture radar observations. Journal of Geophysical Research: Solid Earth, 123, 9202– 9222. https://doi-org.proxy.mul.missouri.edu/10.1029/2017JB015305

Zhu, Z., & Woodcock, C. E. (2012). Object-based cloud and cloud shadow detection in Landsat imagery. Remote sensing of environment, 118, 83-94.